Volume 30, Number 2 October, 2022
ISSN:1521-1398 PRINT,1572-9206 ONLINE

Journal of Computational Analysis and Applications

EUDOXUS PRESS, LLC

Journal of Computational Analysis and Applications
ISSNno.'s:1521-1398 PRINT,1572-9206 ONLINE

SCOPE OF THE JOURNAL

An international publication of Eudoxus Press, LLC
(twice annually)

Editor in Chief: George Anastassiou
Department of Mathematical Sciences,
University of Memphis, Memphis, TN 38152-3240, U.S.A
ganastss@memphis.edu
http://www.msci.memphis.edu/~ganastss/jocaaa

The main purpose of "J.Computational Analysis and Applications" is to publish high quality research articles from all subareas of Computational Mathematical Analysis and its many potential applications and connections to other areas of Mathematical Sciences. Any paper whose approach and proofs are computational,using methods from Mathematical Analysis in the broadest sense is suitable and welcome for consideration in our journal, except from Applied Numerical Analysis articles. Also plain word articles without formulas and proofs are excluded. The list of possibly connected mathematical areas with this publication includes, but is not restricted to: Applied Analysis, Applied Functional Analysis, Approximation Theory, Asymptotic Analysis, Difference Equations, Differential Equations, Partial Differential Equations, Fourier Analysis, Fractals, Fuzzy Sets, Harmonic Analysis, Inequalities, Integral Equations, Measure Theory, Moment Theory, Neural Networks, Numerical Functional Analysis, Potential Theory, Probability Theory, Real and Complex Analysis, Signal Analysis, Special Functions, Splines, Stochastic Analysis, Stochastic Processes, Summability, Tomography, Wavelets, any combination of the above, e.t.c.

"J.Computational Analysis and Applications" is a peer-reviewed Journal. See the instructions for preparation and submission of articles to JoCAAA. Assistant to the Editor: Dr.Razvan Mezei,mezei_razvan@yahoo.com, St.Martin Univ.,Olympia,WA,USA.

Journal of Computational Analysis and Applications(JoCAAA) is published by **EUDOXUS PRESS,LLC**,1424 Beaver Trail Drive,Cordova,TN38016,USA,anastassioug@yahoo.com http://www.eudoxuspress.com. **Annual Subscription Prices**:For USA and Canada,Institutional:Print $800, Electronic OPEN ACCESS. Individual:Print $300. For any other part of the world add $140 more(handling and postages) to the above prices for Print. No credit card payments.

JoCAAA is reviewed and abstracted by AMS Mathematical Reviews,MATHSCI, Elsevier-Scopus.

Editorial Board
Associate Editors of Journal of Computational Analysis and Applications

George Cybenko
Thayer School of Engineering
Dartmouth College
8000 Cummings Hall,
Hanover, NH 03755-8000
603-646-3843 (X 3546 Secr.)
e-mail:george.cybenko@dartmouth.edu
Approximation Theory and Neural Networks

Sever S. Dragomir
School of Computer Science and Mathematics, Victoria University,
PO Box 14428,
Melbourne City,
MC 8001, AUSTRALIA
Tel. +61 3 9688 4437
Fax +61 3 9688 4050
sever.dragomir@vu.edu.au
Inequalities, Functional Analysis, Numerical Analysis, Approximations, Information Theory, Stochastics.

Oktay Duman
TOBB University of Economics and Technology,
Department of Mathematics, TR-06530,
Ankara, Turkey,
oduman@etu.edu.tr
Classical Approximation Theory, Summability Theory, Statistical Convergence and its Applications

Saber N. Elaydi
Department Of Mathematics
Trinity University
715 Stadium Dr.
San Antonio, TX 78212-7200
210-736-8246
e-mail: selaydi@trinity.edu
Ordinary Differential Equations, Difference Equations

J .A. Goldstein
Department of Mathematical Sciences
The University of Memphis
Memphis, TN 38152
901-678-3130
jgoldste@memphis.edu
Partial Differential Equations, Semigroups of Operators

H. H. Gonska
Department of Mathematics
University of Duisburg
Duisburg, D-47048
Germany
011-49-203-379-3542
e-mail: heiner.gonska@uni-due.de
Approximation Theory, Computer Aided Geometric Design

John R. Graef
Department of Mathematics
University of Tennessee at Chattanooga
Chattanooga, TN 37304 USA
John-Graef@utc.edu
Ordinary and functional differential equations, difference equations, impulsive systems, differential inclusions, dynamic equations on time scales, control theory and their applications

Weimin Han
Department of Mathematics
University of Iowa
Iowa City, IA 52242-1419
319-335-0770
e-mail: whan@math.uiowa.edu
Numerical analysis, Finite element method, Numerical PDE, Variational inequalities, Computational mechanics

Tian-Xiao He
Department of Mathematics and Computer Science
P.O. Box 2900, Illinois Wesleyan University
Bloomington, IL 61702-2900, USA
Tel (309)556-3089
Fax (309)556-3864
the@iwu.edu
Approximations, Wavelet, Integration Theory, Numerical Analysis, Analytic Combinatorics

Margareta Heilmann
Faculty of Mathematics and Natural Sciences, University of Wuppertal
Gaußstraße 20
D-42119 Wuppertal, Germany,
heilmann@math.uni-wuppertal.de
Approximation Theory (Positive Linear Operators)

Xing-Biao Hu
Institute of Computational Mathematics
AMSS, Chinese Academy of Sciences

Beijing, 100190, CHINA
hxb@lsec.cc.ac.cn
Computational Mathematics

Jong Kyu Kim
Department of Mathematics
Kyungnam University
Masan Kyungnam,631-701,Korea
Tel 82-(55)-249-2211
Fax 82-(55)-243-8609
jongkyuk@kyungnam.ac.kr
Nonlinear Functional Analysis, Variational Inequalities, Nonlinear Ergodic Theory, ODE, PDE, Functional Equations.

Robert Kozma
Department of Mathematical Sciences
The University of Memphis
Memphis, TN 38152, USA
rkozma@memphis.edu
Neural Networks, Reproducing Kernel Hilbert Spaces,
Neural Percolation Theory

Mustafa Kulenovic
Department of Mathematics
University of Rhode Island
Kingston, RI 02881,USA
kulenm@math.uri.edu
Differential and Difference Equations

Irena Lasiecka
Department of Mathematical Sciences
University of Memphis
Memphis, TN 38152
PDE, Control Theory, Functional Analysis, lasiecka@memphis.edu

Burkhard Lenze
Fachbereich Informatik
Fachhochschule Dortmund
University of Applied Sciences
Postfach 105018
D-44047 Dortmund, Germany
e-mail: lenze@fh-dortmund.de
Real Networks, Fourier Analysis, Approximation Theory

Hrushikesh N. Mhaskar
Department Of Mathematics
California State University
Los Angeles, CA 90032
626-914-7002
e-mail: hmhaska@gmail.com
Orthogonal Polynomials, Approximation Theory, Splines, Wavelets, Neural Networks

Ram N. Mohapatra
Department of Mathematics
University of Central Florida
Orlando, FL 32816-1364
tel.407-823-5080
ram.mohapatra@ucf.edu
Real and Complex Analysis, Approximation Th., Fourier Analysis, Fuzzy Sets and Systems

Gaston M. N'Guerekata
Department of Mathematics
Morgan State University
Baltimore, MD 21251, USA
tel: 1-443-885-4373
Fax 1-443-885-8216
Gaston.N'Guerekata@morgan.edu
nguerekata@aol.com
Nonlinear Evolution Equations, Abstract Harmonic Analysis, Fractional Differential Equations, Almost Periodicity & Almost Automorphy

M.Zuhair Nashed
Department Of Mathematics
University of Central Florida
PO Box 161364
Orlando, FL 32816-1364
e-mail: znashed@mail.ucf.edu
Inverse and Ill-Posed problems, Numerical Functional Analysis, Integral Equations, Optimization, Signal Analysis

Mubenga N. Nkashama
Department OF Mathematics
University of Alabama at Birmingham
Birmingham, AL 35294-1170
205-934-2154
e-mail: nkashama@math.uab.edu
Ordinary Differential Equations, Partial Differential Equations

Vassilis Papanicolaou
Department of Mathematics
National Technical University of Athens
Zografou campus, 157 80
Athens, Greece
tel:: +30(210) 772 1722
Fax +30(210) 772 1775
papanico@math.ntua.gr
Partial Differential Equations,

Probability

Choonkil Park
Department of Mathematics
Hanyang University
Seoul 133-791
S. Korea, baak@hanyang.ac.kr
Functional Equations

Svetlozar (Zari) Rachev,
Professor of Finance, College of Business, and Director of Quantitative Finance Program,
Department of Applied Mathematics & Statistics
Stonybrook University
312 Harriman Hall, Stony Brook, NY 11794-3775
tel: +1-631-632-1998,
svetlozar.rachev@stonybrook.edu

Alexander G. Ramm
Mathematics Department
Kansas State University
Manhattan, KS 66506-2602
e-mail: ramm@math.ksu.edu
Inverse and Ill-posed Problems, Scattering Theory, Operator Theory, Theoretical Numerical Analysis, Wave Propagation, Signal Processing and Tomography

Tomasz Rychlik
Polish Academy of Sciences
Instytut Matematyczny PAN
00-956 Warszawa, skr. poczt. 21
ul. Śniadeckich 8
Poland
trychlik@impan.pl
Mathematical Statistics, Probabilistic Inequalities

Boris Shekhtman
Department of Mathematics
University of South Florida
Tampa, FL 33620, USA
Tel 813-974-9710
shekhtma@usf.edu
Approximation Theory, Banach spaces, Classical Analysis

T. E. Simos
Department of Computer Science and Technology
Faculty of Sciences and Technology
University of Peloponnese
GR-221 00 Tripolis, Greece
Postal Address:
26 Menelaou St.
Anfithea - Paleon Faliron
GR-175 64 Athens, Greece
tsimos@mail.ariadne-t.gr
Numerical Analysis

H. M. Srivastava
Department of Mathematics and Statistics
University of Victoria
Victoria, British Columbia V8W 3R4
Canada
tel.250-472-5313; office,250-477-6960 home, fax 250-721-8962
harimsri@math.uvic.ca
Real and Complex Analysis, Fractional Calculus and Appl., Integral Equations and Transforms, Higher Transcendental Functions and Appl.,q-Series and q-Polynomials, Analytic Number Th.

I. P. Stavroulakis
Department of Mathematics
University of Ioannina
451-10 Ioannina, Greece
ipstav@cc.uoi.gr
Differential Equations
Phone +3-065-109-8283

Manfred Tasche
Department of Mathematics
University of Rostock
D-18051 Rostock, Germany
manfred.tasche@mathematik.uni-rostock.de
Numerical Fourier Analysis, Fourier Analysis, Harmonic Analysis, Signal Analysis, Spectral Methods, Wavelets, Splines, Approximation Theory

Roberto Triggiani
Department of Mathematical Sciences
University of Memphis
Memphis, TN 38152
PDE, Control Theory, Functional Analysis, rtrggani@memphis.edu

Juan J. Trujillo
University of La Laguna
Departamento de Analisis Matematico
C/Astr.Fco.Sanchez s/n
38271. LaLaguna. Tenerife.
SPAIN

Tel/Fax 34-922-318209
Juan.Trujillo@ull.es
Fractional: Differential Equations-Operators-Fourier Transforms, Special functions, Approximations, and Applications

Ram Verma
International Publications
1200 Dallas Drive #824 Denton, TX 76205, USA
Verma99@msn.com
Applied Nonlinear Analysis, Numerical Analysis, Variational Inequalities, Optimization Theory, Computational Mathematics, Operator Theory

Xiang Ming Yu
Department of Mathematical Sciences
Southwest Missouri State University
Springfield, MO 65804-0094
417-836-5931
xmy944f@missouristate.edu
Classical Approximation Theory, Wavelets

Xiao-Jun Yang
State Key Laboratory for Geomechanics and Deep Underground Engineering, China University of Mining and Technology, Xuzhou 221116, China
*Local Fractional Calculus and Applications, Fractional Calculus and Applications, General Fractional Calculus and Applications, Variable-order Calculus and Applications, Viscoelasticity and Computational methods for Mathematical Physics.*dyangxiaojun@163.com

Richard A. Zalik
Department of Mathematics
Auburn University
Auburn University, AL 36849-5310 USA.
Tel 334-844-6557 office
Fax 334-844-6555
zalik@auburn.edu
Approximation Theory, Chebychev Systems, Wavelet Theory

Ahmed I. Zayed
Department of Mathematical Sciences
DePaul University
2320 N. Kenmore Ave.
Chicago, IL 60614-3250
773-325-7808
e-mail: azayed@condor.depaul.edu
Shannon sampling theory, Harmonic analysis and wavelets, Special functions and orthogonal polynomials, Integral transforms

Ding-Xuan Zhou
Department Of Mathematics
City University of Hong Kong
83 Tat Chee Avenue
Kowloon, Hong Kong
852-2788 9708,Fax:852-2788 8561
e-mail: mazhou@cityu.edu.hk
Approximation Theory, Spline functions, Wavelets

Xin-long Zhou
Fachbereich Mathematik, Fachgebiet Informatik
Gerhard-Mercator-Universitat Duisburg
Lotharstr.65, D-47048 Duisburg, Germany
e-mail:Xzhou@informatik.uni-duisburg.de
Fourier Analysis, Computer-Aided Geometric Design, Computational Complexity, Multivariate Approximation Theory, Approximation and Interpolation Theory

Jessada Tariboon
Department of Mathematics
King Mongut's University of Technology N. Bangkok
1518 Pracharat 1 Rd., Wongsawang, Bangsue, Bangkok, Thailand 10800
jessada.t@sci.kmutnb.ac.th, Time scales Differential/Difference Equations, Fractional Differential Equations

Jagdev Singh
JECRC University, Jaipur, India
jagdevsinghrathore@gmail.com
Fractional Calculus, Mathematical Modelling, Special Functions, Numerical Methods

Instructions to Contributors
Journal of Computational Analysis and Applications

An international publication of Eudoxus Press, LLC, of TN.

Editor in Chief: George Anastassiou

Department of Mathematical Sciences
University of Memphis
Memphis, TN 38152-3240, U.S.A.

1. Manuscripts files in Latex and PDF and in English, should be submitted via email to the Editor-in-Chief:

Prof.George A. Anastassiou
Department of Mathematical Sciences
The University of Memphis
Memphis,TN 38152, USA.
Tel. 901.678.3144
e-mail: ganastss@memphis.edu

Authors may want to recommend an associate editor the most related to the submission to possibly handle it.

Also authors may want to submit a list of six possible referees, to be used in case we cannot find related referees by ourselves.

2. Manuscripts should be typed using any of TEX,LaTEX,AMS-TEX,or AMS-LaTEX and according to EUDOXUS PRESS, LLC. LATEX STYLE FILE. (Click HERE to save a copy of the style file.)They should be carefully prepared in all respects. Submitted articles should be brightly typed (not dot-matrix), double spaced, in ten point type size and in 8(1/2)x11 inch area per page. Manuscripts should have generous margins on all sides and should not exceed 24 pages.

3. Submission is a representation that the manuscript has not been published previously in this or any other similar form and is not currently under consideration for publication elsewhere. A statement transferring from the authors(or their employers,if they hold the copyright) to Eudoxus Press, LLC, will be required before the manuscript can be accepted for publication.The Editor-in-Chief will supply the necessary forms for this transfer.Such a written transfer of copyright,which previously was assumed to be implicit in the act of submitting a manuscript,is necessary under the U.S.Copyright Law in order for the publisher to carry through the dissemination of research results and reviews as widely and effective as possible.

4. The paper starts with the title of the article, author's name(s) (no titles or degrees), author's affiliation(s) and e-mail addresses. The affiliation should comprise the department, institution (usually university or company), city, state (and/or nation) and mail code.

The following items, 5 and 6, should be on page no. 1 of the paper.

5. An abstract is to be provided, preferably no longer than 150 words.

6. A list of 5 key words is to be provided directly below the abstract. Key words should express the precise content of the manuscript, as they are used for indexing purposes.

The main body of the paper should begin on page no. 1, if possible.

7. All sections should be numbered with Arabic numerals (such as: 1. INTRODUCTION) .
Subsections should be identified with section and subsection numbers (such as 6.1. Second-Value Subheading).
If applicable, an independent single-number system (one for each category) should be used to label all theorems, lemmas, propositions, corollaries, definitions, remarks, examples, etc. The label (such as Lemma 7) should be typed with paragraph indentation, followed by a period and the lemma itself.

8. Mathematical notation must be typeset. Equations should be numbered consecutively with Arabic numerals in parentheses placed flush right, and should be thusly referred to in the text [such as Eqs.(2) and (5)]. The running title must be placed at the top of even numbered pages and the first author's name, et al., must be placed at the top of the odd numbed pages.

9. Illustrations (photographs, drawings, diagrams, and charts) are to be numbered in one consecutive series of Arabic numerals. The captions for illustrations should be typed double space. All illustrations, charts, tables, etc., must be embedded in the body of the manuscript in proper, final, print position. In particular, manuscript, source, and PDF file version must be at camera ready stage for publication or they cannot be considered.

Tables are to be numbered (with Roman numerals) and referred to by number in the text. Center the title above the table, and type explanatory footnotes (indicated by superscript lowercase letters) below the table.

10. List references alphabetically at the end of the paper and number them consecutively. Each must be cited in the text by the appropriate Arabic numeral in square brackets on the baseline.
References should include (in the following order):
initials of first and middle name, last name of author(s)
title of article,

name of publication, volume number, inclusive pages, and year of publication.

Authors should follow these examples:

Journal Article

1. H.H.Gonska,Degree of simultaneous approximation of bivariate functions by Gordon operators, (journal name in italics) *J. Approx. Theory*, 62,170-191(1990).

Book

2. G.G.Lorentz, (title of book in italics) *Bernstein Polynomials* (2nd ed.), Chelsea,New York,1986.

Contribution to a Book

3. M.K.Khan, Approximation properties of beta operators,in(title of book in italics) *Progress in Approximation Theory* (P.Nevai and A.Pinkus,eds.), Academic Press, New York,1991,pp.483-495.

11. All acknowledgements (including those for a grant and financial support) should occur in one paragraph that directly precedes the References section.

12. Footnotes should be avoided. When their use is absolutely necessary, footnotes should be numbered consecutively using Arabic numerals and should be typed at the bottom of the page to which they refer. Place a line above the footnote, so that it is set off from the text. Use the appropriate superscript numeral for citation in the text.

13. After each revision is made please again submit via email Latex and PDF files of the revised manuscript, including the final one.

14. Effective 1 Nov. 2009 for current journal page charges, contact the Editor in Chief. Upon acceptance of the paper an invoice will be sent to the contact author. The fee payment will be due one month from the invoice date. The article will proceed to publication only after the fee is paid. The charges are to be sent, by money order or certified check, in US dollars, payable to Eudoxus Press, LLC, to the address shown on the Eudoxus homepage.

No galleys will be sent and the contact author will receive one (1) electronic copy of the journal issue in which the article appears.

15. This journal will consider for publication only papers that contain proofs for their listed results.

Markovian Queueing Model with Single Working Vacation and Server Breakdown

M.SEENIVASAN,
Mathematics Wings - DDE, Annamalai University,
Annamalainagar-608002, India.
Email: emseeni@yahoo.com
R.ABINAYA,
Department of Mathematics, Annamalai University,
Annamalainagar-608002, India.
Email: anuyaabi2@gmail.com

December 14, 2021

In this article, we investigate a Markovian queuing model with server breakdown and Single working vacation. Arrival follows Poisson process with parameter λ. Service while the single working vacation epoch, normal working epoch together with vacation epoch are all exponentially assigned with rate μ_b, μ_v and ηrespectively. After taking first vacation the server wait idle in the system to serve. This type of vacation is called Single Working Vacation (SWV). If the queue length increases, service rate changes from slow rate to normal rate. When the server may subject to sudden breakdown with rate α and after it should be repaired and goes to normal service with rate β. This queue model has been analysed with the help of Matrix Geometric Method (MGM) to find steady state probability vectors. Using it some performance measure is also determined.

AMS subject classification number— 60K25,60K30 and 90B22
Key Words —- Working Vacation (WV), Single Working Vacation (SWV) , Stability condition, Server breakdown, Matrix Geometric Method (MGM);

1 Introduction

Queueing systems with SWV and absolute service have acquired importance over the most recent twenty years because of large extent uses mainly manufacturing system, service system, telecommunications, and computer system. Its discoveries might be utilized to give quicker client support, increment traffic stream, further develop request shipments from a stockroom, or plan information organizations and call focuses. Numerous significant utilization of the

queueing theory are traffic flow vehicles, airplane, individuals, correspondences, booking patients in medical clinics, occupations on machines, programs on PC, and office configuration banks, mail depots, stores. In numerous genuine queueing circumstances, after assistance fulfillment, if no customer in the queue, a server goes on a vacation epoch. This type is known as vacation queue. Using survey paper by Doshi (1986) many researchers introduced queueing model with vacations.

Servi and Finn (2002) developed an M/M/1 queueing model upon WV. Wu and Takagi (2003) analysed an M/G/1 queueing model upon MWV. Analysis of GI/M/1 queueing model upon MWV studied by Baba (2005). Server will only take one WV if the queue become null. So, if the queue has no customers when the server come back from SWV, he will idle on the system and wait for the customers to arrive instead of picking up another WV. A multi-server system with an SWV were proposed by Lin and Ke (2009). The use of inactive epoch a M/G/1 model were studied by Levy and Yechiali (1975).

The vacation models and the model in which the server may goes to breakdowns and repairs, is well ascertained in survey papers B.T. Doshi. William J. Gray et al (2000) overworked on multiple types of server breakdowns in queueing theory. A queueing model with server breakdowns, repairs, vacations, and backup server is studied by Srinivas R.Chakravarthy (2020).Agelenbe et al (1991) analyzed the queues with negative arrivals. A matrix-Geometric method approach is a useful tool for solving the more complex queueing problems. Neuts (1978) deliberate Markov c hains with applications queueing theory, which have a matrix geometric invariant probability vector. Neuts (1981) derived Matrix Geometric solution in stochastic models.

Transient solution for the queue-size distribution in a finite-buffer model with general independent input stream and single working vacation was explained by Wojciech M Kempa et al (2018). Rachita Sethi et al (2019) studied performance analysis of machine repair problem with working vacation and service interruptions. Seenivasan et al (2021) studied performance examination of two heterogeneous servers queuing model with an irregularly reachable server utilizing MGM. Seenivasan et al (2021) investigated a retrial queueing model with two heterogeneous servers using the MGM. Praveen Deora et al (2021) analyzed the cost analysis and optimization of machine repair model with working vacation and feedback policy. M/M/1 queueing model with working vacation and two type of server breakdown was discussed by Praveen Kumar Agrawal et al (2021).

[1] Our study, deals with an SWV and server breakdown in M/M/1 queueing model. In accordance with FCFS principle customers are served. This model has been analysed using MGM. The excess of this study designated as follows. We providing construction of model in section 2. Performance measures formalized in section 3. Mathematical illustrations solved in section 4. And brief conclusion in final section.

[1]Corresponding Author: M.Seenivasan, Mathematics Wings - DDE, Annamalai University, Annamalainagar-608002,India.
Email: emseeni@yahoo.com

2 Construction of the Model

We consider a Single Working Vacation (SWV) and Server breakdown in M/M/1 model. The customers show up in line as per Poisson process with parameter λ. They create a queue dependent on her/his request for appearance. At a normal working period, influx customers served at a service rate μ_b, following an exponential distribution. The server starts a single vacation of arbitrary length if there is no customer in the system with parameter η follows an exponential distribution. During a SWV period, influx customers get service with rate μ_v, following an exponential distribution. If the queue forms, then the server chop and shift its rate from μ_v to μ_b, the normal working interval starts. For next vacation server waits idle to serve influx customers. This type of vacation is called Single Working Vacation (SWV). If not, the server starts a normal working period when a customer arrival occurs.

When the server may subject to sudden breakdown with rate α and after it should be repaired and goes to normal service with rate β. The transition rate diagram is shown in Figure 1.

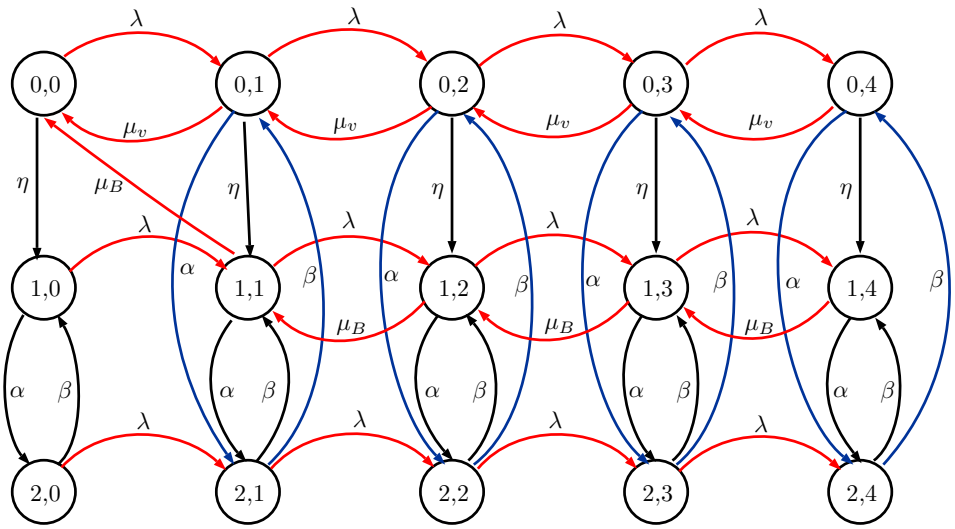

Figure 1: The transition rate diagram

Let $\{k(t), n(t) : t \geq 0\}; \lim_{t\to\infty} p\{k(t) = i, n(t) = j\}$ be a Markov process, where $k(t)$ and $n(t)$ represent state of process at time t respectively.
$k(t) = 0$, when server is on SWV,
$k(t) = 1$, when server is on normal working epoch
$k(t) = 2$, when server is on breakdown
n(t) denotes total customer in the system.
The Quasi-birth and death Process along with the state space Ω as follow

$\Omega = \{(0,0)U(1,0)U(2,0)U(i,j); i = 0,1,2, j = 1,2,....,n \geq 1\}$

Consider a QBD process with Infinitesimal generator matrix Q is presented below

$$Q = \begin{pmatrix} A_0 & C_1 & \cdots & \cdots & \cdots & \cdots & \cdots & \cdots \\ C_0 & C_2 & C_3 & \cdots & \cdots & \cdots & \cdots & \cdots \\ 0 & C_3 & C_2 & C_3 & \cdots & \cdots & \cdots & \cdots \\ 0 & \cdots & C_3 & C_2 & \cdots & \cdots & \cdots & \cdots \\ 0 & \cdots & \cdots & C_3 & \cdots & \cdots & \cdots & \cdots \\ \cdots & \cdots & \cdots & \cdots & \cdots & \cdots & \cdots & \cdots \end{pmatrix}$$

Where

$$A_0 = \begin{pmatrix} -(\lambda+\eta) & \eta & 0 \\ 0 & -(\lambda+\alpha) & \alpha \\ 0 & \beta & -(\beta+\lambda) \end{pmatrix}; C_1 = \begin{pmatrix} \lambda & 0 & 0 \\ 0 & \lambda & 0 \\ 0 & 0 & \lambda \end{pmatrix};$$

$$C_0 = \begin{pmatrix} \mu_v & 0 & 0 \\ \mu_b & 0 & 0 \\ 0 & 0 & 0 \end{pmatrix}; C_2 = \begin{pmatrix} -(\lambda+\mu_v+\alpha+\eta) & \eta & \alpha \\ 0 & -(\lambda+\mu_b+\alpha) & \alpha \\ \beta & \beta & -(2\beta+\lambda) \end{pmatrix};$$

$$C_3 = \begin{pmatrix} \mu_v & 0 & 0 \\ 0 & \mu_b & 0 \\ 0 & 0 & 0 \end{pmatrix}$$

We define $p_{ij} = \{k = i, n = j\}$; where j denote number of customers in the system & i denote the server state.

Probability vector are defined as $P = (P_0, P_1, P_2, \ldots)$ where, $P_j = (p_{0j}, p_{1j}, p_{2j})$, $j = 0,1,2,3,...$

The static probability row matrix is represented by using $PQ = O$. (1)

$P_j = P_0 R^j$ where $j \geq 1$ (2)

The normalizing equation is defined by

$P_0 [I - R]^{-1} e = 1$ (3)

Where 'e' is the column unit vector with all its element equal to one.

The static condition of such a QBD, (See Neuts (1981)) can be obtained by the drift condition

$PC_1 e < PC_3 e$ (4)

Where the row vector $P = (P_0, P_1, P_2)$ is obtained from the Infinitesimal generator

$S = C_1 + C_2 + C_3$. S is given by

$$S = \begin{pmatrix} -(\alpha+\eta) & \eta & \alpha \\ 0 & -\alpha & \alpha \\ \beta & \beta & 2\beta \end{pmatrix} \quad (5)$$

S is irreducible and the row vector P can be shown to be unique such that

$PS = 0$ and $Pe = 1$ (6)

From Equation(6), we have

$P_1 = (\frac{2\eta-\alpha}{\alpha})P_0$

$P_2 = (\frac{\eta+\alpha}{\beta})P_0$

$P_0 = [1 + (\frac{\eta+\alpha}{\beta}) + (\frac{2\eta-\alpha}{\alpha})]^{-1}$ (7)

The static condition takes format

$\lambda[P_0 + P_1 + P_2] < \mu_b P_0 + \mu_v P_1$ (8)

Equation(5) gives the static probability of S.

Once the rate matrix R obtained, the probability vectors P_j's ($j \geq 1$) are obtained from Eq.(2) and Eq.(3).

3 Performance Measures

Performance measure have been found using steady-state probabilities as given below

When the server is idle mean no. of customers presented $E(I) = P_0$ (9)

When the server is SWV mean no. of customers presented

$$E(SWV) = \sum_{j=0}^{\infty} jp_{0j} \tag{10}$$

When the server is normal busy period mean no. of customers presented

$$E(BP) = \sum_{j=1}^{\infty} jp_{1j} \tag{11}$$

When the server is on breakdown mean no. of customers presented

$$E(BD) = \sum_{j=1}^{\infty} jp_{1j} \tag{12}$$

Mean no. of customer in the system is

$$E(N) = E(I) + E(WV) + E(BP) + E(BD) \tag{13}$$

4 Mathematical Study

Here, we make mathematical calculation for model given by the segment above. Our goals are to show effect of a parameter on system features. By modifying λ, four illustrations are presented in these sections.

The parameter λ value varies and all other argument values are fixed. Illustration 1 to Illustration 4 is presented below.

Illustration 1

We take $\lambda = 0.1$,$\mu_b = 0.6$,$\mu_v = 0.5$,$\alpha = 0.2$,$\eta = 0.5$,$\beta = 0.7$ and the rate matrix is

$$R = \begin{pmatrix} 0.0942 & 0.0781 & 0.0193 \\ 0.0126 & 0.1347 & 0.0167 \\ 0.0534 & 0.1106 & 0.0834 \end{pmatrix}$$

Table 1.Probability vectors

	p_{0j}	p_{1j}	p_{2j}	Total
P_0	0.1215	0.5476	0.1479	0.8170
P_1	0.0262	0.0996	0.0232	0.1496
P_2	0.0050	0.0181	0.0042	0.0273
P_3	0.0009	0.0033	0.0007	0.0049
P_4	0.0002	0.0006	0.0001	0.0009
P_5	0.0000	0.0001	0.0000	0.0001
Total				0.9998

By substituting R matrix in equation (1) vector P_0 are obtained and normalization equation $P_0\left[I-R\right]^{-1}e=1$ for the mathematical argument selected previously, row vector P_1 is granted by $P_0=(0.1215,0.05476,0.1479)$. More, the balance vector P_j's gained from $P_j=P_0R^j, j=1,2,3,\ldots$ and are shown in Table 1. Column 2, 3 and 4 contains the three elements of $P_j, j=0,1,2,\ldots$. Final column constitutes the total of two elements. Total probability was confirmed to be $0.9998\approx 1$.

Illustration 2

We take $\lambda=0.2$,$\mu_b=0.6$,$\mu_v=0.5$,$\alpha=0.2$,$\eta=0.5$,$\beta=0.7$ and the rate matrix is

$$R=\begin{pmatrix}0.1807 & 0.1644 & 0.0313\\ 0.0250 & 0.2694 & 0.0274\\ 0.1024 & 0.2328 & 0.1507\end{pmatrix}$$

Table 2.Probability vectors

	p_{0j}	p_{1j}	p_{2j}	Total
P_0	0.1655	0.3782	0.0979	0.6416
P_1	0.0494	0.1519	0.0303	0.2316
P_2	0.0158	0.0561	0.0103	0.0822
P_3	0.0053	0.0201	0.0036	0.0290
P_4	0.0018	0.0070	0.0013	0.0101
P_5	0.0006	0.0025	0.0004	0.0035
P_6	0.0002	0.0009	0.0002	0.0013
P_7	0.0001	0.0003	0.0001	0.0005
P_8	0.0000	0.0001	0.0000	0.0001
Total				0.9999

By substituting R matrix in equation (1) vector P_0 are obtained and normalization equation $P_0\left[I-R\right]^{-1}e=1$ for the mathematical argument selected previously, row vector P_1 is granted by $P_0=(0.1655,0.3782,0.0979)$. More, the

balance vector P_j's gained from $P_j = P_0 R^j, j = 1, 2, 3, \ldots$ and are shown in Table 1. Column 2, 3 and 4 contains the three elements of $P_j, j = 0, 1, 2, \ldots$. Final column constitutes the total of two elements. Total probability was confirmed to be $0.9999 \approx 1$.

Illustration 3

We take $\lambda = 0.3$,$\mu_b = 0.6$,$\mu_v = 0.5$,$\alpha = 0.2$,$\eta = 0.5$,$\beta = 0.7$ and the rate matrix is

$$R = \begin{pmatrix} 0.2587 & 0.2552 & 0.0391 \\ 0.0363 & 0.4018 & 0.0345 \\ 0.1452 & 0.3612 & 0.2067 \end{pmatrix}$$

Table 3.Probability vectors

	p_{0j}	p_{1j}	p_{2j}	Total
P_0	0.1615	0.2511	0.0640	0.4766
P_1	0.0602	0.1612	0.0282	0.2536
P_2	0.0257	0.0919	0.0139	0.1315
P_3	0.0120	0.0485	0.0070	0.0675
P_4	0.0059	0.0251	0.0036	0.0346
P_5	0.0030	0.0129	0.0018	0.0177
P_6	0.0015	0.0066	0.0009	0.0090
P_7	0.0008	0.0034	0.0005	0.0047
P_8	0.0004	0.0017	0.0002	0.0023
P_9	0.0002	0.0009	0.0001	0.0012
P_{10}	0.0001	0.0005	0.0001	0.0007
P_{11}	0.0001	0.0002	0.0000	0.0003
P_{12}	0.0000	0.0001	0.0000	0.0001
Total				0.9997

By substituting R matrix in equation (1) vector P_0 are obtained and normalization equation $P_0 [I - R]^{-1} e = 1$ for the mathematical argument selected previously, row vector P_1 is granted by $P_0 = (0.1615, 0.2511, 0.0640)$. More, the balance vector P_j's gained from $P_j = P_0 R^j, j = 1, 2, 3, \ldots$ and are shown in Table 1. Column 2, 3 and 4 contains the three elements of $P_j, j = 0, 1, 2, \ldots$. Final column constitutes the total of two elements. Total probability was confirmed to be $0.9997 \approx 1$.

Illustration 4

We take $\lambda = 0.4$,$\mu_b = 0.6$,$\mu_v = 0.5$,$\alpha = 0.2$,$\eta = 0.5$,$\beta = 0.7$ and the rate matrix is

$$R = \begin{pmatrix} 0.3275 & 0.3420 & 0.0441 \\ 0.0453 & 0.5253 & 0.0392 \\ 0.1802 & 0.4836 & 0.2546 \end{pmatrix}$$

Table 4.Probability vectors

	p_{0j}	p_{1j}	p_{2j}	Total
P_0	0.1304	0.1578	0.0421	0.3303
P_1	0.0574	0.1478	0.0227	0.2279
P_2	0.0296	0.1083	0.0141	0.1520
P_3	0.0171	0.0738	0.0091	0.1000
P_4	0.0106	0.0491	0.0060	0.0657
P_5	0.0068	0.0323	0.0039	0.0430
P_6	0.0044	0.0212	0.0026	0.0282
P_7	0.0029	0.0139	0.0017	0.0185
P_8	0.0019	0.0091	0.0011	0.0121
P_9	0.0012	0.0059	0.0007	0.0078
P_{10}	0.0008	0.0039	0.0005	0.0052
P_{11}	0.0005	0.0025	0.0003	0.0033
P_{12}	0.0003	0.0017	0.0002	0.0022
P_{13}	0.0003	0.0011	0.0001	0.0014
P_{14}	0.0001	0.0007	0.0001	0.0009
P_{15}	0.0001	0.0004	0.0001	0.0006
P_{16}	0.0001	0.0003	0.0000	0.0004
P_{17}	0.0000	0.0002	0.0000	0.0002
P_{18}	0.0000	0.0001	0.0000	0.0001
Total				0.9998

By substituting R matrix in equation (1) vector P_0 are obtained and normalization equation $P_0\left[I-R\right]^{-1}e=1$ for the mathematical argument selected previously, row vector P_1 is granted by $P_0=(0.1304,0.1578,0.0421)$. More, the balance vector P_j's gained from $P_j=P_0R^j, j=1,2,3,\ldots$ and are shown in Table 1. Column 2, 3 and 4 contains the three elements of $P_j, j=0,1,2,\ldots$. Final column constitutes the total of two elements. Total probability was confirmed to be $0.9998\approx 1$.

Table 4.Performance Measures

λ	$E(I)$	$E(SWV)$	$E(BP)$	$E(BD)$	$E(N)$
0.1	0.8170	0.0397	0.1486	0.0347	1.0400
0.2	0.6416	0.1090	0.3736	0.0708	1.1950
0.3	0.4766	0.2079	0.7529	0.1128	1.5502
0.4	0.3303	0.3412	1.4211	0.1792	2.2718

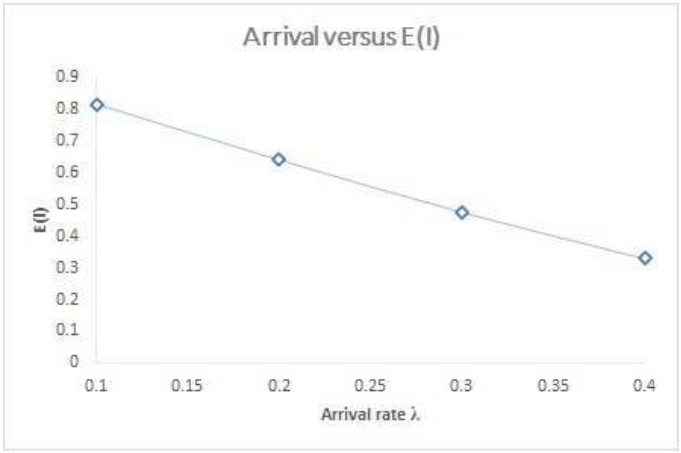

Figure 2

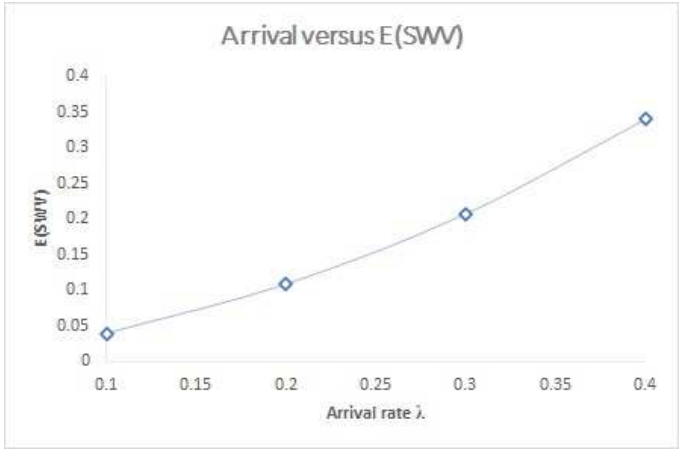

Figure 3

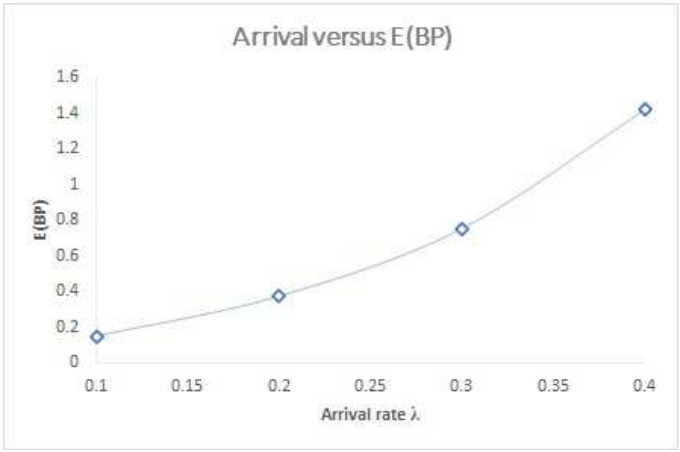

Figure 4

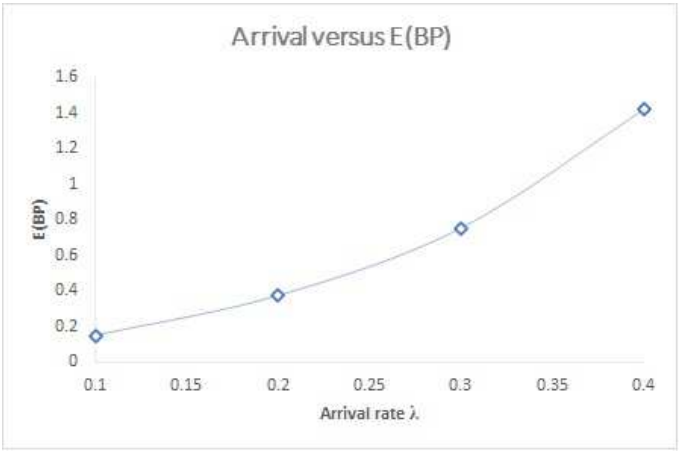

Figure 5

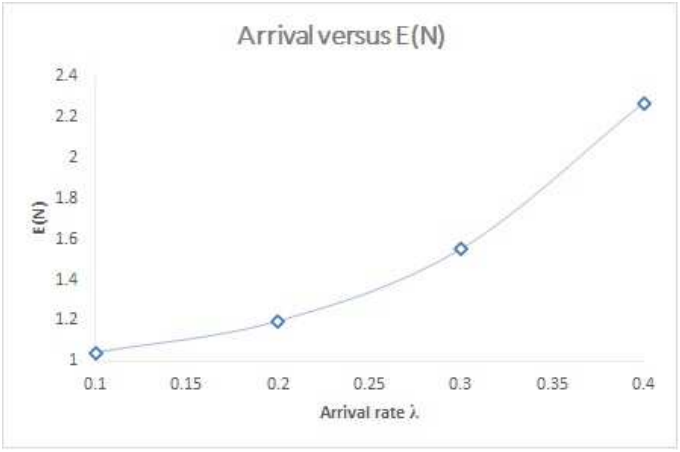

Figure 6

Out of the above figures, we derived few performance measurements with the effect of λ such as mean no., of customer if server is idle, mean no., of customer if server is on SWV, mean no., of customer if server is on busy period, mean no., of customer if server is on breakdown and mean no., of customers throughout system respectively. From Figure 2 shows that arrival rate increases, mean no., of customer if server is idle decreases, Figure 3, Figure 4, Figure 5 and Figure 6 shows arrival rate increases, mean no., of customer if server is SWV, busy period, breakdown and mean no., of customers throughout system increases.

5 CONCLUSION

In this article, we have studied a single-server queueing model along with SWV and server breakdown. We derived the static probability row vector by MGM and also we derived some performance measures for mean no., of customers in the system during server is idle, SWV, normal busy period, breakdown and mean no., of customers throughout system respectively with the effect of λ.

References

[1] Baba, Y., Analysis of a GI/M/1 queue with multiple working vacations, Operations research Letters vol.33, pp.201-209, (2005).

[2] Doshi, B.T., Single - server queue with vacation a servey, Queueing Systems, vol.1, pp. 29-66, (1986).

[3] Gelenbe, E., Glynn, P., and Sigman, k., Queues with negative arrivals, Appl prob vol.28, pp. 245-250, (2003).

[4] Levy, y. and Yechiali, U., Utilization of idle time in an M/G/1 queueing system, Manag. Sci. Vol.22, pp. 202-211, (1975).

[5] Lin, C.H. and Ke, J.C., Multi-server system with single working vacation, Appl Math Model, Vol.33, pp.2967-2977, (2009).

[6] Madhu Jain, Anamika Jain, Working vacations queueing model with multiple types of server breakdowns, Appl Math Model, Vol.34, pp. 1-13, (2010).

[7] Neuts, M.F., Markov chains with applications queueing theory, which have a matrix geometric invariant probability vector, Adv Appl Prob, Vol. 10, pp. 185-212, (1978).

[8] Neuts, M.F., Matrix-Geometric solutions in stochastic models, vol. 2 of johns Hopkins series in the mathematical series, Johns Hopkins University Press, Baltimore, USA, (1981).

[9] Praveen Deora, Umesh Kumari, and DC Sharma, Cost analysis and optimization of machine repair model with working vacation and feedback policy, International Journal of Applied Computational Mathematics, Vol. 6, pp. 1-14, (2021).

[10] Praveen Kumar Agrawal, Anamika Jain, and Madhu Jain, M/M/1 queueing model with working vacation and two type of server breakdown, Phys Conf Ser, Vol. 1849, (2021).

[11] Rachita Sethi, Amita Bhagat, Performance analysis of machine repair problem with working vacation and service interruptions, AIP Conf Proceedings, Vol. 2061, (2019).

[12] Seenivasan, M., Rajarajan, G., and Indumathi, M., Retrial queueing model with two heterogeneous servers using the Matrix Geometric Method, Mater Sci Eng, Vol. 1070, (2021).

[13] Seenivasan, M. and Indumathi, M., Performance Analysis Of Two Heterogeneous Server Queuing Model with Intermittently Obtainable Server Using Matrix Geometric Method, Phys Conf Ser, Vol. 1724, (2021).

[14] Srinivas R.Chakravarthy, Shruti Rakhee and Kulshrestha, A queueing model with server breakdowns, repairs, vacations, and backup server, Operations research perspectives, Vol. 7, (2020).

[15] Servi, L.D. and Finn, S.G., M/M/1 queues with working vacation (M/M/1/WV), Perform Eval, Vol. 50, pp. 41-52, (2002).

[16] William J. Gray, Patrick Wang, P. and Meckinley Scott, A Queueing Model with Multiple Types of Server Breakdowns, Quality Technology and Quantitative Management, pp. 245-255, Vol. 1, (2004).

[17] Wojciech M Kempa and Martyna Kobielnik, Transient solution for the queue-size distribution in a finite-buffer model with general independent input stream and single working vacation, Appl Math Modelling, Vol. 59, pp. 614-628, (2018).

[18] Wu, D. and Takagi, H., M/G/1 queue with multiple working vacation, In proceedings of the Queueing Symposium, Stochastic models and their Application, Kakegowa, pp. 51-60, (2003).

Generalized fractional operators and their image formulas

Manish Kumar Bansal[1,*], Kottakkaran Sooppy Nisar[2], Junesang Choi[3] and Devendra Kumar[4]

[1]Department of Mathematics, Jaypee Institute of Information Technology, Noida-201309, Uttar Pradesh, India.

Email: manish.bansal@mail.jiit.ac.in, bansalmanish443@gmail.com

[2]Department of Mathematics, College of Arts and Sciences, Wadi Aldawaser Prince Sattam bin Abdulaziz University, Saudi Arabia. Email: n.sooppy@psau.edu.sa

[3]Department of Mathematics, Dongguk University Gyeongju 38066, Republic of Korea. Email: junesangchoi@gmail.com

[4]Department of Mathematics, University of Rajasthan, Jaipur 302004, Rajasthan, India. Email: devendra.maths@gmail.com

Abstract

Numerous image formulae for a diversity of polynomials and functions subjected to a variety of fractional integrals and derivatives have been given. In this paper, we aimto construct image formulae for the product of incomplete H-functions and a general class of polynomials under the Katugampola fractional integral and derivative operators . We also provide some particular instances of our main findings in corollaries, among many others.

Keywords: Fractional Integral operators, Incomplete H-functions, Fox's H-function, Mellin-Barnes type contour integral.
Mathematics Subject Classification 2010: 26A33; 33C60; 44A10; 34A08; 33B20.

1 Introduction and preliminaries

We begin by recalling the well-known Gamma function Γ defined by (see, e.g., [19, Section 1.1])

$$\Gamma(\mu) = \begin{cases} \int_0^\infty e^{-\mathfrak{v}}\mathfrak{v}^{\mu-1}d\mathfrak{v} & (\Re(\mu) > 0) \\ \frac{\Gamma(\mu+k)}{(\mu)_k} & (\mu \in \mathbb{C} \setminus \mathbb{Z}_{\leq 0};\ k \in \mathbb{N}_0), \end{cases} \tag{1.1}$$

* Corresponding author

where the Pochhammer symbol $(\mu)_\nu$ ($\mu,\ \nu \in \mathbb{C}$) is defined, in terms of Gamma function Γ (see, e.g., [19, p. 2 and p. 5]), by

$$\begin{aligned}(\mu)_\nu &= \frac{\Gamma(\mu+\nu)}{\Gamma(\mu)} \quad (\mu+\nu \in \mathbb{C}\setminus\mathbb{Z}_{\leq 0},\ \nu \in \mathbb{C}\setminus\{0\};\ \mu \in \mathbb{C}\setminus\mathbb{Z}_{\leq 0},\ \nu = 0)\\ &= \begin{cases} 1 & (\nu = 0,\ \mu \in \mathbb{C}\setminus\{0\}),\\ \mu(\mu+1)\cdots(\mu+n-1) & (\nu = n \in \mathbb{N},\ \mu \in \mathbb{C}), \end{cases}\end{aligned} \tag{1.2}$$

it being assumed that $(0)_0 = 1$. Here and throughout, let $\mathbb{C}$, $\mathbb{R}$, $\mathbb{R}^+$, $\mathbb{Z}$, and $\mathbb{N}$ denote the sets of complex numbers, real numbers, positive real numbers, integers, and positive integers, respectively. Also let $\mathbb{N}_0 := \mathbb{N}\cup\{0\}$ and $\mathbb{Z}_{\leq \ell}$ be the set of integers which are less than or equal to some integer $\ell \in \mathbb{Z}$. The incomplete Gamma function $\gamma(\mu,u)$ and its complement $\Gamma(\mu,u)$ defined by

$$\gamma(\mu,u) = \int_0^u e^{-\mathfrak{v}}\mathfrak{v}^{\mu-1}d\mathfrak{v} \qquad (u \geq 0;\ \Re(\mu) > 0), \tag{1.3}$$

and

$$\Gamma(\mu,u) = \int_u^\infty e^{-\mathfrak{v}}\mathfrak{v}^{\mu-1}d\mathfrak{v} \qquad (u \geq 0;\ \Re(\mu) > 0 \ \text{ when } \ u = 0), \tag{1.4}$$

respectively, satisfy the following relation:

$$\gamma(\mu,u) + \Gamma(\mu,u) = \Gamma(\mu) \qquad (\Re(\mu) > 0). \tag{1.5}$$

Srivastava et al. [21] used the incomplete Gamma functions to introduce the following incomplete H-functions (see also [5]):

$$\begin{aligned}\gamma^{\mathsf{m},\mathsf{n}}_{\mathsf{p},\mathsf{q}}(z) &= \gamma^{\mathsf{m},\mathsf{n}}_{\mathsf{p},\mathsf{q}}\left[\ z\ \middle|\ \begin{matrix}(\mathsf{e}_1,\mathsf{E}_1,\mathsf{y}),(\mathsf{e}_i,\mathsf{E}_i)_{2,\mathsf{p}}\\ \\ (\mathsf{f}_i,\mathsf{F}_i)_{1,\mathsf{q}}\end{matrix}\ \right]\\ &= \gamma^{\mathsf{m},\mathsf{n}}_{\mathsf{p},\mathsf{q}}\left[\ z\ \middle|\ \begin{matrix}(\mathsf{e}_1,\mathsf{E}_1,\mathsf{y}),(\mathsf{e}_2,\mathsf{E}_2),\cdots,(\mathsf{e}_\mathsf{p},\mathsf{E}_\mathsf{p})\\ \\ (\mathsf{f}_1,\mathsf{F}_1),(\mathsf{f}_2,\mathsf{F}_2),\cdots,(\mathsf{f}_\mathsf{q},\mathsf{F}_\mathsf{q})\end{matrix}\ \right]\\ &:= \frac{1}{2\pi\mathrm{i}}\int_{\mathfrak{C}} \mathbb{G}(\xi,\mathsf{y})\ z^{-\xi}d\xi,\end{aligned} \tag{1.6}$$

where

$$\mathbb{G}(\xi,\mathsf{y}) = \frac{\gamma(1-\mathsf{e}_1-\mathsf{E}_1\xi,\mathsf{y})\prod_{i=1}^{\mathsf{m}}\Gamma(\mathsf{f}_i+\mathsf{F}_i\xi)\prod_{i=2}^{\mathsf{n}}\Gamma(1-\mathsf{e}_i-\mathsf{E}_i\xi)}{\prod_{i=\mathsf{m}+1}^{\mathsf{q}}\Gamma(1-\mathsf{f}_i-\mathsf{F}_i\xi)\prod_{i=\mathsf{n}+1}^{\mathsf{p}}\Gamma(\mathsf{e}_i+\mathsf{E}_i\xi)}; \tag{1.7}$$

$$\begin{aligned}\Gamma_{\mathsf{p},\mathsf{q}}^{\mathsf{m},\mathsf{n}}(z) &= \Gamma_{\mathsf{p},\mathsf{q}}^{\mathsf{m},\mathsf{n}}\left[\begin{array}{c|l} z & (\mathsf{e}_1,\mathsf{E}_1,\mathsf{y}),(\mathsf{e}_i,\mathsf{E}_i)_{2,\mathsf{p}} \\ & (\mathsf{f}_i,\mathsf{F}_i)_{1,\mathsf{q}} \end{array}\right] \\ &= \Gamma_{\mathsf{p},\mathsf{q}}^{\mathsf{m},\mathsf{n}}\left[\begin{array}{c|l} z & (\mathsf{e}_1,\mathsf{E}_1,\mathsf{y}),(\mathsf{e}_2,\mathsf{E}_2),\cdots,(\mathsf{e}_\mathsf{p},\mathsf{E}_\mathsf{p}) \\ & (\mathsf{f}_1,\mathsf{F}_1),(\mathsf{f}_2,\mathsf{F}_2),\cdots,(\mathsf{f}_\mathsf{q},\mathsf{F}_\mathsf{q}) \end{array}\right] \\ &:= \frac{1}{2\pi\mathrm{i}}\int_{\mathfrak{C}} \mathbb{F}(\xi,\mathsf{y})\; z^{-\xi}d\xi, \end{aligned} \tag{1.8}$$

where

$$\mathbb{F}(\xi,\mathsf{y}) = \frac{\Gamma(1-\mathsf{e}_1-\mathsf{E}_1\xi,\mathsf{y})\prod_{i=1}^{\mathsf{m}}\Gamma(\mathsf{f}_i+\mathsf{F}_i\xi)\prod_{i=2}^{\mathsf{n}}\Gamma(1-\mathsf{e}_i-\mathsf{E}_i\xi)}{\prod_{i=\mathsf{m}+1}^{\mathsf{q}}\Gamma(1-\mathsf{f}_i-\mathsf{F}_i\xi)\prod_{i=\mathsf{n}+1}^{\mathsf{p}}\Gamma(\mathsf{e}_i+\mathsf{E}_i\xi)}. \tag{1.9}$$

For convergence conditions of these incomplete H-functions as well as the description of the contour $\mathfrak{C}$, one may refer to [21]. They [21] explored a variety of intriguing properties of these incomplete H-functions, such as decomposition and reduction formulas, derivative formulas, various integral transforms, and computational representations, as well as applied some significantly general RiemannLiouville and Weyl type fractional integral operators to each of these incomplete H-functions.

Srivastava [17] introduced the following general class of polynomials:

$$S_{\mathsf{n}}^{\mathsf{m}}[x] = \sum_{k=0}^{[\mathsf{n}/\mathsf{m}]}\frac{(-\mathsf{n})_{\mathsf{m}k}}{k!}\,A_{\mathsf{n},k}\,x^k \qquad (\mathsf{m}\in\mathbb{N},\ \mathsf{n}\in\mathbb{N}_0)\,, \tag{1.10}$$

where the coefficients $A_{\mathsf{n},k}$ $(\mathsf{n},\ k\in\mathbb{N}_0)$ are arbitrary real or complex constants. By properly specializing $A_{\mathsf{n},k}$, the general class of polynomials may generate many existing polynomials as special instances, including Jacobi and Laguerre polynomials (see, e.g., [15]). In particular, setting $A_{0,0}=1$ and $x=0$ reduces $S_{\mathsf{n}}^{\mathsf{m}}[x]$ to unity.

There have been many introductions and investigations of fractional integrals and derivatives. Two of them are recalled here. The left-sided and right-sided Riemann-Liouville fractional integrals $I_{a+}^{\alpha}f$ and $I_{b-}^{\alpha}f$ of order $\alpha\in\mathbb{C}$ are defined as (see, e.g., [10, 12–14])

$$\left(I_{a+}^{\alpha}f\right)(x) = \frac{1}{\Gamma(\alpha)}\int_a^x (x-\tau)^{\alpha-1}f(\tau)\,d\tau \quad (x>a,\ \Re(\alpha)>0), \tag{1.11}$$

and

$$\left(I_{b-}^{\alpha}f\right)(x) = \frac{1}{\Gamma(\alpha)}\int_x^b (\tau-x)^{\alpha-1}f(\tau)\,d\tau \quad (b>x,\ \Re(\alpha)>0), \tag{1.12}$$

respectively. The Riemann-Liouville fractional derivatives $D^{\alpha}_{a+}f$ and $D^{\alpha}_{b-}f$ of order $\alpha \in \mathbb{C}$ $(\Re(\alpha) \geq 0)$ are defined by

$$(D^{\alpha}_{a+}f)(x) = \left(\frac{d}{dx}\right)^{\mathsf{n}} \left(I^{\mathsf{n}-\alpha}_{a+}f\right)(x) \quad (x > a) \tag{1.13}$$

and

$$(D^{\alpha}_{b-}f)(x) = \left(-\frac{d}{dx}\right)^{\mathsf{n}} \left(I^{\mathsf{n}-\alpha}_{b-}f\right)(x) \quad (x < b), \tag{1.14}$$

where $\mathsf{n} = [\Re(\alpha)] + 1$.

For $\rho \in \mathbb{R} \setminus \{0\}$, the left-sided and right-sided Katugampola fractional integrals, respectively, denoted by ${}^{\rho}I^{\lambda}_{a+}$ and ${}^{\rho}I^{\lambda}_{b-}$ of order $\lambda \in \mathbb{C}$ $(\Re(\lambda) > 0)$, are defined as (see [7])

$$\left({}^{\rho}I^{\lambda}_{a+}\phi\right)(s) = \frac{\rho^{1-\lambda}}{\Gamma(\lambda)} \int_a^s \frac{\tau^{\rho-1}\phi(\tau)}{(s^{\rho}-\tau^{\rho})^{1-\lambda}} d\tau \quad (s > a), \tag{1.15}$$

and

$$\left({}^{\rho}I^{\lambda}_{b-}\phi\right)(s) = \frac{\rho^{1-\lambda}}{\Gamma(\lambda)} \int_s^b \frac{\tau^{\rho-1}\phi(\tau)}{(\tau^{\rho}-s^{\rho})^{1-\lambda}} d\tau \quad (b > s). \tag{1.16}$$

It is noted that

(i) when $\rho = 1$, (1.15) and (1.16), respectively, reduce to Riemann-Liouville fractional integrals (1.11) and (1.12);

(ii) taking $\rho \to 0^{+}$, (1.15) and (1.16), respectively, reduce to the famous Hadamard fractional integrals (see [6]; see also [7]):

$$\left(H^{\lambda}_{a+}\phi\right)(s) = \frac{1}{\Gamma(\lambda)} \int_a^s \left(\log\frac{s}{\tau}\right)^{\lambda-1} \frac{\phi(\tau)}{\tau}\, d\tau \quad (s > a,\, \Re(\lambda) > 0), \tag{1.17}$$

and

$$\left(H^{\lambda}_{b-}\phi\right)(s) = \frac{1}{\Gamma(\lambda)} \int_s^b \left(\log\frac{\tau}{s}\right)^{\lambda-1} \frac{\phi(\tau)}{\tau}\, d\tau \quad (s < b,\, \Re(\lambda) > 0). \tag{1.18}$$

The matching Katugampola fractional derivatives on the left and right sides, designated respectively by ${}^{\rho}D^{\lambda}_{a+}$ and ${}^{\rho}D^{\lambda}_{b-}$, are defined as (see [8])

$$\begin{aligned}\left({}^{\rho}D^{\lambda}_{a+}\phi\right)(s) &= \left(s^{1-\rho}\frac{d}{ds}\right)^{\mathsf{n}} \left({}^{\rho}I^{\mathsf{n}-\lambda}_{a+}\phi\right)(s) \\ &= \frac{\rho^{\lambda-\mathsf{n}+1}}{\Gamma(\mathsf{n}-\lambda)} \left(s^{1-\rho}\frac{d}{ds}\right)^{\mathsf{n}} \int_a^s \frac{\tau^{\rho-1}\phi(\tau)}{(s^{\rho}-\tau^{\rho})^{\lambda-\mathsf{n}+1}} d\tau,\end{aligned} \tag{1.19}$$

and

$$\begin{aligned}\left({}^{\rho}D_{b-}^{\lambda}\phi\right)(s) &= \left(-s^{1-\rho}\frac{d}{ds}\right)^{\mathsf{n}}\left({}^{\rho}I_{b-}^{\mathsf{n}-\lambda}\phi\right)(s)\\ &= \frac{\rho^{\lambda-\mathsf{n}+1}}{\Gamma(\mathsf{n}-\lambda)}\left(-s^{1-\rho}\frac{d}{ds}\right)^{\mathsf{n}}\int_{s}^{b}\frac{\tau^{\rho-1}\phi(\tau)}{(\tau^{\rho}-s^{\rho})^{\lambda-\mathsf{n}+1}}d\tau, \end{aligned} \tag{1.20}$$

where $\mathsf{n} = [\Re(\lambda)] + 1$.

The identities in Lemmas 1.1 and 1.2 provide the image formulae for the power function t^{α} when the fractional integral and derivative operators of Katugampola are used. In this case, we make major use of the well-known beta function (see, e.g., [19, p. 8]):

$$B(\alpha,\,\beta) = \begin{cases} \displaystyle\int_0^1 t^{\alpha-1}(1-t)^{\beta-1}\,\mathrm{d}t \quad (\Re(\alpha)>0,\ \Re(\beta)>0) \\ \displaystyle\frac{\Gamma(\alpha)\,\Gamma(\beta)}{\Gamma(\alpha+\beta)} \qquad\qquad\qquad (\alpha,\,\beta\in\mathbb{C}\setminus\mathbb{Z}_{\leq 0})\,. \end{cases} \tag{1.21}$$

Proofs have been omitted.

Lemma 1.1 *Let $\rho > 0$, $\Re(\alpha) > 0$, and $\Re(\lambda) > 0$. Then*

$$\left({}^{\rho}I_{0+}^{\lambda}t^{\alpha}\right)(s) = \rho^{-\lambda}\frac{\Gamma\left(\frac{\alpha}{\rho}+1\right)}{\Gamma\left(\frac{\alpha}{\rho}+1+\lambda\right)}s^{\alpha+\rho\lambda} \tag{1.22}$$

and

$$\left({}^{\rho}I_{0-}^{\lambda}t^{\alpha}\right)(s) = (-\rho)^{-\lambda}\frac{\Gamma\left(\frac{\alpha}{\rho}+1\right)}{\Gamma\left(\frac{\alpha}{\rho}+1+\lambda\right)}s^{\alpha+\rho\lambda}. \tag{1.23}$$

Lemma 1.2 *Let $\rho > 0$, $\Re(\alpha) > 0$, $\Re(\lambda) > 0$, and $n = [\Re(\lambda)] + 1$. Then*

$$\left({}^{\rho}D_{0+}^{\lambda}t^{\alpha}\right)(s) = \rho^{\lambda}\frac{\Gamma\left(\frac{\alpha}{\rho}+1\right)}{\Gamma\left(\frac{\alpha}{\rho}+1-\lambda\right)}s^{\alpha-\rho\lambda} \tag{1.24}$$

and

$$\left({}^{\rho}D_{0-}^{\lambda}t^{\alpha}\right)(s) = (-\rho)^{\lambda}\frac{\Gamma\left(\frac{\alpha}{\rho}+1\right)}{\Gamma\left(\frac{\alpha}{\rho}+1-\lambda\right)}s^{\alpha-\rho\lambda}. \tag{1.25}$$

Numerous image formulae for a diversity of polynomials and functions subjected to a variety of fractional integrals and derivatives have been given (see,

e.g., [1], [2], [3], [4], [9], [18], [22], [23], [24], [25]). The purpose of this article isto establish image formulae for the product of incomplete H-functions and a general class of polynomials under the Katugampola fractional integral and derivative operators. Among many others, we also present some specific examples of our major results.

2 Katugampola fractional integral operators involving incomplete H-functions and general class of polynomials

In this part, we state the following theorems that establish the image formulae for product of the incomplete H-functions and the general class of polynomials under the left- and right-sided Katugampola fractional integral operators.

Theorem 2.1 *Let* $\Re(\lambda) > 0$, $a, b \in \mathbb{R}$, $\rho, \alpha, \beta \in \mathbb{R}^+$, $\mathsf{y} \geq 0$, *and* $s > 0$. *Then*

$$\left({}^{\rho}I_{0+}^{\lambda} S_{\mathsf{n}}^{\mathsf{m}}[at^{\alpha}]\Gamma_{\mathsf{p},\mathsf{q}}^{\mathsf{m},\mathsf{n}}\left[bt^{\beta}\middle|\begin{matrix}(\mathsf{e}_1,\mathsf{E}_1,\mathsf{y}),(\mathsf{e}_j,\mathsf{E}_j)_{2,\mathsf{p}}\\ (\mathsf{f}_j,\mathsf{F}_j)_{1,\mathsf{q}}\end{matrix}\right]\right)(s) = \rho^{-\lambda}s^{\rho\lambda}\sum_{k=0}^{[\frac{\mathsf{n}}{\mathsf{m}}]}\frac{(-\mathsf{n})_{\mathsf{m}k}}{k!}A_{\mathsf{n},k}(as^{\alpha})^k \times \Gamma_{\mathsf{p}+1,\mathsf{q}+1}^{\mathsf{m},\mathsf{n}+1}\left[bs^{\beta}\middle|\begin{matrix}(\mathsf{e}_1,\mathsf{E}_1,\mathsf{y}),(\mathsf{e}_j,\mathsf{E}_j)_{2,\mathsf{p}}(\frac{-\alpha k}{\rho},\frac{\beta}{\rho})\\ (\mathsf{f}_j,\mathsf{F}_j)_{1,\mathsf{q}},(-\lambda-\frac{\alpha k}{\rho},\frac{\beta}{\rho})\end{matrix}\right] \tag{2.1}$$

and

$$\left({}^{\rho}I_{0+}^{\lambda} S_{\mathsf{n}}^{\mathsf{m}}[at^{\alpha}]\gamma_{\mathsf{p},\mathsf{q}}^{\mathsf{m},\mathsf{n}}\left[bt^{\beta}\middle|\begin{matrix}(\mathsf{e}_1,\mathsf{E}_1,\mathsf{y}),(\mathsf{e}_j,\mathsf{E}_j)_{2,\mathsf{q}}\\ (\mathsf{f}_j,\mathsf{F}_j)_{1,w}\end{matrix}\right]\right)(s) = \rho^{-\lambda}s^{\rho\lambda}\sum_{k=0}^{[\frac{\mathsf{n}}{\mathsf{m}}]}\frac{(-\mathsf{n})_{\mathsf{m}k}}{k!}A_{\mathsf{n},k}(as^{\alpha})^k \times \gamma_{\mathsf{p}+1,\mathsf{q}+1}^{\mathsf{m},\mathsf{n}+1}\left[bs^{\beta}\middle|\begin{matrix}(\mathsf{e}_1,\mathsf{E}_1,\mathsf{y}),(\mathsf{e}_j,\mathsf{E}_j)_{2,\mathsf{p}}(\frac{-\alpha k}{\rho},\frac{\beta}{\rho})\\ (\mathsf{f}_j,\mathsf{F}_j)_{1,\mathsf{q}},(-\lambda-\frac{\alpha k}{\rho},\frac{\beta}{\rho})\end{matrix}\right]. \tag{2.2}$$

Proof. Let Δ be the left-handed member of (2.1). Using (1.15), (1.10) and (1.8), and changing the order of integrals, which may be readily verified under the constraints, we have

$$\Delta = \sum_{k=0}^{[\mathsf{n}/\mathsf{m}]}\frac{(-\mathsf{n})_{\mathsf{m}k}}{k!}A_{\mathsf{n},k}\,a^k\int_{\mathfrak{C}}\mathbb{F}(\xi,\mathsf{y})b^{-\xi}\left({}^{\rho}I_{0+}^{\lambda}\left[t^{\alpha k-\beta\xi}\right]\right)(s)\,d\xi. \tag{2.3}$$

Employing (1.22) to evaluate the right-handed Katugampola fractional integral

in (2.3), we obtain

$$\Delta = \rho^{-\lambda} s^{\rho\lambda} \sum_{k=0}^{[\mathsf{n}/\mathsf{m}]} \frac{(-\mathsf{n})_{\mathsf{m}k}}{k!} A_{\mathsf{n},k} (s^{\alpha} a)^k \frac{1}{2\pi i} \int_{\mathfrak{C}} \mathbb{F}(\xi, \mathsf{y}) (bs^{\beta})^{-\xi} \frac{\Gamma\left[1 + \frac{\alpha k}{\rho} - \frac{\beta}{\rho}\xi\right]}{\left[1 + \lambda + \frac{\alpha k}{\rho} - \frac{\beta}{\rho}\xi\right]} d\xi,$$

which, upon expressing the integral in terms of (1.8), yields the desired right-handed member of (2.1).

The proof of (2.2) would run in parallel with that of (2.1). We omit the specific. □

Theorem 2.2 *Let* $\Re(\lambda) > 0$, $a, b \in \mathbb{R}$, $\rho, \alpha, \beta \in \mathbb{R}^+$, $\mathsf{y} \geq 0$, *and* $s < 0$. *Then*

$$\left({}^{\rho} I_{0-}^{\lambda} S_{\mathsf{n}}^{\mathsf{m}} [at^{\alpha}] \Gamma_{\mathsf{p},\mathsf{q}}^{\mathsf{m},\mathsf{n}} \left[bt^{\beta} \middle| \begin{matrix} (\mathsf{e}_1, \mathsf{E}_1, \mathsf{y}), (\mathsf{e}_j, \mathsf{E}_j)_{2,\mathsf{p}} \\ (\mathsf{f}_j, \mathsf{F}_j)_{1,\mathsf{q}} \end{matrix} \right] \right)(s) = (-\rho)^{-\lambda} s^{\rho\lambda} \sum_{k=0}^{[\frac{\mathsf{n}}{\mathsf{m}}]} \frac{(-\mathsf{n})_{\mathsf{m}k}}{k!} A_{\mathsf{n},k} (as^{\alpha})^k$$
$$\times \Gamma_{\mathsf{p}+1,\mathsf{q}+1}^{\mathsf{m},\mathsf{n}+1} \left[b\, s^{\beta} \middle| \begin{matrix} (\mathsf{e}_1, \mathsf{E}_1, \mathsf{y}), (\mathsf{e}_j, \mathsf{E}_j)_{2,\mathsf{p}} (-\frac{\alpha k}{\rho}, \frac{\beta}{\rho}) \\ (\mathsf{f}_j, \mathsf{F}_j)_{1,\mathsf{q}}, (-\lambda - \frac{\alpha k}{\rho}, \frac{\beta}{\rho}) \end{matrix} \right] \tag{2.4}$$

and

$$\left({}^{\rho} I_{0-}^{\lambda} S_{\mathsf{n}}^{m} [at^{\alpha}] \gamma_{\mathsf{p},\mathsf{q}}^{\mathsf{m},\mathsf{n}} \left[bt^{\beta} \middle| \begin{matrix} (\mathsf{e}_1, \mathsf{E}_1, \mathsf{y}), (\mathsf{e}_j, \mathsf{E}_j)_{2,\mathsf{p}} \\ (\mathsf{f}_j, \mathsf{F}_j)_{1,\mathsf{q}} \end{matrix} \right] \right)(s) = (-\rho)^{-\lambda} s^{\rho\lambda} \sum_{k=0}^{[\frac{\mathsf{n}}{\mathsf{m}}]} \frac{(-\mathsf{n})_{\mathsf{m}k}}{k!} A_{\mathsf{n},k} (as^{\alpha})^k$$
$$\times \gamma_{\mathsf{p}+1,\mathsf{q}+1}^{\mathsf{m},\mathsf{n}+1} \left[bs^{\beta} \middle| \begin{matrix} (\mathsf{e}_1, \mathsf{E}_1, \mathsf{y}), (\mathsf{e}_j, \mathsf{E}_j)_{2,\mathsf{p}} (-\frac{\alpha k}{\rho}, \frac{\beta}{\rho}) \\ (\mathsf{f}_j, \mathsf{F}_j)_{1,\mathsf{q}}, (-\lambda - \frac{\alpha k}{\rho}, \frac{\beta}{\rho}) \end{matrix} \right]. \tag{2.5}$$

Proof. The proof would proceed in the same manner as the proof of Theorem 2.1. We omit specifics. □

3 Katugampola fractional derivative operators with incomplete H-functions and general class of polynomials

The following two theorems provide the image formulae for product of the incomplete H-functions and the general class of polynomials under the left- and right-sided Katugampola fractional derivative operators. Since the proofs here would be identical to those used in Theorems 2.1 and 2.2, we omit the required proofs.

Theorem 3.1 *Let* $\Re(\lambda) > 0$, $a, b \in \mathbb{R}$, $\rho, \alpha, \beta \in \mathbb{R}^+$, $\mathsf{y} \geq 0$, *and* $s > 0$. *Then*

$$\left({}^{\rho}\mathcal{D}^{\lambda}_{0+} S^{\mathsf{m}}_{\mathsf{n}}[at^{\alpha}] \Gamma^{\mathsf{m},\mathsf{n}}_{\mathsf{p},\mathsf{q}} \left[bt^{\beta} \middle| \begin{matrix} (\mathsf{e}_1, \mathsf{E}_1, \mathsf{y}), (\mathsf{e}_j, \mathsf{E}_j)_{2,\mathsf{p}} \\ (\mathsf{f}_j, \mathsf{F}_j)_{1,\mathsf{q}} \end{matrix} \right] \right)(s)$$

$$= \rho^{\lambda} s^{\rho\lambda} \sum_{k=0}^{[\mathsf{n}/\mathsf{m}]} \frac{(-\mathsf{n})_{\mathsf{m}k}}{k!} A_{\mathsf{n},k} (as^{\alpha})^k \Gamma^{\mathsf{m},\mathsf{n}+1}_{\mathsf{p}+1,\mathsf{q}+1} \left[bs^{\beta} \middle| \begin{matrix} (\mathsf{e}_1, \mathsf{E}_1, \mathsf{y}), (\mathsf{e}_j, \mathsf{E}_j)_{2,\mathsf{p}}, (-\frac{\alpha k}{\rho}, \frac{\beta}{\rho}) \\ (\mathsf{f}_j, \mathsf{F}_j)_{1,\mathsf{q}}, (\lambda - \frac{\alpha k}{\rho}, \frac{\beta}{\rho}) \end{matrix} \right] \tag{3.1}$$

and

$$\left({}^{\rho}\mathcal{D}^{\lambda}_{0+} S^{\mathsf{m}}_{\mathsf{n}}[at^{\alpha}] \gamma^{\mathsf{m},\mathsf{n}}_{\mathsf{p},\mathsf{q}} \left[bt^{\beta} \middle| \begin{matrix} (\mathsf{e}_1, \mathsf{E}_1, \mathsf{y}), (\mathsf{e}_j, \mathsf{E}_j)_{2,\mathsf{p}} \\ (\mathsf{f}_j, \mathsf{F}_j)_{1,\mathsf{q}} \end{matrix} \right] \right)(s)$$

$$= \rho^{\lambda} s^{\rho\lambda} \sum_{k=0}^{[\mathsf{n}/\mathsf{m}]} \frac{(-\mathsf{n})_{\mathsf{m}k}}{k!} A_{\mathsf{n},k} (as^{\alpha})^k \gamma^{\mathsf{m},\mathsf{n}+1}_{\mathsf{p}+1,\mathsf{q}+1} \left[bs^{\beta} \middle| \begin{matrix} (\mathsf{e}_1, \mathsf{E}_1, \mathsf{y}), (\mathsf{e}_j, \mathsf{E}_j)_{2,\mathsf{p}}, (-\frac{\alpha k}{\rho}, \frac{\beta}{\rho}) \\ (\mathsf{f}_j, \mathsf{F}_j)_{1,\mathsf{q}}, (\lambda - \frac{\alpha k}{\rho}, \frac{\beta}{\rho}) \end{matrix} \right]. \tag{3.2}$$

Theorem 3.2 *Let* $\Re(\lambda) > 0$, $a, b \in \mathbb{R}$, $\rho, \alpha, \beta \in \mathbb{R}^+$, $\mathsf{y} \geq 0$, *and* $s < 0$. *Then*

$$\left({}^{\rho}\mathcal{D}^{\lambda}_{0-} S^{\mathsf{m}}_{\mathsf{n}}[at^{\alpha}] \Gamma^{\mathsf{m},\mathsf{n}}_{\mathsf{p},\mathsf{q}} \left[bt^{\beta} \middle| \begin{matrix} (\mathsf{e}_1, \mathsf{E}_1, \mathsf{y}), (\mathsf{e}_j, \mathsf{E}_j)_{2,\mathsf{p}} \\ (\mathsf{f}_j, \mathsf{F}_j)_{1,\mathsf{q}} \end{matrix} \right] \right)(s)$$

$$= (-\rho)^{\lambda} s^{\rho\lambda} \sum_{k=0}^{[\mathsf{n}/\mathsf{m}]} \frac{(-\mathsf{n})_{\mathsf{m}k}}{k!} A_{\mathsf{n},k} (as^{\alpha})^k \Gamma^{\mathsf{m},\mathsf{n}+1}_{\mathsf{p}+1,\mathsf{q}+1} \left[bs^{\beta} \middle| \begin{matrix} (\mathsf{e}_1, \mathsf{E}_1, \mathsf{y}), (\mathsf{e}_j, \mathsf{E}_j)_{2,\mathsf{p}}, (-\frac{\alpha k}{\rho}, \frac{\beta}{\rho}) \\ (\mathsf{f}_j, \mathsf{F}_j)_{1,\mathsf{q}}, (\lambda - \frac{\alpha k}{\rho}, \frac{\beta}{\rho}) \end{matrix} \right] \tag{3.3}$$

and

$$\left({}^{\rho}\mathcal{D}^{\lambda}_{0-} S^{\mathsf{m}}_{\mathsf{n}}[at^{\alpha}] \gamma^{\mathsf{m},\mathsf{n}}_{\mathsf{p},\mathsf{q}} \left[bt^{\beta} \middle| \begin{matrix} (\mathsf{e}_1, \mathsf{E}_1, \mathsf{y}), (\mathsf{e}_j, \mathsf{E}_j)_{2,\mathsf{p}} \\ (\mathsf{f}_j, \mathsf{F}_j)_{1,\mathsf{q}} \end{matrix} \right] \right)(s)$$

$$= (-\rho)^{\lambda} s^{\rho\lambda} \sum_{k=0}^{[\mathsf{n}/\mathsf{m}]} \frac{(-\mathsf{n})_{\mathsf{m}k}}{k!} A_{\mathsf{n},k} (as^{\alpha})^k \gamma^{\mathsf{m},\mathsf{n}+1}_{\mathsf{p}+1,\mathsf{q}+1} \left[bs^{\beta} \middle| \begin{matrix} (\mathsf{e}_1, \mathsf{E}_1, \mathsf{y}), (\mathsf{e}_j, \mathsf{E}_j)_{2,\mathsf{p}}, (-\frac{\alpha k}{\rho}, \frac{\beta}{\rho}) \\ (\mathsf{f}_j, \mathsf{F}_j)_{1,\mathsf{q}}, (\lambda - \frac{\alpha k}{\rho}, \frac{\beta}{\rho}) \end{matrix} \right]. \tag{3.4}$$

4 Particular cases and remarks

Due to the generality of both incomplete H-functions and the general class polynomials, the main identities established in the preceding sections may result

in a variety of simpler formulae as special instances. For example, the case $\mathsf{y}=0$ of (1.8) reduces to the Fox's H-function (see, e.g., [20, p. 10]; see also [11], [16]):

$$\Gamma_{\mathsf{p},\mathsf{q}}^{\mathsf{m},\mathsf{n}}\left[\begin{array}{c|c} z & \begin{array}{c}(\mathsf{e}_1,\mathsf{E}_1),(\mathsf{e}_i,\mathsf{E}_i)_{2,\mathsf{p}}\\ \\ (\mathsf{f}_i,\mathsf{F}_i)_{1,\mathsf{q}}\end{array}\end{array}\right]=H_{\mathsf{p},\mathsf{q}}^{\mathsf{m},\mathsf{n}}\left[\begin{array}{c|c} z & \begin{array}{c}(\mathsf{e}_1,\mathsf{E}_1),(\mathsf{e}_i,\mathsf{E}_i)_{2,\mathsf{p}}\\ \\ (\mathsf{f}_i,\mathsf{F}_i)_{1,\mathsf{q}}\end{array}\end{array}\right]$$
$$=H_{\mathsf{p},\mathsf{q}}^{\mathsf{m},\mathsf{n}}\left[\begin{array}{c|c} z & \begin{array}{c}(\mathsf{e}_1,\mathsf{E}_1),(\mathsf{e}_2,\mathsf{E}_2),\cdots,(\mathsf{e}_\mathsf{p},\mathsf{E}_\mathsf{p})\\ \\ (\mathsf{f}_1,\mathsf{F}_1),(\mathsf{f}_2,\mathsf{F}_2),\cdots,(\mathsf{f}_\mathsf{q},\mathsf{F}_\mathsf{q})\end{array}\end{array}\right]. \tag{4.1}$$

For another example, putting $\mathsf{m}=1$, $\mathsf{n}=\mathsf{p}$, q being replaced by $\mathsf{q}+1$ and taking appropriate parameters, the functions (1.6) and (1.8) reduce, respectively, to the incomplete Fox-Wright Ψ-functions ${}_{\mathsf{p}}\Psi_{\mathsf{q}}^{(\gamma)}$ and ${}_{\mathsf{p}}\Psi_{\mathsf{q}}^{(\Gamma)}$ (see [21, Eqs. (6.3) and (6.4)]; see also [2, Eqs. (14) and (15)]):

$$\gamma_{\mathsf{p},\mathsf{q}+1}^{1,\mathsf{p}}\left[\begin{array}{c|c} -z & \begin{array}{c}(1-\mathsf{e}_1,\mathsf{E}_1,\mathsf{y}),(1-\mathsf{e}_j,\mathsf{E}_j)_{2,\mathsf{p}}\\ \\ (0,1),(1-\mathsf{b}_j,\mathsf{B}_j)_{1,\mathsf{q}}\end{array}\end{array}\right]={}_{\mathsf{p}}\Psi_{\mathsf{q}}^{(\gamma)}\left[\begin{array}{c}(\mathsf{e}_1,\mathsf{E}_1,\mathsf{y}),(\mathsf{e}_j,\mathsf{E}_j)_{2,\mathsf{p}};\\ z\\ (\mathsf{b}_j,\mathsf{B}_j)_{1,\mathsf{q}};\end{array}\right] \tag{4.2}$$

and

$$\Gamma_{\mathsf{p},\mathsf{q}+1}^{1,\mathsf{p}}\left[\begin{array}{c|c} -z & \begin{array}{c}(1-\mathsf{e}_1,\mathsf{E}_1,\mathsf{y}),(1-\mathsf{e}_j,\mathsf{E}_j)_{2,\mathsf{p}}\\ \\ (0,1),(1-\mathsf{b}_j,\mathsf{B}_j)_{1,\mathsf{q}}\end{array}\end{array}\right]={}_{\mathsf{p}}\Psi_{\mathsf{q}}^{(\Gamma)}\left[\begin{array}{c}(\mathsf{e}_1,\mathsf{E}_1,\mathsf{y}),(\mathsf{e}_j,\mathsf{E}_j)_{2,\mathsf{p}};\\ z\\ (\mathsf{b}_j,\mathsf{B}_j)_{1,\mathsf{q}};\end{array}\right]. \tag{4.3}$$

The following corollaries cover some of them.

Corollary 4.1 *Let $\Re(\lambda)>0$, a, $b\in\mathbb{R}$, and ρ, α, $\beta\in\mathbb{R}^+$. Then*

$$\left({}^{\rho}I_{0+}^{\lambda}S_{\mathsf{n}}^{\mathsf{m}}[at^{\alpha}]H_{\mathsf{p},\mathsf{q}}^{\mathsf{m},\mathsf{n}}\left[bt^{\beta}\left|\begin{array}{c}(\mathsf{e}_j,\mathsf{E}_j)_{1,\mathsf{p}}\\ \\ (\mathsf{f}_j,\mathsf{F}_j)_{1,\mathsf{q}}\end{array}\right.\right]\right)(s)=\rho^{-\lambda}s^{\rho\lambda}\sum_{k=0}^{[\mathsf{n}/\mathsf{m}]}\frac{(-\mathsf{n})_{\mathsf{m}k}}{k!}A_{\mathsf{n},k}(as^{\alpha})^k$$
$$\times H_{\mathsf{p}+1,\mathsf{q}+1}^{\mathsf{m},\mathsf{n}+1}\left[bs^{\beta}\left|\begin{array}{c}(\mathsf{e}_j,\mathsf{E}_j)_{1,\mathsf{p}}(-\frac{\alpha k}{\rho},\frac{\beta}{\rho})\\ \\ (\mathsf{f}_j,\mathsf{F}_j)_{1,\mathsf{q}},(-\lambda-\frac{\alpha k}{\rho},\frac{\beta}{\rho})\end{array}\right.\right] \tag{4.4}$$
$$(s>0)$$

and

$$\left({}^{\rho}I_{0-}^{\lambda}S_{\mathsf{n}}^{\mathsf{m}}[at^{\alpha}]H_{\mathsf{p},\mathsf{q}}^{\mathsf{m},\mathsf{n}}\left[bt^{\beta}\left|\begin{array}{c}(\mathsf{e}_j,\mathsf{E}_j)_{1,\mathsf{p}}\\ \\ (\mathsf{f}_j,\mathsf{F}_j)_{1,\mathsf{q}}\end{array}\right.\right]\right)(s)=(-\rho)^{-\lambda}s^{\rho\lambda}\sum_{k=0}^{[\mathsf{n}/\mathsf{m}]}\frac{(-\mathsf{n})_{\mathsf{m}k}}{k!}A_{\mathsf{n},k}(as^{\alpha})^k$$
$$\times H_{\mathsf{p}+1,\mathsf{q}+1}^{\mathsf{m},\mathsf{n}+1}\left[bs^{\beta}\left|\begin{array}{c}(\mathsf{e}_j,\mathsf{E}_j)_{1,\mathsf{p}}(\frac{-\alpha k}{\rho},\frac{\beta}{\rho})\\ \\ (\mathsf{f}_j,\mathsf{F}_j)_{1,\mathsf{q}},(-\lambda-\frac{\alpha k}{\rho},\frac{\beta}{\rho})\end{array}\right.\right] \tag{4.5}$$

$$(s<0).$$

Proof. Taking $\mathsf{y}=0$ in (2.1) and (2.4), we get the required results. □

Corollary 4.2 *Let* $\Re(\lambda)>0$, a, $b\in\mathbb{R}$, *and* ρ, α, $\beta\in\mathbb{R}^+$. *Then*

$$\left({}^{\rho}\mathcal{D}^{\lambda}_{0+}S^{\mathsf{m}}_{\mathsf{n}}[at^{\alpha}]H^{\mathsf{m},\mathsf{n}}_{\mathsf{p},\mathsf{q}}\left[bt^{\beta}\middle|\begin{matrix}(\mathsf{e}_j,\mathsf{E}_j)_{1,\mathsf{p}}\\(\mathsf{f}_j,\mathsf{F}_j)_{1,\mathsf{q}}\end{matrix}\right]\right)(s)=\rho^{\lambda}s^{\rho\lambda}\sum_{k=0}^{[\frac{\mathsf{n}}{\mathsf{m}}]}\frac{(-\mathsf{n})_{\mathsf{m}k}}{k!}A_{\mathsf{n},k}(as^{\alpha})^k$$
$$\times H^{\mathsf{m},\mathsf{n}+1}_{\mathsf{p}+1,\mathsf{q}+1}\left[bs^{\beta}\middle|\begin{matrix}(\mathsf{e}_j,\mathsf{E}_j)_{1,\mathsf{p}},(-\frac{\alpha k}{\rho},\frac{\beta}{\rho})\\(\mathsf{f}_j,\mathsf{F}_j)_{1,\mathsf{q}},(\lambda-\frac{\alpha k}{\rho},\frac{\beta}{\rho})\end{matrix}\right] \tag{4.6}$$

$$(s>0)$$

and

$$\left({}^{\rho}\mathcal{D}^{\lambda}_{0-}S^{\mathsf{m}}_{\mathsf{n}}[at^{\alpha}]H^{\mathsf{m},\mathsf{n}}_{\mathsf{p},\mathsf{q}}\left[bt^{\beta}\middle|\begin{matrix}(\mathsf{e}_j,\mathsf{E}_j)_{1,\mathsf{p}}\\(\mathsf{f}_j,\mathsf{F}_j)_{1,\mathsf{q}}\end{matrix}\right]\right)(s)=\rho^{\lambda}s^{\rho\lambda}\sum_{k=0}^{[\mathsf{n}/\mathsf{m}]}\frac{(-\mathsf{n})_{\mathsf{m}k}}{k!}A_{\mathsf{n},k}(as^{\alpha})^k$$
$$\times H^{\mathsf{m},\mathsf{n}+1}_{\mathsf{p}+1,\mathsf{q}+1}\left[bs^{\beta}\middle|\begin{matrix}(\mathsf{e}_j,\mathsf{E}_j)_{1,\mathsf{p}},(-\frac{\alpha k}{\rho},\frac{\beta}{\rho})\\(\mathsf{f}_j,\mathsf{F}_j)_{1,\mathsf{q}},(\lambda-\frac{\alpha k}{\rho},\frac{\beta}{\rho})\end{matrix}\right] \tag{4.7}$$

$$(s<0).$$

Proof. Taking $\mathsf{y}=0$ in (3.1) and (3.3), we get the required results. □

Corollary 4.3 *Let* $\Re(\lambda)>0$, a, $b\in\mathbb{R}$, ρ, α, $\beta\in\mathbb{R}^+$, $\mathsf{y}\geq 0$, *and* $s>0$. *Then*

$$\left({}^{\rho}I^{\lambda}_{0+}S^{\mathsf{m}}_{\mathsf{n}}[at^{\alpha}]_{\mathsf{p}}\Psi^{(\Gamma)}_{\mathsf{q}}\left[bt^{\beta}\middle|\begin{matrix}(\mathsf{e}_1,\mathsf{E}_1,\mathsf{y}),(\mathsf{e}_j,\mathsf{E}_j)_{2,\mathsf{p}}\\(\mathsf{f}_j,\mathsf{F}_j)_{1,\mathsf{q}}\end{matrix}\right]\right)(s)=\rho^{-\lambda}s^{\rho\lambda}\sum_{k=0}^{[\mathsf{n}/\mathsf{m}]}\frac{(-\mathsf{n})_{\mathsf{m}k}}{k!}A_{\mathsf{n},k}(as^{\alpha})^k$$
$$\times {}_{\mathsf{p}+1}\Psi^{(\Gamma)}_{\mathsf{q}+1}\left[bs^{\beta}\middle|\begin{matrix}(\mathsf{e}_1,\mathsf{E}_1,\mathsf{y}),(\mathsf{e}_j,\mathsf{E}_j)_{2,\mathsf{p}}(1+\frac{\alpha k}{\rho},\frac{\beta}{\rho})\\(\mathsf{f}_j,\mathsf{F}_j)_{1,\mathsf{q}},(1+\lambda+\frac{\alpha k}{\rho},\frac{\beta}{\rho})\end{matrix}\right] \tag{4.8}$$

and

$$\left({}^{\rho}I^{\lambda}_{0+}S^{\mathsf{m}}_{\mathsf{n}}[at^{\alpha}]_{\mathsf{p}}\Psi^{(\gamma)}_{\mathsf{q}}\left[bt^{\beta}\middle|\begin{matrix}(\mathsf{e}_1,\mathsf{E}_1,\mathsf{y}),(\mathsf{e}_j,\mathsf{E}_j)_{2,\mathsf{p}}\\(\mathsf{f}_j,\mathsf{F}_j)_{1,\mathsf{q}}\end{matrix}\right]\right)(s)=\rho^{-\lambda}s^{\rho\lambda}\sum_{k=0}^{[\mathsf{n}/\mathsf{m}]}\frac{(-\mathsf{n})_{\mathsf{m}k}}{k!}A_{\mathsf{n},k}(as^{\alpha})^k$$
$$\times {}_{\mathsf{p}+1}\Psi^{(\gamma)}_{\mathsf{q}+1}\left[bs^{\beta}\middle|\begin{matrix}(\mathsf{e}_1,\mathsf{E}_1,\mathsf{y}),(\mathsf{e}_j,\mathsf{E}_j)_{2,\mathsf{p}}(1+\frac{\alpha k}{\rho},\frac{\beta}{\rho})\\(\mathsf{f}_j,\mathsf{F}_j)_{1,\mathsf{q}},(1+\lambda+\frac{\alpha k}{\rho},\frac{\beta}{\rho})\end{matrix}\right]. \tag{4.9}$$

Proof. Using (4.2) and (4.3) in (2.1) and (2.2) gives the required identities. □

Corollary 4.4 *Let* $\Re(\lambda) > 0$, a, $b \in \mathbb{R}$, ρ, α, $\beta \in \mathbb{R}^+$, $\mathsf{y} \geq 0$, *and* $s < 0$. *Then*

$$\left({}^{\rho}I_{0-}^{\lambda} S_{\mathsf{n}}^{\mathsf{m}}[at^{\alpha}]_{\mathsf{p}} \Psi_{\mathsf{q}}^{(\Gamma)} \left[bt^{\beta} \middle| \begin{matrix} (\mathsf{e}_1, \mathsf{E}_1, \mathsf{y}), (\mathsf{e}_j, \mathsf{E}_j)_{2,\mathsf{p}} \\ (\mathsf{f}_j, \mathsf{F}_j)_{1,\mathsf{q}} \end{matrix} \right] \right)(s)$$

$$= (-\rho)^{-\lambda} s^{\rho\lambda} \sum_{k=0}^{[\mathsf{n}/\mathsf{m}]} \frac{(-\mathsf{n})_{\mathsf{m}k}}{k!} A_{\mathsf{n},k} (as^{\alpha})^k {}_{\mathsf{p}+1}\Psi_{\mathsf{q}+1}^{(\Gamma)} \left[bs^{\beta} \middle| \begin{matrix} (\mathsf{e}_1, \mathsf{E}_1, \mathsf{y}), (\mathsf{e}_j, \mathsf{E}_j)_{2,\mathsf{p}} (1 + \frac{\alpha k}{\rho}, \frac{\beta}{\rho}) \\ (\mathsf{f}_j, \mathsf{F}_j)_{1,\mathsf{q}}, (1 + \lambda + \frac{\alpha k}{\rho}, \frac{\beta}{\rho}) \end{matrix} \right] \tag{4.10}$$

and

$$\left({}^{\rho}I_{0-}^{\lambda} S_{\mathsf{n}}^{\mathsf{m}}[at^{\alpha}]_{\mathsf{p}} \Psi_{\mathsf{q}}^{(\gamma)} \left[bt^{\beta} \middle| \begin{matrix} (\mathsf{e}_1, \mathsf{E}_1, \mathsf{y}), (\mathsf{e}_j, \mathsf{E}_j)_{2,\mathsf{p}} \\ (\mathsf{f}_j, \mathsf{F}_j)_{1,\mathsf{q}} \end{matrix} \right] \right)(s)$$

$$= (-\rho)^{-\lambda} s^{\rho\lambda} \sum_{k=0}^{[\frac{\mathsf{n}}{\mathsf{m}}]} \frac{(-\mathsf{n})_{\mathsf{m}k}}{k!} A_{\mathsf{n},k} (as^{\alpha})^k {}_{\mathsf{p}+1}\Psi_{\mathsf{q}+1}^{(\gamma)} \left[bs^{\beta} \middle| \begin{matrix} (\mathsf{e}_1, \mathsf{E}_1, \mathsf{y}), (\mathsf{e}_j, \mathsf{E}_j)_{2,\mathsf{p}} (1 + \frac{\alpha k}{\rho}, \frac{\beta}{\rho}) \\ (\mathsf{f}_j, \mathsf{F}_j)_{1,\mathsf{q}}, (1 + \lambda + \frac{\alpha k}{\rho}, \frac{\beta}{\rho}) \end{matrix} \right] \tag{4.11}$$

Proof. Employing (4.2) and (4.3) in (2.4) and (2.5) provides the desired identities. □

Corollary 4.5 *Let* $\Re(\lambda) > 0$, a, $b \in \mathbb{R}$, ρ, α, $\beta \in \mathbb{R}^+$, $\mathsf{y} \geq 0$, *and* $s > 0$. *Then*

$$\left({}^{\rho}\mathcal{D}_{0+}^{\lambda} S_{\mathsf{n}}^{\mathsf{m}}[at^{\alpha}]_{\mathsf{p}} \Psi_{\mathsf{q}}^{(\Gamma)} \left[bt^{\beta} \middle| \begin{matrix} (\mathsf{e}_1, \mathsf{E}_1, \mathsf{y}), (\mathsf{e}_j, \mathsf{E}_j)_{2,\mathsf{p}} \\ (\mathsf{f}_j, \mathsf{F}_j)_{1,\mathsf{q}} \end{matrix} \right] \right)(s)$$

$$= \rho^{\lambda} s^{\rho\lambda} \sum_{k=0}^{[\mathsf{n}/\mathsf{m}]} \frac{(-\mathsf{n})_{\mathsf{m}k}}{k!} A_{\mathsf{n},k} (as^{\alpha})^k {}_{\mathsf{p}+1}\Psi_{\mathsf{q}+1}^{(\Gamma)} \left[bs^{\beta} \middle| \begin{matrix} (\mathsf{e}_1, \mathsf{E}_1, \mathsf{y}), (\mathsf{e}_j, \mathsf{E}_j)_{2,\mathsf{p}}, (1 + \frac{\alpha k}{\rho}, \frac{\beta}{\rho}) \\ (\mathsf{f}_j, \mathsf{F}_j)_{1,\mathsf{q}}, (1 - \lambda + \frac{\alpha k}{\rho}, \frac{\beta}{\rho}) \end{matrix} \right] \tag{4.12}$$

and

$$\left({}^{\rho}\mathcal{D}_{0+}^{\lambda} S_{\mathsf{n}}^{\mathsf{m}}[at^{\alpha}]_{\mathsf{p}} \Psi_{\mathsf{q}}^{(\gamma)} \left[bt^{\beta} \middle| \begin{matrix} (\mathsf{e}_1, \mathsf{E}_1, \mathsf{y}), (\mathsf{e}_j, \mathsf{E}_j)_{2,\mathsf{p}} \\ (\mathsf{f}_j, \mathsf{F}_j)_{1,\mathsf{q}} \end{matrix} \right] \right)(s)$$

$$= \rho^{\lambda} s^{\rho\lambda} \sum_{k=0}^{[\frac{\mathsf{n}}{\mathsf{m}}]} \frac{(-\mathsf{n})_{\mathsf{m}k}}{k!} A_{\mathsf{n},k} (as^{\alpha})^k {}_{\mathsf{p}+1}\Psi_{\mathsf{q}+1}^{(\Gamma)} \left[bs^{\beta} \middle| \begin{matrix} (\mathsf{e}_1, \mathsf{E}_1, \mathsf{y}), (\mathsf{e}_j, \mathsf{E}_j)_{2,\mathsf{p}}, (1 + \frac{\alpha k}{\rho}, \frac{\beta}{\rho}) \\ (\mathsf{f}_j, \mathsf{F}_j)_{1,\mathsf{q}}, (1 - \lambda + \frac{\alpha k}{\rho}, \frac{\beta}{\rho}) \end{matrix} \right]. \tag{4.13}$$

Proof. Applying (4.2) and (4.3) to (3.1) and (3.2) offers the desired results. □

Corollary 4.6 *Let* $\Re(\lambda) > 0$, $\delta \in \mathbb{C} \setminus \mathbb{Z}_{\leq -1}$, $a, b \in \mathbb{R}$, $\rho, \alpha, \beta \in \mathbb{R}^+$, $\mathsf{y} \geq 0$, *and* $s > 0$. *Then*

$$\left({}^{\rho}I_{0+}^{\lambda} L_{\mathsf{n}}^{(\delta)}(at^{\alpha}) \Gamma_{\mathsf{p},\mathsf{q}}^{1,\mathsf{n}} \left[bt^{\beta} \middle| \begin{matrix} (\mathsf{e}_1, \mathsf{E}_1, \mathsf{y}), (\mathsf{e}_j, \mathsf{E}_j)_{2,\mathsf{p}} \\ (\mathsf{f}_j, \mathsf{F}_j)_{1,\mathsf{q}} \end{matrix} \right] \right)(s) = \rho^{-\lambda} s^{\rho\lambda} \sum_{k=0}^{[\mathsf{n}]} \frac{(-\mathsf{n})_k}{k!\,\mathsf{n}!} \frac{(1+\delta)_{\mathsf{n}}}{(1+\delta)_k} (as^{\alpha})^k \times \Gamma_{\mathsf{p}+1,\mathsf{q}+1}^{1,\mathsf{n}+1} \left[bs^{\beta} \middle| \begin{matrix} (\mathsf{e}_1, \mathsf{E}_1, \mathsf{y}), (\mathsf{e}_j, \mathsf{E}_j)_{2,\mathsf{p}} (-\frac{\alpha k}{\rho}, \frac{\beta}{\rho}) \\ (\mathsf{f}_j, \mathsf{F}_j)_{1,\mathsf{q}}, (-\lambda - \frac{\alpha k}{\rho}, \frac{\beta}{\rho}) \end{matrix} \right] \tag{4.14}$$

and

$$\left({}^{\rho}I_{0+}^{\lambda} L_{\mathsf{n}}^{(\delta)}(at^{\alpha}) \gamma_{\mathsf{p},\mathsf{q}}^{1,\mathsf{n}} \left[bt^{\beta} \middle| \begin{matrix} (\mathsf{e}_1, \mathsf{E}_1, \mathsf{y}), (\mathsf{e}_j, \mathsf{E}_j)_{2,\mathsf{q}} \\ (\mathsf{f}_j, \mathsf{F}_j)_{1,w} \end{matrix} \right] \right)(s) = \rho^{-\lambda} s^{\rho\lambda} \sum_{k=0}^{[\mathsf{n}]} \frac{(-\mathsf{n})_k}{k!\,\mathsf{n}!} \frac{(1+\delta)_{\mathsf{n}}}{(1+\delta)_k} (as^{\alpha})^k \times \gamma_{\mathsf{p}+1,\mathsf{q}+1}^{1,\mathsf{n}+1} \left[bs^{\beta} \middle| \begin{matrix} (\mathsf{e}_1, \mathsf{E}_1, \mathsf{y}), (\mathsf{e}_j, \mathsf{E}_j)_{2,\mathsf{p}} (-\frac{\alpha k}{\rho}, \frac{\beta}{\rho}) \\ (\mathsf{f}_j, \mathsf{F}_j)_{1,\mathsf{q}}, (-\lambda - \frac{\alpha k}{\rho}, \frac{\beta}{\rho}) \end{matrix} \right], \tag{4.15}$$

where $L_{\mathsf{n}}^{(\delta)}(x)$ *are Laguerre polynomials.*

Proof. Setting $\mathsf{m} = 1$ and choosing $A_{\mathsf{n},k} = (1+\delta)_{\mathsf{n}} / \{(1+\delta)_k\, \mathsf{n}!\}$ in the results in Theorem 2.1, with the aid of Laguerre polynomials $L_{\mathsf{n}}^{(\delta)}(x)$ (see, e.g., [15, p. 201, Eq. (3)]), we obtain the desired identities here. □

Likewise, as with Corollary 4.6, substituting $\mathsf{m} = 1$ and selecting $A_{\mathsf{n},k} = (1+\delta)_{\mathsf{n}} / \{(1+\delta)_k\, \mathsf{n}!\}$ in the identities in Theorems 2.2–3.2 and Corollaries 4.1–4.5 results in the corresponding formulae involving the Laguerre polynomials.

References

[1] P. Agarwal and J. Choi, Fractional calculus operators and their image formulas, *J. Korean Math. Soc.* **53**(5) (2016), 1183-1210 `http://dx.doi.org/10.4134/JKMS.j150458`

[2] M. K. Bansal and J. Choi, A note on pathway fractional integral formulas associated with the incomplete H-functions, *Int. J. Appl. Comput. Math.* **5**(5) (2019), Article ID 133. `https://doi.org/10.1007/s40819-019-0718-8`

[3] M. K. Bansal, D. Kumar and R. Jain, A study of Marichev-Saigo-Maeda fractional integral operators associated with S-generalized Gauss hypergeometric function, *KYUNGPOOK Math. J.* **59**(3) (2019), 433–443. `https://doi.org/10.5666/KMJ.2019.59.3.433`

[4] M. K. Bansal, D. Kumar, K. S. Nisar and J. Singh, Certain fractional calculus and integral transform results of incomplete $\aleph$-functions with applications, *Math. Meth. Appl. Sci.* **43**(8)(2020), 5602–5614. https://doi.org/10.1002/mma.6299

[5] M. K. Bansal, D. Kumar, J. Singh and K. S. Nisar, On the solutions of a class of integral equations pertaining to incomplete H-function and incomplete $\overline{H}$-function, *Mathematics* **8**(5) (2020), Article ID 819. https://doi.org/10.3390/math8050819

[6] J. Hadamard, Essai sur l'etude des fonctions donnees par leur developpment de Taylor, *J. Pure Appl. Math.* **4**(8) (1892), 101–186.

[7] U. N. Katugampola, New approach to a generalized fractional integral, *Appl. Math. Comput.* **218**(3) (2011), 860–865. https://doi.org/10.1016/j.amc.2011.03.062

[8] U. N. Katugampola, New approach to generalized fractional derivatives, *Bull. Math. Anal. Appl.* **6**(4) (2014), 1–15.

[9] O. Khan, N. Khan, K. S. Nisar, M. Saif and D. Baleanu, Fractional calculus of a product of multivariable Srivastava polynomial and multi-index Bessel function in the kernel F_3, *AIMS Math.* **5**(2) (2020), 1462–1475. DOI:10.3934/math.2020100

[10] A. A. Kilbas, H. M. Srivastava, and J. J. Trujillo, *Theory and Applications of Fractional Differential Equations*, North-Holland Mathematical Studies, Vol. **204**, Elsevier (North-Holland) Science Publishers, Amsterdam, London and New York, 2006.

[11] D. Kumar and J. Singh, Application of generalized M-series and $\overline{H}$-function in electric circuit theory, *MESA* **7**(3) (2016), 503–512.

[12] K. S. Miller and B. Ross, *An Introduction to the Fractional Calculus and Fractional Differential Equations*, John Wiley & Sons, INC, New York, 1993.

[13] K. Oldham and J. Spanier, *Fractional Calculus: Theory and Applications of Differentiation and Integration of Arbitrary Order*, Academic Press, New York, 1974.

[14] I. Podlubny, *Fractional Differential Equations*, Academic Press, California, USA, 1999.

[15] E. D. Rainville, *Special Functions*, Macmillan Company, New York, 1960; Reprinted by Chelsea Publishing Company, Bronx, New York, 1971.

[16] J. Singh and D. Kumar, On the distribution of mixed sum of independent random variables one of them associated with Srivastava's polynomials and $\overline{H}$-function, *J. Appl. Math. Stat. Inform.* **10**(1) (2014), 53–62. https://doi.org/10.2478/jamsi-2014-0005

[17] H. M. Srivastava, A contour integral involving Fox's H-function, *Indian J. Math.* **14** (1972), l–6.

[18] H. M. Srivastava, M. K. Bansal and P. Harjule, A study of fractional integral operators involving a certain generalized multi-index Mittag-Leffler function, *Math. Meth. Appl. Sci.* **41**(16) (2018), 6108–6121. https://doi.org/10.1002/mma.5122

[19] H. M. Srivastava and J. Choi, *Zeta and q-Zeta Functions and Associated Series and Integrals*, Elsevier Science Publishers, Amsterdam, London and New York, 2012.

[20] H. M. Srivastava, K. C. Gupta and S. P. Goyal, *The H-Functions of One and Two Variables with Applications*, South Asian Publishers, New Delhi and Madras, 1982.

[21] H. M. Srivastava, R. K. Saxena and R. K. Parmar, Some families of the incomplete H-functions and the incomplete $\bar{H}$-functions and associated integral transforms and operators of fractional calculus with applications, *Russian J. Math. Phys.* **25**(1) (2018), 116–138. DOI10.1134/S1061920818010119

[22] H. M. Srivastava and Ž. Tomovski, Fractional calculus with an integral operator containing a generalized Mittag-Leffler function in the kernel, *Appl. Math. Comput.* **211**(1) (2009), 198–210. doi:10.1016/j.amc.2009.01.055

[23] K. Jangid, S.D. Purohit, K.S. Nisar and S. Araci, Generating functions involving the incomplete H-functions, *Analysis* **41(4)** (2021), 239–244. https://doi.org/10.1515/anly-2021-0038

[24] A. Bhargava, R.K. Jain and J. Singh, Certain New Results Involving Multivariable Aleph(ℵ) -Function, Srivastava Polynomials, Hypergeometric Functions and $\bar{H}$Function, *Int. J. Appl. Comput. Math* **7** (2021), 196. doi.org/10.1007/s40819-021-01071-w

[25] D.L. Suthar, A.M. Khan, A. Alaria, S.D. Purohit and J. Singh, Extended Bessel-Maitland function and its properties pertaining to integral transforms and fractional calculus, *AIMS Mathematics*, **5(2)** (2020), 1400–1410. doi:10.3934/math.2020096

New Fixed Points Outcomes for Fractal Creation by Applying Different Fixed Point Technique

Narayan partap[1], Sarika Jain and Renu Chugh

December 25, 2021

Abstract

Fractal like Julia set is regarded as one of the striking and significant mathematical fractals in the field of science and technology. There are different numerical iterative techniques which generate these fractals and in fact these numerical iterative techniques are the strength of fractal geometry. In recent past, Julia sets have been studied through numerical techniques like Picard, Mann, and Ishikawa etc. which are the examples of one-step, two-step, and three-step iterative techniques respectively. In this article, we have concentrated our research work on the computation as well as the different features of cubic Julia sets for the complex polynomial $P_{m,n}(z) = z^3 + mz + n$. This generation process has been carried-over through a new numerical four-step iterative technique. We have generated new and ever seen cubic Julia sets for the above complex polynomial. The cubic Julia sets generated through above polynomial have important mathematical properties. It is also fascinating that some of the generated cubic Julia sets are analogous to fractal shaped antennas, butterfly and some categories of ants. Some of the generated cubic Julia sets can also be categorized as wall-decorated pictures.

Key words: Cubic Julia sets; Four-Step Iterative Technique; Escape Criterion; Complex Cubic Equation

Mathematics Subject Classification(2010): 37C25; 28A80; 54E35; 54E50

1

1 Introduction

Fractals have many applications in various fields of science and technology. The production of cell phone has become possible only due to fractal shaped antennas. This was not possible before the introduction of this notion. The Chaos theory is what fractals are all about, and that is at the core of most Cosmological Models which describe our entire Universe on both the scales of very small and large. Fractal geometry is very practical for all sorts of things from biology to physics to cosmology to even the stock market. For instance veins and arteries form fractal trees, some mineral deposits are distributed under the fractal laws through the soil, and the stock market, perhaps not quite a natural phenomenon, behaves according to fractal laws.

If we look back into the history of fractal geometry, we find that the interest in fractal geometry with respect to Julia sets began in the 19th century. Named after

[1]Corresponding author: Haryana Education Department, Haryana, India

the esteemed French mathematician Gaston Julia, the Julia set expresses a complex and rich set of dynamics, giving rise to a large range of breathtaking visuals. Gaston was first who invented Julia sets and examined their features [27] $(p-122)$. In 1918, a masterpiece of him on Julia sets was published which was the major event in the history of fractal geometry. In this masterpiece, Gaston Julia first proposed the latest idea on a Julia set and that made him famous in the world of mathematics. Julia sets live in complex plane and this is the place where all chaotic behavior of complex plane occurs [9] $(p-221)$. When all the computational experiments were far ahead of its time, Herald Cramer gave the first approximate graphical representation to Julia sets. Mathematical items like Julia sets were recognized when computer graphics became user friendly [28].

What makes Julia sets interesting to analysis is that, despite being borne out of apparently easy iterative techniques, they can be very tangled and often fractal in nature. Due to fascination of computer experiments and incredulity of their graphical representation, Mandelbrot and Julia asets remain a topic of modern research with much interest being in evoking the tangled structure of Julia sets and in calculating their properties such as 'fractal dimension' [14]. For detailed investigation on Mandelbrot and Julia sets, one can follow the related work and complex dynamics system in references like [4, 5, 6, 8, 9, 12, 16, 18, 25, 26, 39].These sets (Julia sets) have been computed and examined for cubic [2, 3, 7, 9, 12, 13], quadratic [9, 19, 27], and also for higher degree polynomials using Picard iteration,which is an example of one-step numerical procedure.

Julia sets may be generated for any order complex polynomial. In this research Paper, we have emphasized our research work on cubic Julia sets with reference to complex polynomial of order 3. In 1988, Branner and Hubbard, by a series of papers, paid concerned with the way in which the space of polynomial of degree $d > 3$ is decomposed when the polynomial are classified according to their active behavior using iterative procedure. However their results are satisfied only for $d = 3$. They also dispense with the good framework of the locus connectedness for cubic polynomials [2]. In 1992, their second paper of this series was also dedicated to the account of dynamical system complex cubic polynomial. They also raised the query when the Julia set of a cubic polynomial became a Cantor set [3].

In 1998, Liaw found the regularities for the parameter space of the cubic polynomials in the two dimensional projections. The projection of the parameter points that have non-totally disconnected Julia sets can be observe as a combination of Mandelbrot-like sets [20]. In the same year Cheng and Liaw established asymptotic similarity between the parameter spaces (the Mandelbrot set) and the dynamic space (the Julia sets) of cubic mappings. The dynamic spaces and the parametric spaces of cubic polynomials consist many small copies of the Julia sets and Mandelbrot sets respectively of the standard quadratic mapping [7]. In 2001, Liaw studied the orientations, sizes, and positions of above small copies to understand the formation of the cubic polynomials [21].

In 1999, Yan, Liu, and Zhu worked on a general complex cubic iteration and produced results on the range of Mandelbrot and Julia sets generated from above cubic iteration[41]. These results are helpful in plotting the above generated sets. In 2003, Tomova produced results about the limits of cubic Julia and Mandelbrot sets for complex polynomial $z^3 + pz + q$ and also for Julia and Mandelbrot sets of higher orders polynomial of the form $z^n + c$, [40].

In 2006, Fu *et.al.* generated higher order Julia set and Mandelbrot sets by applying fast computing algorithm [15]. Mamta *et.al.* studied and computed superior Julia sets for nth degree complex polynomial [32, 33], for cubic [6] and for quadratic complex

polynomials [17, 30, 31] using superior iterates (a two-step feedback procedure). Superior Julia sets have also been analysed under the effect of noises [34, 35]. In 2018, Narayan*et.al.* computed and analysed new collection of antifractals for the complex polynomial $\bar{z}^n + c$ in the GK-orbit [23].

In our previous article, we have computed and examined new collection of fractals using faster iteration with *s*-convexity [24].Recently, Rahman, Nisar and Golamankaneh, also studied the generalized Riemann–Liouville fractional integral for the functions with fractal support. They explored reverse Minkowski's inequalities and certain other related inequalities by employing generalized Riemann–Liouville fractional integral for the functions with fractal support [29].

Fractals have also vital role in various domains ranging from mathematical to engineering applications, nano technology to bio medical domain. However, for a deep understanding of fractals and to review the relevant areas, one must go through some recent implementations of non-linear concepts in various areas of machine learning, microprocessors and computer science related to data analysis [10, 37]. For more applications of numerical computing techniques one may see [11, 38].

In this research paper, we have explored new and ever seen cubic fractal sets for the complex cubic polynomial $z \to z^3 + mz + n$, using new different numerical iterative technique (a four-step feedback system) with improved escape criterion. We have also analysed the characteristics of the above generated cubic Julia sets.

2 Material and Method

In past years, researchers focused mainly on three types of feedback procedures like Picard iterates, a one-step feedback system [27], Mann iterates, a two-step feedback system [17, 36], Ishikawa iterates, a three-step feedback system [6] etc. In 2014, Mujahid *et. al.* introduced a new four-step iterative procedure and proved that it is faster than all of Mann, Picard and Agarwal *et. al.* processes. They supported analytic proof by a numerical example and mentioned that this process is independent of all above processes. They also demonstrated some strong and weak convergence results for two non-expansive functions [1].

In this research paper, we have computed Julia sets for the cubic complex polynomial using this faster four-step feedback procedure with improved escape criterion which provides the different results than the previous results.

Definition 2.1. Let S be a non-empty set and p be a self-map from S to S. For a point s_0 in S, the **Picard orbit** (generally called orbit of p) is the set of all iterates of a point s_0, that is: $P(p,s_0) = \{s_n : s_n = p(s_{n-1}),\ n = 1,2,\cdots\}$, where $P(p,s_0)$ of p at the initial point s_0 is the sequence $(p^n s_0)$

Definition 2.2. The filled in Julia set of the function $F(z) = z^n + c$ is defined as

$$K(F) = \{z \in C : F^k(z) \textit{ does not tend to } \infty\}$$

where $F^k(z)$ is the k^{th} iterate of function F, *K(F)* denotes the filled in Julia set and C is the complex space. The boundary of *K(F)* is known as Julia set of the function F. Julia set is the set of those points whose orbits are bounded under $F_c(z) = z^n + c$.

Definition 2.3. (New Iterative Procedure-NIP) Let X be a non-empty set such that $T : X \to X$ and $\{x_n\}$ be a sequence of iterates of initial point $x_0 \in X$ such that

$$\{x_{n+1}:\ x_{n+1} = (1-u_n)Ty_n + u_nTz_n\ ;$$
$$y_n = (1-v_n)Tx_n + v_nTz_n\ ;$$
$$z_n = (1-w_n)x_n + w_nTx_n;\ n = 0,1,2,\cdots,\},$$

where $u_n, v_n, w_n \in [1,0]$ and $\{u_n\}, \{v_n\}, \{w_n\}$ are sequences of positive numbers. For the sake of simplicity, we take $u_n = u, v_n = v, w_n = w$.

2.1 Escape Criterion for Cubic Complex Polynomial

In computation of fractals like Julia and Mandelbrot sets, there is always need to establish a criterion called 'Escape criterion' which enacts a chief role in the graphical representation of Mandelbrot as well as Julia sets and these criteria are different for different order complex polynomials.
Here, in this part, we demonstrate the new escape criterion using NIP for the complex cubic polynomials:

$$P_{m,n}(z) = z^3 + mz + n$$

where m and n are complex numbers.
The following theorem and results provide the escape criterion using NIP for the above mentioned complex polynomial.

Theorem 2.1. *Consider that* $|z| > |n| > (|m| + 2/|u|)^{1/2}$, $|z| > |n| > (|m| + 2/|v|)^{1/2}$, *and* $|z| > |n| > (|m| + 2/|w|)^{1/2}$, *where* $0 < u < 1$, $0 < v < 1$, $0 < w < 1$, *and c is in the complex plane.*
Define

$$z_1 = (1-u)P_{m,n}(z) + uP_{m,n}(z)\ ,$$
$$z_2 = (1-u)P_{m,n}(z_1) + uP_{m,n}(z_1)\ ,$$
$$\vdots$$
$$z_n = (1-u)P_{m,n}(z_{n-1}) + uP_{m,n}(z_{n-1})\ , n = 2,3,4,\cdots$$

where $P_{m,n}(z)$ *is the fuction of z.*
Then $|z| \to \infty$ *as* $n \to \infty$

Proof. Consider

$$\begin{aligned}
|P'_{m,n}(z)| &= |(1-w)z + wP''_{m,n}(z)| \ \ where P''_{m,n}(z) = z^3 + mz + n \\
&= |(1-w)z + w(z^3 + mz + n)| \\
&= |z - wz + wz^3 + mwz + wn)| \\
&\geq |wz^3 + mwz + z - wz| - |wn| \\
&\geq |z|(|wz^2 + mw + 1 - w|) - w|z|, \qquad (\because |z| \geq n) \\
&\geq |z|(|wz^2 + mw| - |1-w|) - w|z| \\
&= |z|(w|z^2 + m| - 1)
\end{aligned}$$

i.e.

$$|P'_{m,n}(z)| \geq |z|(w|z^2 + m| - 1) \tag{2.1}$$

Also

$$\begin{aligned}
|P_{m,n}(z)| &= |(1-v)P''_{m,n}(z) + vP'_{m,n}(z)| \\
&\geq |(1-v)(z^3+mz+n+v|z|(w|z^2+m|-1|)) \qquad [By\ using\ Eq.(2.1)] \\
&= |(1-v)z^3+m(1-v)z+n(1-v)+vw|z|(|z^2+m|-v|z||) \\
&\geq |(1-v)z^3+m(1-v)z|-(1-v)|z|+vw|z|(|z^2+m|-v|z|) \\
&= |z|[(1-v)|z^2+m|-1]+vw|z||z^2+m| \\
&\geq |z|[(vw-v+1)(|z^2|-|m|-1)]
\end{aligned}$$

Since,

$$z_n = (1-u)P_{m,n}(z_{n-1}) + uP'_{m,n}(z_{n-1})$$

We have

$$\begin{aligned}
|z_1| &= |(1-u)P_{m,n}(z) + uP'_{m,n}(z)| \\
&\geq |(1-u)[|z|(vw-v+1)|z^2+m|-1]+u[|z|(w|z^2+m|-1)] \\
&\geq |z||(uv+vw-uvw-u-v+1)|z^2+m|-|(1-u)|z|| \\
&\quad +uw|z||z^2+m|-u|z| \\
&= |z|[(uv+vw+uw-uvw-u-v+1)|z^2+m|-1] \\
&\geq |z|[(uv+vw+uw-uvw-u-v+1)(|z^2|-|m|)-1] \\
&= |z|R[|z^2|-(|m|+1/R)]
\end{aligned}$$

where

$$R = uv+vw+uw-uvw-u-v+1$$

Since, $|z|>|n|>(|m|+2/|u|)^{1/2}$, $|z|>|n|>(|m|+2/|v|)^{1/2}$, and $|z|>|n|>(|m|+2/|w|)^{1/2}$, so that we have $|z|>(|m|+2/R)^{1/2}$, this mean $|z^2|-(|m|+1/R)>(1/R)$ so that $R(|z^2|-(|m|+1/R))>1$. Therefore there exists a $\lambda>0$ such that

$$|z_1|>(1+\lambda)|z|$$

Repeating the same argument, we get

$$|z_n|>(1+\lambda)^n|z|$$

Thus, orbit of z tends to infinity as $n\to\infty$. This completes the proof. □

Corollary 2.1.1. *Consider the complex cubic polynomial $P_{m,n}(z)=z^3+mz+n$ where m, n are complex numbers and assume*
$|z|>max[\,|n|,(|m|+2/|u|)^{1/2},(|m|+2/|v|)^{1/2},(|m|+2/|w|)^{1/2}]$ then $|z_n|>(1+\lambda)^n|z|$ and $|z_n|\to\infty$ as $n\to\infty$. This provides the 'escape criterion' for the above complex cubic polynomial.

Corollary 2.1.2. *Assume*
$|z_k| > max[\,|n|, (|m|+2/|u|)^{1/2}, (|m|+2/|v|)^{1/2}, (|m|+2/|w|)^{1/2}]$ *for some* $k \geq 0$ *then* $|z_k| > (1+\lambda)^n |z_{k-1}|$ *and* $|z_n| \to \infty$ *as* $n \to \infty$.
This result provides an algorithm to generate cubic Julia sets for the above mentioned complex polynomial.

3 Result And Discussion

3.1 Fractals as Cubic Julia sets

Cubic Julia sets, applying new different fixed point technique, are generated through complex polynomial $P_{m,n}(z) = z^3 + mz + n$, using cubic escape criterion with the software Mathematica 10.0, See Figures 1-20.

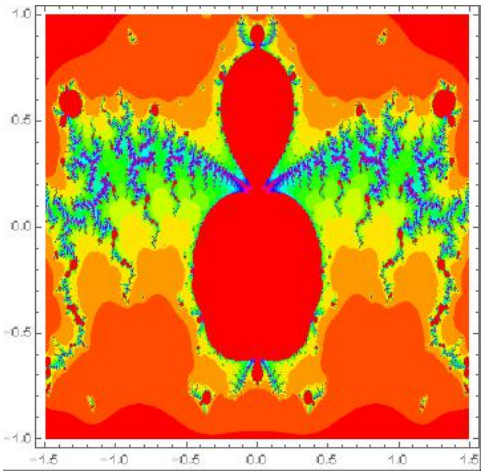

Figure 1: Ants Cubic Julia set for u= v=.48, w=.28, m=-3.2, n=.56I

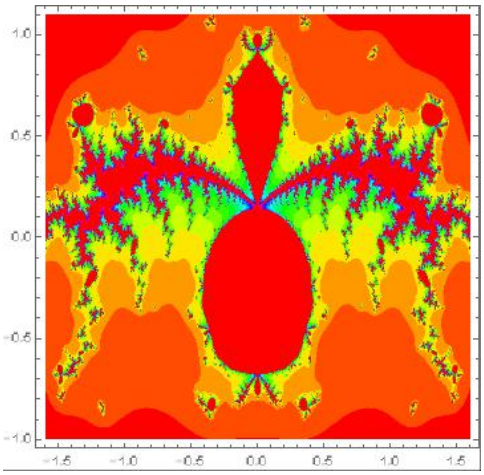

Figure 2: Ants Cubic Julia set for u= v=.477, w=.283, m=-3.13, n=.59I

3.2 Graphical Execution of Cubic Julia Sets Employed NIP

For the graphical execution of cubic Julia sets we iterate complex cubic polynomial $P_{m,n}(z) = z^3 + mz + n$, and define the prisoner set using escape criterion under the above new different iterative procedure. We have also generated some interested and ever seemed cubic Julia sets.

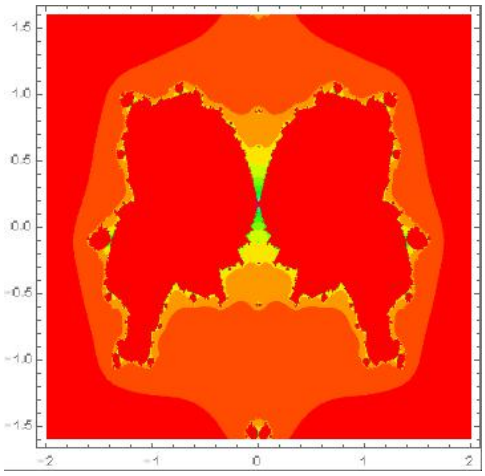

Figure 3: Cubic Julia set for u= v=.42, w=.05, m=-1.6, n=.45I

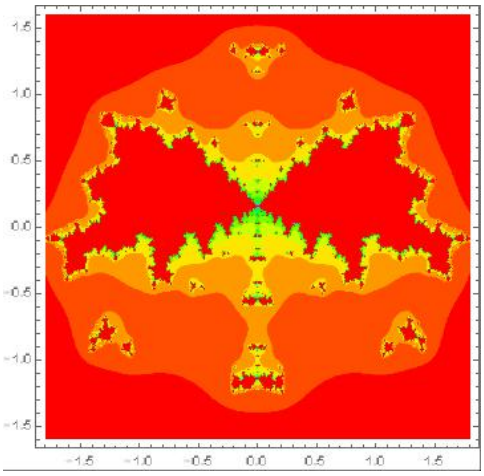

Figure 4: Cubic Julia set for u= v=.45, w=.09, m=-2.3, n=.52I

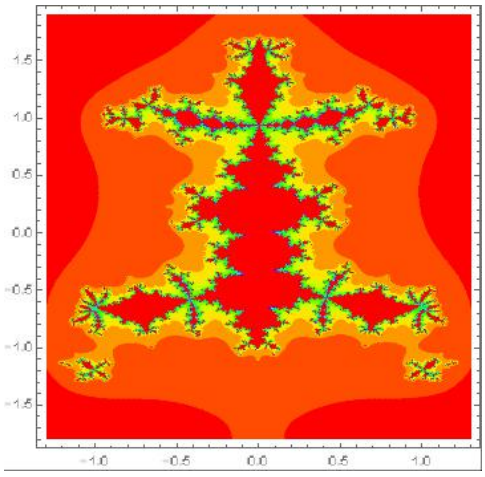

Figure 5: Cubic Julia set for u= v=.44 w=.07 m=.6-.01I n=1.2I

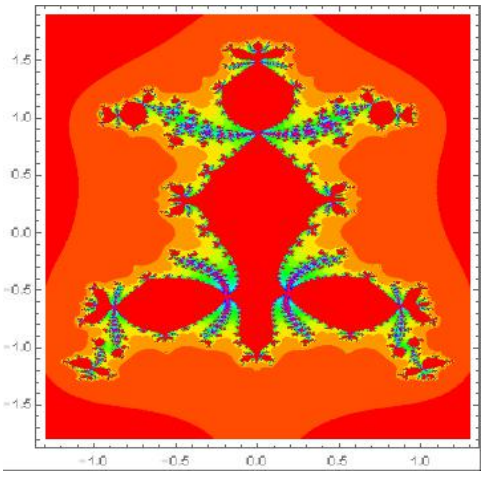

Figure 6: Cubic Julia set for u= v=.44 w=.03 m=.62-.01I n=1I

In this paper we have used two sets of parameters, $u, v, w$and m, n, and by changing parametric cost of these set of pairs, we have also noticed many important observations as follow:

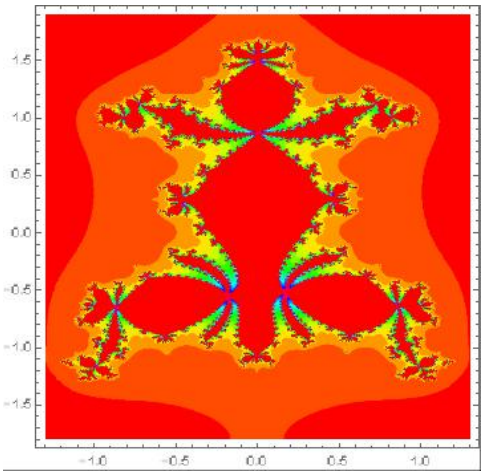

Figure 7: Cubic Julia set for u= v=.44 w=.07 m=.62-.01I n=1I

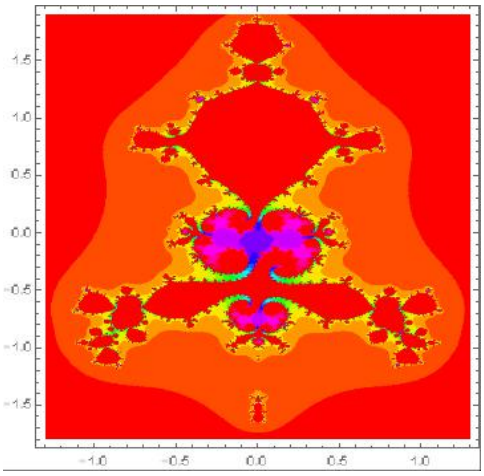

Figure 8: Cubic Julia set for u= v=.57 w=.05 m=.6+.01I n=1.2I

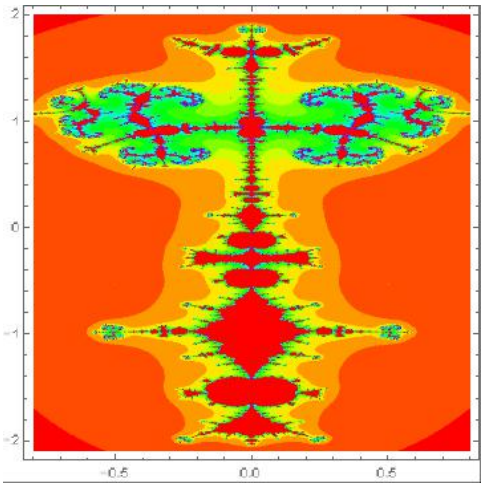

Figure 9: Antenna Cubic Julia set for u= v=.15 w=.83 m=2.5 n=-.80I

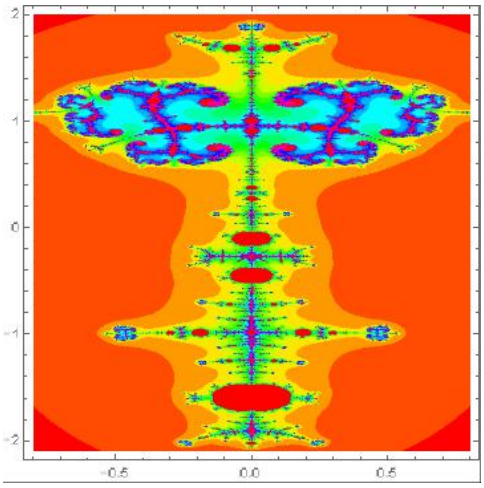

Figure 10: Antenna Cubic Julia set for u= v=.15 w=.83 m=2.62 n=-.80I

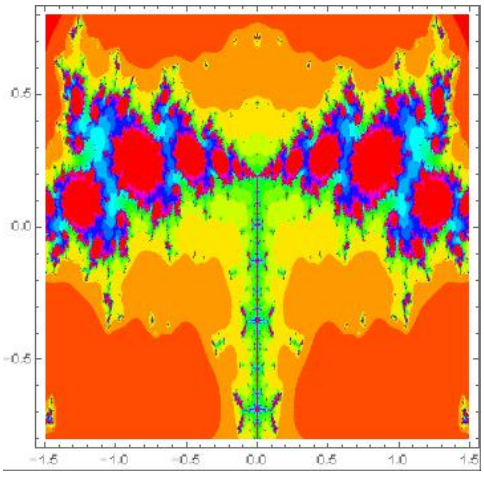

Figure 11: Antenna Cubic Julia set for u= v=.46 w=.366 m=-29.1 n=.75I

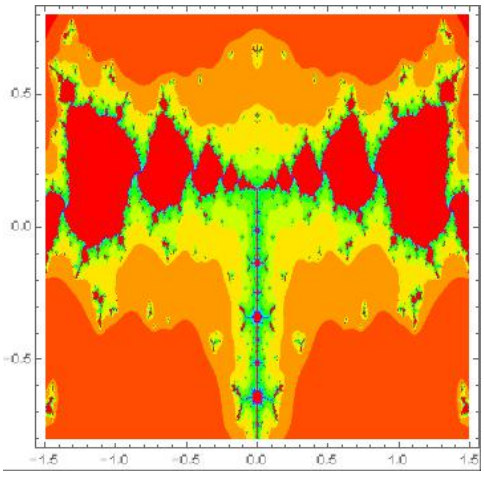

Figure 12: Antenna Cubic Julia set for u= v=.46 w=.366 m=-3.1 n=.59I

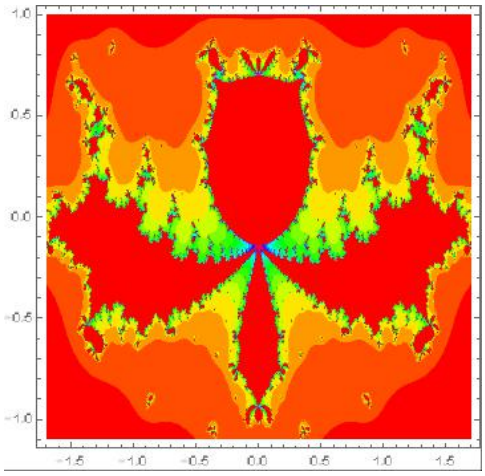

Figure 13: Cubic Julia set for u= v=.48,w=.32 m=-3.13, n=-.59I

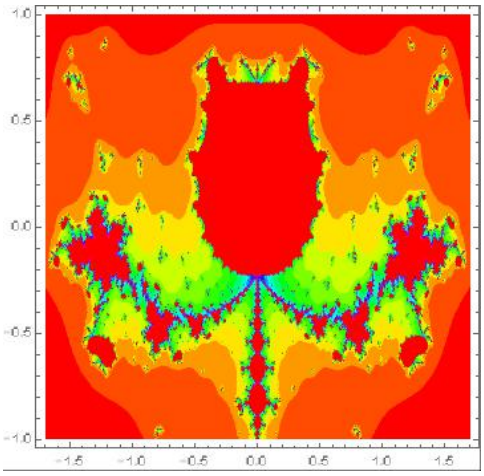

Figure 14: Cubic Julia set for u= v=.48, w=.32 m=-3.03, n=-.89I

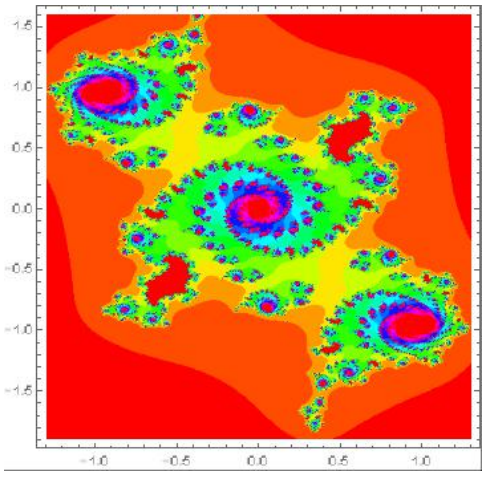

Figure 15: Cubic Julia set for u= v=.5, w=.03, m=1.2I n=0

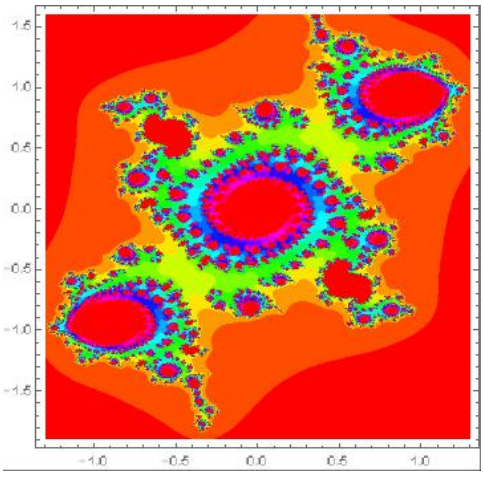

Figure 16: Cubic Julia set for u= v=.5, w=.05,m=-1.17I n=0

- It has been observed that the Figures 1 - 14 and Figures 17 - 20 show the perfect mathematical reflexive symmetry about imaginary axes only whereas the Figures 15 - 16 show the perfect mathematical reflexive symmetry about both the axes (real as well as imaginary axes).
- It is noticed that the prisoner sets of the cubic Julia sets in the Figures 1 - 5, Figure 17 and Figures 11 - 16 are mathematically disconnected whereas the prisoner sets of the remaining cubic Julia sets are mathematically connected.

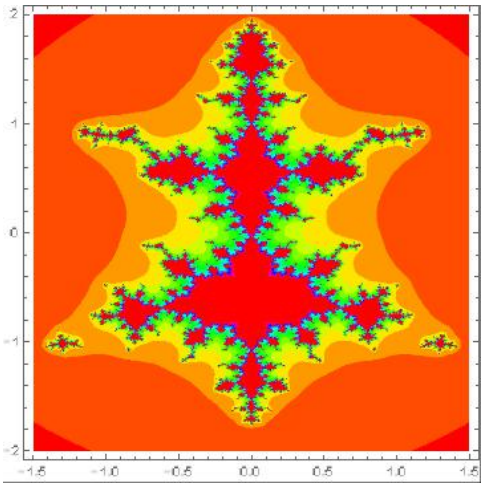

Figure 17: Cubic Julia set for u= v=.03 w=.95 m=1.0 n=1.001I

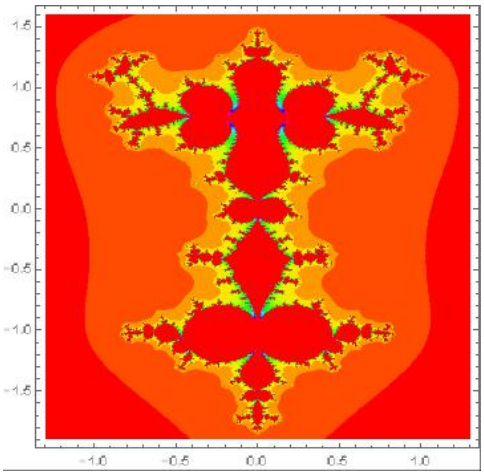

Figure 18: Cubic Julia set for u= v=.5 w=.01 m=1.3 n=-.80I

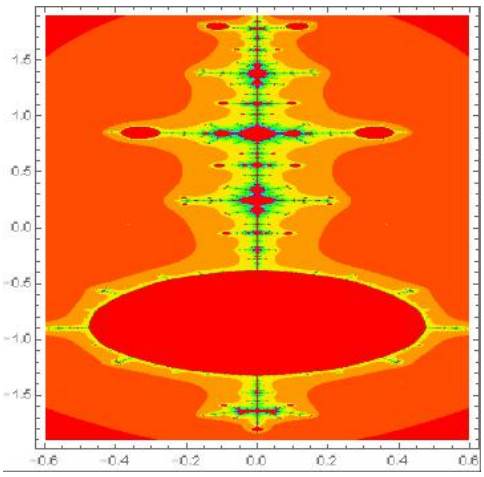

Figure 19: Cubic Julia set for u= v=.19 w=.376 m=2.2 n=.40I

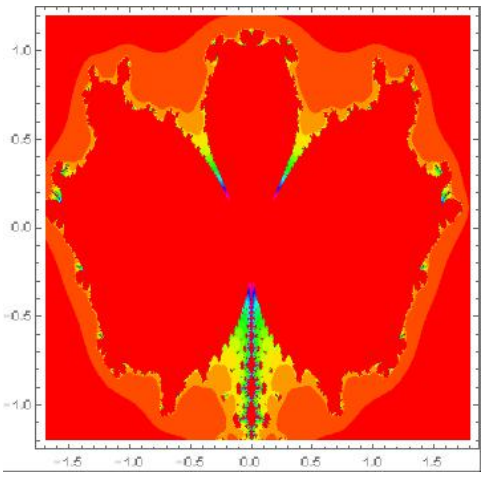

Figure 20: Butterfly Cubic Julia set for u= v=.5 w=.3 m=-2.03 n=-.6I

- It is also noticed that the cubic Julia sets in Figure 1 and Figure 2 capture the shape of ants, Figures 4 - 8, look like as meditating posture, the cubic Julia in Figures 9-12 and Figure 19 take the shape of antennas, the cubic Julia set in Figure 20 take the shape of a butterfly and the Julia sets in Figure 3-4 and Figures 13-14 are wall-decorated pictures.

Conclusion

In this research paper, a new different four-step iterative procedure has been applied to the complex cubic polynomial $P_{m,n}(z) = z^3 + mz + n$, and significant as well as exciting results have been obtained.We have obtained new and ever seen cubic Julia sets as output for the above complex cubic polynomial. Some of the generated cubic Julia sets have perfect mathematical reflexive symmetry about the axes. From above generated

cubic Julia sets, some Julia sets are connected and some are disconnected which is also an important mathematical property of fractals.It is also fascinating to see that some of the generated cubic Julia sets take the shape of antennas which is an important application of fractals, some cubic Julia sets capture the shape of ants and the butterfly, some cubic Julia sets look like as meditating posture, and some other look like as wall-decorated pictures.

References

[1] Abbas M and Nazir T (2014) A new iteration process applied to constained minimization and feasibility problems, Matemathykm Bechnk , 66, (2), 223-234.

[2] Branner B and Hubbard JH (1988) The Iteration of Cubic Polynomials Part I: The global topology of parameter space, Acta Math, 160, 143-206.

[3] Branner B and Hubbard JH (1992) The Iteration of Cubic Polynomials Part II: Patterns and para-patterns, Acta Math, 169(3-4), 229-325.

[4] Beardon AF (1991)Iteration of Rational Functions, Springer-Verlag, New York.

[5] Bunde A and Havlin S (1996) Fractals and Disordered Systems, Springer-Verlag, Berlin, Heidelberg.

[6] Chauhan YS, Rana R and Negi A (2010) New Julia sets of Ishikawa Iterates, International Journal of Computer Applications, 7(13), 34-42.

[7] Cheng C and Liaw S (1998) Similarity between the dynamic and parameter spaces in cubic mappings, Fractals, 6(3), 293-299.

[8] Conway JB (1978) Functions of One Complex Variable, Second Edition, Springer-Verlag, New York.

[9] Devaney RL (1992) A First Course in Chaotic Dynamical Systems: Theory and Experiment, Addison Wesley.

[10] Dubey VP, Singh J, Alshehri AM, Dubey S and Kumar D (2021) A comparative analysis of two computational schemes for solving local fractional Laplace equations, Mathematical Methods in the Applied Sciences, 44(17), 13540-13559.

[11] Dubey VP, Dubey S, Kumar D and Singh S (2021) A computational study of fractional model of atmospheric dynamics of carbon dioxide gas, Chaos, Solitons and Fractals, 142, 110375.

[12] Douady A and Hubbard JH (1984) Etude dynamique des pïolynomes complexes, Publications Mathematiques d'Orsay , Universitïe de Paris-Sud.

[13] Epstein A and Yampolsky M (1999) Geography of the cubic connectedness locus: intertwining surgery, Ann. Sci. École Norm Sup.4, 32, 151-185.

[14] Fraser J (2009) An Introduction to Julia sets, http://www.mcs.st and.ac.uk/ jmf32/julia.pdf.

[15] Fu C, Jiang H, Yi X and Zhang Z (2006) An accelerated algorithm of constructing general high-order Mandelbrot and Julia sets, Advances in Natural Computation, Proc. Part II ICNC (Sep 24-28, Xi'an, China), Springer, Berlin Heidelberg, 4222, 793-796.

[16] Holmgren RA (1994) A First Course in Discrete Dynamical Systems, Springer-Verlag, New York, Inc.

[17] Kumar M and Rani M (2005) A new approach to superior Julia sets,J. Nature. Phys. Sci., 19(2), 148-155.

[18] Kigami J (2001) Analysis on Fractals, Cambridge Univ. Press, Cambridge.

[19] Lei T (1990) Similarity between the Mandelbrot sets and Julia sets, Commun. Math. Phys., 134(3), 587-617.

[20] Liaw S (1998) The parameter spaces of the cubic polynomials, Fractals, 6(2), 181-189.

[21] Liaw S (2001) Structure of the cubic mappings, Fractals,9(2), 231-235.

[22] Milnor J (2000) Local connectivity of Julia sets: expository lectures, The Mandelbrot Set, Theme and Variations (Edited by Lei Ten), London Math. Soc. Lecture Note Ser., 274, Cambridge University Press, 67-116.

[23] Partap N, Jain S and Chugh R (2018) Computation of Antifractals-Tricorns and Multicorns with their complex nature, Pertanika Journal of science and technology, 26(2), 863 - 872.

[24] Partap N, Jain S and Chugh R (2019) Supremacy of s-convexity scheme and generation of advanced fractal using faster iteration, *Nonlinear Studies*, 26(2), 289 - 301.

[25] Partap N, Jain S and Chugh R (2020) Computation of Newborn J-Sets via Fixed Point Iteration and Their Complex Nature, in: IEEE Proc. ICRITO 2020, Noida, India, 1089 - 1093.

[26] Partap N, Jain S and Chugh R (2020) Reckoning of Newborn M-Sets with Their Complex Nature via Fixed Point Iteration, in: IEEE Proc. ICRITO 2020, Noida, India, 1123 - 1126.

[27] Peitgen HO, Jurgens H and Saupe D (1992) Chaos and Fractals, Springer-Verlag, New York, Inc.

[28] Peitgen HO, Jurgens H and Saupe D (2004) Chaos and Fractals: New frontiers of science (2nd ed.), Springer-Verlag, New York, Inc.

[29] Rahman G, Nisar KS and Golamankaneh AK (2021) The Nonlocal Fractal Integral Reverse Minkowski's and Other Related Inequalities on Fractal Sets, Mathematical Problems in Engineering, 21, 10 pages. Article ID 4764891.

[30] Rani M and Nagi A (2008) New Julia sets for complex Carotid-Kundalini function, Chaos,Solitons and Fractals, 36(2), 226-236.

[31] Rani M and Agarwal R (2009) Generation of fractals from complex logistic map, *Chaos,Solitons and Fractals* **41**, 1, 447-452, 2009.

[32] Rani M (2010) Superior antifractals, in:IEEE Proc. ICCAE 2010,1(1), 798-802.

[33] Rani M (2010a) Superior tricorns and multicorns,in: WSEAS Proc. 9th Int. conf. on Applications of Computer Engineering (ACE '10): Recent Advances and Applications of Computer Engineering, 58-61.

[34] Rani M and Agarwal R (2010) Effect of noise on Julia sets generated by logistic map, in: Proc. 2nd IEEE International Conference on Computer and Automation Engineering (ICCAE 2010), 2, 55-59.

[35] Rani M and Agarwal R (2010) Effect of stochastic noise on superior Julia sets, J. Math. Imaging Vis., 36, 63-68.

[36] Rani M (2011) Cubic superior Julia sets, in: Proc. European Computing Conference,80-84.

[37] Rashid *et.al*.(2020) Multidimensional fixed points in generalized distance spaces,Advances in Difference Equations, 20, 20 pages. Article Number 571.

[38] Singh J,Kumar D,Purohit SD, Mishra AM and Bohra M (2020) An efficient numerical approach for fractional multidimensional diffusion equations with exponential memory,Numerical Methods for Partial Differential Equations, 37(2), 1631-1651.

[39] Steinmnetz N (1993)Rational Iteration: Complex Analytic Dynamical Systems, Walter de Cruyter, Berlin, New York.

[40] Tomova AV(2003) The Mandelbrot set for Julia sets of arbitrary order; A remark on the shape of cubic Mandelbrot and Julia sets, Mandelbrot and Julia sets for the polynomials of arbitrary order, Proc ICT and P, Varna, Bulgaria, FOI-COMMERCE, Sofia, 78-88.

[41] Yan D, Liu X and Zhu W (1999) A Study of Mandelbrot and Julia Sets generated from a general complex cubic Iteration, Fractals, 7(4), 433-437.

The complement on the existence of fixed points that belong to the zero set of a certain function due to Karapinar et al.

Pathaithep Kumrod, Wutiphol Sintunavarat[1]

December 26, 2021

Abstract

Recently, the idea of φ-fixed point and the elementary results on φ-fixed points were first investigated by Jleli et al. [Jleli M, Samet B, Vetro C (2014) Fixed point theory in partial metric spaces via φ-fixed point's concept in metric spaces. Journal of Inequalities and Applications, 2014(1):1-9.]. Based on this work, Karapinar et al. [Karapinar E, O'Regan D, Samet B (2015) On the existence of fixed points that belong to the zero set of a certain function. Fixed Point Theory and Applications, 2015(1):1-14.] established the new φ-fixed point results, which can be reduced to the famous fixed point result of Boyd and Wong in 1969. However, the main result of Karapinar et al. does not cover the φ-fixed point results of Jleli et al. This paper aims to fulfill this gap by proving φ-fixed point results covering several φ-fixed point results and fixed point results. **Key words**: φ-fixed point; φ-Picard mapping; Control function
Mathematics Subject Classification(2010): 46T99; 47H10; 54H25

[1]

1 Introduction and preliminaries

In 2014, Jleli et al. [1] had initiated the concept of (F, φ)-contraction with the help of some control function, which is one of the interesting generalizations of the classical Banach contraction principle and first introduced the concepts of φ-fixed point and φ-Picard mapping. Moreover, they also proved some φ-fixed point theorems for contractive mappings expanded some fixed point results in metric spaces. Consistent with Jleli et al. [1], we will be needed the following notations, definitions, and results in this research.

[1]Corresponding author: Department of Mathematics and Statistics,
Faculty of Science and Technology, Thammasat University Rangsit Center,
Pathum Thani 12120, Thailand

Let X be a nonempty set, $\varphi : X \to [0, \infty)$ be a given function and $T : X \to X$ be a mapping. By F_T and Z_φ the set of all fixed points of T and the set of all zeros of the function φ, respectively, i.e., $F_T := \{x \in X : Tx = x\}$ and $Z_\varphi := \{x \in X : \varphi(x) = 0\}$.

Definition 1.1 ([1])**.** Let X be a nonempty set and $\varphi : X \to [0, \infty)$ be a given function. An element $z \in X$ is said to be a φ-fixed point of the mapping $T : X \to X$ if and only if z is a fixed point of T and $\varphi(z) = 0$ (i.e., $z \in F_T \cap Z_\varphi$).

Definition 1.2 ([1])**.** Let (X, d) be a metric space and $\varphi : X \to [0, \infty)$ be a given function. A mapping $T : X \to X$ is said to be a φ-Picard mapping if and only if, for each $x, z \in X$, the following conditions are satisfied:

(i) $F_T \cap Z_\varphi = \{z\}$ for some $z \in X$;

(ii) $T^n x \to z$ as $n \to \infty$ for each $x \in X$.

To describe the control function, which is an important class of this work, let $\mathcal{F}$ be the family of all functions $F : [0, \infty)^3 \to [0, \infty)$ satisfying the following conditions:

$(F1)$ $\max\{a, b\} \leq F(a, b, c)$ for all $a, b, c \in [0, \infty)$;

$(F2)$ $F(0, 0, 0) = 0$;

$(F3)$ F is continuous.

As examples, the following functions $F_1, F_2, F_3 : [0, \infty)^3 \to [0, \infty)$ belong to $\mathcal{F}$:

(i) $F_1(a, b, c) = a + b + c$ for all $a, b, c \in [0, \infty)$;

(ii) $F_2(a, b, c) = \max\{a, b\} + c$ for all $a, b, c \in [0, \infty)$;

(iii) $F_3(a, b, c) = a + a^2 + b + c$ for all $a, b, c \in [0, \infty)$.

Definition 1.3 ([1])**.** Let (X, d) be a metric space, $\varphi : X \to [0, \infty)$ be a given function, and $F \in \mathcal{F}$. A mapping $T : X \to X$ is said to be an (F, φ)-contraction mapping if there exists $k \in [0, 1)$ such that

$$F(d(Tx, Ty), \varphi(Tx), \varphi(Ty)) \leq kF(d(x, y), \varphi(x), \varphi(y))) \quad \forall (x, y) \in X^2. \quad (1.1)$$

Theorem 1.4 ([1])**.** *Let (X, d) be a complete metric space, $\varphi : X \to [0, \infty)$ be a lower semi-continuous function, $F \in \mathcal{F}$ and $T : X \to X$ be an (F, φ)-contraction mapping. Then $F_T \subseteq Z_\varphi$ and T is a φ-Picard mapping.*

Remark 1.5. Note that if we set $F(a, b, c) = a + b + c$ for all $a, b, c \in [0, \infty)$ and $\varphi(x) = 0$ for all $x \in X$ in (1.1), then the contractive condition (1.1) reduces to the Banach contractive condition.

In recent years, Jleli et al.'s fixed point theorem has been generalized and extended in several directions. One such generalization was introduced by Karapinar et al. [2] by replacing the constant k of the contractive condition (1.1) with the control function, which was first introduced by Boyd and Wong [3]. They also proved the existence and uniqueness results of a φ-fixed point for new nonlinear mappings. Nevertheless, this result expands all conditions of results of [1], except that the condition $(F2)$ is replaced by

$(F2^\star)$ $F(a,0,0)=a$ for all $a\geq 0$.

Here, we recall the definition of the following class as given by Boyd and Wong [3]. Denote Ψ the set of functions $\psi:[0,\infty)\to[0,\infty)$ satisfying the following conditions:

$(\psi 1)$ ψ is upper semi-continuous from the right;

$(\psi 2)$ $\psi(t)<t$ for each $t>0$.

Combining this definition with Jleli et al.'s theorem, Karapinar et al. [2] proved the following theorem:

Theorem 1.6 ([2]). *Let (X,d) be a complete metric space. Suppose that the mapping $T:X\to X$ satisfies the following condition:*

$$F(d(Tx,Ty),\varphi(Tx),\varphi(Ty))\leq\psi(F(d(x,y),\varphi(x),\varphi(y)))\quad\forall(x,y)\in X^2,\quad(1.2)$$

where $\varphi:X\to[0,\infty)$ is lower semi-continuous, $\psi\in\Psi$, and $F:[0,\infty)^3\to[0,\infty)$ is a function satisfying the following conditions:

$(F1)$ $\max\{a,b\}\leq F(a,b,c)$ *for all $a,b,c\in[0,\infty)$;*

$(F2^\star)$ $F(a,0,0)=a$ *for all $a\geq 0$;*

$(F3)$ *F is continuous.*

Then $F_T\subseteq Z_\varphi$ and T is a φ-Picard mapping.

In the case of ψ defined by $\psi(t)=kt$ for some $k\in[0,1)$, Theorem 1.6 seem almost similar to a generalization of Theorem 1.4 except that Theorem 1.6 use the control function F satisfying conditions $(F1)$, $(F2^\star)$, $(F3)$ rather than Theorem 1.4 use the control function F satisfying conditions $(F1)$, $(F2)$, $(F3)$. It is easy to see that the condition $(F2^\star)$ is stronger than the condition $(F2)$ since there are many functions satisfying the condition $(F2)$ but it does not satisfy the condition $(F2^\star)$. For example, functions $F_1,F_2,F_3:[0,\infty)^3\to[0,\infty)$ defined by $F_1(a,b,c)=a+a^2+b+c$, $F_2(a,b,c)=\ln(a+1)+(a+b)e^c+\max\{a,b\}$, and $F_3(a,b,c)=\max\{2a,b\}+c$ for all $a,b,c\geq 0$. From the above observation, we can conclude that the main theorem of [2] is not a proper extension of Theorem 1.4.

The main goal of this work is to fulfill the mentioned gap by using the new technique for improving Theorem 1.6 via the original control function, which was introduced by Jleli et al. in [1]. For simplicity, the following diagram shows the relation of Karapinar et al.'s results and our results, which describes the objectives of this research.

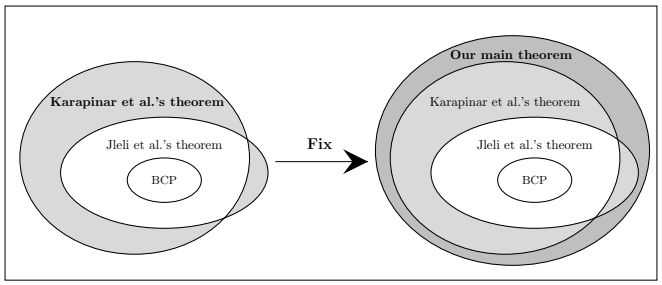

Figure 1: The conceptual research framework

2 Main results

In section, we will prove the generalized φ-fixed point results by using the new technique, which is the improved version of the φ-fixed point theorem of Karapinar et al. [2], but it replaces the condition $(F2^{\star})$ by the condition $(F2)$.

Theorem 2.1. *Let (X, d) be a complete metric space and T be a self mapping on X such that*

$$F(d(Tx, Ty), \varphi(Tx), \varphi(Ty)) \leq \psi(F(d(x, y), \varphi(x), \varphi(y))) \quad \forall (x, y) \in X^2, \quad (2.1)$$

where $\varphi : X \to [0, \infty)$ is lower semi-continuous, $F \in \mathcal{F}$ and $\psi \in \Psi$. Then $F_T \subseteq Z_\varphi$ and T is a φ-Picard mapping.

Proof. The first step is to prove that $F_T \subseteq Z_\varphi$. Let $x \in F_T$. Letting $y = x$ in (2.1), we have

$$F(0, \varphi(x), \varphi(x)) \leq \psi(F(0, \varphi(x), \varphi(x))). \quad (2.2)$$

Assume that $\varphi(x) > 0$. It follows from $(F1)$ that $F(0, \varphi(x), \varphi(x)) > 0$. By (2.2) and $(\psi 1)$, we get

$$F(0, \varphi(x), \varphi(x)) \leq \psi(F(0, \varphi(x), \varphi(x))) < F(0, \varphi(x), \varphi(x)),$$

which is a contradiction. Therefore, $\varphi(x) = 0$, which implies that

$$F_T \subseteq Z_\varphi. \quad (2.3)$$

Next, we will show that T is a φ-Picard mapping. Let x_0 be an arbitrary point in X. Define the sequence $\{x_n\} \subseteq X$ by $x_n = Tx_{n-1}$ for all $n \in \mathbb{N}$. If $x_{n^*} = x_{n^*-1}$ for some $n^* \in \mathbb{N}$, then x_{n^*} is a fixed point of T. Hence, for the rest of the proof, we assume that $x_n = x_{n-1}$ for all $n \in \mathbb{N}$, that is,

$$d(x_n, x_{n-1}) > 0 \quad (2.4)$$

for each $n \in \mathbb{N}$. Now, we will claim that

$$\lim_{n\to\infty} d(x_{n+1}, x_n) = \lim_{n\to\infty} \varphi(x_n) = 0. \quad (2.5)$$

From $(F1)$ and (2.4), we obtain

$$F(d(x_n, x_{n-1}), \varphi(x_n), \varphi(x_{n-1})) > 0$$

for all $n \in \mathbb{N}$. This allows to use the condition $(\psi 2)$ and so by using the contractive condition (2.1), we obtain

$$\begin{aligned} F(d(x_{n+1}, x_n), \varphi(x_{n+1}), \varphi(x_n)) &\leq \psi(F(d(x_n, x_{n-1}), \varphi(x_n), \varphi(x_{n-1}))) \\ &< F(d(x_n, x_{n-1}), \varphi(x_n), \varphi(x_{n-1})) \end{aligned} \tag{2.6}$$

for all $n \in \mathbb{N}$. This shows that $\{F(d(x_{n+1}, x_n), \varphi(x_{n+1}), \varphi(x_n))\}$ is a decreasing sequence. Furthermore, it is easy to see that it is also bounded below by 0 and hence it converges to some point $r \geq 0$, that is,

$$\lim_{n\to\infty} F(d(x_{n+1}, x_n), \varphi(x_{n+1}), \varphi(x_n)) = r. \tag{2.7}$$

From (2.6), (2.7) and the squeeze theorem, we get

$$\lim_{n\to\infty} \psi(F(d(x_n, x_{n-1}), \varphi(x_n), \varphi(x_{n-1}))) = r. \tag{2.8}$$

Assume that $r > 0$. So we have

$$\begin{aligned} r &\overset{(2.8)}{=} \limsup_{n\to\infty} \psi(F(d(x_n, x_{n-1}), \varphi(x_n), \varphi(x_{n-1}))) \\ &\overset{(\psi 1)}{\leq} \psi(r) \\ &\overset{(\psi 2)}{<} r \end{aligned}$$

which provides a contradiction. Therefore, $r = 0$, that is,

$$\lim_{n\to\infty} F(d(x_{n+1}, x_n), \varphi(x_{n+1}), \varphi(x_n)) = 0,$$

and thus, by $(F1)$, we get

$$\lim_{n\to\infty} d(x_{n+1}, x_n) = \lim_{n\to\infty} \varphi(x_n) = 0,$$

that is, Equation (2.5) holds.

Now, we shall prove that $\{x_n\}$ is a Cauchy sequence. Assume on the contrary that $\{x_n\}$ is not a Cauchy sequence. Then there exists $\epsilon > 0$ for which we can find subsequences $\{x_{m(k)}\}$ and $\{x_{n(k)}\}$ of $\{x_n\}$ with $n(k) > m(k) \geq k$ and

$$d\left(x_{m(k)}, x_{n(k)}\right) \geq \epsilon \tag{2.9}$$

for all $k \in \mathbb{N}$. Corresponding to $m(k)$, we may choose $n(k)$ such that it is the smallest integer satisfying (2.9). Then we have

$$d\left(x_{m(k)}, x_{n(k)-1}\right) < \epsilon.$$

By the triangular inequality, we have

$$\begin{aligned}\epsilon &\leq d\left(x_{m(k)}, x_{n(k)}\right)\\ &\leq d\left(x_{m(k)}, x_{n(k)-1}\right) + d\left(x_{n(k)-1}, x_{n(k)}\right)\\ &< \epsilon + d\left(x_{n(k)-1}, x_{n(k)}\right).\end{aligned}$$

Letting $k \to \infty$ in the above inequality and using (2.5), we have

$$\lim_{k\to\infty} d\left(x_{m(k)}, x_{n(k)}\right) = \epsilon. \tag{2.10}$$

By a similar way, we can show that

$$\lim_{k\to\infty} d\left(x_{m(k)+1}, x_{n(k)+1}\right) = \epsilon. \tag{2.11}$$

Using $(F3)$, (2.5), (2.10) and (2.11), it follows that

$$\lim_{k\to\infty} F\left(d\left(x_{m(k)}, x_{n(k)}\right), \varphi\left(x_{m(k)}\right), \varphi\left(x_{n(k)}\right)\right) = F(\epsilon, 0, 0) \tag{2.12}$$

and

$$\lim_{k\to\infty} F\left(d\left(x_{m(k)+1}, x_{n(k)+1}\right), \varphi\left(x_{m(k)+1}\right), \varphi\left(x_{n(k)+1}\right)\right) = F(\epsilon, 0, 0). \tag{2.13}$$

Now, we choose $x = x_{m(k)}$ and $y = x_{n(k)}$ in (2.1), we infer

$$F\left(d\left(x_{m(k)+1}, x_{n(k)+1}\right), \varphi\left(x_{m(k)+1}\right), \varphi\left(x_{n(k)+1}\right)\right) \leq \psi\left(F\left(d(x_{m(k)}, x_{n(k)}), \varphi(x_{m(k)}), \varphi(x_{n(k)})\right)\right).$$

Taking the limit superior as $k \to \infty$ on both sides of the above inequality and using (2.13), we deduce

$$F(\epsilon, 0, 0) \leq \limsup_{k\to\infty} \psi\left(F\left(d(x_{m(k)}, x_{n(k)}), \varphi(x_{m(k)}), \varphi(x_{n(k)})\right)\right). \tag{2.14}$$

Using the condition $(\psi 1)$ and (2.12), we obtain

$$\limsup_{k\to\infty} \psi\left(F\left(d(x_{m(k)}, x_{n(k)}), \varphi(x_{m(k)}), \varphi(x_{n(k)})\right)\right) \leq \psi(F(\epsilon, 0, 0)) < F(\epsilon, 0, 0). \tag{2.15}$$

From (2.14) and (2.15) together with $(\psi 2)$, we obtain

$$F(\epsilon, 0, 0) \leq \psi(F(\epsilon, 0, 0)) < F(\epsilon, 0, 0),$$

which is a contradiction. Therefore, $\{x_n\}$ is a Cauchy sequence. By the completeness of X, there exists a point $z \in X$ such that

$$\lim_{n\to\infty} d(x_n, z) = 0. \tag{2.16}$$

Using (2.5), (2.16) and the lower semi-continuity of φ, we get

$$0 \leq \varphi(z) \leq \liminf_{n\to\infty} \varphi(x_n) = 0,$$

which implies that

$$\varphi(z) = 0. \tag{2.17}$$

Next, we will prove that z is a fixed point of T. From $(F2)$, $(F3)$, (2.5) and (2.16), we get

$$\lim_{n\to\infty} F(d(x_n, z), \varphi(x_n), 0) = F(0, 0, 0) = 0.$$

Note that from $(\psi 2)$, it follows that $\lim_{t\to 0^+} \psi(t) = 0$. Then

$$\lim_{n\to\infty} \psi(F(d(x_n, z), \varphi(x_n), 0)) = \lim_{t\to 0^+} \psi(t) = 0. \tag{2.18}$$

Hence, from $(F1)$, (2.1), (2.17) and (2.18), we conclude that

$$d(x_{n+1}, Tz) \leq \psi(F(d(x_n, z), \varphi(x_n), 0)) \to 0 \text{ as } n \to \infty.$$

Therefore, by the uniqueness of the limit, we obtain $z = Tz$, i.e., z is a fixed point of T.

Finally, we will show that T has a unique fixed point. Suppose that u and v are fixed points of T such that $u \neq v$. Then $d(u, v) > 0$. Therefore,

$$\begin{aligned} F(d(u, v), 0, 0) &= F(d(Tu, Tv), 0, 0) \\ &\overset{(2.1)}{\leq} \psi(F(d(u, v), 0, 0)) \\ &\overset{(\psi 2)}{<} F(d(u, v), 0, 0), \end{aligned}$$

which is a contradiction. Thus, the fixed point of T is unique. This completes the proof. □

The following example shows that Theorem 2.1 is more applicable than many other results in the literature.

Example 2.2. Let $X = [0, \infty)$ and $d : X \times X \to \mathbb{R}$ be defined by $d(x, y) = |x - y|$ for all $x, y \in X$. Then (X, d) is a complete metric space. Assume that $T : X \to X$ and $\psi : [0, \infty) \to [0, \infty)$ are defined by

$$Tx = \begin{cases} \frac{x^2}{2}, & 0 \leq x < \frac{1}{2}, \\ \frac{1}{8x}, & x \geq \frac{1}{2}, \end{cases} \quad \text{and} \quad \psi(t) = \begin{cases} \frac{t}{2}, & 0 \leq t < 1, \\ \frac{1}{2}\sin\left(\frac{1}{2t-1}\right) + \frac{1}{2}, & t \geq 1. \end{cases}$$

Clearly, by the graph in Figure 2, we have $\psi \in \Psi$.

Now, we will show that the fixed point result of Boyd and Wong [3] can not be applied in this example. For any $x \in \left(0, \frac{1}{2}\right)$ and $y = \frac{1}{2}$, we obtain

$$d(Tx, Ty) = \left|\frac{x^2}{2} - \frac{1}{4}\right| = \frac{1}{4} - \frac{x^2}{2} > \frac{1}{4} - \frac{x}{2} = \left|\frac{x}{2} - \frac{1}{4}\right| = \psi\left(\left|x - \frac{1}{2}\right|\right) = \psi\left(d(x, y)\right).$$

Hence, T does not satisfy the Boyd and Wong's contractive condition. Also, the Banach contraction principle is not applicable, since T is not continuous at $\frac{1}{2}$.

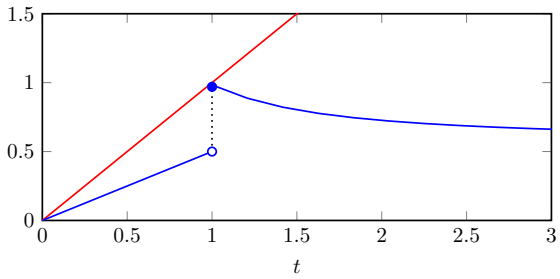

Figure 2: The graph of ψ in blue line

Next, we will show that Theorem 2.1 can be applied in this example. Let $\varphi : X \to [0,\infty)$ and $F : [0,\infty)^3 \to [0,\infty)$ be defined by

$$\varphi(x) = x, \quad x \in X \qquad \text{and} \quad F(a,b,c) = a + a^2 + b + c, \quad a,b,c \geq 0.$$

It is easy to see that $F \in \mathcal{F}$ and φ is lower semi-continuous. Now, we claim that the mapping T satisfies the contractive condition (2.1). Suppose that $x, y \in X$. We have to consider the following cases:

Case 1. If $(x,y) \in \left[0, \frac{1}{2}\right)^2$, then we get

$$\begin{aligned}
F(d(Tx,Ty),\varphi(Tx),\varphi(Ty)) &= d(Tx,Ty) + (d(Tx,Ty))^2 + \varphi(Tx) + \varphi(Ty) \\
&= |Tx - Ty| + |Tx - Ty|^2 + Tx + Ty \\
&= \frac{|x^2 - y^2|}{2} + \frac{|x^2 - y^2|^2}{4} + \frac{x^2}{2} + \frac{y^2}{2} \\
&= \frac{|(x+y)(x-y)|}{2} + \frac{|(x+y)(x-y)|^2}{4} + \frac{x^2}{2} + \frac{y^2}{2} \\
&\leq \frac{|x-y|}{2} + \frac{|x-y|^2}{2} + \frac{x}{2} + \frac{y}{2} \qquad (2.19) \\
&\leq \psi(|x-y| + |x-y|^2 + x + y) \\
&= \psi(d(x,y) + (d(x,y))^2 + \varphi(x) + \varphi(y)) \\
&= \psi(F(d(x,y),\varphi(x),\varphi(y))).
\end{aligned}$$

Case 2. If $(x,y) \in \left[\frac{1}{2},\infty\right)^2$, then we get

$$\begin{aligned} F(d(Tx,Ty),\varphi(Tx),\varphi(Ty)) &= d(Tx,Ty)+(d(Tx,Ty))^2+\varphi(Tx)+\varphi(Ty) \\ &= |Tx-Ty|+|Tx-Ty|^2+Tx+Ty \\ &= \left|\frac{1}{8x}-\frac{1}{8y}\right|+\left|\frac{1}{8x}-\frac{1}{8y}\right|^2+\frac{1}{8x}+\frac{1}{8y} \\ &< \frac{1}{2}\sin\left(\frac{1}{2(|x-y|+|x-y|^2+x+y)+1}\right)+\frac{9}{16} \\ &= \psi(|x-y|+|x-y|^2+x+y) \\ &= \psi(d(x,y)+(d(x,y))^2+\varphi(x)+\varphi(y)) \\ &= \psi(F(d(x,y),\varphi(x),\varphi(y))). \end{aligned} \tag{2.20}$$

Case 3. Let $(x,y) \in \left[0,\frac{1}{2}\right)\times\left[\frac{1}{2},\infty\right)\cup\left[\frac{1}{2},\infty\right)\times\left[0,\frac{1}{2}\right)$. Without loss of generality, we may assume that $x \in \left[0,\frac{1}{2}\right)$ and $y \in \left[\frac{1}{2},\infty\right)$ and so $|x-y|+|x-y|^2+x+y>1$, then

$$\begin{aligned} F(d(Tx,Ty),\varphi(Tx),\varphi(Ty)) &= d(Tx,Ty)+(d(Tx,Ty))^2+\varphi(Tx)+\varphi(Ty) \\ &= |Tx-Ty|+|Tx-Ty|^2+Tx+Ty \\ &= \left|\frac{x^2}{2}-\frac{1}{8y}\right|+\left|\frac{x^2}{2}-\frac{1}{8y}\right|^2+\frac{x^2}{2}+\frac{1}{8y} \\ &\leq \frac{1}{2}\sin\left(\frac{1}{2(|x-y|+|x-y|^2+x+y)+1}\right)+\frac{9}{16} \\ &= \psi(|x-y|+|x-y|^2+x+y) \\ &= \psi(d(x,y)+(d(x,y))^2+\varphi(x)+\varphi(y)) \\ &= \psi(F(d(x,y),\varphi(x),\varphi(y))). \end{aligned} \tag{2.21}$$

The validity of the conditions (2.19), (2.20) and (2.21) can be checked by plotting 3D surface in MATLAB, shown as Figure 3. Without loss of generality and for the sake of simplicity, we restrict the domain in Figure 3 to $[0,3]$. Therefore, all the required hypotheses of Theorem 2.1 are fulfilled, and so T has a unique φ-fixed point. In this case, the point 0 is a unique φ-fixed point of T.

Remark 2.3. If we take $\varphi(x)=0$ for all $x \in X$ in Theorem 2.1, then we get the real proper generalization of the Boyd and Wong fixed point theorem. However, if we take the same function φ in Theorem 1.6 and use $(F2^\star)$, we can see that the obtained result is equivalent to the Boyd and Wong fixed point theorem. This yields the advantage of our main result with the several results in the literature as shown in Figure 4.

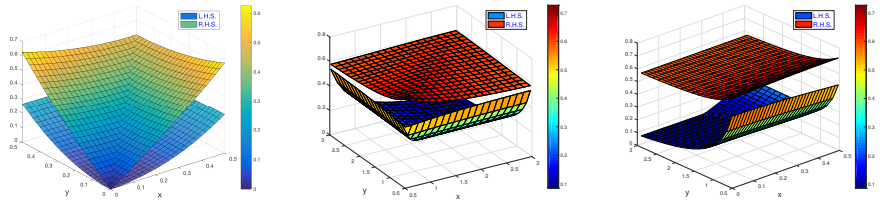

Figure 3: The value of the comparison of the L.H.S. and the R.H.S. of (2.19) and (2.21)

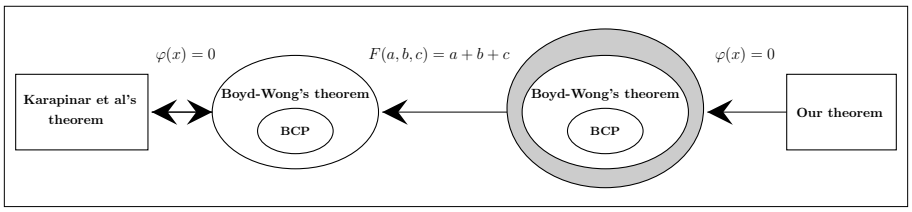

Figure 4: The difference of consequence between our theorem and Karapinar et al.'s theorem

3 Conclusions

Inspired by the problem of the relaxing of the hypothesis of the control function F in Theorem 1.6, we proposed a new technique for solving this problem. By the help of this suggested technique, our main theorem has the new proof, which seems to be simpler than the proof in [2]. The obtained result of this paper is a real proper generalization of the result in [1], and it also covers several famous fixed point results and φ-fixed point results in the literature. For the part of an application, we can use the main result in this work for applying in the homotopy result, and the fixed point results in partial metric spaces like the application in [2] since the class $\mathcal{F}$ is weaker than the class defined in [2].

Acknowledgement

This work was supported by Thammasat University Research Unit in Fixed Points and Optimization.

References

[1] Jleli M, Samet B, Vetro C (2014) Fixed point theory in partial metric spaces via φ-fixed point's concept in metric spaces. Journal of Inequalities and Applications, 2014(1):1-9.

[2] Karapinar E, O'Regan D, Samet B (2015) On the existence of fixed points that belong to the zero set of a certain function. Fixed Point Theory and Applications, 2015(1):1-14.

[3] Boyd DW, Wong JS (1969) On nonlinear contractions. Proceedings of the American Mathematical Society, 20:458-464.

Dynamical Analysis on Two Dose Vaccines in the Presence of Media

Payal Rana[1], Dinkar Jha[1], and Sudipa Chauhan*[1]

[1]Department Of Mathematics, Amity Institute Of Applied Science, Amity University , Sector 125 , Noida , INDIA

Abstract

The Covid-19 outbreak hit us as a serious health crisis with vaccination to be seen as the only way out of it. And media can play the role of an advocate to fight against this epidemic by spreading important awareness regarding various protocols and vaccination strategies. Since breakthrough infections are becoming highly common, a two dose vaccine regime may be the need of the hour even for individuals with a pre-existing illness to build better immunity. Thus in this paper, our aim is to analyse a mathematical model with two dose vaccination strategy in the presence of media and breakthrough infections. An SIV_1V_2R model is formulated and the dynamical analysis is done. The basic reproduction number is obtained and the local stability analysis of both the disease-free and endemic equilibrium point is discussed based on reproduction number. The global stability of the endemic equilibrium point is done by graph theoretic approach. Finally, the numerical validation of the analytic solution is done using MATLAB using the real data of India for some important parameters to address a few vital questions which involves the role of media on the vaccination strategy. And sensitive model parameters effecting the basic reproduction number and endemic equilibrium points are identified using sensitivity analysis techniques like PRCC(partial rank correlation coefficient). Thus, the outcomes demonstrated the trend a two-dose vaccine model can follow and how the effect of media can help bring down the infections. This model provides support that two dose vaccination against COVID-19 with media presence for awareness is highly effective in controlling this epidemic.

Keywords: Vaccine; Covid-19; Global Stability; Parameter Sensitivity

1 Introduction

Since the advancements in medication and technology particularly with the initiation of vaccination, there has been an improvement in the quality of life

in the age of infectious diseases. After the primary creation of vaccine by a doctor for pox from a live pox virus in 1796, in order to produce vaccines for alternative diseases several scientists and doctors followed his path as well. Many diseases are currently preventable like contagious disease, mumps, rubella, serum hepatitis, and respiratory illness due to the use of such vaccines[1, 2]. Due to the spread of SARS-CoV-2 virus, the COVID-19 outbreak was declared a pandemic and since then the development of COVID-19 vaccines has been the top priority of responsible stakeholders to control the outbreak. Afterwards with the availability of various types of vaccines to the world, the focus shifted to process of vaccination. There is an urgent need for the disbursement of vaccines to the general public so that the vaccines are effective to suppress the infection and in a very timely manner. Therefore, coming up with concerned strategies is crucial to the success of vaccination and control of epidemic as several of the vaccines need over one dose over a lifespan. Specially since the talk has now been shifted on the number of doses(one or two) [3], decisions regarding single or multi dose vaccines is a matter of great importance to avoid confusion among the general public.

1.1 Two-Dose Vaccine

For the ongoing Covid-19 epidemic, the often suggested vaccine strategy may be a two-dose program and even a booster dose in future[4, 5]. The second dose isn't thought of to be a booster vaccine but rather the use of this particular dose is with the aim to produce immunity to those that don't answer the primary dose. For example, more or less two to five of individuals don't develop immunity once the primary dose of the MMR(Measles, Mumps and Rubella) vaccine is given emphasising on the need of multi dose regime. Recently Covid-19 Vaccines have received emergency use authorization developed by Oxford-AstraZeneca, Pfizer-BioNTech and Moderna in different countries. Mass vaccination campaigns and clinical trials can provide high levels of protection against severe and symptomatic disease using 2 dose vaccines [6]. Due to a weak one-dose vaccine immunity in some vaccines, there could be short-term benefits where the virus may still continue to replicate [7]. This could eventually lead to immune escape mutations by the virus and thus a two-dose strategy may be able to mitigate this effect. Even for individuals who already have some existing illness, when co-infected with Covid may show better immunity when administered by two dose of vaccines than one dose vaccine as seen in the case of cancer patients in [8]. Multidose vaccines when compared to single-dose injection may offer a stronger protection against infection of the same vaccines and communication initiatives are needed to spread information about such regimes[9]. The ongoing discussions related to vaccination regimes are often led by media and influences the decision making of individuals.

1.2 Effect of media

The behavior of public with respect to vaccination may be altered due to involvement of media. People who may be infected may not come in contact with others because of the weakening effects due to their illness or due to the suggestions by public health organizations to quarantine to avoid infecting others. Hygienic measures may be taken up by general public to reduce the chance of getting infected and take steps to avoid large public gatherings. An example is of the 1994 outbreak of plague which presented with complex dynamics in a state in India [10]. After the outbreak of the disease many people in order to escape the disease fled the state of Surat and led to the transmission of the disease to other parts of the country. Thus, there is a need of proper discourse of information to the public. The media in particular greatly influences an individual's behavior toward a diseases and may also lead to interventions to control disease spread by governmental health care institutions. Awareness programs by media can make people comprehensive about a disease towards taking precautionary measures like wearing protective masks, social distancing and more importantly vaccination to suppress the chances of infection.

1.3 Empirical Literature and Structure of study

The most recent development in mathematical modelling in the field of biology or epidemic can be seen in [11, 12, 13, 14, 15]. There has been innumerable developments in mathematical modeling and numerical methods and its applications which is able to provide a better understanding and prediction for various types of systems like models depicting the relationship between computer viruses and epidemiology [16, 17, 18, 19, 20]. Mathematical models are able to provide a compatible understanding with the real-world dynamics of infection diseases. In order to exhibit the dynamics of Covid-19, there are many models available in the literatures for systems of nonlinear differential equations, making the models more realistic [21]. We have seen good researches in epidemic or infectious disease models[22, 23]. In [24], a deterministic model for Varicella Zoster Virus dynamics with vaccination is studied. Mathematical model on the outbreaks of influenza and to manage it by vaccination is discussed in [25]. A Dengue Epidemic model is considered amid vaccination in [26] and in [27] dynamic models is discussed with the importance of vaccination. And as of the recent Covid-19 outbreak some models with respect to vaccinations are discussed are discussed in [28, 29]. In [7] one dose regime is recommend if it produces a strong immune response. However, if a single vaccine dose is poor then the manufacturer recommended two-dose regime is suggested for a potential positive long term outcomes. Thus, a two dose vaccine Covid-19 model needs to be studies to understand its impact on the transmission of infection.

There may be some countries like the developing nations that may not be able to sustain a two-dose vaccination program for respiratory illness, and definitely would not be able to get funding for the multi-dose respiratory illness inoculation process. Thus, one needs to address the following questions: is it

doable to form one dose respiratory illness vaccination program that would replace a two-dose respiratory illness vaccination strategy? Is the involvement of media important in increasing vaccination process and reducing infection?. We shall aim to address these questions by developing a multi-dose vaccine model consisting of the susceptible, infected, vaccinated(First and second dose) and recovered (SIV_1V_2R) individuals in Section 2 and investigating the impact of media involvement to dispense information to the public. In section 3 the model dynamics are analyzed for the equilibrium point. We shall establish the local and global(graph theoretic method) for the endemic equilibrium. In Section 5 we will proceed with the numerical simulation where in we shall valid our results and understand the behaviour of our system. Under numerical discuss, we aim to find the sensitivity Indices of endemic equilibrium point to find the relevant parameters and their impact on the populations, followed by uncertainty analysis for the basic reproduction number to find important parameters related to transmission of infection in a two dose regime system. As part of our study, numerical discussion will help quantify the sensitivity index of the various parameters and give an insight to understand the effectiveness of the two dose regime and media to our variables and transmission of infection.
The novelty of our study is to encapsulate a two dose vaccination regime and the role of the media for a Covid-19 system and dynamically analysing thoroughly along with real data numerical validation.

2 The Model

The Model developed in this paper is motivated by the model by Kermack and McKendrick [30] which consists of the Susceptible, Infected and Removed (SIR) epidemiological class. SIR model was one of the revolutionary in its time but in present life with full of advanced technology, SIR model is one of the cornerstones of Mathematical Epidemiology. While assuming constant birth and death rate, SIR model divided the population into three different classes; Susceptible(S),Infected(I) and Recovered (R). The working of the SIR model can bee seen in Fig 1 for better understanding.

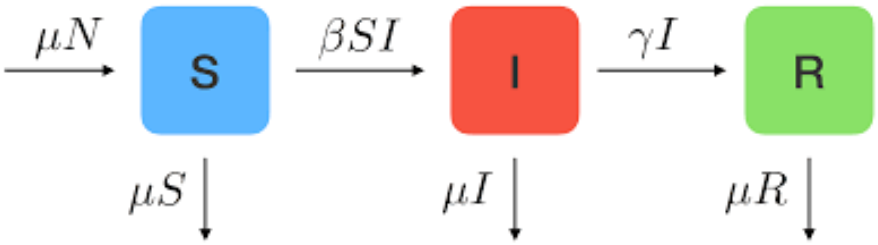

Figure 1: Flowchart of Model

The differential Equations for the basic **SIR** model is ans follows:

$$\frac{dS}{dt} = \mu N - \beta SI - \mu S$$
$$\frac{dI}{dt} = \beta SI - \gamma I - \mu I$$
$$\frac{dR}{dt} = \gamma I - \mu R.$$

A two-dose regime may be able to provide better immunity to the general public and even to those who have some pre-existing illness [8]. Thus with this as motivation, we have extended the paper by incorporating two new vaccinated classes V_1 and V_2 in reference to the current scenario of covid. The model assumptions are considered as follows:

- Only a fraction of susceptible population get vaccinated due to the rumours regarding vaccinations.
- The interaction between susceptible and infected classes follow Holling type-II functional response.
- The population can still join the susceptible class and be prone to getting infected after two doses. These kind of infections are termed as 'Breakthrough' infections [31, 32] and exist for all types of vaccines prescribed against SARS-COVID-2. Breakthrough infections can be attributed to occurrence of severe variants (such as the delta variant), low immune response to vaccination and traveling to places that are seeing significant surge in cases. But the infections are mild in nature and may not lead to hospitalisation.
- The natural recovery is also not permanent and they can still get reinfected as defined by Indian Council Of Medical Research (ICMR). ICMR defines this reinfection as occurrence of two positive tests at a gap of at least 102 days with one interim negative test [31] .

Therefore, in reference to the assumptions, the extended model SIV_1V_2R is given by,

$$\begin{aligned}
\frac{dS}{dt} &= (1-p)\mu N - \mu S - \frac{b_1 IS}{(1+\alpha I)} + \psi R \\
\frac{dI}{dt} &= \frac{b_1 IS}{(1+\alpha I)} - \mu I - \gamma I \\
\frac{dV_1}{dt} &= p\mu N - \mu V_1 - p_1 V_1 \\
\frac{dV_2}{dt} &= p_1 V_1 - \mu V_2 - p_2 V_2 \\
\frac{dR}{dt} &= \gamma I + p_2 V_2 - \mu R - \psi R.
\end{aligned} \tag{1}$$

The system is bounded in the region $\{S, I, V_1, V_2, R; S + I + V_1 + V_2 + R = N\}$.

Table 1: Table for Variables and Parameters

Variables and Parameters	**Interpretation**
S	Susceptible Individual Density
I	Infected Individual Density
R	Recovered Individual Density
V_1	Vaccinated Individual Density After 1st Dose
V_2	Vaccinated Individual Density After 2nd Dose
N	Total Population Density
μ	Birth and Death rate
p	Rate of First Dose of Vaccine
p_1	Rate of Second Dose of Vaccine
p_2	Rate at which Vaccinated Individuals get Recovered
b_1	Rate of Infection
γ	Rate at which Infected Individuals Recover/ Natural Recovery Rate
ψ	Rate at which Recovered Individuals get Susceptible Again
α	Effect of Media

The description of the parameters and variables can be seen in Table 1 for our system. We can see the mechanism graphically in the schematic diagram in Fig 2 for the proposed model.

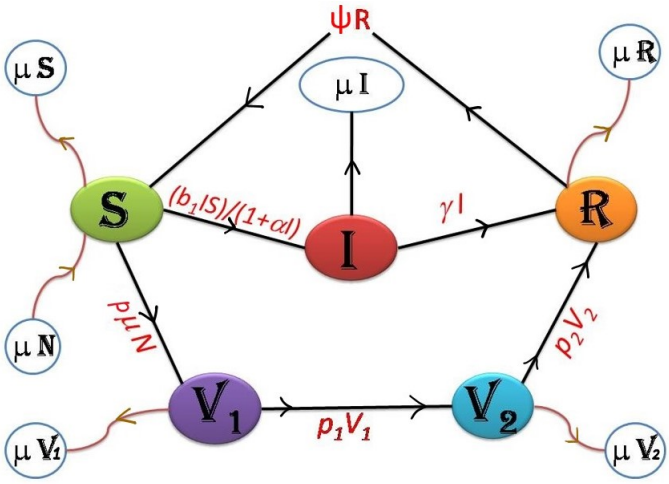

Figure 2: Schematic diagram of the SIV_1V_2R model. Susceptible individuals S can either move to the infected I or the vaccinated class V_1. At the rate of p, the susceptible who get vaccinated with the first dose will join vaccinated class V_1 . After recovering naturally the infected individuals join the recovered class R at the rate of γ. At the rate of p_1 individuals who receive the second dose of vaccination after getting the first dose will move towards the vaccinated class V_2. Individuals move towards the recovered class R at the rate of p_2 after receiving both the doses. Individuals from the recovered class R join back to the class of susceptible S at the rate of ψ owing to breakthrough infections/reinfections even after after getting vaccinated with both the doses or recovering from the infection naturally.

2.0.1 Questions Addressed by the Research Work

Our research takes a dig at the following unaddressed issues:

- Exploring the calibre of infected class response to complete vaccination. Can vaccination act as a lodestar to reduce infection ?
- The relation of media and pandemic. What is the role of media in infected and susceptible classes ?
- What is the degree of correlation, if there exist any, between the parametric values and the endemic equilibrium?.

3 Model Dynamics

3.1 Basic Reproduction Number

The basic reproduction number particularly for the study infectious diseased is considered a central concept and is the spectral radius of the next generation

method. For the dynamic analysis of any general disease transmission model, the basic reproduction number R_0 [33, 34] is a crucial element. The trend or behaviour of R_0 can give significant implications for upcoming outbreaks. It gives the number of secondary infections arising due to a single infection. In the system, if $R_0 > 1$ then the disease will continue and if $R_0 \leq 1$ then the disease will die out. To explore the impact of vaccination we will be dealing with $R_0 > 1$ when the infection is present in the system. R_0 can be written as,

$$R_0 = \frac{b_1 N}{(\mu + \gamma)}.$$

3.2 Existence of equilibrium points

Equilibrium points are the steady state solutions where the system may approach in the long run. Our analysis will be around the equilibrium points and its stability as it can help to study the system behaviour in long run in reference to multi-dose vaccination. Thus, we shall first obtain the equilibrium points and the conditions for their existence. Our main focus will be on disease-free equilibrium point and endemic equilibrium point [35]. The system (1) posses a disease free or boundary equilibrium point $E^0(S^0, 0, V_1^0, V_2^0, R^0)$ given by,

$$S^0 = \frac{(1-p)N(\mu+\psi)(\mu+p_1)(\mu+p_2) + pp_1p_2\psi N}{(\mu+\psi)(\mu+p_1)(\mu+p_2)}, \quad V_1^0 = \frac{p\mu N}{(\mu+p_1)}$$

$$V_2^0 = \frac{pp_1\mu N}{(\mu+p_1)(\mu+p_2)}, \quad R^0 = \frac{pp_1p_2\mu N}{(\mu+\psi)(\mu+p_1)(\mu+p_2)}.$$

Endemic or interior equilibrium point $E^*(S^*, I^*, V_1^*, V_2^*, R^*)$ for the system (1) is given by

$$S^* = \frac{(\mu+\gamma)(1+\alpha I^*)}{b_1} = \frac{(1+\alpha I^*)N}{R_0},$$

$$V_1^* = \frac{p\mu N}{(\mu+p_1)}, \quad V_2^* = \frac{pp_1\mu N}{(\mu+p_1)(\mu+p_2)},$$

$$I^* = \frac{\mu(\mu+\psi)(\mu+p_1)(\mu+p_2)[(1-p)Nb_1 - (\mu+\gamma)] + \psi b_1 pp_1p_2\mu N}{[(\mu+\psi)(\mu+\gamma)(\alpha\mu+b_1) - \psi b_1\gamma](\mu+p_1)(\mu+p_2)},$$

$$R^* = \frac{\gamma\mu(\mu+\psi)(\mu+p_1)(\mu+p_2)[(1-p)Nb_1 - (\mu+\gamma)] + \psi b_1 pp_1p_2\mu N\gamma + pp_1p_2\mu N[(\mu+\gamma)(\mu+\psi)(\alpha\mu+b_1-\psi b_1\gamma)]}{(\mu+\psi)(\mu+p_1)(\mu+p_2)[(\mu+\psi)(\mu+\gamma)(\alpha\mu+b_1) - \psi b_1\gamma]},$$

where the equilibria exists if $R_0 > \frac{1}{(1-p)}$ and $(\alpha\mu + b_1) > \psi b_1\gamma$.

We will now be analysing the stability of boundary and interior equilibrium points for the system (1).

3.3 Local Stability analysis

We shall prove the local stability for the model about the disease free and endemic equilibrium point to visualize the conditions under which the epidemic system can be stabilized [36]. General Jacobian matrix for our system is given by,

$$J = \begin{vmatrix} (-\mu - \frac{b_1 I}{1+\alpha I}) & -\frac{b_1 S}{(1+\alpha I)^2} & 0 & 0 & \psi \\ \frac{b_1 I}{(1+\alpha I)} & (\frac{b_1 S}{(1+\alpha I)^2} - \mu - \gamma) & 0 & 0 & 0 \\ 0 & 0 & (-\mu - p_1) & 0 & 0 \\ 0 & 0 & p_1 & (-\mu - p_2) & 0 \\ 0 & \gamma & 0 & p_2 & (-\mu - \psi). \end{vmatrix}$$

General characteristic equation pertaining to the jacobian matrix above is given by,

$$\left[\left(\mu + \frac{b_1 I}{1+\alpha I} + \lambda\right)\left(\frac{b_1 S}{(1+\alpha I)^2} - \mu - \gamma - \lambda\right)(\mu + p_1 + \lambda)(\mu + p_2 + \lambda)(\mu + \psi + \lambda)\right],$$

$$\left[\left(-\frac{b_1 I}{1+\alpha I}\right)\left(\frac{b_1 S}{(1+\alpha I)^2}\right)(\mu + p_1 + \lambda)(\mu + p_2 + \lambda)(\mu + \psi + \lambda)\right]\left[\left(\frac{b_1 I \gamma \psi}{1+\alpha I}\right)(\mu + p_1 + \lambda)(\mu + p_2 + \lambda)\right] = 0.$$

Characteristic equation pertaining to the boundary equilibrium point E^0 is given by,

$$(\mu + \lambda)(b_1 S^0 - \mu - \gamma - \lambda)(\mu + p_1 + \lambda)(\mu + p_2 + \lambda)(\mu + \psi + \lambda) = 0.$$

Eigen values corresponding to boundary equilibrium point E^0 are $\lambda_1 = -\mu, \lambda_2 = b_1 S^0 - (\mu + \gamma) < 0$ if $b_1 S^0 < (\mu + \gamma)$ or $R_0 < \frac{N}{S^0}, \lambda_3 = -(\mu + p_1), \lambda_4 = -(\mu + p_2), \lambda_5 = -(\mu + \psi)$. Consequently, E^0 is stable if $R_0 < \frac{N}{S^0}$. Next, the characteristic equation pertaining to interior equilibrium point $E^*(S^*, I^*, V_1^*, V_2^*, R^*)$ is given as follows:

$$\lambda^5 + a_1\lambda^4 + a_2\lambda^3 + a_3\lambda^2 + a_4\lambda + a_5 = 0,$$

where
$a_1 = 5\mu + \psi + p_1 + p_2 + \gamma + \frac{b_1 I}{1+\alpha I} - \frac{b_1 S}{(1+\alpha I)^2}$,
$a_2 = -(\mu + \frac{b_1 I}{1+\alpha I})(\frac{b_1 S}{(1+\alpha I)^2} - \mu - \gamma) + \frac{b_1^2 SI}{(1+\alpha I)^3} + (3\mu + \psi + p_1 + p_2)(2\mu + \gamma + \frac{b_1 I}{1+\alpha I} - \frac{b_1 S}{(1+\alpha I)^2}) + (\mu + \psi)(2\mu + p_1 + p_2) + (\mu + p_1)(\mu + p_2)$,
$a_3 = (3\mu+\psi+p_1+p_2)\{\frac{b_1^2 SI}{(1+\alpha I)^3} - (\mu + \frac{b_1 I}{1+\alpha I})(\frac{b_1 S}{(1+\alpha I)^2} - \mu - \gamma)\} + [(2\mu+p_1+p_2)(\mu+\psi) + (\mu+p_1)(\mu+p_2)][2\mu+\gamma+\frac{b_1 I}{1+\alpha I} - \frac{b_1 S}{(1+\alpha I)^2}] + (\mu+\psi)(\mu+p_1)(\mu+p_2) - \frac{b_1 I \psi \gamma}{1+\alpha I}$,
$a_4 = \{(2\mu + p_1 + p_2)(\mu + \psi) + (\mu + p_1)(\mu + p_2)\}\{\frac{b_1^2 SI}{(1+\alpha I)^3} - (\mu + \frac{b_1 I}{1+\alpha I})(\frac{b_1 S}{(1+\alpha I)^2} - \mu - \gamma)\} + (\mu + \psi)(\mu + p_1)(\mu + p_2)[2\mu + \gamma + \frac{b_1 I}{1+\alpha I} - \frac{b_1 S}{(1+\alpha I)^2}] - (2\mu + p_1 + p_2)\frac{b_1 I \psi \gamma}{1+\alpha I}$,
$a_5 = (\mu + \psi)(\mu + p_1)(\mu + p_2)[\frac{b_1^2 SI}{(1+\alpha I)^3} - (\mu + \frac{b_1 I}{1+\alpha I})(\frac{b_1 S}{(1+\alpha I)^2} - \mu - \gamma)] - (\mu + p_1)(\mu + p_2)\frac{b_1 I \psi \gamma}{1+\alpha I}$.
Thus, the endemic equiliria is locally stable according to Routh- Hurwitz criteria

if $a_i's > 0, i = 1, 2, 3, 4, 5$ under the following conditions: $I^*(1+\alpha I^*) > S^*$, $R_0 > \frac{N(1+\alpha I^*)^2}{S^*}$, $\frac{b_1^2 S^* I^*}{(1+\alpha I^*)^3} > (\mu + \frac{b_1 I^*}{1+\alpha I^*})(\frac{b_1 S^*}{(1+\alpha I^*)^2} - \mu - \gamma)$, $\frac{I^*}{1+\alpha I^*} < \frac{(\mu+\psi)(\mu+p_1)(\mu+p_2)}{b_1\psi\gamma}$, $(\mu+\psi)(\mu+p_1)(\mu+p_2)[2\mu+\gamma+\frac{b_1 I^*}{1+\alpha I^*} - \frac{b_1 S^*}{(1+\alpha I^*)^2}] > (2\mu+p_1+p_2)\frac{b_1 I^*\psi\gamma}{1+\alpha I^*}$ and $(\mu+\psi)[\frac{b_1^2 S^* I^*}{(1+\alpha I^*)^3} - (\mu + \frac{b_1 I^*}{1+\alpha I^*})(\frac{b_1 S^*}{(1+\alpha I^*)^2} - \mu - \gamma)] > \frac{b_1 I^*\psi\gamma}{1+\alpha I^*}$ along with $a_1a_2a_3 > a_3^2 + a_1^2 a_4$ and $(a_1a_4 - a_5)(a_1a_2a_3 - a_3^2 - a_1^2a_4) > a_5(a_1a_2 - a_3)^2 + a_5^2 a_1$.

4 Global stability

To establish global stability we shall use the graph-theoretic method as in [37, 38, 39]. We shall construct the lyapunov function through a directed graph with the help of the terminologies from [37]. To construct the lyapunov function we shall use a directed graph . A directed graph has a set of ordered pair say (i, j) and vertices where (i, j) is known as arc to terminal vertex j from initial vertex i. For the terminal vertex j, $d^-(j)$ is the in-degree of j which denotes the number of arcs in the digraph. And for initial vertex is i, $d^+(i)$ is the out-degree of vertex i which denotes the number of arcs in the digraph. Let us consider a weighted directed graph say $\chi(J)$ over a $q \times q$ weighted matrix J where the weights(a_{ij}) of each arc if they exist are $a_{ij} > 0$, and if otherwise then $a_{ij} = 0$. we consider c_i as the co-factor of l_{ij} of the Laplacian of $\chi(J)$ which is given by:

$$l_{ij} = \begin{cases} -a_{ij} & i \neq j \\ \sum_{k \neq i} a_{ij} & i = j. \end{cases}$$

If there is a strongly connected path i.e directed to and fro path for the arcs in $\chi(J)$ then $c_i > 0 \forall i = 1, 2..., q$. We shall also use Theorem 3.3 and Theorem 3.4 from [37, 39], which will help us in the construction of lyapunov function. The theorems states:

- **Theorem3.3 of [37]**: if $a_{ij} > 0$ and $d^-(i) = 1$, for some i, j, then

$$c_i a_{ij} = \sum_{k=1}^{q} c_j a_{jk}.$$

- **Theorem 3.4 of [37]**: if $a_{ij} > 0$ and $d^+(j) = 1$, for some i, j, then

$$c_i a_{ij} = \sum_{k=1}^{q} c_k a_{ki}.$$

We shall also use **Theorem 3.5** of [37] as below:

Theorem 4.1. *Let us consider an open set $L \subset R^m$ and a function $f : L \to R^m$ for a system*

$$\dot{z} = f(z) \tag{2}$$

and assuming:
a) $\exists$ $M_i : L \to R$, $H_{ij} : L \to R$ and $a_{ij} \geq 0$ such that

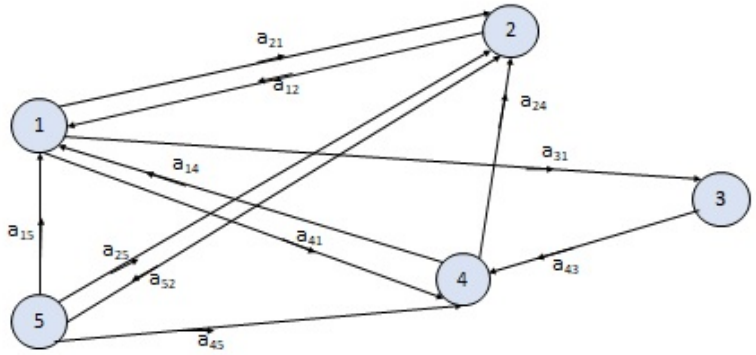

Figure 3: Directed graph for $\alpha = 1$ for the associated weights

$$M_i' = M_i'|_2 \leq \sum_{j=1}^{q} a_{ij} H_{ij}(z), \text{ with } z \in L,\ i = 1, \ldots, q.$$

b) For $J = [a_{ij}]$, of (H, J) each directed cycle B_c satisfies:

$$\sum_{(i,j)\in\epsilon(B_c)} H_{ij}(z) \leq 0\ ,\ z \in L$$

where $\epsilon(B_c)$ is set of arcs in B_c.
Then for $c_i \geq 0, i = 1, \ldots, q$ the function is:

$$M(z) = \sum_{i=1}^{q} c_i M_i(z)$$

satisfies $M'|_2 \leq 0$, that is, $M(z)$ is a Lyapunov function for 2.

4.1 Lyapunov Function Construction

Construction: $M_1 = \frac{(S-S^*)^2}{2}$, $M_2 = I - I^* - I^* \ln \frac{I}{I^*}$, $M_3 = \frac{(V_1-V_1^*)^2}{2}$, $M_4 = \frac{(V_2-V_2^*)^2}{2}$ and $M_5 = \frac{(R-R^*)^2}{2}$. Now by differentiation;
$M_1' = (S - S^*)S' \leq ((1-p)\mu N + \mu S^*)(S + V_2) + \frac{b_1 S^* IS}{(1+\alpha I)} + \psi RS = a_{14}H_{12} + a_{12}H_{12} + a_{15}H_{15}$ where $a_{14} = (1-p)\mu N + \mu S^*, a_{12} = b_1 S^*, a_{15} = \psi$.
$M_2' = (\frac{I-I^*}{I})I' \leq \frac{b_1 IS}{(1+\alpha I)} + (\mu+\gamma)I^*(I + V_2 + 1) = a_{21}H_{21} + a_{24}H_{24}$ where $a_{21} = b_1, a_{24} = (\mu+\gamma)I^*$.
$M_3' = (V_1 - V_1^*)V_1' \leq (p\mu N + \mu V_1^* + p_1 V_1^*)(V_1 + S) = a_{31}G_{31}$ where $a_{31} = (p\mu N + \mu V_1^* + p_1 V_1^*)$.
$M_4' = (V_2 - V_2^*)V_2' \leq p_1 V_1 V_2 + (\mu + p_2)(V_2 + S) = a_{43}G_{43} + a_{41}G_{41}$ where $a_{43} = p_1, a_{41} = (\mu + p_2)$.
$M_5' = (R-R^*)R' \leq \gamma IR + p_2 V_2 R + (\mu+\psi)(R+I) = a_{25}G_{25} + a_{45}G_{45} + a_{52}G_{52}$ where $a_{25} = \gamma, a_{45} = p_2, a_{52} = (\mu+\psi)$. We get an associated weighted directed graph as shown in Fig 3. Then by Theorem3.5[37] $\exists c_i's, 1 \leq i \leq 5$ such that $M = \sum_{i=1}^{q} c_i M_i$ is a lyapunov function. Using Theorem 3.3 and 3.4 we get the relation between c_i.

For $a_{31} > 0$ and $d^-(3) = 1$, we get $c_3a_{31} = c_4a_{43}$ and for $a_{52} > 0$ and $d^-(5) = 1$ we get $c_5a_{52} = c_1a_{15} + c_2a_{25} + c_4a_{45}$. Hence, $c_1 = c_4 = c_2 = 1$, $c_3 = \frac{a_{43}}{a_{31}}$ and $c_5 = \frac{a_{15}+a_{25}+a_{45}}{a_{52}}$. Thus, the lyapunov function is $M = M_1 + M_2 + \frac{p_1}{(p\mu N+\mu V_1^*+p_1V_1^*)}M_3 + M_4 + \frac{p_2+\gamma+\psi}{(\mu+\psi)}M_5$. And for M':
$M' = (S - S^*)S' + (\frac{I-I^*}{I})I' + \frac{p_1}{(p\mu N+\mu V_1^*+p_1V_1^*)}(V_1 - V_1^*)V_1' + (V_2 - V_2^*)V_2' + \frac{p_2+\gamma+\psi}{(\mu+\psi)}(R - R^*)R'$.
If we consider the set $U = \{x \in R_+^5 : M' = 0\}$ then we see that $S = S^*$, $V_1 = V_1^*$, $V_2 = V_2^*$, $I = I^*$ and $R = R^*$. Hence, we get the unique equilibrium point $(S^*, I^*, V_1^*, V_2^*, R^*)$. Therefore we say that the equilibrium point is globally stable using LaSalle's Invariance principle .

5 Numerical Simulation

In this section, we will discuss a numerical example in support of the analytic results of our system. We would try to encapsulate the sensitivity analysis of endemic equilibrium, global sensitivity analysis of basic reproduction number along with validation of our analytic solution for media effect. So, on computing

Parameters	Values/Units	Source
μ	0.0035342	Assumed
p	0.004545	https://www.mygov.in/covid-19
p_1	0.0001	https://www.mygov.in/covid-19
p_2	0.00909	https://www.mygov.in/covid-19
b_1	0.62	Assumed
γ	0.0476	Assumed
ψ	0.0011	https://www.mygov.in/covid-19
α	0.5	Assumed
N	140	Assumed

Table 2: Parameters and Values for SIV_1V_2R model

the values using the parameters (mentioned in Table 2 where some values taken from the mygov.in site on 15 june,2021.) in the system of equations and we'll get unique positive equilibrium at (SIV_1V_2R) resting at (0.3348, 6.0267, 16.8756, 1.5341 ,25.3862) as seen in Fig 4, giving a glimpse about the behaviour or the condition of epidemic in future. Now, if we focus on the effect of vaccination on other classes like Susceptible and Infected, then we get to know by graph that:

- From Fig 5a, graph to analyse the relation between susceptible and Vaccinated class(First dose). Here we can see that the susceptible individuals are constant with increase in the vaccination process but on further increasing the vaccination, the susceptible individuals are exponentially increasing. As more and more people get vaccinated then through word of mouth and more confidence build on the idea of vaccination, more susceptible people will be willing to get vaccinated.

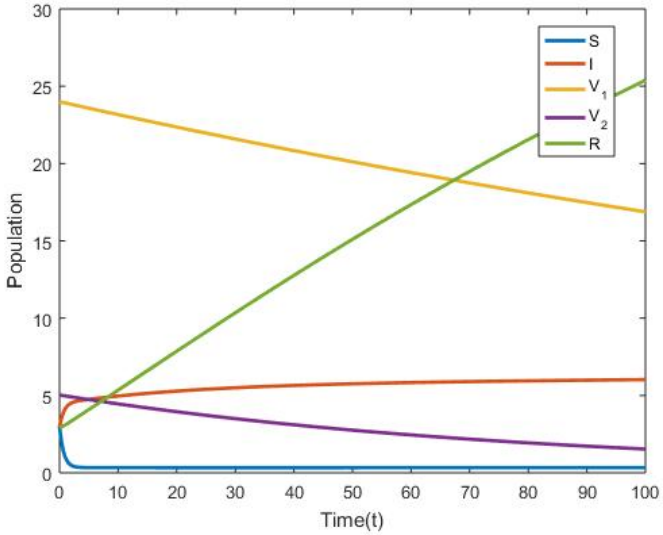

Figure 4: SIV_1V_2R Dynamic Graph

- Now by analysing the effect of complete(two dose) vaccination over infection rate (from Fig 5b), we get to know that the infectants goes on declining as individuals are getting vaccinated. This implies that two dose vaccination regime will help suppress transmission of infection and suppress the outbreak.

5.1 Sensitivity Indices of endemic equilibrium point

We shall now discuss the sensitivity analysis of equilibrium point with respect to the estimated parameters of our system. We aim to investigate the degree to which a parameter may affect the concerned variable through an affirmative relationship or a negative relationship through this process of parameter sensitivity analysis. We get the proportion that a relative change in a parameter brings to the relative change in a variable through the sensitivity index obtained. *Definition*[40, 41]: For the variable v that depends differentiably on a parameter h, we define the normalised forward sensitivity index Ω of a variable as:

$$\Omega_h^v = \frac{\partial v}{\partial h} \times \frac{h}{v}. \tag{3}$$

Thus, using the above method we get the sensitivity indices for each variable with respect to the parameters for endemic equilibrium as given in Table 3 and shown in Fig 6. For interpretation, if the index is positive it means that an increase in parameter will lead to the increase in the variable with the index value/magnitude. And a negative index implies that a increase in the parameter will lead to decrease in variable by the index value.

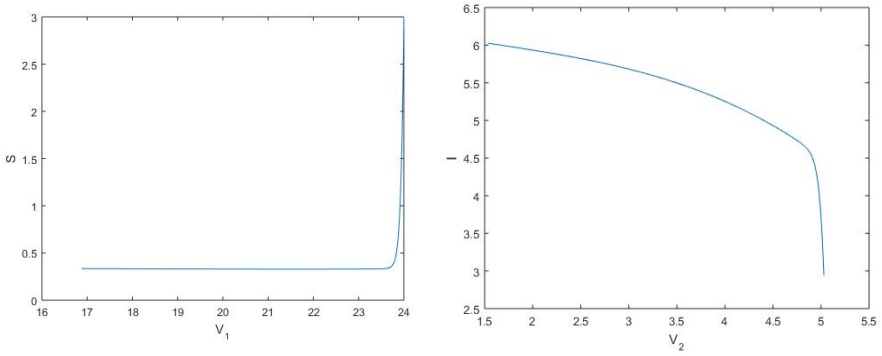

(a) Relation between Susceptible and Vaccinated classes

(b) Relation between Vaccinated and Infected classes

Figure 5: Relations with respect to Vaccinated class

-	S^*	I^*	V_1^*	V_2^*	R^*
p	-0.039	$-.0046$	1.1240	1.0837	-0.0096
α	-0.8494	0.0036	0	0	0.0042
p_1	$1.0794 * 10^{-4}$	$1.2664 * 10^{-4}$	-0.2222	0.7498	$6.6345 * 10^{-4}$
p_2	$3.9757 * 10^{-5}$	$4.7074 * 10^{-5}$	0	-0.7214	$2.4647 * 10^{-4}$
γ	0.1506	-0.9124	0	0	0.1019
μ	0.7197	0.7636	-0.7854	-1.0332	0.1196
ψ	0.1591	0.1867	0	0	-0.0219
N	0.8817	1.0461	1.1336	1.1475	1.2177
b_1	-0.9964	0.0042	0	0	0.0049

Table 3: Sensitivity indices, $\Omega_{h_j}^{v_i} = \frac{\partial v_i}{\partial h_j} * \frac{h_j}{v_i}$, of the state variables at the endemic equilibrium, v_i, to the parameters, h_j

5.2 Uncertainty analysis of R_0

For our model we shall also determine uncertainty analysis for R_0 by LHS method to get more validation for the relation between R_0 and its parameters. PRCC(partial rank correlation coefficient)[42] is one technique which will help us quantify the uncertainty for any model. We consider the four parameters from R_0 and have chosen normal distribution for them as in Fig 7. We find the PRCC values using Matlab with the following pdfs and shown in:
$b_1 \sim \quad Normal(0.62, 0.01)$,
$N \sim \quad Normal(140, 0.2)$,
$\gamma \sim \quad Normal(0.0476, 0.01)$,
$\mu \sim \quad Normal(0.0035342, 0.01)$.

We get the PRCC values for our input parameters which can be seen in Fig8. We get the following indexes for the parameters: $b_1 = 0.21, N = 0.26, \mu = -0.96$

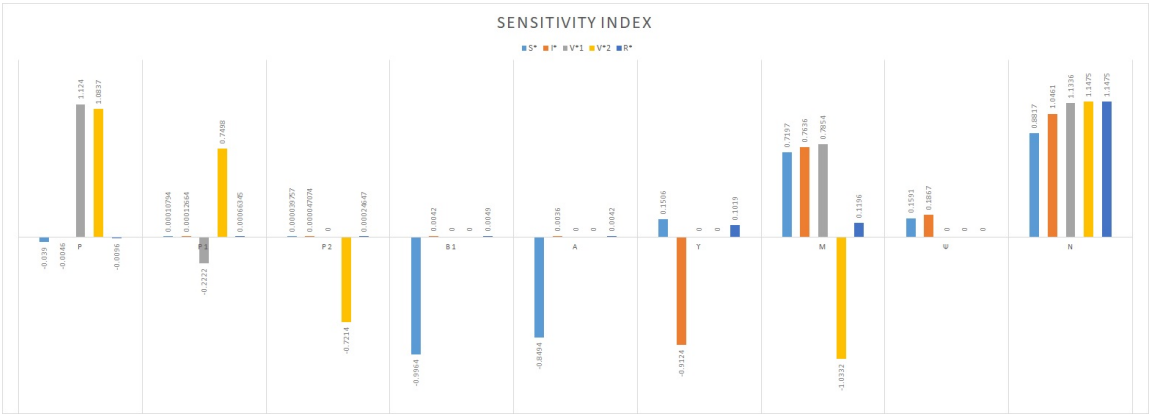

Figure 6: Bar graph for Sensitivity Index of $S^*, I^*, V_1^*, V_2^*, R^*$ with respect to the parameters

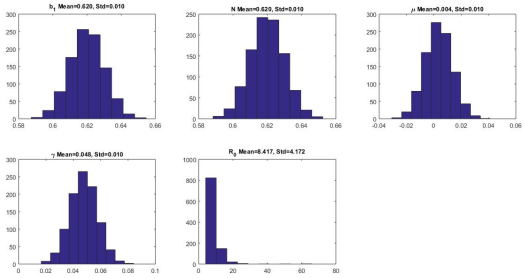

Figure 7: Distribution of parameters for R_0

and $\gamma = -0.96$. The graphs shows that R_0 is positively correlated to b_1 and N. The effect of the parameter μ and γ will bring about an opposite change in the transmission of infection as it is negatively correlated. Since the value μ and γ parameters are close to 1, it indicates a strong correlation to change in R_0. Thus, these two parameters are strongly negatively correlated to R_0.
We shall now check the contour plot for R_0 with respect to some combination of important parameters as in Fig 9. In Fig 9a we can see that the b_1 has a direct response to R_0, as the value of b_1 increases the gradation of color approaches to the highest color which is yellow. In a similar manner in Fig 9b we see that N too has direct response as we can see the color gradation approach yellow as N increases. And μ has a high indirect response to R_0, as the value of μ increases the gradation of color approaches to the lowest color which is dark blue and R_0 decreases.

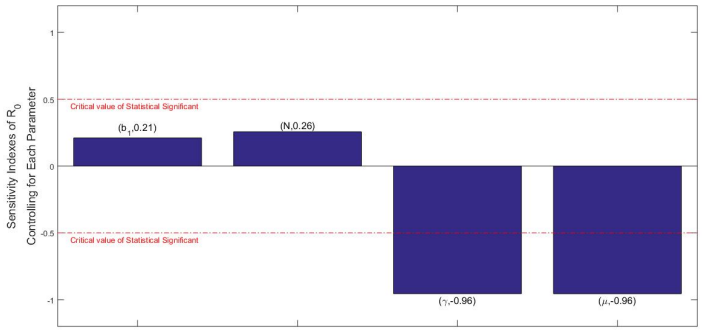

Figure 8: PRCC: input variables

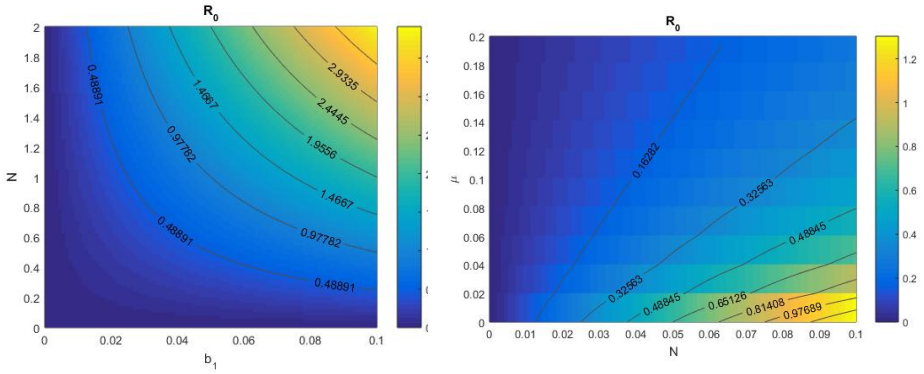

(a) (b)

Figure 9: Contour plots of ρ^0.

5.3 Media Effect (α) on Susceptible and Infected class

Media Effect helps in spreading awareness among people to stay safe from epidemic and has an ideal impact on the epidemic dynamics which can be seen through graph line when α is either at 0.5 or at 0 in the following:

- In Fig 10a, both values of α effect on susceptible population are shown. As the value of α increases, S also increases as now they will be less vulnerable to catching infection and avoiding decrease in S population. Thus, media will have a positive impact on S individuals as they get awareness of the implications of catching infections, advantages of vaccinations or protocols to follow to avoid risk of getting infected.

- We see in Fig 10b, that media causes a decreasing effect in infected class. Its shows that media effect plays an effective role in decreasing infection

and spreading awareness among population about the epidemic outbreak.

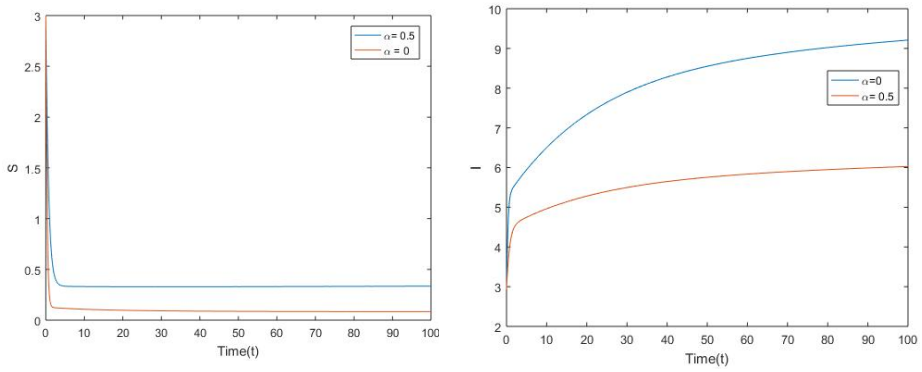

(a) Media effect on Susceptible class

(b) Media effect on Infected class

Figure 10: Media Effect

6 Conclusion

In this paper our aim is to completely analyze the model and be able to become answerable to all those question we aimed to address at the start of our study. As novelty we have studied a two dose vaccination regime and the role of the media for a Covid-19 system and dynamically analysed our system thoroughly along with real data numerical validation. We have looked up on the analysis of model and studied their steady states like Disease Free Equilibrium(DFE) and Endemic Equilibrium(EE). We also found their local stability by finding their eigen values and using Routh-Hurwitz Stability Criteria. In context to the endemic equilibria, global stability analysis of the system has been performed using the graph-theoretic method. For numerical analysis we have taken some real data from Government site of India as an example of Covid-19 to make graph on them thus to analyse the situation created. The incorporation of two dose vaccination regime in the system brings about a desirable outcome for reducing infection. Later we used sensitivity analysis technique to identify sensitive model parameters effecting the R_0 and endemic equilibrium point. It was able to provide us with the degree of positive or negative correlation with which each variable is bound to the parameters present in the model. We have performed Latin hypercube sampling method for our model to determine uncertainty analysis for R_0 to understand the role certain parameters play in the transmission of infection. We also showed the effective role media plays in spreading awareness among population and help reduce infection. Also it is understood that α (the effect of media) will bring down the infections and increase the susceptible population by offering subsequent protection by awareness.

Therefore, on analysing we have seen that without media effect there is no such great awareness among people because media is one of the important ways that makes a country united or be aware of the various protocols and regimes related to an outbreak. Also, a two dose vaccination regime may be the need of the hour to vanquish such an infectious diseases. *As the cases of breakthrough infections and co-infections of already existing ailments increase, so the application of a two dose vaccine regime along with media influence can help provide better immunity and suppress infections as seen in our results.* Thus, a two dose vaccination regime and the role of the media is of paramount importance in policy formation and execution for this deadly epidemic.

Conflict of interest

All authors declare no conflicts of interest in this paper.

References

[1] Ask the Experts: Diseases Vaccines. Diptheria, Tetanus, and Pertussis. Immunization Action Coalition. http://www.immunize.org/askexperts/experts per.asp.

[2] Vaccines and Immnuizations. Pertussis (Whooping Cough) Vaccine. Center for Disease Control and Prevention. http://www.cdc.gov/vaccines/vpdvac/pertussis/default.htm?s cid=cs 074.

[3] Hill, E. M., & Keeling, M. J., Comparison between one and two dose SARS-CoV-2 vaccine prioritisation for a fixed number of vaccine doses. medRxiv, (2021).

[4] Hethcote, H. W., Simulations of pertussis epidemiology in the United States: effects of adult booster vaccinations. Mathematical Biosciences, 158(1),47-73, (1999).

[5] Batty, C., Examining the Implications of a 7th Grade Pertussis Booster Program in the State of Ohio, Master's Thesis Dissertation, The Ohio State University 2013.

[6] Voysey M, Clemens SAC, Madhi SA, Weckx LY, Folegatti PM, Aley PK, et al. Safety and efficacy of the ChAdOx1 nCoV-19 vaccine (AZD1222) against SARS-CoV-2: an interim analysis of four randomised controlled trials in Brazil, South Africa, and the UK. Lancet., 397,99–111,(2021).

[7] Saad-Roy, C. M., Morris, S. E., Metcalf, C., Mina, M. J., Baker, R. E., Farrar, J., Holmes, E. C., Pybus, O. G., Graham, A. L., Levin, S. A., Grenfell, B. T., & Wagner, C. E. . Epidemiological and evolutionary considerations of

SARS-CoV-2 vaccine dosing regimes. Science (New York, N.Y.), 372(6540), 363–370,(2021).

[8] Monin, L., Laing, A.G., Muñoz-Ruiz, M., McKenzie, D.R., Del Barrio, I.D.M., Alaguthurai, T., Domingo-Vila, C., Hayday, T.S., Graham, C., Seow, J. & Abdul-Jawad, S., Safety and immunogenicity of one versus two doses of the COVID-19 vaccine BNT162b2 for patients with cancer: interim analysis of a prospective observational study. The Lancet Oncology,(2021).

[9] Crutcher, M., & Seidler, P. M., Maximizing Completion of the Two-Dose COVID-19 Vaccine Series with Aid from Infographics. Vaccines, 9(11), 1229,(2021), https://doi.org/10.3390/vaccines9111229.

[10] Ramalingaswami V. Psychosocial effects of the 1994 plague outbreak in Surat, India. Military Med. 166,29-30, (2001).

[11] Singh, J., Ganbari, B., Kumar, D., & Baleanu, D. Analysis of fractional model of guava for biological pest control with memory effect. Journal of Advanced Research, 32, 99-108,(2021).

[12] Singh, J., Analysis of fractional blood alcohol model with composite fractional derivative. Chaos, Solitons & Fractals, 140, 110127,(2020).

[13] Yadav, S., Kumar, D., Singh, J., & Baleanu, D., Analysis and dynamics of fractional order Covid-19 model with memory effect. Results in physics, 24, 104017,(2021).

[14] Danane, J., Hammouch, Z., Allali, K., Rashid, S., & Singh, J., A fractional-order model of coronavirus disease 2019 (COVID-19) with governmental action and individual reaction. Mathematical Methods in the Applied Sciences,(2021).

[15] Marco-Franco, J. E., Pita-Barros, P., González-de-Julián, S., Sabat, I., & Vivas-Consuelo, D., Simplified Mathematical Modelling of Uncertainty: Cost-Effectiveness of COVID-19 Vaccines in Spain. Mathematics, 9(5), 566, (2021).

[16] Dubey, V. P., Kumar, R., & Kumar, D., A reliable treatment of residual power series method for time-fractional Black–Scholes European option pricing equations. Physica A: Statistical Mechanics and its Applications, 533, 122040,(2019).

[17] Dubey, V. P., Kumar, R., & Kumar, D., A hybrid analytical scheme for the numerical computation of time fractional computer virus propagation model and its stability analysis. Chaos, Solitons & Fractals, 133, 109626,(2020).

[18] Dubey, V. P., Kumar, R., & Kumar, D., Numerical solution of time-fractional three-species food chain model arising in the realm of mathematical ecology. International Journal of Biomathematics, 13(02), 2050011, (2020).

[19] Dubey, V. P., Kumar, R., Singh, J., & Kumar, D., An efficient computational technique for time-fractional modified Degasperis-Procesi equation arising in propagation of nonlinear dispersive waves. Journal of Ocean Engineering and Science, 6(1), 30-39, (2021).

[20] Dubey, V. P., Dubey, S., Kumar, D., & Singh, J., A computational study of fractional model of atmospheric dynamics of carbon dioxide gas. Chaos, Solitons & Fractals, 142, 110375, (2021).

[21] Akman, O., Chauhan, S., Ghosh, A., Liesman, S., Michael, E., Mubayi, A., Perlin, R., Seshaiyer, P. & Tripathi, J.P., The Hard Lessons and Shifting Modeling Trends of COVID-19 Dynamics: Multiresolution Modeling Approach. Bulletin of Mathematical Biology, 84(1), 1-30,(2022).

[22] Edelstein-Keshet, L., Mathematical Models in Biology, SIAM, (2005).

[23] Siettos, C., Russo, L., Mathematical modeling of infectious disease dynamics, Virulence, 4(4), (2013).

[24] Edward, S. Modeling and Stability Analysis for a Varicella Zoster Virus Model with Vaccination. Applied and Computational Mathematics, 3(4), 150 ,(2014).

[25] Arino, J., Brauer, F., Driessche, P. V., Watmough, J., & Wu, J., Simple models for containment of a pandemic. Journal of The Royal Society Interface, 3(8), 453-457,(2006).

[26] Carvalho, S. A., Silva, S. O., & Charret, I. D. Mathematical modeling of dengue epidemic: Control methods and vaccination strategies. Theory in Biosciences, 138(2), 223-239,(2019).

[27] Gjini, E., & Gomes, M. G. Expanding vaccine efficacy estimation with dynamic models fitted to cross-sectional prevalence data post-licensure. Epidemics, 14, 71-82, (2016).

[28] Bubar, K. M., Kissler, S. M., Lipsitch, M., Cobey, S., Grad, Y. H., & Larremore, D. B. Model-informed COVID-19 vaccine prioritization strategies by age and serostatus, (2020).

[29] Iboi, E. A., Ngonghala, C. N., & Gumel, A. B., Will an imperfect vaccine curtail the COVID-19 pandemic in the U.S.?

[30] Kermack, W., McKendrick, A., 1927. A Contribution to the Mathematical Theory of Epidemics, Proceedings of the Royal Society of London A 115, 700–721, (2020).

[31] Coronavirus — ICMR study provides a new definition for SARS-CoV-2 reinfection, https://www.thehindu.com/sci-tech/science/icmr-study-provides-a-new-definition-for-sars-cov-2-re-infection/article34213132.ece.

[32] COVID-19 Vaccine Breakthrough Case Investigation and Reporting, https://www.cdc.gov/vaccines/covid-19/health-departments/breakthrough-cases.html.

[33] Van den Driessche P., Watmough J. Reproduction Numbers and Sub-Threshold endemic Equilibria for Compartmental Models of Disease Transmission. Mathematical Biosciences. 180(1-2), 29-48, (2002).

[34] Kretzschmar, M., Teunis, P., Pebody, R., Incidence and Reproduction Numbers of Pertussis: Estimates from Serological and Social Contact Data in Five European Countries. PLOS Medicine. 7(6),1-10,(2010).

[35] Chauhan, S., Misra, O. P., & Dhar, J., Stability analysis of SIR model with vaccination. American journal of computational and applied mathematics, 4(1), 17-23, (2014).

[36] Barik, M., Chauhan, S., & Bhatia, S. K., Efficacy of pulse vaccination over constant vaccination in COVID-19: a dynamical analysis. Commun. Math. Biol. Neurosci., (2020).

[37] Shuai Z , Driessche , P V D, Global Stability of Infectious Disease Models Using Lyapunov Functions *SIAM Journal on Applied Mathematics* 73,1513-1532, (2013).

[38] Guo H , Li M Y , Shuai Z, A graph-theoretic approach to the method of global Lyapunov functions *Proceedings of the American Mathematical Society*, 136,2793–2802, (2008).

[39] Bessey, K. , Mavis, M. , Rebaza, J. , Zhang, J., Global stability analysis of a general model of zika virus *Non autonomous Dynamical Systems* 6, 18–34, (2019).

[40] Berhe, H. W., Makinde, O. D., & Theuri, D. M., Parameter Estimation and Sensitivity Analysis of Dysentery Diarrhea Epidemic Model. Journal of Applied Mathematics, 2019, 1–13, (2019), doi: 10.1155/2019/8465747.

[41] Chitnis, N., Hyman, J. M., & Cushing, J. M., Determining Important Parameters in the Spread of Malaria Through the Sensitivity Analysis of a Mathematical Model. Bulletin of Mathematical Biology, 70(5), 1272–1296, (2008), doi: 10.1007/s11538-008-9299-0.

[42] S. Marino, I. B. Hogue, C. J. Ray, and D. E. Kirschner. A methodology forperforming global uncertainty and sensitivity analysis in systems biology.Journal of Theoretical Biology, 254(1):178–196, (2008).

Certain problems in ordered partial metric space using mixed g-monotone

Richa Sharma[1], Virendra Singh Chauhan[2] and Garima Agarwal[3]

December 23, 2021

Abstract

Motivated from the fixed point hypothesis, we demonstrate the presence and uniqueness for coupled coincidence type point including a contractive condition for a map in partially metric utilizing mixed g-monotone. A model is likewise outfitted to exhibit the legitimacy of the speculations of our outcomes.

Key words: Complete Metric Space; Coupled Fixed Point; mixed g-monotone property

Mathematics Subject Classification(2010): 54H25; 47H10

1

1 Introduction

A different idea of generalized metric space perceived as partial metric space offered by Matthews [6]. Many authors had given imperative results on such type of spaces [8, 9, 10].

Bhaskar and Lakshmikantam [2] established coupled fixed point and demonstrated certain coupled fixed point results for maps which gratify the property of mixed monotone. Also, present applications for periodic boundary value problem. Authors have extended numerous outcomes on coupled fixed point hypotheses on metric spaces, e.g., in [1, 2, 3, 4, 5, 7, 11].

We foremost verify the presence of coupled coincidence points. Then, we demonstrate uniqueness of coupled coincidence point results for a map having the property of mixed g-monotone in partial metric spaces. At the end we support the result by giving an example.

[1]Corresponding author: [2]Virendra Singh Chouhan,
[1]Department of Mathematics, Chandigarh University, Mohali(India),
Email- richa.tuknait@yahoo.in,
[2,3]Department of Mathematics and Statistics, Manipal University Jaipur (India),
[2]Email-darbarvsingh@yahoo.com(Corresponding Author)
[3]Email-garima.agarwal@jaipur.manipal.edu

The view of partial metric spaces given by Matthews [6].

Definition 2.1. [6] Presuppose Z be a null set. A partial metric on Z defines as a function $p : Z \times Z \to \mathbb{R}_n$ for every $s, t, z \in Z$:

$$(1) \quad s = t \iff p(s,s) = p(s,t) = p(t,t)$$
$$(2) \quad p(s,s) \leq p(s,t),$$
$$(3) \quad p(s,t) = p(t,s)$$
$$(4) \quad p(s,t) \leq p(s,t) + p(z,t) - p(z,z)$$

A pair (Z,p) known as partial metric space, and p is partial metric on Z where, Z is a null set.

If p is a partial metric on Z, the function $p^r : Z \times Z \to \mathbb{R}_+$ defined as

$$p^r(s,t) = 2\, p(s,t) - p(s,s) - p(t,t)$$

is a metric on Z.

The prevailing definitions given by [2].

Definition 2.2. [2] A point $(s,v) \in Z \times Z$ for a map $T : Z \times Z \to Z$ possesses $T(s,v) = s, T(v,s) = h$ then it is known as coupled fixed point.

Definition 2.3. [4] Assume $(S, \leq)$ is partially ordered set, let two mappings $F : S \times S \to S$ and $g : S \to S$. Then F possesses property of the mixed g-monotone if $F(s,w)$ is g-non-decreasing in its starting element and is g-non-increasing in its next element, for $s, w \in S$

$$s_1, s_2 \in S, gs_1 \leq gs_2 \implies F(s_1, w) \leq F(s_2, w)$$
$$w_1, w_2 \in S, gw_1 \leq gw_2 \implies F(s, w_1) \geq F(s, w_2).$$

2 Main Theorem

Theorem 2.1. *Presuppose $(Z, \leq, p)$ be a complete partially ordered set. Presuppose mappings $T : Z \times Z \to Z$ and $g : Z \to Z$ possesses property of mixed g-monotone. Presuppose $T(Z \times Z) \subseteq g(Z)$ and for any $s_0, v_0 \in Z$ with $gs_0 \leq T(s_0, v_0)$ and $gv_0 \geq T(v_0, s_0)$*

$$\begin{aligned} p(T(s,v), T(u,z)) \leq\ & p(gs, gu) - \psi(p(gv, gz)) \\ & + L\ min\{p(gs, T(s,v)), p(gu, T(u,z)), \\ & p(gu, T(s,v)), p(gs, T(u,z))\}. \end{aligned} \tag{2.1}$$

for every $s, u, v, z \in Z$ with $gs \geq gu$, $gv \leq gz$, and $L \geq 0$. Here ψ : [0,∞)→[0,∞) is a map which is non-decreasing, continuous and non-negative in (0,∞), $\psi(0) = 0$ and $\lim_{t\to\infty} \psi(t) = \infty$. Presuppose either Z has the subsequent properties or T is continuous.

1. *If a decreasing sequence $\{v_m\} \to Z$, therefore $gv_m \geq v$ for every m.*
2. *If an increasing sequence $\{s_m\} \to Z$, therefore $gs_m \leq s$ for every m.*

Then T and g possesses coupled coincidence point.

Proof. Presuppose $s_0, v_0 \in Z$ such that $gs_0 \leq T(s_0, v_0)$ and $gv_0 \geq T(v_0, s_0)$. Since $T(Z \times Z) \subseteq g(Z)$, select $s_1, v_1 \in Z$ thus $gs_1 = T(s_0, v_0)$ and $gv_1 = T(v_0, z_0)$.

Again, take $s_2, v_2 \in Z$ such that $gs_2 = T(s_1, v_1)$ and $gv_2 = T(v_1, s_1)$. As T possesses the property of mixed g- monotone, we have $gs_0 \leq gs_1 \leq gs_2$ and $gv_2 \leq gv_1 \leq gv_0$. Persistent the same procedure, we can create $\{z_m\}$ and $\{v_m\}$ in Z such that

$$gs_m = T(s_{m-1}, v_{m-1}) \leq gs_{m+1} = T(s_m, v_m)$$

and

$$gv_{m+1} = T(v_m, s_m) \leq gv_m = T(v_{m-1}, s_{m-1}).$$

If, for some integer m, we have $(gs_{m+1}, gv_{m+1}) = (gs_m, gv_m)$, then $T(s_m, v_m) = gs_m$ and $T(v_m, s_m) = gv_m$,thus T and g has a coincidence point (s_m, v_m).
We presume that $(gs_{m+1}, gv_{m+1}) \neq (gs_m, gv_m)$ for all $m \in \mathbb{N}$, that is, we assume that either $gs_{m+1} \neq gs_m$ or $gv_{m+1} \neq gv_m$. we have,

$$\begin{aligned} p(gs_{m+1}, gs_m) &= p(T(s_m, v_m), T(s_{m-1}, v_{m-1})) \\ &\leq p(gs_m, gs_{m-1}) - \psi(p(gv_m, gv_{m-1})) \\ &+ L\ min\{p(gs_m, T(s_m, v_m)), p(gs_{m-1}, T(s_{m-1}, v_{m-1})), \\ &\qquad p(gs_m, T(gs_{m-1}, v_{m-1})), p(gs_{m-1}, T(s_m, v_m))\} \\ &= p(gs_m, gs_{m-1}) - \psi(p(gv_m, gv_{m-1})) \end{aligned} \tag{2.2}$$

similarly,

$$p(gv_{m+1}, gv_m) \leq p(gv_m, gv_{m-1}) - \psi(p(gs_m, gs_{m-1})) \tag{2.3}$$

Let $\delta_m = p(gs_{m+1}, gs_m) + p(gv_{m+1}, gv_m)$.
Add (2) and (3), we have

$$\delta_m \leq \delta_{m-1} - \psi(\delta_{m-1}) \tag{2.4}$$

If $\exists m_1 \in N^*$ s.t. $p(gs_{m_1}, gs_{m_1-1}) = 0, p(gv_{m_1}, gv_{m_1-1}) = 0$, then $gs_{m_1-1} = gs_{m_1} = T(gs_{m_1-1}, gv_{m_1-1}); gv_{m_1-1} = gv_{m_1} = T(gv_{m_1}, gs_{m_1-1})$ and T has coupled coincidence point and the evidence is done. In other case $p(gs_{m+1}, gs_m) \neq 0$; $p(gv_{m+1}, gv_m) \neq 0$ for every $m \in \mathbb{N}$. At that point utilizing presumption on ψ , we get

$$\delta_m \leq \delta_{m-1} - \psi(\delta_{m-1}) \leq \delta_{m-1} \tag{2.5}$$

δ_m is a positive sequence and possesses a limit δ^*. Take limit $m \to \infty$, we have

$$\delta^* \leq \delta^* - \psi(\delta^*)$$

Thus $\psi(\delta^*) = 0$, utilizing supposition on ψ , we accomplished $\delta^* = 0$, ie. $\lim_{m\to\infty}(\delta_m) = 0$

$$\lim_{m\to\infty} p(s_{m+1}, s_m) + p(v_{m+1}, v_m) = 0$$
$$\implies \lim_{m\to\infty} p(s_{m+1}, s_m) = \lim_{m\to\infty} p(v_{m+1}, v_m) = 0 \tag{2.6}$$

We will show that $\{gs_m\}$, $\{gv_m\}$ are Cauchy groupings in Z. Assume that in any event one $\{gs_m\}$ or $\{gv_m\}$ be not a Cauchy sequence. At that point there exists $\epsilon > 0$ and two subsequence $m_k > n_k \geq k$ such that

$$r_k = p(gs_{m_k}, gs_{n_k}) + p(gv_{m_k}, gv_{n_k}) \geq \epsilon, \tag{2.7}$$

$\forall\ k = 1, 2, 3, \ldots$. Further, relating to n_k, select m_k such that it is smallest integer $m_k > n_k \geq k$ gratify (2.7), we have

$$p(gs_{m_k}, gs_{n_k}) + p(gv_{m_k}, gv_{n_k}) < \epsilon. \tag{2.8}$$

Using triangle inequality and (2.7) and (2.8), we get

$$\begin{aligned}\epsilon \leq r_k &= p(gs_{m_k}, gs_{n_k}) + p(gv_{m_k}, gv_{n_k}) \\ &\leq p(gs_{m_k}, gs_{n-1_k}) + p(gs_{n-1_k}, gs_{n_k}) + p(gv_{m_k}, gv_{n-1_k}), p(gv_{n-1_k}, gv_{n_k}) \\ &< \epsilon + \delta_{m_{k-1}}\end{aligned}$$

Let $k \to \infty$ and taking equation (2.6), we have $\lim_{n,m\to\infty} r_k = \epsilon > 0$.
Now, we get

$$\begin{aligned}p(gs_{m_{k+1}}, gs_{n_{k+1}}) &= p(T(gs_{m_k}, gv_{m_k}), T(gs_{n_k}, gv_{n_k})) \\ &\leq p(gs_{m_k}, gs_{n_k}) - \psi(p(gv_{m_k}, gv_{n_k}) + L\ min\{p(gs_{m_k}, T(gs_{m_k}, gv_{m_k})), p(gs_{n_k}, T(gs_{n_k}, gv_{n_k})), \\ &\qquad p(gs_{n_k}, T(gs_{n_k}, gv_{n_k})), p(gs_{m_k}, T(gs_{m_k}, gv_{m_k}))\} \\ &\leq p(gs_{m_k}, gs_{n_k}) - \psi(p(gv_{m_k}, gv_{n_k}).\end{aligned} \tag{2.9}$$

Similarly,

$$p(gv_{m_{k+1}}, gv_{n_{k+1}}) \leq p(gv_{m_k}, gv_{n_k}) - \psi(p(gs_{m_k}, gs_{n_k}). \tag{2.10}$$

Using (2.9) and (2.10), we get

$$r_{k+1} \leq r_k - \psi(r_k) \tag{2.11}$$

$\forall\ k \in 1, 2, 3, \ldots$ take $k \to \infty$ in equation (11).

$$\epsilon = \lim_{k\to\infty} r_{k+1} \leq \lim_{k\to\infty} [r_k - \psi(r_k)] < \epsilon. \tag{2.12}$$

a contraction. Thus $\{gs_m\}$ and $\{gv_m\}$ are Cauchy sequence.
Using lemma, $\{gs_m\}$ and $\{gv_m\}$ are Cauchy sequence in (Z, p^t). As, (Z, p) is complete, thus (Z, p^t) is complete, so $\exists\ s, v \in Z$
$\lim_{m\to\infty} p^t(gs_m, s) = \lim_{m\to\infty} p^t(v_m, v) = 0$
By lemma, we get

$$p(s,s) = \lim_{m\to\infty} p(gs_m, s) = \lim_{m\to\infty} p(gs_m, gs_m)$$
$$p(v,v) = \lim_{m\to\infty} p(gv_m, v) = \lim_{m\to\infty} p(gv_m, gv_m)$$

By condition and equation we get $\lim_{m\to\infty} p(gs_m, gs_m) = 0$.
Thus follows as $p(u,u) = \lim_{m\to\infty} p(gs_m, u) = \lim_{m\to\infty} p(gs_m, gs_m) = 0$, similarly $p(v,v) = \lim_{m\to\infty} p(gv_m, v) = \lim_{m\to\infty} p(gv_m, gv_m) = 0$
We now prove that$T(s,v) = s, T(v,s) = v$.

Case1: As Z is a complete, $\exists\ s, v \in Z$
$\lim_{m\to\infty} s_m = s, \lim_{m\to\infty} v = v$ we prove that (s,v) is coupled coincidence point of T and g.

$$\begin{aligned} s &= \lim_{m\to\infty} gs_{m+1} = \lim_{n\to\infty} T(s_m, v_m) = T(\lim_{m\to\infty} s_m, \lim_{m\to\infty} v_m) \\ v &= \lim_{m\to\infty} gv_{m+1} = \lim_{m\to\infty} T(v_m, s_m) = T(\lim_{m\to\infty} v_m, \lim_{m\to\infty} s_m) \end{aligned} \tag{2.13}$$

As g is continuous, we attain

$$\lim_{m\to\infty} g(gs_m) = gs,\ \lim_{m\to\infty} g(gv_m) = gv. \tag{2.14}$$

Commutativity of T and g gives

$$\begin{aligned} g(gs_{m+1}) &= g(T(s_m, v_m)) = T(gs_m, gv_m) \\ g(gv_{m+1}) &= g(T(v_m, s_m)) = T(gv_m, gs_m). \end{aligned} \tag{2.15}$$

By continuity of T, $\{g(gs_{m+1})\}$ is converges to $T(s,v)$ and $\{g(gv_{m+1})\}$ converges to $T(v,z)$. From uniqueness of the limit and (2.14), we accomplish $T(s,v) = gs$ and $T(v,s) = gv$, consequently, T and g possesses a coupled incident point.
Case2: Presuppose that the condition (a) and (b) of the result holds.
The sequence $\{gs_m\} \to s$, $\{gv_m\} \to v$

$$\begin{aligned} p(T(s,v), gs) &\le p(T(s,v), gs_{m+1}) + p(gs_{m+1}, gs) \\ &= p(T(s,v), T(s_m, v_m)) + p(gs_{m+1}, gs) \\ &\le p(gs, gs_m) - \psi(p(gv, gv_m)) \\ &+ L\ min\{p(gs, T(s,v)), p(gs_m, T(s_m, v_m)), p(gs_m, T(s,v)), p(gs, T(s_m, v_m))\} + p(gs_{m+1}, gs) \end{aligned}$$

Letting $m\to\infty$, we have $p(T(s,v), s) \le 0$
Thus $T(s,v) = s$, correspondingly, in similar way we can prove that $T(v,s) = v$. □

Theorem 2.2. *Presuppose the assumptions of Theorem 3.1 hold. Presuppose there exists $z \in Z$ which is comparable to s and v for every $s, v \in Z$. Thus T and g possesses only one coupled coincidence point.*

Proof. Succeeding the proof of Theorem 3.1, the arrangement of coupled coincidence points of T and g is non-empty. We will prove that coupled coincidence

points are (s, v) and $(\acute{s}, \acute{v})$, then

$$g(s) = T(s, v),\ g(v) = T(v, s)$$
$$\text{and } g(\acute{s}) = T(\acute{s}, \acute{v}),\ g(\acute{v}) = T(\acute{v}, \acute{s}),$$

then

$$gs = g\acute{s} \text{ and } gv = g\acute{v}. \tag{2.16}$$

Select $(d, z) \in Z \times Z$ comparable with both.

Let $d_0 = d, z_0 = z$ and choose $d_1, z_1 \in Z$ so that $gd_1 = T(d_0, z_0)$ and $gz_1 = T(z_0, d_0)$.

Then, similarly to the evidence of Theorem 3.1, we can inductively define sequences $\{gd_m\}$ and $\{gz_m\}$ as follows

$$gd_{m+1} = T(d_m, z_m) \ \ and \ \ gz_{m+1} = T(z_m, d_m).$$

Since $(gs, gv) = (T(s, v), T(v, s))$ and $(T(d, z), T(z, d)) = (gd_1, gz_1)$ are comparable, then $gs \leq gd_1$ and $gv \geq gz_1$. It is easy to prove using the mathematical induction,

$$gs \leq gd_m \ \ gv \geq gz_m \ \ \forall\ m \in \mathbb{N}.$$

Now, from the contractive condition (1)

$$\begin{aligned} p(gs, gs_{m+1}) &= p(T(s, v), T(s_m, v_m)) \\ &\leq p(gs, gs_m) - \psi(p(gv, gv_m)) \\ &\quad + L\ min\{p(gs, T(s, v)), p(gs_m, T(s_m, v_m)), p(gs_m, T(s, v)), p(gs, T(s_m, v_m))\} \\ &\leq p(gs, gs_m) - \psi(p(gv, gv_m)) \end{aligned} \tag{2.17}$$

Similarly

$$p(gv, gv_{m+1}) = p(gv, gv_m) - \psi(p(gs, gs_m)) \tag{2.18}$$

Adding (2.17) and (2.18), we get

$$p(gs, gs_{m+1}) + p(gv, gv_{m+1}) \leq p(gs, gs_m) + p(gv, gv_m) - [\psi(p(gv, gv_m)) + \psi(p(gs, gs_m))] \tag{2.19}$$

This implies

$$p(gs, gs_{m+1}) + p(gv, gv_{m+1}) \leq p(gs, gs_m) + p(gv, gv_m) \tag{2.20}$$

Thus, the sequence is non-increasing. hence, there exist $\alpha \geq 0$.

$$\lim_{m \to \infty} p(gs, gs_m) + p(gv, gv_m) = \alpha \tag{2.21}$$

We shall prove that $\alpha = 0$. Presuppose in contrary, $\alpha > 0$. Take $m \to \infty$ in equation (2.21), we have

$$\alpha \leq \alpha - \psi(\alpha) < \alpha \tag{2.22}$$

a contradiction. Therefore, $\alpha = 0$, that is

$$\lim_{m\to\infty} p(gs, gs_m) + p(gv, gv_m) = 0.$$

It implies

$$\lim_{m\to\infty} p(gs, gs_m) = \lim_{m\to\infty} p(gv, gv_m) = 0.$$

Similarly, we can prove

$$\lim_{m\to\infty} p(g\acute{s}, gs_m) = \lim_{m\to\infty} p(g\acute{v}, gv_m) = 0.$$

From last equalities, we have $gs = g\acute{s}$ and $gv = g\acute{v}$. □

Example 2.3. Presume $Z = [0, 1]$ with usual partial metric p defined as $p : Z \times Z \to$ [0,1] with $p(s, v) = max(s, v)$. The (Z, p) is complete partial metric space for any $s, v \in Z$.

$$p(s, v) = |s - v|$$

Thus (Z, p^t) is complete Euclidean metric space.
Presume the mapping $T : Z \times Z \to Z$ given as $T(s, v) = \frac{2s-v}{4}; s \geq v$

Take $\psi : [0, \infty) \to [0, \infty)$ such that $\psi(t) = \frac{t}{4}$

As, T has the property of mixed g-monotone property and is continuous.
Now, we discuss the following possibilities for (s, v) and (u, z) with $gs \leq gu,\ gv \geq gz$

Case 1- If $(s, v) = (u, z) = (0, 0)$
Then clearly $p(T(s, v), T(u, z)) = 0$
Thus (1) holds.
Case 2- If $(s, v) = (u, z) = (1, 0)$
Then LHS of (1)
$= p(T(s, v), T(u, z)) = p(T(1, 0), T(1, 0)) = p(\frac{1}{2}, \frac{1}{2}) = \frac{1}{2}$,
which is less than RHS of (1)
Thus (1) holds.
Case 3- If $(s, v) = (u, z) = (1, 1)$
Thus (1) holds.
Case 4- If $(s, v) = (1, 0); (u, z) = (0, 0)$
Thus (1) holds.
Case5- If $(s, v) = (1, 0); (u, z) = (1, 1)$
Thus (1) holds.

Therefore, all the properties of Theorem 3.1 are gratified.
Also, g and T possesses unique coupled coincidence point as $(0, 0)$.

Conclusions

As introduced toward the start of this work, Bhaskar and Laksmikantham, stretch out this hypothesis to partially ordered metric spaces and present the idea of coupled fixed point for mixed-monotone map.

Acquiring results as concerns the presence and the uniqueness of certain coupled coincidence point hypotheses for a map possesses the property of mixed g-monotone in partial metric spaces.

Acknowledgement

The authors express their sincere thanks to the reviewers and editors for their valuable comments and suggestions.

References

[1] Aydi H (2011) Some coupled fixed point results on partial metric spaces. International Journal of Mathematical Sciences, Article ID 647091.

[2] Bhaskar T G, Lakshmikantham V (2006) Fixed point theorems in partially ordered metric spaces and applications. Nonlinear Analysis: Theory, Methods and Apllications, 65(7:1379-1393.

[3] Chouhan V S, Sharma R (2017) Coupled fixed point theorems involving rational expressions in partially ordered cone metric spaces. Communications in Optimization Theory, 2017:1-15.

[4] Ciric L, Lakshmikantham V (2009) Coupled fixed point theorems for nonlinear contractions in partially ordered metric spaces. Nonlinear Analysis: Theory, Methods and Applications, 70(12):4341-4349.

[5] Ciric L, Olatinwo M O, Gopal D, Akinbo G (2012) Coupled fixed point theorems for mappings satisfing a contractions of rational type on a partially ordered metric space. Advances in Fixed Point Theory, 2(1):1-8.

[6] Matthews S G (1994) Partial metric topology. Proc 8th summer conference on general topology and application, in Annals of the New York Academy of Sciences, 728:183-197.

[7] Nabil T (2021) Applying hybrid coupled fixed point theory to the nonlinear hybrid system of second order differential equations. J. Computational Analysis and Applications, 29(3):494-504.

[8] Nazam M, Arshad M, Park C, Yun S (2019) Fixed points of Ciric type ordered F-contractions on partial metric spaces. J. Computational Analysis and Applications, 26(8):1459-1470.

[9] O'Neill S J (1995) Two topologies are better than one. Tech. Rep., University of Warwick, Coventry, UK.

[10] O'Neill S J (1996) Partial metrics, valuations and domain theory. Proc 11th summer conference on general topology and application, in Annals of the New York Academy of Sciences, 806: 304-315.

[11] Sharma R, Chouhan V S, Mishra S (2019) Coupled fixed point theorems for rational contractions in partially ordered cone metric spaces. AIP Conference Proceedings 2095, 030022, doi.org/10.1063/1.5097533.

Numerical Study of Viscous Dissipation, Suction/Injection Effects and Dufour Number also with Chemical Reaction Impacts of MHD Casson Nanofluid in Convectively Heated Non-Linear Extending Surface

Sanju Jangid[1], *Ruchika Mehta*[1*] *and Devendra Kumar*[2]
[1,1*] *Department of Mathematics and Statistics*,
Manipal University Jaipur, Jaipur(Raj.), India
[2] *Departmentof Mathematics*,
University of Rajasthan, Jaipur(Raj.), India
[1*] *ruchika.mehta*1981@*gmail.com*

January 1, 2022

Abstract

This numerical study looked at the effects of thermophoresis diffusion, Brownian motion parameter influences, and suction/injection influence in a hydromagnetic (MHD) Casson nanofluid in a convectively heated nonlinear extending surface (in 2D). Using similarity transformations, the leading partial differential equations (PDEs) are renewed into a set of ordinary differential equations (ODEs) with suitable boundary conditions, and then numerically resolved using a 4^{th}order Runge-Kutta approach based on the shooting technique and the MATLAB application. Graphs are used to investigate the effects of dimensionless parameters such as local Grashof temperature and concentration parameter, permeability, Joule impact, thermo radiative impression, Dufour and chemical reactive impression on nanoparticle volume fraction profiles, temperature, and movement. Tables and graphs are used to examine other characteristics of importance, such as the skin friction coefficient, heat, and mass transfer in a variety of situations, as well as the relationship between these parameters.

Key words: Casson Nanofluid; MHD; Heat Generation/Absorption, Thermophoresis Diffusion, RK-4^{th} order.

1 Introduction

There are several applications, including the learning of non-Newtonian fluids across an extended sheet, which was completed with extreme kindness. Although the elasticity of non-Newtonian fluid behaviour may be assessed, their fundamental equations are occasionally used to classify the rheological features. The fundamental relations in non-Newtonian fluids are extra difficult because they provide the rheological non-dimensional characteristics. Non-Newtonian fluids include a variation of fluids used in the oil industry, as well as cooling courses for micro-ships, unclosed-flow switching, and multiplex systems.

Because of its applications in paramedical sciences, geo and astrophysics, oil reservoirs, and geothermal engineering, free convective heat transport is a mean-

ingful part of fluid dynamics. The term "thermal radiation" refers to a method of converting internal energy into electromagnetic waves. Thermal radiation and nonlinear thermal radiation are employed in a variety of applications, including space vehicles, paper and glass manufacture, gas turbines, space technologies, and hypersonic combat. The flow model is based on a mix of Tiwari and Das models, as well as the Buongiorno's model.The influence of MHD Casson fluid flow through a convective surface with crossdiffusion, chemical reaction, and nonlinear radiative heat is accounted for using convective and boundary conditions, according to Ramudu et al. [1].Butt et al. [2] assessed the entropy generative impression of a flow traversed by a permeable stretched surface of hydromagnetic Casson nanofluid. Afify [3] addresses Casson nano fluid's work in the presence of viscid dissipative impression on a stretched sheet with slip limits. AlHossainy et al [4] address a SQLM (spectral quasi linearization method) mathematical work for the impact of stress on hydromagneto nanofluid flow with permeability influence in three dimensions. The timedependent nonlinearly convective stream of thin film nano liquid across an inclined stretchable sheet with a magnetic effect was studied by Saeed et al. [5]. The use of this current fractional operator to investigate Newtonian heating impacts for the generalized Casson fluid flow is the focus of Tassaddiq et al. [6] research. In this study, the MHD and porous impacts of such fluids are also taken into account. MHD Casson nanofluid (Ag and Cu water) boundary layer flow and heat transference across a stretched surface through a porous mode were studied by Siddiqui and Shankar [7]. Faraz [8] investigated a mathematical study on an axisymmetric Casson nanofluid flow over a radially stretched sheet with hydromagnetic impact. Hady et al. [9] inspected the radiative effect and heat transmission of a viscid nanofluid across a nonlinear stretched sheet. In the company of porous mode, Mahantha and Shaw [10] proposed a 3dimensional convective Casson fluid flow with convective limits passing through a linear stretched sheet. Vendabai [11] investigate a hydromagnetic boundary layer Casson nanofluid flow passing through an upright exponentially stretched cylinder with transverse magneto impact and heat generating or absorptive impression. Alotaibi et al. [12] investigated the influence of viscid dissipative impact over a convectively intensive nonlinear spreading surface, as well as suction or injection and heat absorption or generation impacts, on a hydromagnetic boundary layer flow of Casson nanofluid flow. Oyelakin et al. [13] studied a flow of timedependent Casson nanofluid across a stretched surface with thermal radiative imprint and slip limiting settings.

Many studies of Newtonian and nonNewtonian fluids have been directed in order to examine the impacts of fluid movements, as well as various types of nanofluid flows across various surfaces. In fresh years, a large number of inspections on the boundary layer flow of Casson nanofluids in a variety of geometries have been carried out. Ullah et al. [14] looked at the effect of thermo radiative, convective limiting circumstances, and heat generation/absorption on a timedependent hydromagnetic mixed connective slip Casson fluid flow, as well as chemically reactive influence, on a nonlinearly stretched sheet in a porous mode. The local fractional linear transport equations (LFLTE) in fractal porous media are studied by Singh et al. [15]. Dwivedi and Singh [16] produced a new finite difference collocation approach that was designed using the Fibonacci polynomial and then used to one super and two sub-diffusion problems with better reliability. Imtiaz et al. [17] examined how a convective Casson nanofluid flow goes through a stretched cylinder and the restrictions that come with it. Eid and Mahny [18] describe a computational study to determine the heatgenerating influence of Sisko nanofluid across a nonlinear stretched sheet with porous mode. Eid [19] investigated a twophase nanofluid flow with hydromagnetic influence, as well as chemical reactive and heat generating effects, across an exponentially stretched sheet. Chemical reaction effects on a convectively heated nonlinear stretched surface of Carreau nanofluid were explored by Eid et al [20].

Eid [21] investigated the chemical reactive effects of H_2O-NPs (nanoparticles) in unsteady and stagnation point flow on a stretched sheet in the soaking porous mode. Mustafa and Khan [22] investigated a Casson model flow over a nonlinear stretched sheet with magneto impacts. Wahiduzzaman et al [23] did a mathematical investigation of hydromagnetic Casson fluid flow in the presence of porous mode passing through a nonisotherm stretched sheet. The Casson nanofluid flow between stretched discs with radiative influence was deliberated by Khan et al [24]. The viscid dissipative impression of hydromagnetic Casson nanofluid passing through permeable stretched sheet was observed by Besthapu and Bandari [25]. Pramanik [26] discusses the thermo radiative and Nusselt number impressions in the presence of a porous mode of nonNewtonian Casson flow passing over an exponentially stretched surface.

The vast range of commercial and manufacturing experiments of flow behaviour across stretched surfaces has attracted numerous writers, including artificial fibres, metallic sheet manufacture, petroleum industries, metal spinning, polymer processing, and so on. Reddy[27] examined the thermal radiative effect and chemically reactive impact of a hydromagnetic Casson fluid flow over an exponentially persuaded permeable stretched surface. Vijayaragavan [28] used a permeable stretched sheet to investigate the heat source or sink effect of timeindependent hydromagnetic Casson fluid flow. Haq et al. [29] examined timedependeny free convection slip flow of secondgrade fluid across an endless hot inclined plate. Lahmar et al. [30] examined the impacts of thermal conductivity and Nusselt number on the squeezing of a timedependent nanofluid by a tending magneto. Nadeem et al. [31] considered a nonNewtonian shear thinning Casson fluid flow with permeability impact passes across a stretchy linear sheet. Mass transference of hydromagnetic Casson fluid with suction and chemical reactive impression was explored by Shehzad et al [32]. Dahab et al. [33] investigated the influence of extending surface over a nonlinearly heated extending surface using hydromagnetic Casson nanofluid flow. Ibrahim et al. [34] conducted a mathematical investigation of a dissipative hydromagnetic mixed convective Casson nanofluid with chemical reactive effect across a nonlinear permeable stretched sheet with heat source impression. Hayat et al. [35] took into account mixed convective stagnation point Casson fluid flow as well as convective constraints. The goal of Puneeth et al. [36] is to figure out what function mixed convection, Brownian motion, and thermophoresis play in the dynamics of a Casson hybrid nanofluid in a bidirectional nonlinear stretching sheet. The heat transfer and entropy of an unstable Casson nanofluid flow, where fluid is positioned across a stretched flat surface flowing nonuniformly, were explored by Jamshed et al. [37]. Over a nonlinear stretched sheet, Shah et al [38] discussed chemically reactive hydromagnetic Casson nanofluid flow with radiation influence and entropy generating impression. Soret or diffusion thermo or thermo difusion effect is described as matter diffusion caused by a gradient of heat, whereas Dufour efect is defined as heat diffusion caused by a gradient of concentration. For excessively big temperature and concentration gradients, these consequences have played a substantial influence. The majority of the time, these two impacts are regarded as secondorder effects. Its uses include contaminant movement in groundwater, chemical reactors, and geosciences. Several academics are drawn to the field of heat flux mass transfer because of its wide range of applications in numerous fields. Fiber optics manufacturing, plastic emulsion, glass cutting, nanoelectronics freezing, catalytic reactors, wire drawing, and improved oil extraction are all examples of Brownian motion effects and thermophoresis in the scientific and technical sphere.

The current study attentions on the Casson nanofluid flow over a nonlinear inclined stretching surface with Buoyancy and Dufour impacts, as a result of the above mentioned literature review and the rising need for nonNewtonian nanofluid

flows in industry and engineering. When compared to Newtonian based nanofluid flow, Casson nanofluid is more useful for cooling and friction-reducing agents. The goal of this research is to show a comprehensive mathematical investigation of the impression of buoyancy force, permeability, joule heating impression, and chemical reactive with heat generative or absorption, suction or blowing impact, and viscid dissipative impression of 2-dimensional hydromagneto Casson fluid flow permits through nonlinear outspreading plate along with CBC (convective boundary conditions) ref [12]. PDEs (dimension form) of existing effort were turned into ODEs with the support of several similarity transformations. The RK4th order process cracked nondimensional ODEs with the help of the shooting procedure. MATLAB software is used to create graphs and tables that highlight the rooted parameter behaviour.

2 Problem Structure:

Deliberate hydromagnetic convective nanofluid flow in the section ($y > 0$) over an exponentially extensible sheet as 2-dimensional incompressible (density is constant) time-independent viscid along with the impact of the viscous dissipative and several non-dimensional parameters. X-axis indicated for surface and y-axis erect to surface. The extensible surface is projected to have a velocity outline of the power law $u_w(x) = ax^n$ where a, n is non-zero constants. Magnetic field is covered with $B(x) = B_0 x^{(n-1/2)}$ and the electric field is zero, but the induced magnetic field is unnoticed by the weak magnetic amount of Reynolds. $T_w(x) = T_\infty + Ax^n$, where A is non-zero secure rate, T_∞ displays the free stream temperature. C_∞ displays the ambient nano-particles concentration. Flow chart of existing work is exposed in [Figure 1].

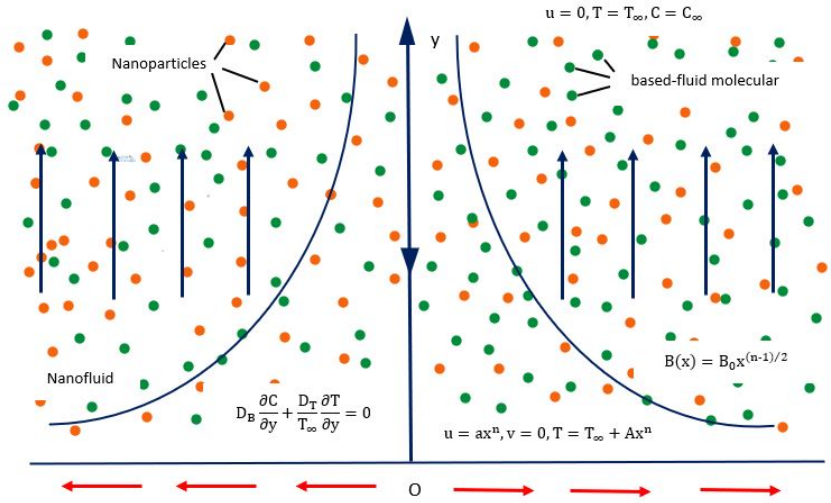

Figure 1: Bodily Modal of recent effort.

The Casson fluid rheological state equation [references [21], [31]] is:

$$\tau_{ij} = \begin{cases} 2(\mu_B + \frac{\tau_y}{\sqrt{2\pi}})e_{ij} & \text{if } \pi > \pi_c \\ 2(\mu_B + \frac{\tau_y}{\sqrt{2\pi}})e_{ij} & \text{if } \pi < \pi_c \ . \end{cases} \tag{1}$$

Where deformation component rate product $\pi = e_{ij}e_{ij}$, where e_{ij} displays the $(i, j)^{th}$ deformation component rate, π is the multiple of the sections of deformation

component rate product, π_c indicates to the non-Newtonian fluid critical rate of this deformation component rate product, μ_B signifies Casson fluid plastic viscosity, τ_y shows yield stress.

Consider the apparatuses of velocity function $V = [u(x,y), v(x,y), 0]$, the temperature function $T = T(x,y)$ and concentration function $C = C(x,y)$. The motion, temperature and the concentration relations in a Casson nanofluid are inscribed as

$$\frac{\partial u}{\partial x} + \frac{\partial v}{\partial y} = 0, \tag{2}$$

$$u\frac{\partial u}{\partial x} + v\frac{\partial v}{\partial y} = \nu(1+\frac{1}{\beta})\frac{\partial^2 u}{\partial y^2} - \frac{\sigma B^2(x)u}{\rho_f} - \frac{\nu}{k'}u + g_0\beta_T(T-T_\infty) + g_0\beta_C(C-C_\infty), \tag{3}$$

$$u\frac{\partial T}{\partial x} + v\frac{\partial T}{\partial y} = \alpha\frac{\partial^2 T}{\partial y^2} + \frac{Q_0}{\rho c_p}(T-T_\infty) + \tau[D_B(\frac{\partial T}{\partial y}\frac{\partial C}{\partial y}) + \frac{D_T}{T\infty}(\frac{\partial T}{\partial y})^2] + \frac{\mu}{\rho c_p}(1+\frac{1}{\beta})(\frac{\partial u}{\partial y})^2$$
$$+ \frac{\sigma B^2(x)u^2}{\rho c_p} - \frac{1}{\rho c_p}\frac{\partial q_r}{\partial y} + \frac{D_B K_T}{c_s c_p}\frac{\partial^2 C}{\partial y^2}, \tag{4}$$

$$u\frac{\partial C}{\partial x} + v\frac{\partial C}{\partial y} = D_B\frac{\partial^2 C}{\partial y^2} + \frac{D_T}{T_\infty}\frac{\partial^2 T}{\partial y^2} - k_1(C - C_\infty). \tag{5}$$

where, u and v show the x-axis and y-axis velocity apparatuses respectively, ν displays the kinematic viscosity, $\beta = \mu_B\frac{\sqrt{2\pi_C}}{\tau_y}$ indicates the Casson fluid parameter, σ displays the conductivity electrical field, ρ indicates the fluid density, the thermophoresis and Brownian diffusions coefficients are direct by D_T, and D_B respectively, Q_0 specifies the dimensional heat source or sink coefficient, α shows the thermal diffusivity, T pointed for temperature,$\tau = \frac{(\rho C)_p}{(\rho C)_f}$ directs the ratio of the effective heat capacity to efficient liquid heat capacity, and C_p indicates the specific heat.

The existing work boundary conditions are specified by

$$u = u_w = ax^n,\ v = v_w,\ T = T_w = T_\infty + Ax^n,\ D_B\frac{\partial C}{\partial y} + \frac{D_T}{T_\infty}\frac{\partial T}{\partial y} = 0,\ \ at\ y = 0.$$

$$u \to 0, \qquad T \to T_\infty, \qquad C \to C_\infty, \qquad at\ \ y \to \infty. \tag{6}$$

Where, $a > 0$ is for the stretching channel walls.

The Roseland approximation of the radiative heat flux is arranged by

$$q_r = \frac{-4\sigma^*}{3k^*}\frac{\partial T^4}{\partial y}, \tag{7}$$

Here T^4 as a linear relation of temperature via Taylor's sequence expansion about T_∞ and ignoring advanced terms, thus

$$T^4 \approx 4{T_\infty}^3 T - {T_\infty}^4. \tag{8}$$

In view of the similarity transformation

$$u = ax^n f'(\eta), \qquad v = -ax^{(n-1)/2}\sqrt{\frac{\nu}{a}}(\frac{n+1}{2}f(\eta) + \frac{n-1}{2}\eta f'(\eta)), \tag{9}$$

$$\eta = \sqrt{\frac{a}{\nu}}x^{(n-1)/2}y, \qquad \theta(\eta) = \frac{T - T_\infty}{T_w - T_\infty}, \qquad \phi(\eta) = \frac{C - C_\infty}{C_w - C_\infty}. \tag{10}$$

With (7)-(10), equations (2)-(6)are reduced to the next arrangement.

$$(1+\frac{1}{\beta})f'''-n(f')^2+(\frac{n+1}{2})ff''-Mnf'+k_2f'+G_T\theta+G_C\phi=0, \tag{11}$$

$$((1+Nr)/Pr)\theta''-nf'\theta+(\frac{n+1}{2})f\theta'+Nb\theta'\phi'+Nt(\theta')^2+(1+\frac{1}{\beta})Ec(f'')^2$$
$$+Q\theta+MnEc(f')^2+Du\phi''=0, \tag{12}$$

$$\phi''+(\frac{n+1}{2})Scf\phi'+\frac{Nt}{Nb}\theta''-ScK\phi=0. \tag{13}$$

With limit circumstances

$$f(0)=f_w,\quad f'(0)=1,\quad \theta(0)=1,\quad Nb\phi'(0)+Nt\theta'(0)=0,\quad at\ \ \eta=0. \tag{14a}$$

$$f'(\infty)\to 0,\quad \theta(\infty)\to 0,\quad \phi(\infty)\to 0,\quad at\ \ \eta\to\infty. \tag{14b}$$

Where, $Mn=\frac{\sigma B^2(x)}{\rho a x^{n-1}}$ shows the magnetic parameter, $k_2=\frac{\nu}{k' a x^{n-1}}$ indicates the permeability parameter, $G_T=\frac{g_0\beta_T(T_w-T_\infty)}{a^2x^{2n-1}}$ and $G_C=\frac{g_0\beta_C(C_w-C_\infty)}{a^2x^{2n-1}}$ indicate the local temperature and concentration Grashof number respectively, $Pr=\frac{\nu}{\alpha}$ shows the Prandtl number, $Q=\frac{Q_0}{\rho a c_p x^{n-1}}$ indicates the heat generation or absorption, $Nr=\frac{16\sigma^* {T_\infty}^3}{3kk^*}$ directs the radiation parameter, $Ec=\frac{u_w^2}{c_p(T_w-T_\infty)}$ shows the Eckert number, $Nb=\frac{\tau D_B(C_w-C_\infty)}{\nu}$ directs the Brownian motion parameter, $Nt=\frac{\tau D_T(T_w-T_\infty)}{\nu T_\infty}$ indicates the thermophoresis diffusion influence, $Du=\frac{D_BK_T(C_w-C_\infty)}{c_sc_p\nu(T_w-T_\infty)}$ specifies the Dufour number, $Sc=\frac{\nu}{D_B}$ directs the Schmidt number, $K=\frac{k_1}{ax^{n-1}}$ shows the chemical reaction parameter, and $f_w=\frac{-2v_w}{(n+1)\sqrt{\nu a x^{n-1}}}$ indicates the suction or blowing parameter.

Physical Quantities:

Skin Friction Coefficient(C_{fx})**:** The skin friction coefficient is known as follows:

$$C_{fx}=\frac{\tau_w}{\rho u_w^2},\ \ where\ \ \tau_w=\mu_B(1+\frac{1}{\beta})(\frac{\partial u}{\partial y})_{y=0}. \tag{15}$$

Heat Transfer Coefficient: The non-dimensional Nusselt number (Nu_x) is given by

$$Nu_x=\frac{xq_w}{k(T_w-T_\infty)},\ \ where\ \ q_w=-k(\frac{\partial T}{\partial y})_{y=0}. \tag{16}$$

Mass Transfer Coefficient: The rate of mass transfer is derived by a Sherwood number (Sh_x) which is given by

$$Sh_x=\frac{xm_w}{D_B(C_w-C_\infty)},\ \ where\ \ m_w=-D_B(\frac{\partial C}{\partial y})_{y=0}. \tag{17}$$

After solving the equation (15), (16) and (17) with equation (9) and (10), we gain

drag force

$${Re_x}^{1/2}C_{fx}=(1+\frac{1}{\beta})f''(0),$$

local Nusselt

$${Re_x}^{1/2}Nu_x=-\theta'(0),$$

local Sherwood

$$Re_x{}^{1/2}Sh_x = -\phi'(0). \tag{18}$$

Where,τ_w indicates the wall shear stress, k signifies the thermo nano-fluid conductivity, q_w shows the surface heat flux, and m_w directs the surface mass flux, $Re_x = \frac{u_w x}{\nu}$ shows the local Reynolds number.

We explain the reduces equations (11)-(13) with limitations (14a) and (14b) using Runge -Kutta fourth-order method along with shooting technique.

3 Results and Discussion:

The impacts of the numerous types of non-dimensional parameters values to have a physical considerate of the work like, the magneto impact Mn, f_w (suction or blowing), β Casson parameter, heat source or sink impact Q, Dufour impact Du, Brownian diffusivity Nb, Eckert parameter Ec, thermophoresis diffusivity Nt, radiative impact Nr, Prandtl effect Pr, Schmidt impact Sc, chemically reactive influence K, permeability influence k_2, Grashof number impact (G_T *and* G_C), and power law index n, over the momentum graphs $f'(\eta)$, temperature graphs $\theta(\eta)$, and concentration graphs $\phi(\eta)$ discussed through graphs [Figure 2 - Figure 23] and tables along with the influence of drag force $Re_x{}^{1/2}C_{fx}$, local Nusselt $Re_x{}^{1/2}Nu_x$ local Sherwood $Re_x{}^{1/2}Sh_x$. Non-dimensional equations (11)-(13) with limitations (14a) and (14b) solved by Runge- Kutta fourth-order method with shooting technique. After we find the values of heat transfer and mass transfer and draw the graph by MATLAB software. Consider the values of parameters $n = 3$ *or* $1, \beta = 0.1$ *or* $1, Mn = 0.1, k_2 = 0.1, Pr = 0.1, Q = 0.1, Nr = 0.1, Sc = 0.1, K = 0.1, G_T = 0.1, G_C = 0.1, Ec = 0.1, Du = 0.1, Nb = 0.1, Nr = 0.1, f_w = 0.1$.

The influence of the Casson nanofluid parameterβ on the momentum profile with power law index $n = 3$ and 1 is seen in [Figure 2] . The momentum graph drops as β increases in both situations of n, owing to the upsurge in plastic dynamic viscosity, which produces hindrance in the fluid flow. When $n = 3$, the momentum of the Casson nanofluid is greater than that of the Casson nanofluid when $n = 1$. With the track erect to the x-axis, [Figure 3] displays the lowering momentum impact of increased magnetic number Mn owing to the solid Lorentz force, which generates greater resistance in the fluid flow in both situations of Casson fluid $\beta = 0.1$ and 1. [Figure 4] depicts the failure velocity with suction or blowing parameter f_w due to nanofluid heat and thermolayer thickness for $n = 3$ and $n = 1$. When the permeability parameter k_2 rises to $\beta = 0.1$ and 1, the momentum decreases as seen in [Figure 5]. The momentum upsurges due to a rise in buoyant force with growing values of local concentration Grashof number G_C and local temperature Grashof number G_T, in [Figure 6] and [Figure 7] for $\beta = 0.1$ and 1, respectively.

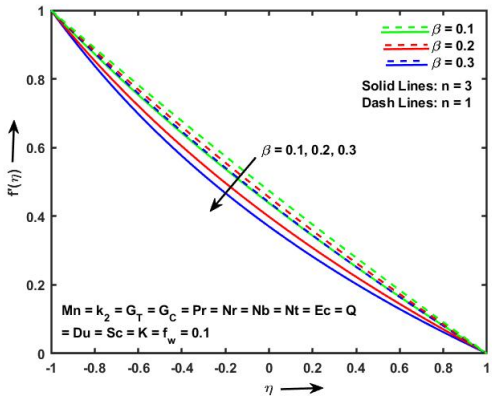

Figure 2: Velocity display of Casson fluid parameter β.

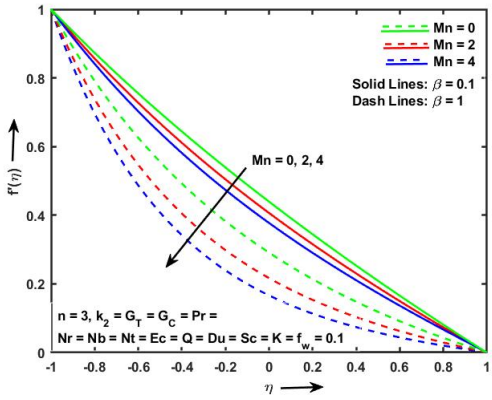

Figure 3: Velocity display of Magnetic parameter Mn.

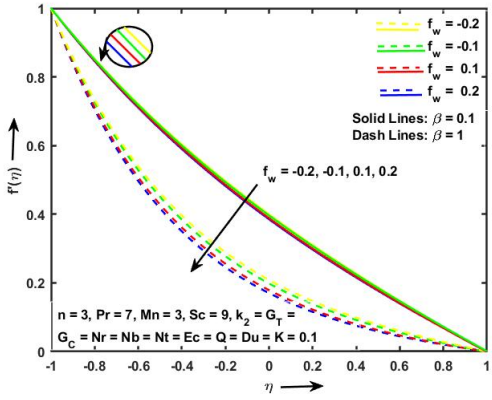

Figure 4: Velocity display of parameter f_w.

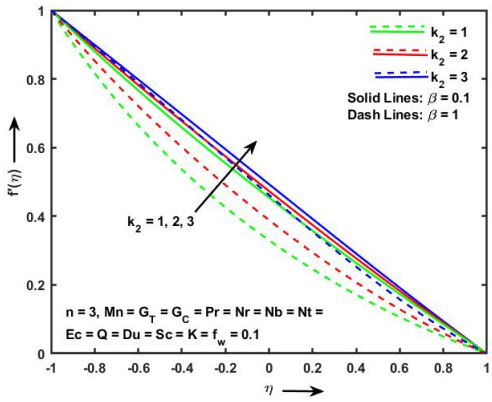

Figure 5: Velocity display of parameter k_2.

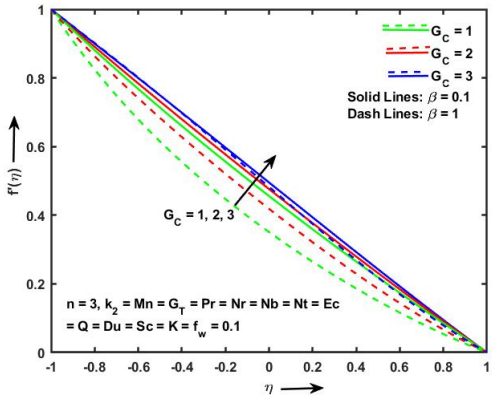

Figure 6: Velocity display of parameter G_C.

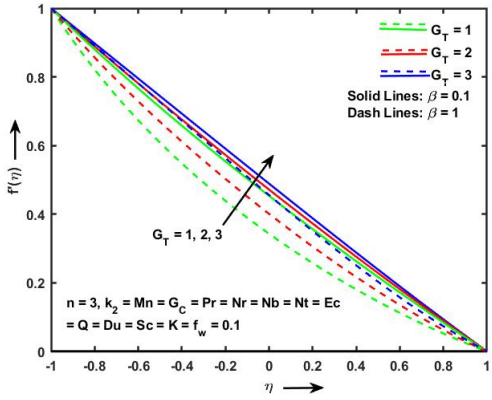

Figure 7: Velocity display of parameter G_T.

[Figure 8] illustrations the result of increasing the Dufour number on temperature between $\beta = 0.1$ and 1. [Figure 9] depicts the increasing influence of temperature on Eckert number Ec. The temperature rise as a result of the viscous dissipative term, which generates heat as a result of frictional heating between the fluid constituents. This additional heat resulted in a rise in temperature, which was connected to an increase in boundary layer breadth. [Figure 10] shows how temperature rises when the radiation parameter Nr between $\beta = 0.1$ and 1 increases. The $k*$ (absorption coefficient) lowers when there is an ascendant in Nr. An increase in f_w falloffs the nanofluid heat and thermolayer width owing to heated nanofluid pulled close to sheet is seen in [Figure 11]. As a result, in both scenarios of $\beta = 0.1$ and 1 with increase f_w, the temperature decreases. The Prandtl number Pr represents the ratio of momentum and thermal diffusivity. The temperature is lowered when Pr is increased (in [Figure 12]). Due to thermal layer thickness, [Figure 13] depicts the temperature increase with increasing heat production or absorption parameter Q (heat create in fluid for $Q > 0$ and heat absolve in fluid for $Q < 0$).

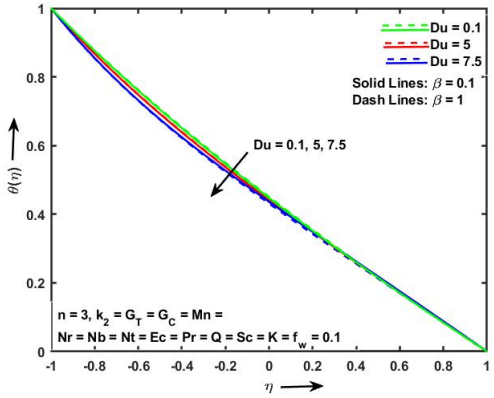

Figure 8: Temperature display of parameter Du,

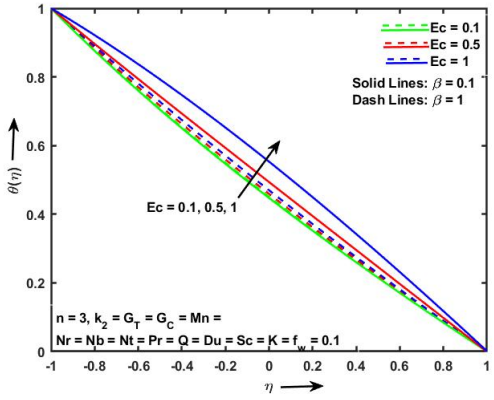

Figure 9: Temperature display of parameter Ec.

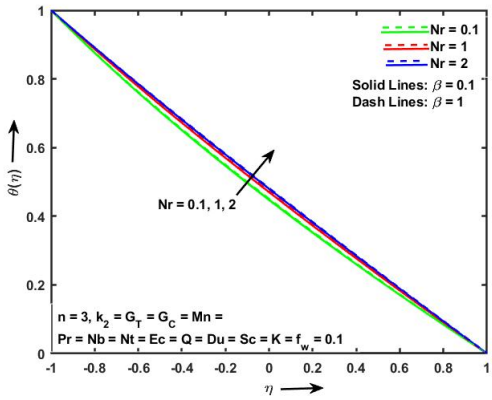

Figure 10: Temperature display of parameter Nr.

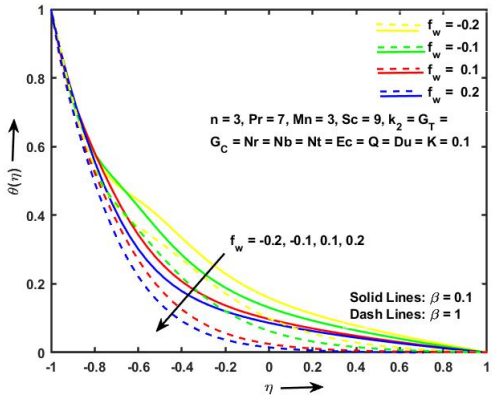

Figure 11: Temperature display of parameter f_w.

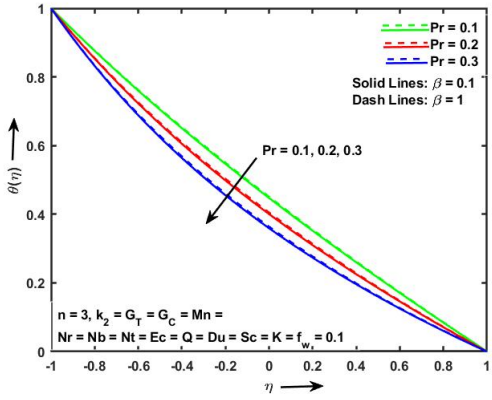

Figure 12: Temperature display of parameter Pr.

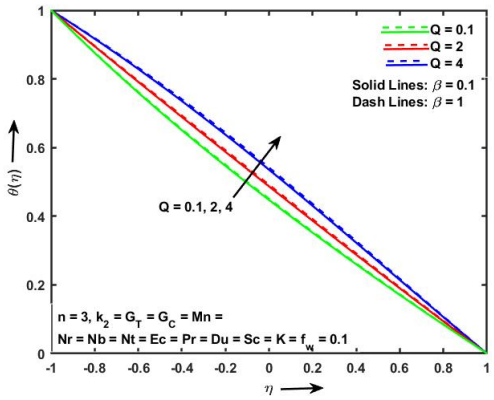

Figure 13: Temperature display of parameter Q.

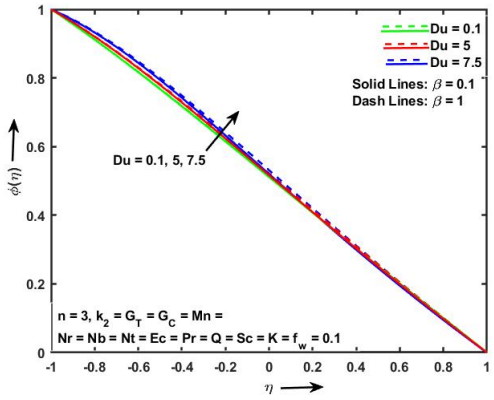

Figure 14: Concentration display of parameter Du.

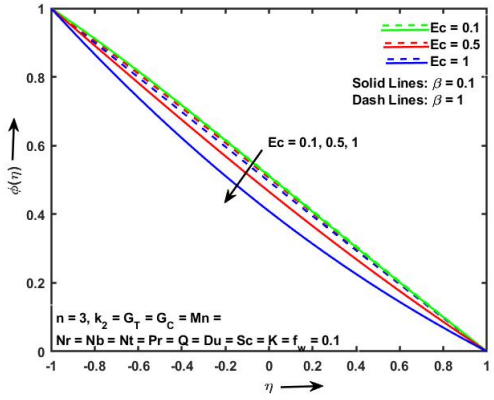

Figure 15: Concentration display of parameter Ec.

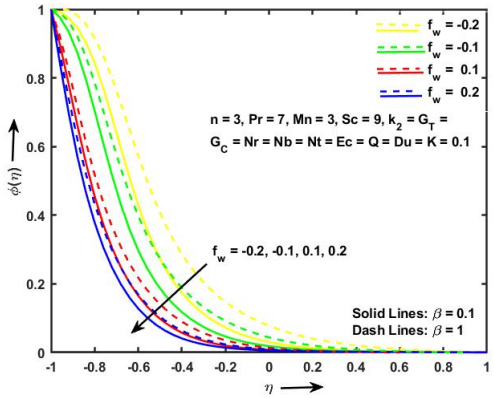

Figure 16: Concentration display of parameter f_w.

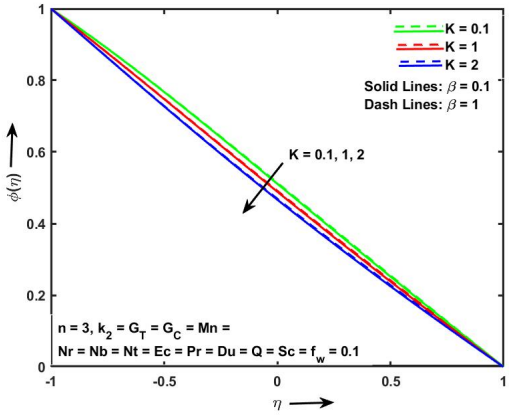

Figure 17: Concentration display of parameter K.

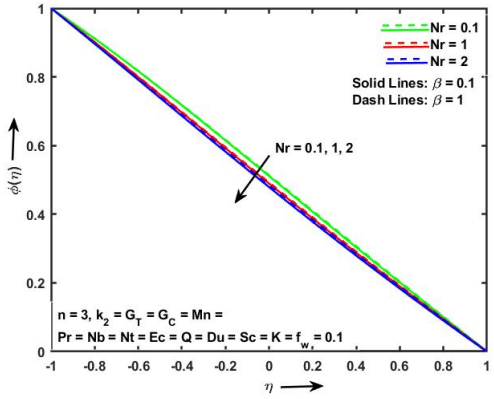

Figure 18: Concentration display of parameter Nr.

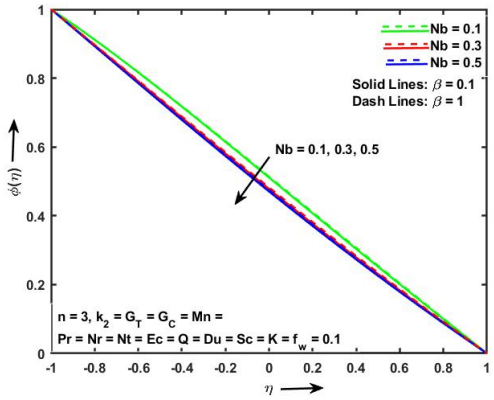

Figure 19: Concentration display of parameter Nb.

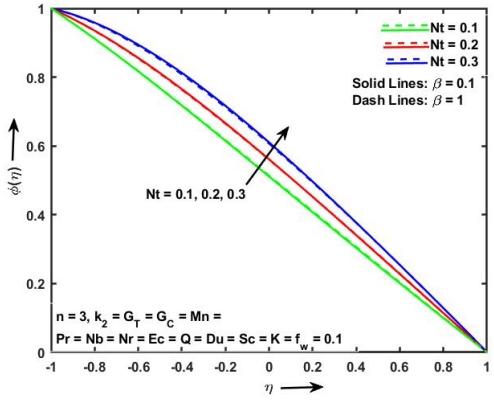

Figure 20: Concentration display of parameter Nt.

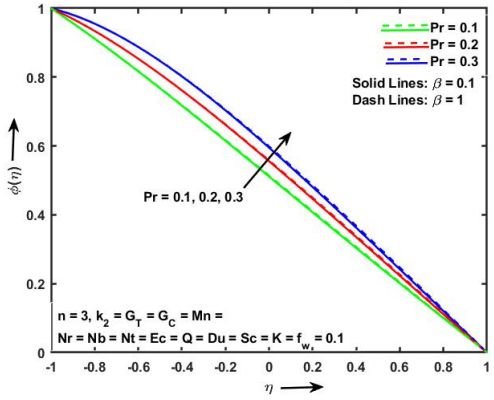

Figure 21: Concentration display of parameter Pr.

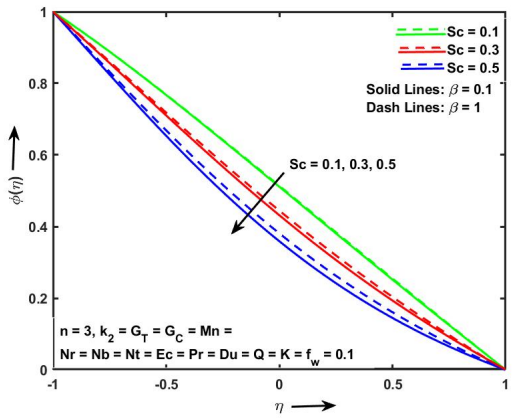

Figure 22: Concentration display of parameter Sc.

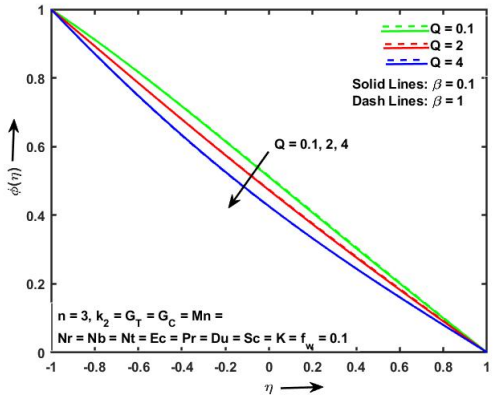

Figure 23: Concentration display of parameter Q.

[Figure 14] depicts an increment of concentration shape with growing Dufour number Du. [Figure 15]-[Figure 19] show the decay volume fraction graph for both $\beta = 0.1$ and 1 of Eckert parameter Ec, suction or blowing impact f_w, chemically reactive imapct K, and radiation parameter Nr. [Figure 20] describes the falling impact of concentration profile of upsurge Brownian parameter Nb for both $\beta = 0.1$ and 1. Similarly, impact of decay volume fraction of increase thermo-diffusion influence showing in [Figure 20]. [Figure 21] shows the effect of rise Prandtl number Pr on growing concentration profile for both $\beta = 0.1$ and 1. Increasing Schmidt number Sc and heat generation and absorption parameter Q impact with declines volume fraction influence explains in [Figure 22] and [Figure 23] respectively.

Table I: Numerical result of drag force coefficient, Nusselt number Nu, and Sherwood number of numerous parameters when $\beta = 0.1$ and 1 and $n = 3$.

Mn	k_2	G_T	G_C	f_w	Pr	Nr	Nb	Nt	Ec	Q	Du	Sc	K	$f''(0)$	$\theta'(0)$	$\phi'(0)$
0 2 4	0.1	0.1	0.1	0.1	0.1	0.1	0.1	0.1	0.1	0.1	0.1	0.1	0.1	-0.6589 -0.7599 -0.8538 -1.1769 -1.5325 -1.8312	-0.6429 -0.6269 -0.6119 -0.6389 -0.6179 -0.6009	-0.4222 -0.4360 -0.4492 -0.4182 -0.4352 -0.4492
0.1	1 2 3	0.1	0.1	0.1	0.1	0.1	0.1	0.1	0.1	0.1	0.1	0.1	0.1	-0.6159 -0.5609 -0.5309 -1.0129 -0.7849 -0.5249	-0.6459 -0.6499 -0.6549 -0.6469 -0.6579 -0.6719	-0.4192 -0.4162 -0.4122 -0.4122 -0.4032 -0.3942
0.1	0.1	1 2 3	0.1	0.1	0.1	0.1	0.1	0.1	0.1	0.1	0.1	0.1	0.1	-0.6169 -0.5639 -0.5119 -0.9879 -0.7638 -0.5458	-0.6459 -0.6499 -0.6539 -0.6489 -0.6599 -0.6699	-0.4192 -0.4162 -0.4132 -0.4102 -0.4022 -0.3952
0.1	0.1	0.1	1 2 3	0.1	0.1	0.1	0.1	0.1	0.1	0.1	0.1	0.1	0.1	-0.6129 -0.5559 -0.4999 -0.9723 -0.7287 -0.4903	-0.6459 -0.6509 -0.6549 -0.6499 -0.6629 -0.6739	-0.4192 -0.4152 -0.4122 -0.4092 -0.4002 -0.3922
3	0.1	0.1	0.1	-0.2 -0.1 0.1 0.2	7	0.1	0.1	0.1	0.1	0.1	0.1	9	0.1	-0.785275 -0.794275 -0.8139 -0.8229 -1.5580 -1.6079 -1.7109 -1.7639	-2.792727 -3.240827 -3.4749 -3.1099 -2.90922 -3.4316 -3.9492 -3.7849	-0.107859 -0.389959 -2.2192 -3.8882 0.11995 -0.0675 -1.5985 -3.0582

0.1	0.1	0.1	0.1	0.1	0.1 0.2 0.3	0.1	0.1	0.1	0.1	0.1	0.1	0.1	0.1	-0.6639 -0.6639 -0.6639 -1.1969 -1.1969 -1.1969	-0.6419 -0.7779 -0.9079 -0.6379 -0.7729 -0.9039	-0.4222 -0.2868 -0.1568 -0.4188 -0.2838 -0.1518
0.1	0.1	0.1	0.1	0.1	0.1	0.1 1 2	0.1	0.1	0.1	0.1	0.1	0.1	0.1	-0.6639 -0.6639 -0.6639 -1.1969 -1.1969 -1.1969	-0.6419 -0.5789 -0.5529 -0.6379 -0.5765 -0.5505	-0.4222 -0.4852 -0.5122 -0.4188 -0.4808 -0.5058
0.1	0.1	0.1	0.1	0.1	0.1	0.1	0.1 0.3 0.5	0.1	0.1	0.1	0.1	0.1	0.1	-0.6639 -0.6639 -0.6639 -1.1971 -1.1977 -1.1977	-0.6419 -0.6479 -0.6539 -0.6379 -0.6439 -0.6499	-0.4222 -0.5152 -0.5342 -0.4188 -0.5092 -0.5272
0.1	0.1	0.1	0.1	0.1	0.1	0.1	0.1	0.1 0.2 0.3	0.1	0.1	0.1	0.1	0.1	-0.6639 -0.6639 -0.6635 -1.1971 -1.1955 -1.1945	-0.6419 -0.6409 -0.6399 -0.6379 -0.6369 -0.6359	-0.4222 -0.2822 -0.1442 -0.4188 -0.2828 -0.1482
0.1	0.1	0.1	0.1	0.1	0.1	0.1	0.1	0.1	0.1 0.5 1	0.1	0.1	0.1	0.1	-0.6639 -0.6636 -0.6636 -1.1971 -1.1971 -1.1971	-0.6419 -0.5239 -0.3749 -0.6379 -0.6009 -0.5549	-0.4222 -0.5412 -0.6902 -0.4188 -0.4558 -0.5018
0.1	0.1	0.1	0.1	0.1	0.1	0.1	0.1	0.1	0.1	0.1 2 4	0.1	0.1	0.1	-0.6639 -0.6639 -0.6639 -1.1971 -1.1971 -1.1971	-0.6419 -0.5309 -0.4019 -0.6379 -0.5249 -0.3939	-0.4222 -0.5337 -0.6627 -0.4188 -0.5318 -0.6638
0.1	0.1	0.1	0.1	0.1	0.1	0.1	0.1	0.1	0.1	0.1	0.1 5 7.5	0.1	0.1	-0.6639 -0.6639 -0.6639 -1.1971 -1.1971 -1.1971	-0.6419 -0.7019 -0.7899 -0.6379 -0.7019 -0.7979	-0.4222 -0.3632 -0.2762 -0.4188 -0.3558 -0.2602

														-0.6639	**-0.6419**	**-0.4222**
														-0.6636	**-0.6409**	**-0.5572**
												0.1		**-0.6642**	**-0.6389**	**-0.6972**
0.1	**0.1**	**0.1**	**0.1**	**0.1**	**0.1**	**0.1**	**0.1**	**0.1**	**0.1**	**0.1**	**0.1**	**0.3**	**0.1**			
												0.5		**-1.1971**	**-0.6379**	**-0.4188**
														-1.1979	**-0.6369**	**-0.5388**
														-1.1999	**-0.6349**	**-0.6628**
														-0.6639	**-0.6419**	**-0.4222**
														-0.6639	**-0.6409**	**-0.4832**
													0.1	**-0.6639**	**-0.6409**	**-0.5472**
0.1	**0.1**	**0.1**	**0.1**	**0.1**	**0.1**	**0.1**	**0.1**	**0.1**	**0.1**	**0.1**	**0.1**	**0.1**	**1**			
													2	**-1.1971**	**-0.6379**	**-0.4188**
														-1.1971	**-0.6369**	**-0.4798**
														-1.1981	**-0.6369**	**-0.5438**

Table II: Mathematical outcome of drag force coefficient, Nusselt number Nu, and Sherwood number of Casson nanofluid parameter β when $n = 3$.

β	Mn	k_2	G_T	G_C	f_w	Pr	Nr	Nb	Nt	Ec	Q	Du	Sc	K	$f^{''}(0)$	$\theta'(0)$	$\phi'(0)$
															-0.5589	**-0.5389**	**-0.4982**
															-0.6049	**-0.5489**	**-0.4872**
0.1															**-0.6419**	**-0.5519**	**-0.4842**
0.2	**0.1**	**0.1**	**0.1**	**0.1**	**0.1**	**0.1**	**0.1**	**0.1**	**0.1**	**0.1**	**0.1**	**0.1**	**0.1**	**0.1**			
0.3															**-0.6639**	**-0.6419**	**-0.4222**
															-0.7819	**-0.6469**	**-0.4152**
															-0.8732	**-0.6469**	**-0.4142**

4 Conclusion:

The impact of hydromagnetic Casson nanofluid's boundary layer on a nonlinear stretching sheet in 2D with the impact of viscid dissipative impact, Dufour number Du, heat absorption or generation Q impact, and suction or blowing impact, among other things, is examined mathematically. The skinfriction coefficient grows as permeability and Grashof number increase. As the Dufour number improves, the Nusselt number drops, whereas the Sherwood number drops as the chemical reactive impression improves. The Runge Kutta 4^{th} order procedure, as well as the shooting technique and MATLAB software, are used to arrive at the mathematical answer. The following are some of the study's key findings:

- Momentum display decreases when β, Mn, and f_w rise, but increases as k_2, G_T, and G_C rise.
- The temperature graph decreases when Du, f_w, and Pr increase, and increases as Ec, Nr, and Q increase.
- The volume fraction distribution improved when Du, Nt, Pr increased and falloffs in Ec, f_w, K, Nr, Nb, Sc, and Q decreased.
- The skin friction coefficient decreases when Mn, Nr, f_w, Nb, Ec, Q, Sc, K increases, while it climbs as k_2, G_T, G_C, β, Pr, Nt, and Du increase.
- The Nusselt number increases as Mn, Nr, Nt, Ec, Q, Sc, and K levels rise, but decreases as k_2, G_T, G_C, β, f_w, Pr, Nb, and Du levels rise.
- The Sherwood number increased when k_2, G_T, G_C, and Nt increased, but decreased as Mn, β, f_w, Nb, Sc, and K increased.

References

[1] AC Venkata Ramudu, K Anantha Kumar, V Sugunamma, and N Sandeep. Impact of soret and dufour on mhd casson fluid flow past a stretching surface with convective–diffusive conditions. *Journal of Thermal Analysis and Calorimetry*, pages 1–11, 2021.

[2] Adnan Saeed Butt, Khadija Maqbool, Syed Muhammad Imran, and Babar Ahmad. Entropy generation effects in mhd casson nanofluid past a permeable stretching surface. *International Journal of Exergy*, 31(2):150–171, 2020.

[3] Ahmed A Afify. The influence of slip boundary condition on casson nanofluid flow over a stretching sheet in the presence of viscous dissipation and chemical reaction. *Mathematical Problems in Engineering*, 2017, 2017.

[4] Ahmed F Al-Hossainy, Mohamed R Eid, and Mohamed Sh Zoromba. Sqlm for external yield stress effect on 3d mhd nanofluid flow in a porous medium. *Physica Scripta*, 94(10):105208, 2019.

[5] Anwar Saeed, Poom Kumam, Saleem Nasir, Taza Gul, and Wiyada Kumam. Non-linear convective flow of the thin film nanofluid over an inclined stretching surface. *Scientific Reports*, 11(1):1–15, 2021.

[6] Asifa Tassaddiq, Ilyas Khan, Kottakkaran Sooppy Nisar, and Jagdev Singh. Mhd flow of a generalized casson fluid with newtonian heating: A fractional model with mittag–leffler memory. *Alexandria Engineering Journal*, 59(5):3049–3059, 2020.

[7] Ayesha Siddiqui and Bandari Shankar. Mhd flow and heat transfer of casson nanofluid through a porous media over a stretching sheet. In *Nanofluid Flow in Porous Media*. IntechOpen, 2019.

[8] Faraz Faraz, Sajjad Haider, and Syed Muhammad Imran. Study of magnetohydrodynamics (mhd) impacts on an axisymmetric casson nanofluid flow and heat transfer over unsteady radially stretching sheet. *SN Applied Sciences*, 2(1):1–17, 2020.

[9] Fekry M Hady, Fouad S Ibrahim, Sahar M Abdel-Gaied, and Mohamed R Eid. Radiation effect on viscous flow of a nanofluid and heat transfer over a nonlinearly stretching sheet. *Nanoscale Research Letters*, 7(1):1–13, 2012.

[10] G Mahanta and S Shaw. 3d casson fluid flow past a porous linearly stretching sheet with convective boundary condition. *Alexandria Engineering Journal*, 54(3):653–659, 2015.

[11] G Sarojamma and K Vendabai. Boundary layer flow of a casson nanofluid past a vertical exponentially stretching cylinder in the presence of a transverse magnetic field with internal heat generation/absorption. *International Journal of Mathematical and Computational Sciences*, 9(1):138–143, 2015.

[12] Hammad Alotaibi, Saeed Althubiti, Mohamed R Eid, and KL Mahny. Numerical treatment of mhd flow of casson nanofluid via convectively heated nonlinear extending surface with viscous dissipation and suction/injection effects. *Computers, Materials & Continua*, 66(1):229–245, 2020.

[13] Ibukun Sarah Oyelakin, Sabyasachi Mondal, and Precious Sibanda. Unsteady casson nanofluid flow over a stretching sheet with thermal radiation, convective and slip boundary conditions. *Alexandria engineering journal*, 55(2):1025–1035, 2016.

[14] Imran Ullah, Krishnendu Bhattacharyya, Sharidan Shafie, and Ilyas Khan. Unsteady mhd mixed convection slip flow of casson fluid over nonlinearly stretching sheet embedded in a porous medium with chemical reaction, thermal radiation, heat generation/absorption and convective boundary conditions. *PloS one*, 11(10):e0165348, 2016.

[15] Jagdev Singh, Devendra Kumar, and Sunil Kumar. An efficient computational method for local fractional transport equation occurring in fractal porous media. *Computational and Applied Mathematics*, 39(3):1–10, 2020.

[16] Kushal Dhar Dwivedi and Jagdev Singh. Numerical solution of two-dimensional fractional-order reaction advection sub-diffusion equation with finite-difference fibonacci collocation method. *Mathematics and Computers in Simulation*, 181:38–50, 2021.

[17] Maria Imtiaz, Tasawar Hayat, and Ahmed Alsaedi. Mixed convection flow of casson nanofluid over a stretching cylinder with convective boundary conditions. *Advanced Powder Technology*, 27(5):2245–2256, 2016.

[18] Mohamed R Eid and Kasseb L Mahny. Flow and heat transfer in a porous medium saturated with a sisko nanofluid over a nonlinearly stretching sheet with heat generation/absorption. *Heat Transfer—Asian Research*, 47(1):54–71, 2018.

[19] Mohamed R Eid. Chemical reaction effect on mhd boundary-layer flow of two-phase nanofluid model over an exponentially stretching sheet with a heat generation. *Journal of Molecular Liquids*, 220:718–725, 2016.

[20] Mohamed R Eid, KL Mahny, Amanullah Dar, and Taseer Muhammad. Numerical study for carreau nanofluid flow over a convectively heated nonlinear stretching surface with chemically reactive species. *Physica A: Statistical Mechanics and its Applications*, 540:123063, 2020.

[21] Mohamed R Eid. Time-dependent flow of water-nps over a stretching sheet in a saturated porous medium in the stagnation-point region in the presence of chemical reaction. *Journal of Nanofluids*, 6(3):550–557, 2017.

[22] M Mustafa and Junaid Ahmad Khan. Model for flow of casson nanofluid past a non-linearly stretching sheet considering magnetic field effects. *AIP advances*, 5(7):077148, 2015.

[23] M Wahiduzzaman, Md Musa Miah, Md Babul Hossain, Fatematuz Johora, and Shamol Mistri. Mhd casson fluid flow past a non-isothermal porous linearly stretching sheet. *Prog. Nonlinear Dynamics Chaos*, 2(2):61–69, 2014.

[24] Nargis Khan, Iram Riaz, Muhammad Sadiq Hashmi, Saed A Musmar, Sami Ullah Khan, Zahra Abdelmalek, and Iskander Tlili. Aspects of chemical entropy generation in flow of casson nanofluid between radiative stretching disks. *Entropy*, 22(5):495, 2020.

[25] Prabhakar Besthapu, Shanker Bandari, et al. Mixed convection mhd flow of a casson nanofluid over a nonlinear permeable stretching sheet with viscous dissipation. *Journal of Applied Mathematics and Physics*, 3(12):1580, 2015.

[26] S Pramanik. Casson fluid flow and heat transfer past an exponentially porous stretching surface in presence of thermal radiation. *Ain Shams Engineering Journal*, 5(1):205–212, 2014.

[27] P Bala Anki Reddy. Magnetohydrodynamic flow of a casson fluid over an exponentially inclined permeable stretching surface with thermal radiation and chemical reaction. *Ain Shams Engineering Journal*, 7(2):593–602, 2016.

[28] R Vijayaragavan. Magnetohydrodynamic radiative casson fluid flow over a stretching sheet with heat source/sink. *Advances in Physics Theories and Applications*, 55:13–23, 2016.

[29] Sami Ul Haq, Saeed Ullah Jan, Syed Inayat Ali Shah, Ilyas Khan, and Jagdev Singh. Heat and mass transfer of fractional second grade fluid with slippage and ramped wall temperature using caputo-fabrizio fractional derivative approach. *AIMS Mathematics*, 5(4):3056–3088, 2020.

[30] Sihem Lahmar, Mohamed Kezzar, Mohamed R Eid, and Mohamed Rafik Sari. Heat transfer of squeezing unsteady nanofluid flow under the effects of an inclined magnetic field and variable thermal conductivity. *Physica A: Statistical Mechanics and Its Applications*, 540:123138, 2020.

[31] Sohail Nadeem, Rizwan Ul Haq, Noreen Sher Akbar, and Zafar Hayat Khan. Mhd three-dimensional casson fluid flow past a porous linearly stretching sheet. *Alexandria Engineering Journal*, 52(4):577–582, 2013.

[32] SA Shehzad, T Hayat, M Qasim, and S Asghar. Effects of mass transfer on mhd flow of casson fluid with chemical reaction and suction. *Brazilian Journal of Chemical Engineering*, 30(1):187–195, 2013.

[33] SM Abo-Dahab, MA Abdelhafez, Fateh Mebarek-Oudina, and SM Bilal. Mhd casson nanofluid flow over nonlinearly heated porous medium in presence of extending surface effect with suction/injection. *Indian Journal of Physics*, pages 1–15, 2021.

[34] SM Ibrahim, G Lorenzini, P Vijaya Kumar, and CSK Raju. Influence of chemical reaction and heat source on dissipative mhd mixed convection flow of a casson nanofluid over a nonlinear permeable stretching sheet. *International Journal of Heat and Mass Transfer*, 111:346–355, 2017.

[35] T Hayat, SA Shehzad, A Alsaedi, and MS Alhothuali. Mixed convection stagnation point flow of casson fluid with convective boundary conditions. *Chinese Physics Letters*, 29(11):114704, 2012.

[36] V Puneeth, S Manjunatha, JK Madhukesh, and GK Ramesh. Three dimensional mixed convection flow of hybrid casson nanofluid past a non-linear stretching surface: A modified buongiorno's model aspects. *Chaos, Solitons & Fractals*, 152:111428, 2021.

[37] Wasim Jamshed, Vivek Kumar, and Vikash Kumar. Computational examination of casson nanofluid due to a non-linear stretching sheet subjected to particle shape factor: Tiwari and das model. *Numerical Methods for Partial Differential Equations*, 2020.

[38] Zahir Shah, Poom Kumam, and Wejdan Deebani. Radiative mhd casson nanofluid flow with activation energy and chemical reaction over past nonlinearly stretching surface through entropy generation. *Scientific Reports*, 10(1):1–14, 2020.

Non-polynomial spline solution of one dimensional singularly perturbed parabolic equations

Shahna[1], Talat Sultana[2] and Arshad Khan[3]

[1] Department of Mathematics, Sri Venkateswara College, University of Delhi, New Delhi-21, India.

[2] Department of Mathematics, Lakshmibai College, University of Delhi, New Delhi-52, India.

[3] Department of Mathematics, Jamia Millia Islamia, New Delhi-25, India.

Email - khan.shahana5@gmail.com, talat@lb.du.ac.in and akhan1234in@rediffmail.com

Abstract

In this paper, two-parameter singularly perturbed parabolic equations are examined by two level method using non-polynomial spline. We have used non-polynomial quadratic spline in space and finite difference discretization in time. Stability analysis is carried out. The approximate solution is shown to converge point-wise to the true solution. Numerical solution of singularly perturbed parabolic equations consisting of linear as well as non-linear has been solved. Three numerical examples are presented to show the efficiency and effectiveness of the developed method.

Key words: Two-parameter singularly perturbed problems; Non-polynomial splines; Stability analysis

Mathematics Subject Classification(2010): 65L10; 65D07

[1]

1 Introduction

We consider the two-parameter singularly perturbed one dimensional parabolic partial differential equation(PDE) of the form:

$$z_\kappa - \epsilon_d z_{\lambda\lambda} + \epsilon_c r(\lambda) z_\lambda + s(\lambda) z = g(\lambda, \kappa), \quad (\lambda, \kappa) \in Q_T, \tag{1.1}$$

subject to

$$z = 0, \ (\lambda, \kappa) \in \partial S \times I, \tag{1.2}$$

[1]Corresponding author: Department of Mathematics
Sri Venkateswara College
University of Delhi, New Delhi, India

and

$$z(\lambda,0) \quad = \quad z_0(\lambda),\ \lambda \in S, \tag{1.3}$$

where, $Q_T = S \times I,\ S \equiv r : l < r < m,\ \partial S \equiv \{l\} \cup \{m\},\ I \equiv (0,T)$ and $l(>0), m(>0) \in \mathbb{R}$, $z = z(\lambda,\kappa)$, $r(\lambda)$ and $s(\lambda)$ are continously differentiable functions and $g(\lambda,\kappa)$ is continuous function defined on Q_T. Also $0 < \epsilon_c \ll 1$ and $0 < \epsilon_d \ll 1$. The above problems occur in various fields of sciences, such as, elasticity, mechanics, chemical reactor theory and convection-diffusion process. There are numerous asymptotic expansion methods available for solution of problems of the above type. But there were difficulties in applying these asymptotic expansions in the inner and outer regions. Many researchers have derived numerical methods for solving singularly perturbed boundary value problems(SPBVPs). Scheme based on parametric spline functions has been developed by Khan et al.[5]. Fractional Kersten-Krasil'shchik coupled KdV mKdV System arising in multi-component plasmas have been numerically solved by Goswami et al.[3]. A uniform convergent numerical method is given by Clavero et al.[2] and Kadalbajoo et al.[4] to solve the one-dimensional time-dependent convection-diffusion problem. Sharma and Kaushik [8] solved a singularly perturbed time delayed convection diffusion problem on a domain which is rectangular. Zahra et al.[10], Aziz and Khan [1] have also used spline methods for solution of SPBVPs. An efficient numerical approach for fractional multi-dimensional diffusion equations with exponential memory is given by Singh et al.[9]. In recent past, Mohanty et al. [7] have solved singularly perturbed parabolic equations using methods based on spline in tension. In this paper, we develop a new algorithm for solving SPBVPs associated with homogeneous Dirichlet boundary conditions.
This paper is divided into 5 sections as follows: In Section 2, the non-polynomial spline scheme is derived. In Section 3, we discuss application of the method for SPBVPs with scheme of $O(k+h^2)$. Truncation error is also discussed in Section 3. In Section 4, stability analysis is carried out. In Section 5 three problems are solved which confirm theoretical behaviour along with the rate of convergence.

2 Non-polynomial Spline

We divide the *[l,m]* interval uniformaly as

$$l = \lambda_0 < \lambda_1 < \lambda_2 < \cdots < \lambda_{n-1} < \lambda_n = m,$$

where

$$\lambda_i = l + ih, \quad 0 \le i \le n \ \ and \ \ h = \frac{(m-l)}{n}.$$

Let

$$R_i(\lambda) = a_i \cos\tau(\lambda - \lambda_{i-1/2}) + b_i \sin\tau(\lambda - \lambda_{i-1/2}) + c_i, \tag{2.1}$$

be a non-polynomial spline defined on closed interval *[l,m]* reduces to polynomial spline which is quadratic as $\tau \longrightarrow 0$ and $\tau > 0$.
To calculate a_i, b_i and c_i, we define

$$\begin{aligned} R_i(\lambda_i) &= z_i,\ R_i'(\lambda_{i-1/2}) = P_{i-1/2}, \\ R_i''(\lambda_i) &= D_i,\ \ 0 \le i \le n-1. \end{aligned} \tag{2.2}$$

Using above interpolatory conditions we get

$$\begin{aligned} a_i &= -\frac{1}{\tau^2} D_i \sec\left(\frac{\vartheta}{2}\right) - \frac{1}{\tau} P_{i-1/2} \tan(\frac{\vartheta}{2}), \\ b_i &= \frac{1}{\tau} P_{i-1/2}, \\ c_i &= z_{i+1} - \frac{1}{\tau^2} D_i, \end{aligned}$$

where, $\vartheta = \tau h$.
Using continuity conditions, $R_{i-1}^{(m)}(\lambda_{i-1/2}) = R_i^{(m)}(\lambda_{i-1/2}), m = 0, 1$ we get the expression as follows:

$$z_{i-1} - 2z_i + z_{i+1} = h^2(\delta D_{i-1} + \eta D_i + \zeta D_{i+1}), 0 \le i \le n-1 \tag{2.3}$$

where,

$$\begin{aligned} \delta &= \frac{\sec(\frac{\vartheta}{2}) - 1}{\vartheta^2}, \\ \eta &= \frac{4\sec(\frac{\vartheta}{2})(1 - \cos^2(\frac{\vartheta}{2})) + 2(1 - \sec(\frac{\vartheta}{2}))}{\vartheta^2}, \\ \zeta &= \delta. \end{aligned}$$

When $\tau \to 0$, it means $\vartheta \to 0$, then $(\delta, \eta, \zeta) \to (1/8, 6/8, 1/8)$, and the scheme given by (2.3) reduces into polynomial quadratic spline relation as:

$$z_{i-1} - 2z_i + z_{i+1} = \frac{1}{8} h^2 (D_{i-1} + 6D_i + D_{i+1}), 0 \le i \le n-1. \tag{2.4}$$

3 Application of the scheme

We consider a SPBVP of the form

$$z_\kappa - \epsilon_d z_{\lambda\lambda} + \epsilon_c r(\lambda) z_\lambda + s(\lambda) z = g(\lambda, \kappa), \quad (\lambda, \kappa) \in Q_T, \tag{3.1}$$

where, $Q_T = S \times I$, $S \equiv r : l < r < m$, $\partial S \equiv \{l\} \cup \{m\}$, $I \equiv (0, T)$ and $l(>0), m(>0) \in \mathbb{R}$. The above equation with

$$z = 0,\ (\lambda, \kappa) \in \partial S \times I,$$

and

$$z(\lambda, 0) = z_0(\lambda),\ \lambda \in S.$$

Here, we use the following derivative approximations of higher order as:

$$\begin{aligned} z_i' &= \frac{z_{i+1}-z_{i-1}}{2h}, \\ z_{i-1}' &= \frac{-3z_{i-1}+4z_i-z_{i+1}}{2h}, \\ z_{i+1}' &= \frac{z_{i-1}-4z_i+3z_{i+1}}{2h}, \\ z_{ti}^j &= \frac{z_i^{j+1}-z_i^j}{k}, \\ z_{ti-1}^j &= \frac{z_{i-1}^{j+1}-z_{i-1}^j}{k}, \\ z_{ti+1}^j &= \frac{z_{i+1}^{j+1}-z_{i+1}^j}{k}. \end{aligned}$$

We consider the following ordinary differential equation

$$\begin{aligned} \epsilon_d \frac{d^2z}{d\lambda^2} &= \epsilon_c r(\lambda)\frac{dz}{d\lambda} + s(\lambda)z - g(\lambda) \\ &\equiv G(\lambda, z, z'). \end{aligned} \tag{3.2}$$

After implementing scheme (2.3) on BVP (3.2), we obtain:

$$z_{i-1} - 2z_i + z_{i+1} = h^2(\delta G_{i-1} + \eta G_i + \zeta G_{i+1}),\ 1 \le i \le n-1 \tag{3.3}$$

where,

$$\begin{aligned} G_{i-1} &= G(\lambda_{i-1}, z_{i-1}, z_{i-1}'), \\ G_i &= G(\lambda_i, z_i, z_i'), \\ G_{i+1} &= G(\lambda_{i+1}, z_{i+1}, z_{i+1}'), \end{aligned}$$

Using derivative approximations, we obtain

$$\tilde{A}z_{i-1} + \tilde{B}z_i + \tilde{C}z_{i+1} = -h^2(\delta g_{i-1} + \eta g_i + \zeta g_{i+1}), 1 \le i \le n-1 \tag{3.4}$$

where,

$$\begin{aligned} \tilde{A} &= \epsilon_d + \frac{3}{2}h\delta\epsilon_c r_{i-1} - \delta h^2 s_{i-1} + \frac{h}{2}\eta\epsilon_c r_i - \frac{h}{2}\zeta\epsilon_c r_{i+1}, \\ \tilde{B} &= -2\epsilon_d - 2h\delta\epsilon_c r_{i-1} - \eta h^2 s_i + 2h\zeta\epsilon_c r_{i+1}, \\ \tilde{C} &= \epsilon_d + \frac{1}{2}h\delta\epsilon_c r_{i-1} - \zeta h^2 s_{i+1} - \frac{h}{2}\eta\epsilon_c r_i - \frac{3h}{2}\zeta\epsilon_c r_{i+1}. \end{aligned}$$

For solving parabolic equation (3.1) we obtain the two level spline scheme by replacing z_i by $\frac{1}{2}(z_i^{j+1} + z_i^j)$, z_{i+1} by $\frac{1}{2}(z_{i+1}^{j+1} + z_{i+1}^j)$, z_{i-1} by $\frac{1}{2}(z_{i-1}^{j+1} + z_{i-1}^j)$, g_i by $(\frac{z_i^{j+1}-z_i^j}{k} + g_i^j)$, g_{i+1} by $(\frac{z_{i+1}^{j+1}-z_{i+1}^j}{k} + g_{i+1}^j)$ and g_{i-1} by $(\frac{z_{i-1}^{j+1}-z_{i-1}^j}{k} + g_{i-1}^j)$ in (3.4) and hence we obtain as follows:

$$\begin{aligned} A_1 z_{i-1}^{j+1} + A_2 z_i^{j+1} + A_3 z_{i+1}^{j+1} &= A_4 z_{i-1}^j + A_5 z_i^j + A_6 z_{i+1}^j - h^2(\delta g_{i-1}^j + \eta g_i^j + \zeta g_{i+1}^j), \\ &\quad 1 \le i \le n-1 \end{aligned} \tag{3.5}$$

where,

$$\begin{aligned}
A_1 &= \frac{-h^2\delta}{k}+\frac{1}{2}(\epsilon_d+\frac{3}{2}h\delta\epsilon_c r_{i-1}-\delta h^2 s_{i-1}+\frac{h}{2}\eta\epsilon_c r_i-\frac{h}{2}\zeta\epsilon_c r_{i+1}),\\
A_2 &= \frac{-h^2\eta}{k}+\frac{1}{2}(-2\epsilon_d-2h\delta\epsilon_c r_{i-1}-\eta h^2 s_i+2h\zeta\epsilon_c r_{i+1}),\\
A_3 &= \frac{-h^2\zeta}{k}+\frac{1}{2}(\epsilon_d+\frac{1}{2}h\delta\epsilon_c r_{i-1}-\zeta h^2 s_{i+1}-\frac{h}{2}\eta\epsilon_c r_i-\frac{3h}{2}\zeta\epsilon_c r_{i+1}),\\
A_4 &= \frac{-h^2\delta}{k}+\frac{1}{2}(-\epsilon_d-\frac{3}{2}h\delta\epsilon_c r_{i-1}+\delta h^2 s_{i-1}-\frac{h}{2}\eta\epsilon_c r_i+\frac{h}{2}\zeta\epsilon_c r_{i+1}),\\
A_5 &= \frac{-h^2\eta}{k}+\frac{1}{2}(2\epsilon_d+2h\delta\epsilon_c r_{i-1}+\eta h^2 s_i-2h\zeta\epsilon_c r_{i+1}),\\
A_6 &= \frac{-h^2\zeta}{k}+\frac{1}{2}(-\epsilon_d-\frac{1}{2}h\delta\epsilon_c r_{i-1}+\zeta h^2 s_{i+1}+\frac{h}{2}\eta\epsilon_c r_i+\frac{3h}{2}\zeta\epsilon_c r_{i+1}).
\end{aligned}$$

Error

Here, we expand the scheme(3.5) in terms of $z(\lambda_i,\kappa_j)$ using Taylor's series and get the expression for truncation error as follows:

$$\begin{aligned}
t_i &= \Big[h^2[1-(\delta+\eta+\zeta)]D_\lambda^2-\frac{1}{2}k[\delta h^2 s_{i-1}+\eta h^2 s_i+\zeta h^2 s_{i+1}]D_t+h^3[\delta-\zeta]D_\lambda^3\\
&\quad +h^4[\frac{1}{12}-\frac{\delta+\zeta}{2}]D_\lambda^4-\frac{1}{4}k^2[\delta h^2 s_{i-1}+\eta h^2 s_i+\zeta h^2 s_{i+1}]D_t^2+h^5[\frac{\delta-\zeta}{3!}]D_\lambda^5\\
&\quad +h^6[\frac{1}{360}-\frac{\delta+\zeta}{24}]D_\lambda^6+...\Big]z_i^j,\ 1\le i\le n-1. \qquad (3.6)
\end{aligned}$$

For $\delta+\eta+\zeta=1$ and $\delta=\zeta$, the method of $O(k+h^2)$ is obtained.

4 Stability Analysis

Here, we obtain the expression which gives information regarding stability of the scheme (3.5). We take Z_i^j as actual solution which satisfies the equation

$$\begin{aligned}
A_1Z_{i-1}^{j+1}+A_2Z_i^{j+1}+A_3Z_{i+1}^{j+1} &= A_4Z_{i-1}^j+A_5Z_i^j+A_6Z_{i+1}^j-h^2(\delta g_{i-1}^j+\eta g_i^j\\
&\quad +\zeta g_{i+1}^j),\ 1\le i\le n-1. \qquad (4.1)
\end{aligned}$$

We assume that an error $e_i^j=Z_i^j-z_i^j$ exist at each point (λ_i,κ_j), then by subtracting (3.5) from (4.1) we get the expression as

$$\begin{aligned}
A_1e_{i-1}^{j+1}+A_2e_i^{j+1}+A_3e_{i+1}^{j+1} &= A_4e_{i-1}^j+A_5e_i^j+A_6e_{i+1}^j,\\
&\quad 1\le i\le n-1. \qquad (4.2)
\end{aligned}$$

To derive stability analysis for the scheme (3.5), we assume that the solution of the homogeneous part of (4.2) is of the form $e_i^j=\varpi^j e^{i\rho}$, where $\varpi\in\mathbb{C}$, $i=\sqrt{-1}$

and $\rho \in \mathbb{R}$. Finally, we get the amplification factor as

$$\varpi = \frac{A_4 e^{-i\rho} + A_5 + A_6 e^{i\rho}}{A_1 e^{-i\rho} + A_2 + A_3 e^{i\rho}}, \tag{4.3}$$

then,

$$\varpi = \frac{-\frac{h^2}{k\epsilon_d}(\delta+\rho) - \frac{h^2}{\epsilon_d}(\delta q_{i-1} - \eta q_i + \zeta q_{i+1}) + 2B_1 \sin^2(\frac{\rho}{2}) + iB_2 \sin(\frac{\rho}{2})}{-\frac{h^2}{k\epsilon_d}(\delta+\rho) + \frac{h^2}{\epsilon_d}(\delta q_{i-1} - \eta q_i + \zeta q_{i+1}) - 2B_1 \sin^2(\frac{\rho}{2}) + iB_2 \sin(\frac{\rho}{2})},$$

where

$$B_1 = 1 + \frac{h^2}{k\epsilon_d}(\delta+\zeta) + h\frac{\epsilon_c}{\epsilon_d}(\delta p_{i-1} - 2\zeta p_{i+1}) + h^2\frac{1}{\epsilon_d}(\delta q_{i-1} + \zeta q_{i+1}),$$

$$B_2 = \frac{h^2}{k\epsilon_d}(\delta-\rho) + \frac{1}{2\epsilon_d}[h\epsilon_c(\delta p_{i-1} + \eta p_i - \zeta p_{i+1}) + h^2(\zeta q_{i+1} - \delta q_{i-1})].$$

The condition for the scheme to be stable is $|\varpi| \leq 1$. As we know that $0 \leq \sin^2(\frac{\rho}{2}) \leq 1$ and $\epsilon_d \propto h$, then from above relation it is easily verified that $|\varpi| \leq 1$ for every ρ. Hence the developed method is unconditionally stable.

5 Numerical Illustrations

We consider three second order SPBVPs. The maximum absolute errors(MAE) are tabulated in Tables 1-4 depending upon the choice of parameters. The convergence rate is denoted by α_n and is computed by following expression:

$$\alpha_n = \ln_2(Er_{n,k}/Er_{2n,k}),$$

and there is a different way to find rate of convergence denoted by $\tilde{\alpha}_n$ and is computed by using

$$\tilde{\alpha}_n = \ln_2(Er_{n,k}/Er_{2n,k/2}).$$

Example 1:

Consider the following problem from Zahra et al.[10].

$$z_\kappa - \epsilon_d\, z_{\lambda\lambda} + z_\lambda = g(\lambda,\kappa), T = 1,$$

in [0,1] associated with $z(0,\kappa) = 0, z(1,\kappa) = 0$ and $z_0(\lambda) = \exp(-1/\epsilon_d) + (1 - \exp(-1/\epsilon_d))\lambda - \exp(-(1-\lambda)/\epsilon_d)$, where
$g(\lambda,\kappa) = \exp(-\kappa)(-c_1 + c_2(1-\lambda) + \exp(-(1-\lambda)/\epsilon_d))$.

The analytical solution is $z(\lambda,\kappa) = \exp(-\kappa)(c_1 + c_2\lambda - \exp(-(1-\lambda)/\epsilon_d))$, where $c_1 = \exp(-1/\epsilon_d), c_2 = 1 - \exp(-1/\epsilon_d)$. The numerical results for $N = 2^4, 2^5, 2^6, 2^7$ and $\epsilon_d = 1/2^8, 1/2^{10}, 1/2^{12}, 1/2^{24}, 1/2^{26}$ using parameters $(\delta,\eta,\zeta) = \frac{1}{8}(1,6,1)$ compared with Zahra et al.[10] are tabulated in Table 1. And for $N = 2^4, 2^5, 2^6, 2^7, 2^8, 2^9$ and $\epsilon_d = 1, 1/4, 1/16, 1/64$ using parameters $(\delta,\eta,\zeta) = \frac{1}{8}(1,6,1)$ compared with Clavero et al.[2] are tabulated in Table 2.

Example 2:

Consider the following PDE from Zahra et al.[10]

$$z_\kappa - \epsilon_d \; z_{\lambda\lambda} + \epsilon_c \; z_\lambda \quad = \quad g(\lambda,\kappa), \; T = 1,$$

in [0,1] associated with $z(0,\kappa) = 0, z(1,\kappa) = 0$ and $z_0(\lambda) = [\phi_1 \cos(\pi\lambda) + \phi_2 \sin(\pi\lambda) + \psi_1 \exp(\theta_1\lambda) + \psi_2 \exp(-\theta_2(1-\lambda))]$, where
$g(\lambda,\kappa) = \exp(-\kappa)[\{-\phi_1 \cos(\pi\lambda) - \phi_2 \sin(\pi\lambda) - \psi_1 \exp(\theta_1\lambda) - \psi_2 \exp(-\theta_2(1-\lambda))\} + \epsilon_d\{\phi_1\pi^2 \cos(\pi\lambda) + \phi_2\pi^2 \sin(\pi\lambda) - \frac{\psi_1}{\theta_1^2} \exp(\theta_1\lambda) - \frac{\psi_2}{\theta_2^2} \exp(-\theta_2(1-\lambda))\} + \epsilon_c\{-\phi_1\pi \cos(\pi\lambda) + \phi_2\pi \sin(\pi\lambda) + \frac{\psi_1}{\theta_1} \exp(\theta_1\lambda) + \frac{\psi_2}{\theta_2} \exp(-\theta_2(1-\lambda))\}]$. The analytical solution is $z(\lambda,\kappa) = \exp(-\kappa)[\phi_1 \cos(\pi\lambda) + \phi_2 \sin(\pi\lambda) + \psi_1 \exp(\theta_1\lambda) + \psi_2 \exp(-\theta_2(1-\lambda))]$ where,

$$\begin{aligned}
\phi_1 &= \frac{\epsilon_d\pi^2 + 1}{\epsilon_c^2\pi^2 + (\epsilon_d\pi^2 + 1)^2}, \\
\phi_2 &= \frac{\epsilon_c\pi}{\epsilon_c^2\pi^2 + (\epsilon_d\pi^2 + 1)^2}, \\
\psi_1 &= -\phi_1 \frac{1 + \exp(-\theta_2)}{1 - \exp(\theta_1 - \theta_2)}, \\
\psi_2 &= \phi_1 \frac{1 + \exp(\theta_1)}{1 - \exp(\theta_1 - \theta_2)}, \\
\theta_1 &= \frac{\epsilon_c - \sqrt{\epsilon_c^2 + 4\epsilon_d}}{2\epsilon_d}, \\
\theta_2 &= \frac{\epsilon_c + \sqrt{\epsilon_c^2 + 4\epsilon_d}}{2\epsilon_d}.
\end{aligned}$$

The numerical results for $N = 2^4, 2^5, 2^6, 2^7, 2^8$, $\epsilon_d = 1, 1/4, 1/16$ and $\epsilon_c = 10^{-3}, 10^{-4}, 10^{-5}$ using parameters $(\delta,\eta,\zeta) = \frac{1}{8}(1,6,1)$ are tabulated in Table 3.

Example 3:

Consider the following PDE from Mohanty et al.[6]

$$\epsilon_d \; z_{\lambda\lambda} - z_\kappa + \frac{1}{\lambda} z_\lambda \quad = \quad g(\lambda,\kappa), \; 0 \le \lambda \le 1, \; \kappa > 0$$

The analytical solution is $z(\lambda,\kappa) = \exp(-\kappa)\sinh\lambda$. The right-hand-side functions, initial and boundary conditions may be obtained using the actual solution given above as a test procedure. The numerical results for $N = 2^4, 2^5, 2^6, 2^7, 2^8$ and $\epsilon_d = 1/2, 1/8, 1/16, 1/32, 1/64, 1/128$ using parameters $(\delta,\eta,\zeta) = \frac{1}{12}(1,10,1)$ compared with Mohanty et al.[6] are tabulated in Table 4.

Table 1: MAE of example 1 for $(\delta, \eta, \zeta) = \frac{1}{8}(1, 6, 1)$

Method	$N \backslash \epsilon_d$	$1/2^8$	$1/2^{10}$	$1/2^{12}$	$1/2^{24}$	$1/2^{26}$
Presented method	2^4	1.2136×10^{-02}	1.3494×10^{-02}	1.3835×10^{-02}	1.3949×10^{-02}	1.3949×10^{-02}
α_n		1.1344	0.9591	0.9231	0.91170	0.91170
Zahra et al.[10]		3.5638×10^{-02}	5.1972×10^{-02}	6.7088×10^{-02}	7.3818×10^{-02}	7.1839×10^{-02}
Presented method	2^5	5.5284×10^{-03}	6.9407×10^{-03}	7.2961×10^{-03}	7.4147×10^{-03}	7.4147×10^{-03}
α_n		1.4946	1.0549	0.9785	0.9554	0.9554
Zahra et al.[10]		1.300×10^{-02}	1.4234×10^{-02}	2.3185×10^{-02}	3.4126×10^{-02}	3.4128×10^{-02}
Presented method	2^6	1.9619×10^{-03}	3.3406×10^{-03}	3.7029×10^{-03}	3.8238×10^{-03}	3.8238×10^{-03}
α_n		2.1590	1.1997	1.0249	0.9776	0.9776
Zahra et al.[10]		9.3378×10^{-03}	8.3305×10^{-03}	8.2129×10^{-03}	1.5756×10^{-02}	1.5761×10^{-02}
Presented method	2^7	4.4173×10^{-04}	1.4543×10^{-03}	1.8198×10^{-03}	1.9419×10^{-03}	1.9419×10^{-03}
Zahra et al.[10]		8.4218×10^{-03}	7.9579×10^{-03}	7.6243×10^{-03}	9.1052×10^{-03}	9.1078×10^{-03}

Table 2: MAE of example 1 for $(\delta, \eta, \zeta) = \frac{1}{8}(1, 6, 1)$

Method	$N \setminus \epsilon_d$	1	1/4	1/16	1/64
Presented Method	2^4	7.8074×10^{-04}	1.2280×10^{-03}	1.0487×10^{-02}	1.0921×10^{-01}
Clavero et al.[2]		1.3076×10^{-03}	1.7398×10^{-03}	4.0133×10^{-02}	5.9664×10^{-02}
	$\tilde{\alpha}_n$	1.7534	1.9008	2.5426	1.3506
Presented Method	2^5	2.3156×10^{-04}	3.2887×10^{-04}	1.8000×10^{-03}	4.2823×10^{-02}
Clavero et al.[2]		7.9078×10^{-04}	9.6845×10^{-03}	2.5552×10^{-03}	3.7372×10^{-02}
	$\tilde{\alpha}_n$	1.8952	1.8851	2.4931	2.0663
Presented Method	2^6	6.2255×10^{-05}	8.9033×10^{-05}	3.1971×10^{-04}	1.0225×10^{-02}
Clavero et al.[2]		3.6986×10^{-04}	5.1056×10^{-03}	1.5865×10^{-02}	2.1792×10^{-02}
	$\tilde{\alpha}_n$	1.9602	1.9124	2.4935	2.6020
Presented Method	2^7	1.5998×10^{-05}	2.3652×10^{-05}	5.6774×10^{-05}	1.6841×10^{-03}
Clavero et al.[2]		1.8894×10^{-04}	2.6223×10^{-03}	9.5603×10^{-03}	1.2381×10^{-03}
	$\tilde{\alpha}_n$	1.9638	1.9347	2.4473	2.5951
Presented Method	2^8	4.1011×10^{-06}	6.1867×10^{-06}	1.0409×10^{-05}	2.7872×10^{-04}
Clavero et al.[2]		9.5517×10^{-05}	1.3289×10^{-03}	5.5999×10^{-03}	6.9704×10^{-03}
	$\tilde{\alpha}_n$	1.9676	1.9514	2.3371	2.6674
Presented Method	2^9	1.0486×10^{-06}	1.5996×10^{-06}	2.0601×10^{-06}	4.3874×10^{-05}
Clavero et al.[2]		4.8028×10^{-05}	6.6891×10^{-04}	3.2019×10^{-03}	3.9052×10^{-03}

Table 3: MAE of example 2 for $(\delta, \eta, \zeta) = \frac{1}{8}(1, 6, 1)$

ϵ_d	1			1/4			1/16		
$\epsilon_c \setminus N$	10^{-3}	10^{-4}	10^{-5}	10^{-3}	10^{-4}	10^{-5}	10^{-3}	10^{-4}	10^{-5}
2^4	5.7028× 10^{-06}	5.6372× 10^{-06}	5.6328× 10^{-06}	7.6099× 10^{-03}	7.5937× 10^{-03}	7.5920× 10^{-03}	3.0375× 10^{-01}	3.0260× 10^{-01}	3.0248× 10^{-01}
α_n	1.4451	1.4479	1.4482	1.8084	1.8084	1.8084	1.8258	1.8258	1.8258
2^5	2.0944× 10^{-06}	2.0671× 10^{-06}	2.0643× 10^{-06}	2.1726× 10^{-03}	2.1681× 10^{-03}	2.1676× 10^{-03}	8.5684× 10^{-02}	8.5356× 10^{-02}	8.5324× 10^{-02}
α_n	1.8444	1.8459	1.8461	1.8568	1.8568	1.8568	1.9140	1.9140	1.9140
2^6	5.8324× 10^{-07}	5.7502× 10^{-07}	5.7420× 10^{-07}	5.9986× 10^{-04}	5.9857× 10^{-04}	5.9845× 10^{-04}	2.2736× 10^{-02}	2.2650× 10^{-02}	2.2640× 10^{-02}
α_n	1.9487	1.9496	1.9497	1.9306	1.9306	1.9306	1.9572	1.9572	1.9572
2^7	1.5108× 10^{-07}	1.4886× 10^{-07}	1.4864× 10^{-07}	1.5736× 10^{-04}	1.5702× 10^{-04}	1.5698× 10^{-04}	5.8551× 10^{-03}	5.8328× 10^{-03}	5.8800× 10^{-03}
α_n	1.9810	1.9815	1.9816	1.9658	1.9658	1.9658	1.9786	1.9786	1.9786
2^8	3.8272× 10^{-08}	3.7696× 10^{-08}	3.7639× 10^{-08}	4.0284× 10^{-05}	4.0197× 10^{-05}	4.0188× 10^{-05}	1.4856× 10^{-03}	1.4799× 10^{-03}	1.4799× 10^{-03}

Table 4: MAE of example 3 for $(\delta, \eta, \zeta) = \frac{1}{12}(1, 10, 1)$

Method	$N \setminus \epsilon_d$	1/2	1/8	1/16	1/32	1/64	1/128
Presented method	2^4	7.2294 × 10^{-04}	8.0022 × 10^{-04}	8.2241 × 10^{-04}	8.3576 × 10^{-04}	8.4320 × 10^{-04}	8.4714 × 10^{-04}
Mohanty et al.[6]		0.2924 × 10^{-03}	0.4454 × 10^{-03}	0.4777 × 10^{-03}	0.5054 × 10^{-03}	0.5344 × 10^{-03}	0.5615 × 10^{-03}
Presented method	2^5	1.2613 × 10^{-05}	1.3899 × 10^{-05}	1.4267 × 10^{-04}	1.4488 × 10^{-04}	1.4610 × 10^{-04}	1.4675 × 10^{-04}
Mohanty et al.[6]		0.7286 × 10^{-04}	0.1129 × 10^{-03}	0.1239 × 10^{-03}	0.1410 × 10^{-03}	0.1869 × 10^{-03}	0.3134 × 10^{-03}
Presented method	2^6	2.2181 × 10^{-05}	2.4391 × 10^{-05}	2.5022 × 10^{-05}	2.5721 × 10^{-05}	2.5610 × 10^{-05}	2.5721 × 10^{-05}
Mohanty et al.[6]		0.1814 × 10^{-04}	0.2835 × 10^{-04}	0.3166 × 10^{-04}	0.3984 × 10^{-04}	0.9429 × 10^{-04}	0.1684 × 10^{-03}
Presented method	2^7	3.9130 × 10^{-06}	4.2982 × 10^{-06}	4.4079 × 10^{-06}	4.5295 × 10^{-06}	4.5102 × 10^{-06}	4.5295 × 10^{-06}
Mohanty et al.[6]		0.4524 × 10^{-05}	0.7091 × 10^{-05}	0.7987 × 10^{-05}	0.1088 × 10^{-04}	0.4743 × 10^{-04}	0.9120 × 10^{-04}
Presented method	2^8	6.9111 × 10^{-07}	7.5878 × 10^{-07}	7.7796 × 10^{-07}	7.9929 × 10^{-07}	7.7590 × 10^{-07}	7.9929 × 10^{-07}
Mohanty et al.[6]		0.1129 × 10^{-05}	0.1771 × 10^{-05}	0.2002 × 10^{-05}	0.2844 × 10^{-05}	0.1821 × 10^{-05}	0.5283 × 10^{-04}

Conclusion

We have presented two level scheme using non-polynomial spline for solving singularly perturbed parabolic equations based on one dimension. In examples 1, 2 and 3, we have computed maximum absolute errors for different values of N and ϵ_d for the sake of comparison with references [2,6,10] and results are tabulated in Tables 1-4. From tables it is shown that our method is much better in accuracy than the methods given by Clavero et al.[2], Mohanty et al.[6] and Zahra et al.[10]. It has already been proved that the presented algorithm gives higher numerical rate of convergence. It has also shown that the scheme is unconditionally stable.

References

[1] Aziz T and Khan A (2002) A spline method for second-order singularly perturbed boundary-value problems. J. Comput. Appl. Math., 147(2):445-452

[2] Clavero C, Jorge JC , Lisbona F (2003) Uniformly convergent scheme on a nonuniform mesh for convection-diffusion parabolic problems. J. Comput. Appl. Math., 154(2):415-429

[3] Goswami A, Sushila, Singh J, Kumar D (2020) Numerical computation of fractional Kersten-Krasil'shchik coupled KdV mKdV System arising in multi-component plasmas. AIMS Math., 5(3):2346-2368

[4] Kadalbajoo MK, Gupta V and Awasthi A (2008) A uniformly convergent B-Spline collocation method on a nonuniform mesh for singularly perturbed one-dimensional time-dependent linear convection-diffusion problem. J. Comput. Appl. Math., 220(1-2):271-289

[5] Khan A, Khan I and Aziz T (2005) A survey on parametric spline function approximation. Appl. Math. Comput., 171(2):983-1003

[6] Mohanty RK, Dahiya V and Khosla N (2012) Spline in compression methods for singularly perturbed 1D parabolic equations with singular coefficients. Open J. Discrete Math., 2(2):70-77

[7] Mohanty RK, Kumar R and Dahiya V (2012) Spline in tension methods for singularly perturbed one space dimensional parabolic equations with singular coefficients. Neural Parallel & Scientific Computing, 20(1):81-92

[8] Sharma M and Kaushik A (2012) Convergence analysis of weighted difference approximations on piecewise uniform grids to a class of singularly perturbed functional differential equations. J. Optim. Theory Appl., 155(1):252-272

[9]Singh J, Kumar D, Purohit SD, Mishra AM, Bohra M (2021) An efficient numerical approach for fractional multi-dimensional diffusion equations with exponential memory. Num. Meth. for Partial Diff. Eqs., 37(2):1631-1651

[10] Zahra WK, El-Azab MS, Mhlawy, Ashraf M El (2014) Spline difference scheme for two parameter singularly perturbed partial differential equations. J. Appl. Math. Inform., 32(1-2):185-201

Solving System of Boundary Value Problems using Non polynomial Spline Methods Based on Off-step Mesh

Sucheta Nayak*, Arshad Khan and R. K. Mohanty

January 1, 2022

Abstract

We present two non polynomial spline methods based on quasi-variable mesh using off-step points to solve the system of boundary value problems which are nonlinear. We also discuss how the methods handle the presence of singularity. The proposed methods has been shown second and third-order convergent for a model linear problem. The methods are implemented on existing problems which are linear, non linear as well as singular. The obtained numerical results approximate the exact solutions very well and validate the theoretical findings.

Key words: Off-step, non polynomial, quasi-variable mesh, singular, nonlinear, system.
Mathematics Subject Classification(2010): 65L10.

1 Introduction

In this paper, we seek solution for the following system of M boundary value problems(BVPs) which are non linear as well as singular.

$$\frac{d^2y^i}{dx^2} = f^i(x, y^1, ..., y^i, ..., y^M, \frac{dy^1}{dx}, ..., \frac{dy^i}{dx}, ..., \frac{dy^M}{dx}), \tag{1.1}$$

$$y^i(0) = a_i, y^i(1) = b_i, \quad \text{where} \quad a_i, b_i \in R, \ i = 1(1)M. \tag{1.2}$$

We consider $-\infty < y^i, \frac{dy^i}{dx} < \infty$ and the conditions such that f^i is continuous and its partial derivatives w.r.t. y^j and $\frac{dy^i}{dx}$ exist, continuous and are positive. Also partial derivative w.r.t. $\frac{dy^i}{dx}$ is bounded by some $K > 0$, $j, i = 1(1)M$, to ensure the existence [13] of a unique solution $(1.1) - (1.2)$.

*Corresponding author: Department of Mathematics, Lady Shri Ram College for Women, University of Delhi, New Delhi-24, India suchetanayak@ lsr.edu.in

Such systems like the fourth order Euler differential equations [5], coupled Navier stokes in fluid dynamics and Maxwell's equations of electromagnetism[9], system of differential equations[28], fourth order non linear differential equations [27] simulates many real world problems. A few more examples are as follows:
(i)In Plate deflection theory

$$(-1)^n y^{(2n)}(x) = f(x, y(x)), n \in N$$
$$y^{(2i)}(a) = A_{2i}, y^{(2i)}(b) = B_{2i}, i \in [0, k-1]$$

(ii)Three box cars on a level track connected by springs is modelled as follows:

$$mx_1'' = -sx_1 + sx_2,$$
$$mx_2'' = sx_1 - 2sx_2 + sx_3,$$
$$mx_3'' = -sx_3,$$

where m, x_1, x_2, x_3 and s are masses,positions of the boxcars and Hooke's constant.

(iii)A horizontal earthquake wave F affects every floor of a building. If there are three floors, then equations for the floor is modelled as follows:

$$M_1x_1'' = -(r_1 + r_2)x_1 + r_2x_2,$$
$$M_2x_2'' = r_2x_1 - (r_2 + r_3)x_2 + r_3x_3,$$
$$M_3x_3'' = r_3x_2 - (r_3 + r_4)x_3,$$

where M_i, x_1, x_2, x_3 and r_i are point masses of each floor, location of masses and Hooke's constant.

Such systems of BVPs comprising first or second order BVPs not only models many real life problems but are also instrumental in solving many higher order problems by decomposing them. Authors like Aftabizadeh[1], Agarwal[2], Regan[24] have developed theories related to existence and uniqueness of solutions for these BVPs. But, for our work, we focus on system of second order BVPs which are non linear as well singular in nature. These problems have extensive application and has been the cause of interest for many authors. Many efficient numerical methods have been developed to solve second order BVPs and 'Splines' have been very instrumental for solving such problems. Mohanty et.al.([15],[16], [18], [21]) developed AGE iterative methods. In these methods, using Taylor's theorem derivatives are approximated and accordingly a finite difference scheme was developed. Then the resultant system solved by splitting the coefficient matrix into sum of three matrices. Also Mohanty et.al.([17],[19],[20],[22]) derived polynomial and non polynomial spline methods based on uniform and variable mesh to solve class of problems ranging from linear, nonlinear, singular and singularly perturbed BVP. A third order cubic spline method based on non uniform mesh was developed by Kadalbajoo et. al[12] to solve singularly perturbed BVPs. BVPs of eighth order were solved by Akram and Rehman[4] using kernel space method. Eighth and sixth order BVPs were solved by Siddiqi and Akram ([30], [31]) using non-polynomial and

septic spline. Jha and Bieniasz[11] developed a scheme based on geometric mesh to solve sixth order differential equation by converting it into system of second order differential equations. Infact, very recently, apart from the schemes based on classical finite differences some other kinds of methods were also developed. Bhrawy et. al.[6] developed collocation method based on Jacobi polynomials and solved nonlinear second-order initial value problems. Dwivedi and Singh [7] developed collocation method based on Fibbonacci polynomial to solve sub diffusion equations. Singh et.al.[32] developed finite difference scheme based on homotopy analysis transform technique to solve fractional non-linear coupled problem. Such considerable amount of work has motivated us to develop a numerical method to solve the higher order problem as well as system of linear and non linear singular BVPs.

In this paper, generalized non polynomial spline schemes have been developed which are based on off-step points using quasi-variable mesh. We use a second order BVP to derive the methods. As per the methods developed, we decompose the higher order BVP into system of second order BVPs (1) alongwith modifying the boundary conditions. Also, we have solved singular BVPs. The off-step points used in the method allows us to overcome the singularity. Moreover, since we use the quasi-variable mesh the error gets uniformly distributed throughout the solution domain. Finally, as we use the boundary conditions in the scheme, we get a tri-diagonal matrix with block elements representing the system of equations to be solved.

We have solved seven problems and demonstrated the accuracy of the proposed methods. The BVPs considered in this paper have been solved by other methods as well. Twizell [29] used modified extrapolation method to solve fourth order linear BVPs, Akram and Siddiqi[3] used non polynomial spline method which is second order convergent to solve linear sixth order BVPs. Khan and Khandelwal[14]and Sakai and Usmani[25] used splines to solve nonlinear fourth and sixth order BVPs.

2 Method Formulation

We use a non linear BVP of second order and derive the method in scalar form:

$$y'' = f(x, y, y'), \text{ subject to } y(0) = a, y(1) = b. \tag{2.1}$$

Now, we divide the solution region [0,1] into $N+1$ points such as $x_j, j = 0(1)N$ with mesh size h_j such that $x_j = x_{j-1} + h_j, \frac{h_{j+1}}{h_j} = \sigma_j, j = 1(1)N-1$ where the σ_j is the mesh ratio. When mesh ratio is one, the quasi-variable mesh converts to a uniform mesh with width, say h. Now, we choose $\sigma_j = \sigma$ a constant $\forall j$ without loss of generality. Also, let the exact solution of (2.1) be $y(x_j)$ or y_j at the grid points x_j. Now, we define the the following non polynomial spline function:

$$S_j(x) = d_j \sin(kx - kx_j) + c_j \cos(kx - kx_j) + b_j(x - x_j) + a_j,\ x_{j-1} \le x \le x_j. \tag{2.2}$$

Here, $S_j(x)$ has continuous second derivative in $[0,1]$ and $S_j(x), S_j'(x)$ interpolates at the mesh points x_j. Using the definition of the spline, we determine values for the unknowns a_j, b_j, c_j and d_j as:

$$a_j = y_j + \frac{f_j}{k^2}, \tag{2.3}$$

$$b_j = \frac{f_j - f_{j-\frac{1}{2}}}{k^2 h_j} - \frac{y_{j-1} - y_j}{h_j},$$

$$c_j = -\frac{f_j}{k^2},$$

$$\text{and} \quad d_j = -\frac{f_k \cos\theta_j - f_{j-\frac{1}{2}}}{k^2 \sin kh_j}. \tag{2.4}$$

Using the spline's first derivative continuity conditions, we get the non polynomial spline method based on off-step points as:

$$\sigma y_{j-1} - y_j(1+\sigma) + y_{j+1} = h_j^2(P\sigma f_{j-\frac{1}{2}} + Q\sigma f_j + R\sigma f_{j+\frac{1}{2}}) + T_j^3, \tag{2.5}$$

where

$$R = \frac{2kh_{j+1} - \sin kh_{j+1}}{2k^2 h_{j+1} \sin kh_{j+1}}, P = \frac{kh_j - \sin kh_j \cos kh_j}{kh_j \sin kh_j}, \tag{2.6}$$

$$Q = \frac{2(\sigma_j+1)(\cos(kh_j\sigma - kh_j) - \cos(kh_j\sigma + kh_j)) - 2\sigma kh_j \sin(kh_j\sigma + kh_j)}{(kh_j)^2(\cos(kh_j\sigma - kh_j) - \cos(kh_j\sigma + kh_j))} \tag{2.7}$$

Now, we also derive the consistency condition using (2.5) − (2.7) i.e.,

$$\tan(\frac{kh_j}{2}) + \tan(\frac{kh_{j+1}}{2}) = \frac{kh_j}{2} + \frac{kh_{j+1}}{2}. \tag{2.8}$$

We solve equation (2.8) for kh_j and consider the non-zero smallest positive root $kh_j = 8.98681891$. But, with this, the order of error term T_j^3 in (2.5) remains four. Now, we derive another off-step method using Taylor's expansion for $j = 1(1)N-1$ as

$$y_{j-1} - y_j(1+\sigma) + \sigma y_{j+1} = h_j^2\sigma(Af_{j-\frac{1}{2}} + Bf_{j+\frac{1}{2}}) + T_j^2, \tag{2.9}$$

$$\text{for } A = \frac{(2+\sigma)}{6}, \ B = \frac{(2\sigma+1)}{6}. \tag{2.10}$$

Now, the following approximations are defined at $x_j, j = 1(1)N-1$,

$$S_j = (\sigma+1)\sigma, \tag{2.11}$$

$$\bar{y}_{j+\frac{1}{2}} = \frac{y_j + y_{j+1}}{2}, \tag{2.12}$$

$$\bar{y}_{j-\frac{1}{2}} = \frac{y_j + y_{j-1}}{2}, \tag{2.13}$$

$$\bar{y'}_{j+\frac{1}{2}} = \frac{y_{j+1} - y_j}{h_j\sigma}, \tag{2.14}$$

$$\bar{y'}_{j-\frac{1}{2}} = \frac{y_j - y_{j-1}}{h_j}, \tag{2.15}$$

$$\bar{y'}_j = \frac{y_{j+1} - y_j(1-\sigma^2) - \sigma^2 y_{j-1}}{S_j h_j}, \tag{2.16}$$

$$\bar{f}_j = f(x_j, y_j, \bar{y'}_j), \tag{2.17}$$

$$\bar{f}_{j-\frac{1}{2}} = f(x_{j-\frac{1}{2}}, \bar{y}_{j-\frac{1}{2}}, \bar{y'}_{j-\frac{1}{2}}), \tag{2.18}$$

$$\bar{f}_{j+\frac{1}{2}} = f(x_{j+\frac{1}{2}}, \bar{y}_{j+\frac{1}{2}}, \bar{y'}_{j+\frac{1}{2}}). \tag{2.19}$$

Next, we define higher order approximation of y_j and y'_j to raise order of the error term T_j^3 in equation (2.5) :

$$\hat{y}_j = y_j + h_j^2\delta(\bar{f}_{j-\frac{1}{2}} + \bar{f}_{j+\frac{1}{2}}), \tag{2.20}$$

$$\hat{y'}_j = \bar{y'}_j - h_j\gamma(\bar{f}_{j-\frac{1}{2}} - \bar{f}_{j+\frac{1}{2}}), \tag{2.21}$$

where γ, δ are unknowns. This gives us the modified $\bar{f}_j$ i.e.,

$$\hat{f}_j = f(x_j, \hat{y}_j, \hat{y'}_j). \tag{2.22}$$

Now, expanding the approximations $(2.12) - (2.22)$ we get the following:

$$P = \frac{\sigma}{3} + O(kh_j{}^2), \tag{2.23}$$

$$R = \frac{1}{3} + O(kh_j{}^2), \tag{2.24}$$

$$Q = \frac{(\sigma+1)}{6} + O(kh_j{}^2), \tag{2.25}$$

$$\bar{y}_{j+\frac{1}{2}} = y_{j+\frac{1}{2}} + \frac{(h_j\sigma)^2}{8}y_j'' + O(h_j^3), \tag{2.26}$$

$$\bar{y}_{j-\frac{1}{2}} = y_{j-\frac{1}{2}} + \frac{(h_j)^2}{8}y_j'' + O(h_j^3), \tag{2.27}$$

$$\bar{y'}_{j+\frac{1}{2}} = y'_{j+\frac{1}{2}} + \frac{(h_j\sigma)^2}{24}y_j''' + O(h_j^3), \tag{2.28}$$

$$\bar{y'}_{j-\frac{1}{2}} = y'_{j-\frac{1}{2}} + \frac{(h_j)^2}{24}y_j''' + O(h_j^3), \tag{2.29}$$

$$\hat{y}_j = y_j + \delta h_j^2(2y_j'') + O(h_j^3), \sigma \neq 1, \tag{2.30}$$

$$\hat{y'}_j = y'_j + \frac{h_j^2 y_j'''}{6}((1+3\gamma)\sigma + 3\gamma) + O(h_j^3), \tag{2.31}$$

$$\bar{f}_{j+\frac{1}{2}} = f_{j+\frac{1}{2}} + \frac{(h_j\sigma)^2 y_j''}{8}\frac{\partial f}{\partial y_j} + \frac{(h_j\sigma)^2 y_j'''}{24}\frac{\partial f}{\partial y_j'} + O(h_j^3), \tag{2.32}$$

$$\bar{f}_{j-\frac{1}{2}} = f_{j-\frac{1}{2}} + \frac{h_j^2 y_j''}{8}\frac{\partial f}{\partial y_j} + \frac{h_j^2 y_j'''}{24}\frac{\partial f}{\partial y_j'} + O(h_j^3), \tag{2.33}$$

$$\hat{f}_j = f_j + 2h_j^2\delta y_j''\frac{\partial f}{\partial y_j} + \frac{h_j^2}{6}(\sigma + 3\gamma(1+\sigma))y_j'''\frac{\partial f}{\partial y_j'} + O(h_j^3). \tag{2.34}$$

Thus, we develop the first method by discretizing the proposed BVP (2.1) based on the method (2.9) as:

$$\sigma y_{j-1} - (1+\sigma)y_j + y_{j+1} = h_j^2(A\sigma\bar{f}_{j-\frac{1}{2}} + B\sigma\bar{f}_{j+\frac{1}{2}}) + T_j^2. \tag{2.35}$$

In this method, we can show that for $\sigma \neq 1$, the order of truncation error T_j^2 is $O(h_j^4)$ using the approximations $(2.32) - (2.33)$. Also, if we use the off-step non-polynomial scheme(2.5) along with the approximation $(2.26) - (2.34)$, we get the second method as:

$$\begin{aligned} y_{j+1} - (1+\sigma)y_j + \sigma y_{j-1} &= h_j^2\sigma(P\bar{f}_{j-\frac{1}{2}} + Q\hat{f}_j + R\bar{f}_{j+\frac{1}{2}}) \\ &- h_j^4[(\frac{R\sigma^2 + Q4((1+3\gamma)\sigma + 3\gamma) + P}{24})y_j'''\frac{\partial f}{\partial y_j'} \\ &+ (\frac{R\sigma^2}{8} + 2Q\delta + \frac{P}{8})y_j''\frac{\partial f}{\partial y_j}] + T_j^3. \end{aligned} \tag{2.36}$$

The coefficients of order four of h_j is equated to zero to get the value of δ, γ so as to raise the order of local truncation error T_j^3. Thus, we get

$\gamma = -\frac{(R\sigma^2+P+4Q\sigma)}{12Q(1+\sigma)}, \delta = -\frac{(R+P\sigma^2)}{16Q}$. In case of uniform mesh, the local truncation error becomes of order six. We also ensure the necessary condition for convergence of the methods provided by Jain [10], that the coefficients A, B in method (2.35)and in method (2.36) P, Q and R are positive for $\sigma > 0$. Hence, both the proposed off-step three point discretization using the approximate solutions Y_j at x_j are as follows:

$$Y_{j+1} - (\sigma+1)Y_j + \sigma Y_{j-1} = h_j^2\sigma(A\bar{F}_{j-\frac{1}{2}} + B\bar{F}_{j+\frac{1}{2}}), \tag{2.37}$$

and

$$Y_{j+1} - (\sigma+1)Y_j + \sigma Y_{j-1} = h_j^2\sigma(R\bar{F}_{j+\frac{1}{2}} + Q\hat{F}_j + P\bar{F}_{j-\frac{1}{2}}). \tag{2.38}$$

3 Generalised Methods

We develop the generalized methods by using the following approximations and scalar methods developed in the last section, thus, solving $(1.1) - (1.2)$ we get,

$$S_j = (\sigma+1)\sigma, \tag{3.1}$$

$$\bar{Y}^i_{j+\frac{1}{2}} = \frac{Y^i_j + Y^i_{j+1}}{2}, \tag{3.2}$$

$$\bar{Y}^i_{j-\frac{1}{2}} = \frac{Y^i_j + Y^i_{j-1}}{2}, \tag{3.3}$$

$$\bar{Y'}^i_{j+\frac{1}{2}} = \frac{Y^i_j - Y^i_{j+1}}{h_j\sigma}, \tag{3.4}$$

$$\bar{Y'}^i_{j-\frac{1}{2}} = \frac{Y^i_j - Y^i_{j-1}}{h_j}, \tag{3.5}$$

$$\bar{Y'}^i_j = \frac{Y^i_{j+1} - (1-\sigma^2)Y^i_j - \sigma^2 Y^i_{j-1}}{S_j h_j}, \tag{3.6}$$

$$\bar{f}_j^i = f^i(x_j, Y_j, Y_j^{(1)}, Y_j^{(2)}, ..., Y_j^i, ..., Y_j^{(M)}, \bar{Y'}_j^{(1)}, \bar{Y'}_j^{(2)}, ..., \bar{Y'}_j^i, ..., \bar{Y'}_j^{(M)}) \quad (3.7)$$

$$\bar{f}_{j-\frac{1}{2}}^i = f^i(x_{j-\frac{1}{2}}, \bar{Y}_{j-\frac{1}{2}}, \bar{Y}_{j-\frac{1}{2}}^{(1)}, \bar{Y}_{j-\frac{1}{2}}^{(2)}, ..., \bar{Y}_{j-\frac{1}{2}}^i, ..., \bar{Y}_{j-\frac{1}{2}}^{(M)}, \bar{Y'}_{j-\frac{1}{2}}^{(1)}, \bar{Y'}_{j-\frac{1}{2}}^{(2)}, ..., \bar{Y'}_{j-\frac{1}{2}}^i, ..., \bar{Y'}_{j-\frac{1}{2}}^{(M)}), \quad (3.8)$$

$$\bar{f}_{j+\frac{1}{2}}^i = f^i(x_{j+\frac{1}{2}}, \bar{Y}_{j+\frac{1}{2}}, \bar{Y}_{j+\frac{1}{2}}^{(1)}, \bar{Y}_{j+\frac{1}{2}}^{(2)}, ..., \bar{Y}_{j+\frac{1}{2}}^i, ..., \bar{Y}_{j+\frac{1}{2}}^{(M)}, \bar{Y'}_{j+\frac{1}{2}}^{(1)}, \bar{Y'}_{j+\frac{1}{2}}^{(2)}, ..., \bar{Y'}_{j+\frac{1}{2}}^i, ..., \bar{Y'}_{j+\frac{1}{2}}^{(M)}), \quad (3.9)$$

$$\hat{Y}_j^i = Y_j^i + h_j^2 \delta_i (\bar{f}_{j+\frac{1}{2}}^i + \bar{f}_{j-\frac{1}{2}}^i), \quad (3.10)$$

$$\hat{Y'}_j^i = \bar{Y'}_j^i + h_j \gamma_i (\bar{f}_{j+\frac{1}{2}}^i - \bar{f}_{j-\frac{1}{2}}^i), \quad (3.11)$$

$$\hat{f}_j^i = f^i(x_j, \hat{Y}_j, \hat{Y}_j^{(1)}, \hat{Y}_j^{(2)}, ..., \hat{Y}_j^i, ..., \hat{Y}_j^{(M)}, \hat{Y'}_j^{(1)}, \hat{Y'}_j^{(2)}, ..., \hat{Y'}_j^i, ..., \hat{Y'}_j^{(M)}) \quad (3.12)$$

$$Y_{j+1}^i - (1+\sigma)Y_j^i + \sigma Y_{j-1}^i = h_j^2 \sigma (A\bar{f}_{j-\frac{1}{2}}^i + B\bar{f}_{j+\frac{1}{2}}^i), \quad (3.13)$$

$$Y_{j+1}^i - (1+\sigma)Y_j^i + \sigma Y_{j-1}^i = h_j^2 \sigma (R\bar{f}_{j+\frac{1}{2}}^i + Q\hat{f}_j^i + P\bar{f}_{j-\frac{1}{2}}^i), \quad (3.14)$$

where

$$A = \frac{(2+\sigma)}{6},\ B = \frac{(2\sigma+1)}{6}, \quad (3.15)$$

$$P = \frac{kh_j - \sin kh_j \cos kh_j}{k^2 kh_j \sin kh_j},\ R = \frac{2kh_{j+1} - \sin kh_{j+1}}{2k^2 kh_{j+1} \sin kh_{j+1}}, \quad (3.16)$$

$$Q = \frac{2(\sigma+1)(\cos(kh_j\sigma - kh_j) - \cos(kh_j\sigma + kh_j)) - 2\sigma kh_j \sin(kh_j\sigma + kh_j)}{(kh_j)^2(\cos(kh_j\sigma - kh_j) - \cos(kh_j\sigma + kh_j))} \quad (3.17)$$

4 Illustration of the Method

Consider a linear singular BVP of fourth order as follows:

$$\frac{d^4y(x)}{dx^4} = a(x)y(x) + d(x), x \neq 0, \quad (4.1)$$

$$y(0) = c_1, y(1) = d_1, \frac{d^2y}{dx^2}(0) = c_2, \frac{d^2y}{dx^2}(1) = d_2. \quad (4.2)$$

where $a(x)$ is singular and c_1, c_2, d_1, d_2 are real constants. Using (1.1), we write the problem $(4.1) - (4.2)$ as follows:

$$\frac{d^2y}{dx^2}(x) = z(x), \quad (4.3)$$

$$\frac{d^2z}{dx^2}(x) = a(x)y(x) + d(x), \quad (4.4)$$

$$y(0) = c_1, y(1) = d_1, \quad (4.5)$$

$$z(0) = c_2, z(1) = d_2. \quad (4.6)$$

We use the method(3.14) to the BVP $(4.3)-(4.6)$. The method is given as follows:

$$\begin{aligned}\sigma Y_{j-1}-Y_j(1+\sigma)+Y_{j+1} &= h_j^2\sigma(R\bar{Z}_{j+\frac{1}{2}}+Q\hat{Z}_j+P\bar{Z}_{j-\frac{1}{2}}), &(4.7)\\ \sigma Z_{j-1}-Z_j(1+\sigma)+Z_{j+1} &= h_j^2\sigma(R(a_{j+\frac{1}{2}}\bar{Y}_{j+\frac{1}{2}}+d_{j+\frac{1}{2}})\\ &\quad +Q(a_j\hat{Y}_j+d_j)+P(a_{j-\frac{1}{2}}\bar{Y}_{j-\frac{1}{2}}+d_{j-\frac{1}{2}})). &(4.8)\end{aligned}$$

Then, we approximate $a_{j\pm\frac{1}{2}}$ for the BVP $(4.7)-(4.8)$ as

$$a_{j-\frac{1}{2}}=a_j-\frac{h_ja_j'}{2}+\frac{h_j^2a_j''}{8}+O(h_j^3), \tag{4.9}$$

$$a_{j+\frac{1}{2}}=a_j+\frac{\sigma h_ja_j'}{2}+\frac{(h_j\sigma)^2a_j''}{8}+O(h_j^3). \tag{4.10}$$

Similarily, we approximate $d_{j\pm\frac{1}{2}}$. Using the relations $(4.9)-(4.10)$ in $(4.7)-(4.8)$ we get,

$$\begin{aligned}\sigma Y_{j-1}-Y_j(1+\sigma)+Y_{j+1} &= h_j^2\sigma(R\bar{Z}_{j+\frac{1}{2}}+Q\hat{Z}_j+P\bar{Z}_{j-\frac{1}{2}}), &(4.11)\\ \sigma Z_{j-1}-Z_j(1+\sigma)+Z_{j+1} &= h_j^2\sigma(R(a_{j+\frac{1}{2}}\bar{Y}_{j+\frac{1}{2}}+d_{j+\frac{1}{2}})\\ &\quad +Q(a_j\hat{Y}_j+d_j)+P(a_{j-\frac{1}{2}}\bar{Y}_{j-\frac{1}{2}}+d_{j-\frac{1}{2}})). &(4.12)\end{aligned}$$

Finally, substituting $(3.1)-(3.12)$ in $(4.11)-(4.12)$ we get the difference equation of BVP $(4.3)-(4.6)$as follows:

$$\begin{bmatrix}b_j^{11} & b_j^{12}\\ b_j^{21} & b_j^{22}\end{bmatrix}\begin{bmatrix}Y_{j-1}\\ Z_{j-1}\end{bmatrix}+\begin{bmatrix}d_j^{11} & d_j^{12}\\ d_j^{21} & d_j^{22}\end{bmatrix}\begin{bmatrix}Y_j\\ Z_j\end{bmatrix}+\begin{bmatrix}p_j^{11} & p_j^{12}\\ p_j^{21} & p_j^{22}\end{bmatrix}\begin{bmatrix}Y_{j+1}\\ Z_{j+1}\end{bmatrix}=\begin{bmatrix}\psi_j^1\\ \psi_j^2\end{bmatrix}, \tag{4.13}$$

where

$$\begin{aligned}
b_j^{11} &= -\sigma + \frac{h_j^4}{2}\sigma^2 Q\delta a_j, \quad b_j^{12} = \frac{h_j^2\sigma^2}{2},\\
b_j^{21} &= \frac{h_j^2}{2}\sigma^2 R a_{j-\frac{1}{2}}, \qquad b_j^{22} = -\sigma + \frac{h_j^4}{2}\sigma^2 Q\delta a_j,\\
d_j^{11} &= (1+\sigma) + Q\delta a_j h_j^4\sigma^2, \qquad d_j^{12} = \frac{h_j^2\sigma^2(2Q+R+P)}{2},\\
d_j^{21} &= \frac{\sigma^2}{2}[h_j^2 a_j(2Q+R+P) + h_j^3(-P+\sigma R)\frac{a_j'}{2} + R\frac{h_j^4\sigma^2 a_j''}{8}],\\
& \qquad\qquad diag_j^{22} = (1+\sigma) + Q\delta a_j h_j^4\sigma^2,\\
p_j^{11} &= -1 + \frac{a_j h_j^4\sigma^2 Q\delta}{2}, \quad p_j^{12} = \frac{R h_j^2\sigma^2}{2},\\
p_j^{21} &= h_j^2\sigma^2\frac{R}{2}a_{j+\frac{1}{2}}, \qquad p_j^{22} = -1 + \frac{a_j h_j^4\sigma^2 Q\delta}{2},\\
\psi_j^1 &= -h_j^4 2 b_j Q\sigma^2,\\
& \qquad\qquad \psi_j^2 = -\sigma^2[h_j^2 d_j(2Q+P+R) + \frac{d_j' h_j^3}{2}(-P+R) + \frac{d_j'' h_j^4}{8}(R+P)].
\end{aligned}$$

5 Convergence Analysis

We provide the convergence of method (3.14) for the coupled second order BVP (4.3) − (4.6). The convergence of scalar singular BVP has been already provided by Mohanty [23]. Now, once the condition (4.5) − (4.6) is substituted in the difference equation (4.13), it is written in matrix form as follows:

$$H\hat{Y} + \hat{\psi} = \begin{bmatrix} b_j & d_j & p_j \end{bmatrix} \begin{bmatrix} \hat{Y_{j-1}} \\ \hat{Y_j} \\ \hat{Y_{j+1}} \end{bmatrix} + \hat{\psi_j} = \hat{0}, \tag{5.1}$$

where b_j, p_j, d_j are block elements of order 2 in tridiagonal block matrix H.

$$\begin{aligned}
\hat{Y} &= [\hat{Y}_1, \hat{Y}_2, ..., \hat{Y}_j, ...\hat{Y}_{N-1}]^T, where \quad \hat{Y_j} = [Y_j, Z_j]^T,\\
\hat{\psi} &= [\hat{\psi}_1 + b_1[c_1, c_2]^T, \hat{\psi}_2, ..., \hat{\psi}_j, ...\hat{\psi}_{N-1} + p_{N-1}[d_1, d_2]^T]^T, \ where\ \hat{\psi_j} = [\psi_j^1, \psi_j^2]^T,\\
& \hat{0} \ \text{is a zero vector with } N-1 \text{ components.}
\end{aligned}$$

Let $[[y_1, z_1]^T, [y_2, z_2]^T ....., [y_j, z_j]^T, ...[y_{N-1}, z_{N-1}]^T]^T \cong \hat{y}$ be the exact solution satisfying

$$H\hat{y} + \hat{\psi} + \hat{T}_j^3 = 0, \tag{5.2}$$

where $\hat{T}_j^3$ is the truncation error, then the error vector E is given by $\hat{y} - \hat{Y}$. We get the error equation from(5.1)and(5.2), *i.e.*, $HE = \hat{T}_j^3$. (5.3)

For some $k_1, k_2 > 0$, let $|a_j| \leq k_1$ and $|a_j'| \leq k_2$. Using (4.13) and neglecting the higher order terms of h_j we get,

$$\|p_j\|_\infty \leq \max_{1\leq j\leq N-2} \begin{cases} 1 + \frac{h_j^2\sigma^2 P}{2}, \\ 1 + \frac{h_j^2\sigma^2 P}{2}(k_1 + \frac{h_j\sigma}{2}k_2), \end{cases} \tag{5.4}$$

$$\|b_j\|_\infty \leq \max_{2\leq j\leq N-1} \begin{cases} \sigma + \frac{h_j^2\sigma^2 R}{2}, \\ \sigma + \frac{h_j^2\sigma^2 R}{2}(k_1 + \frac{h_j}{2}k_2). \end{cases} \tag{5.5}$$

We prove the irreducibility of H for sufficiently small h_j as well as $\|b_j\|_\infty \leq \sigma$ and $\|p_j\|_\infty \leq 1$ from (5.4) − (5.5).
Let the sum of elements of j_{th} row of H be sum_j,

$$sum_j = \begin{cases} \sigma + \frac{h_j^2\sigma^2}{12}(P + 2(R + Q)), j = 1, \\ \sigma + \frac{h_j^2\sigma^2 a_j'}{24}(R + 2(P + Q))a_j + \frac{\sigma^2}{2}(h_j^2 R a_j + h_j^3(-P + 2R\sigma)),\ j = 2, \end{cases} \tag{5.6}$$

$$sum_j = \begin{cases} \frac{h_j^2\sigma^2}{2}(R + Q + P),\ j = 3(2)N - 4, \\ \frac{h_j^2\sigma^2 a_j}{2}(R + Q + P) + \frac{h_j^3\sigma^2 a_j'}{4}(-2P + \sigma R),\ j = 4(2)N - 3, \end{cases} \tag{5.7}$$

$$sum_j = \begin{cases} 1 + \frac{h_j^2\sigma^2}{12}(R + 2(Q + P)),\ j = N - 2, \\ 1 + \frac{h_j^2\sigma^2 a_j}{12}(R + 2(Q + P)) + \frac{h_j^3\sigma^2 a_j'}{4}(-2R + P\sigma),\ j = N - 1. \end{cases} \tag{5.8}$$

We can easily prove that H is Monotone using $0 < L \leq min(L_1, L_2)$ in (5.6) − (5.8) and for sufficiently small h_j. Therefore, $H^{-1} \geq 0$ and exist. Hence by (5.3) we have,

$$||E|| = ||H^{-1}||||\hat{T}_j^3||. \tag{5.9}$$

Now for sufficiently small h_j, by (2.23) − (2.25) and (5.6) − (5.8) we can say that:

$$sum_j > \begin{cases} \frac{h_j^2\sigma(2+3\sigma)}{12}, & j = 1, \\ \frac{h_j^2\sigma(2+3\sigma)L}{12}, j = 2, \end{cases} \tag{5.10}$$

$$sum_j \geq \begin{cases} \frac{h_j^2(\sigma+1)}{2}, & j = 3(2)N - 4, \\ \frac{h_j^2(\sigma+1)L}{2}, & j = 4(2)N - 3, \end{cases} \tag{5.11}$$

$$sum_j > \begin{cases} \frac{h_j^2\sigma(2\sigma+3)}{12}, & j = N - 2, \\ \frac{h_j^2\sigma(2\sigma+3)L}{12}, j = N - 1. \end{cases} \tag{5.12}$$

We can also say for $\sigma \neq 0$:

$$\begin{aligned} sum_j &> \max[\frac{h_j^2\sigma(2+3\sigma)}{12}, \frac{h_j^2\sigma(2+3\sigma)L}{12}] \\ &= \frac{h_j^2\sigma(2+3\sigma)L}{12}, \text{for} \quad j = 1, 2, \end{aligned} \tag{5.13}$$

$$\begin{aligned} sum_j &\geq \max[\frac{h_j^2(1+\sigma)}{2}, \frac{h_j^2(1+\sigma)L}{2}] \\ &= \frac{h_j^2(1+\sigma)L}{2}, \quad \text{for } j = 3(1)N - 3, \end{aligned} \tag{5.14}$$

$$\begin{aligned} sum_j &> \max[\frac{h_j^2\sigma(2\sigma+3)}{12}, \frac{h_j^2\sigma(2\sigma+3)L}{12}] \\ &= \frac{h_j^2\sigma(2\sigma+3)L}{12}, \text{for} \quad j = N - 2, N - 1. \end{aligned} \tag{5.15}$$

Then, we use a result proved by Varga [33] for $i = 1(1)N-1$,

$$H_{i,j}{}^{-1} \leq \frac{1}{sum_j}, \quad \text{where } H_{i,j}{}^{-1} \text{ is the } (i,j)^{th}\text{element of } H^{-1} \tag{5.16}$$

By using $(5.13) - (5.15)$, we have

$$\frac{1}{sum_j} \leq \begin{cases} \frac{12}{h_j^2(3\sigma+2)\sigma L}, & j = 1, 2, \\ \frac{2}{h_j^2(\sigma+1)L}, & j = 3(1)N-3, \\ \frac{12}{h_j^2(2\sigma+3)\sigma L}, & j = N-2, N-1. \end{cases} \tag{5.17}$$

Now, we show that the error defined in equation (5.9) is bounded and is of order $O(h_j^3)$. For this, we define norm of H^{-1} and $\hat{T}_j^3$ such that,

$$\parallel H_{j,i}{}^{-1} \parallel = \max_{j\in[1,N-1]} \sum_{i=1}^{N-1} \mid H_{j,i}{}^{-1} \mid, also \parallel T \parallel = \max_{j\in[1,N-1]} \mid \hat{T}_j^3 \mid . \tag{5.18}$$

Thus, using (5.3) and $(5.16) - (5.18)$ we get the bound for the error term as follows:

$$\parallel E \parallel \leq O(h_j^5)\frac{12}{h_j^2 L\sigma}\frac{(6\sigma^3+18\sigma^2+16\sigma+5)}{(6\sigma^3+19\sigma^2+19\sigma+6)} = O(h_j^3). \tag{5.19}$$

This proves the method (3.14) has third order convergence for BVPs $(4.1) - (4.2)$. Therefore, we can say that method (3.14) has third order convergence for BVP $(1.1) - (1.2)$. Similarly, method (3.13) has second order convergence.

6 Numerical Illustrations

We have solved seven problems. For quasi-variable mesh and uniform mesh, we have tabulated root mean square errors and maximum absolute errors respectively in Tables 1-7. We have chosen $h_1 = \frac{(1-\sigma)}{(1-\sigma^N)}, \sigma \neq 1$. The remaining h_j 's are calculated by the relation $h_j = \sigma h_{j-1}, j = 2(1)N-1$. Figures 1-7 presents the graphs of numerical solution and the exact solution in case of fourth order method based on uniform mesh. Related numerical results are provided in Table 1-7.

Gauss Elimination and Newton's method for block elements has been used for solving system of linear and nonlinear BVPs respectively with initial approximation $y_0 = 0$. The order of convergence (OC) for fourth order method based on uniform mesh is also provided. Matlab 07 has been used for doing all calculations.

Problem 6.1 (Nonlinear boundary value problem)

$$\frac{d^4y(x)}{dx^4} = 6e^{-4\ y} - \frac{12}{(1+x)^4},$$
$$y(0) = 0, y(1) = .6931, \frac{d^2y}{dx^2}(0) = -1, \frac{d^2y}{dx^2}(1) = -.25.$$

Table 1: Problem 6.1

	Off-step mesh			
N	$Method1$	$Method2$	$Uniform\ mesh\ method$	[29]
8	4.4398e-003	4.8610e-006	7.2499e-007	0.37e-005
16	2.0758e-003	1.2961e-006	4.6937e-008	0.29e-006
32	1.3702e-003	6.7628e-007	2.9600e-009	0.19e-007

The exact solution is given by $y(x) = \log(1+x)$. In Table 1, results for quasi-variable mesh taking $\sigma = 0.9$ and for uniform mesh is tabulated.

Problem 6.2 (Sixth order linear boundary value problem):

$$\frac{d^6y(x)}{dx^6} + y(x) = 6(5\sin(x) + 2x\cos(x)), x \in [0,1]$$
$$y(0) = 0, \frac{d^2y}{dx^2}(0) = 0, \frac{d^4y}{dx^4}(0) = 0,$$
$$y(1) = 0, \frac{d^2y}{dx^2}(1) = 3.84416, \frac{d^4y}{dx^4}(1) = -14.42007.$$

The exact solution is $y(x) = (x^2-1)\sin(x)$. In Table 2, results for quasi-variable mesh taking $\sigma = 0.9$ and for uniform mesh is tabulated.

Problem 6.3 (Fourth order non linear boundary value problem)

$$\frac{d^4y(x)}{dx^4} = 3(\frac{dy}{dx})^2 + 4.5y^3, x \in [0,1]$$
$$y(0) = 4, \frac{d^2y}{dx^2}(0) = 24, y(1) = 1, \frac{d^2y}{dx^2}(1) = 1.5e.$$

The exact solution is $y(x) = \frac{4}{(1+2x+x^2)}$. In Table 3, results for quasi-variable mesh taking $\sigma = 0.9$ and for uniform mesh is tabulated.

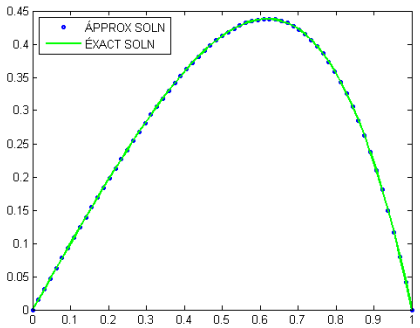

Figure 1: Exact solution vs Numerical solution in uniform mesh method

Table 2: *Problem 6.2*

	Off-step mesh				
N	*Method*1	*Method*2	*Uniform mesh method*	[3]	[26]
8	6.4952e-004	4.2946e-006	6.5901e-007	1.5379 e-006	8.1514e-005
16	5.9397e-004	9.9183e-007	4.1831e-008	1.9790 e-007	2.1052 e-005
32	5.1433e-004	4.7874e-007	2.6133e-009	4.0596 e-008	5.3084 e-006

Table 3: *Problem 6.3*

	Off-step mesh			
N	*Method*1	*Method*2	*Uniform mesh method*	[25]
8	1.2451e-003	8.4710e-005	2.2780e-005	1.44 e-003
16	2.7555e-004	2.1499e-005	1.5362e-006	9.33 e-004
32	4.0919e-004	9.7519e-006	9.8628e-008	5.90 e-005
64	3.1887e-004	6.4390e-006	6.2300e-009	3.69 e-006

Problem 6.4 (Sixth order non linear boundary value problem)

$$\frac{d^6y(x)}{dx^6} = y^2e^{-x},\ x \in [0,1]$$
$$y(0) = 1, y(1) = e,$$
$$\frac{d^2y}{dx^2}(0) = 1, \frac{d^2y}{dx^2}(1) = e,$$
$$\frac{d^4y}{dx^4}(0) = 1, \frac{d^4y}{dx^4}(1) = e.$$

The exact solution is $y(x) = e^x$. In Table 4, results for quasi-variable mesh taking $\sigma = 0.9$ and for uniform mesh is tabulated.

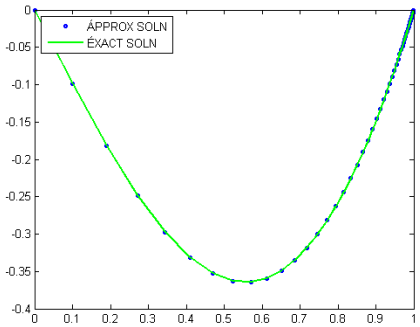

Figure 2: Exact solution vs Numerical solution in uniform mesh method

Table 4: *Problem 6.4*

	Off-step mesh			
N	$Method1$	$Method2$	$Uniform\ mesh\ method$	[14]
8	2.64952e-004	2.0457e-007	5.1651e-008	7.02e-006
16	5.9397e-004	4.9805e-008	3.2495e-009	4.35e-006
32	5.1433e-004	2.4007e-008	2.0334e-010	7.87e-007

Problem 6.5 (Fourth order non-linear singular boundary value problem)

$$x\frac{d^4y(x)}{dx^4} + \frac{4d^3y(x)}{dx^3} = xy^2 - 4\cos(x) - xsin(x), x \neq 0.$$

The exact solution is $y(x) = \sin(x)$. In Table 5, results for quasi-variable mesh taking $\sigma = 0.9$ and for uniform mesh is tabulated.

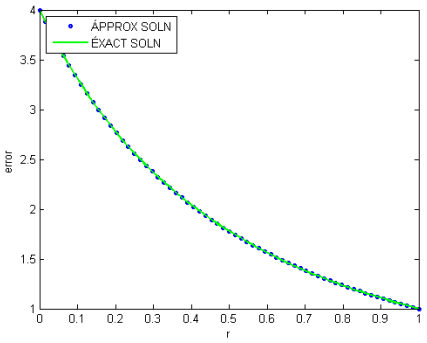

Figure 3: Exact solution vs Numerical solution in uniform mesh method

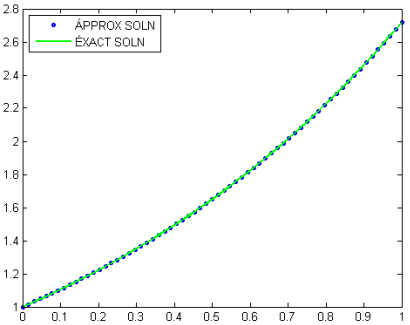

Figure 4: Exact solution vs Numerical solution in uniform mesh method

Table 5: *Problem 6.5*

	Off-step mesh			
N	$Method1$	$Method2$	$Uniform\ mesh\ method$	OC
8	1.4374e-004	4.2067e-006	1.6791e-006	-
16	8.8426e-005	1.2629e-006	1.5413e-007	3.4455
32	5.7765e-005	6.0728e-007	1.2889e-008	3.5810
64	4.0494e-005	4.0146e-007	7.7938e-010	4.1476

Problem 6.6 (Sixth order non-linear singular boundary value problem)

$$x\frac{d^6y(x)}{dx^6} + 6\frac{d^5y(x)}{dx^5} + 2xy(x) = xe^y, x \neq 0.$$

The exact solution is $y(x) = e^x$. In Table 6, results for quasi-variable mesh taking $\sigma = 0.9$ and for uniform mesh is tabulated.

Table 6: *Problem 6.6*

	Off-step mesh			
N	$Method1$	$Method2$	$Uniform\ mesh\ method$	OC
8	6.1864e-004	5.6862e-007	4.5498e-007	-
16	3.1623e-004	1.4817e-007	3.7876e-008	3.5865
32	2.2083e-004	7.6631e-008	2.9520e-009	3.6815
64	2.0493e-004	6.7278e-008	2.2125e-010	3.7379

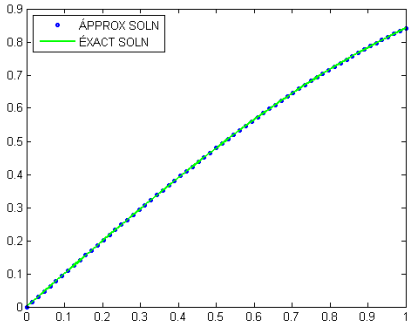

Figure 5: Exact solution vs Numerical solution in uniform mesh method

Problem 6.7 (System of second order boundary value problem)

$$\frac{d^2y(x)}{dx^2} + \frac{dy(x)}{dx} + xy(x) + \frac{dz(x)}{dx} + 2xz(x) = g_1(x),$$
$$\frac{d^2z(x)}{dx^2} + z(x) + 2\frac{dy(x)}{dx} + x^2y(x) = g_2(x),$$
$$y(0) = 0, z(0) = 1, y(1) = 0, z(1) = 1,$$

where $g_1(x) = -2\cos(x)(1+x) + \pi cos(x\pi) + 2xsin(x\pi) + 2\sin(x)(2x - 2 - x^2)$, $g_2(x) = -4\cos(x)(x-1) + 2\sin(x)(2 - x^2 + x^3) + (1 - \pi^2)\sin(x\pi)$ and $x \in [0, 1]$. The exact solution is $y(x) = 2(1-x)\sin(x), z(x) = \sin(x\pi)$.

Table 7: *Problem 6.7*

	z		y	
N	[8]	*Uniform mesh method*	[8]	*Uniform mesh method*
.08	7.5e-004	3.5686e-007	2.2e-004	1.8284e-006
.24	8.2e-004	1.4754e-006	2.3e-004	2.0723e-006
.40	6.5e-004	2.5123e-006	2.3e-004	6.2430e-007
.56	2.8e-004	3.1366e-006	2.2e-004	3.9577e-006
.72	2.6e-004	2.9899e-006	2.6e-004	5.6498e-006
.88	8.0e-004	1.2382e-005	5.5e-004	3.9716e-006
.96	4.8e-004	1.4964e-006	3.1e-004	1.5857e-006

7 Final Remarks

In this paper, two methods of second and third order respectively have been developed to solve singular BVPs both linear as well as nonlinear. For numerical illustration, we have considered seven problems consisting of fourth and sixth order linear and nonlinear BVPs. Table $1-4, 7$ proves improvement in results when compared with problems

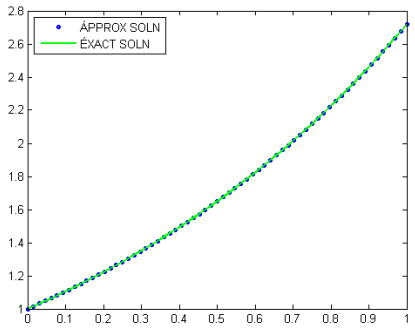

Figure 6: Exact solution vs Numerical solution in uniform mesh method

solved by methods using extrapolation, polynomial and non polynomial splines and also by using reproducing kernel space method.

In our methods minimal grid points i.e., three grid points at a time has been used as compared to existing methods. Due to the use of three grid points, the numerical scheme is converted to a tri-diagonal representation of system of difference equations which can be easily solved by any standard method available in the literature. Also, due to the use of off-step mesh, singularity has been controlled in singular BVPs. We have also solved nonlinear singular BVP and so far such kind of BVP has not been solved. Therefore, for such problems we have presented the numerical order of convergence(OC) based on uniform mesh.

The methods developed are effective and straight forward and can be extended to solve boundary value problems with cartesian as well as polar coordinates. Due to the ability to operate with polar coordinate, many problems on fluid flow with polar symmetry can be attended. Moreover, we can also use the methods to solve wide variety of higher order singularly perturbed BVPs.

References

[1] Aftabizadeh, A.R.(1986), Existence and uniqueness theorems for fourth-order boundary value problems, Journal of Mathematical Analysis and Applications, 116(2), 415-426.

[2] Agarwal, R.P.(1981), Boundary value problems for higher order differential equations, Bulletin of the Institute of Mathematics, Academia Sinica, 9(1), 47-61.

[3] Akram, G. and Siddiqi, S.S.(2006), Solution of sixth order boundary value problems using non-polynomial spline technique, Applied Mathematics and Computation, 181(1), 708-720.

[4] Akram, G. and Rehman, Hamood Ur(2013), Numerical solution of eighth order boundary value problems in reproducing kernel space, Numerical Algorithm , 62, 527-540.

[5] Bernis, F.(1982), Compactness of the support in convex and non-convex fourth order elasticity problem, Nonlinear Analysis, 6, 1221-1243.

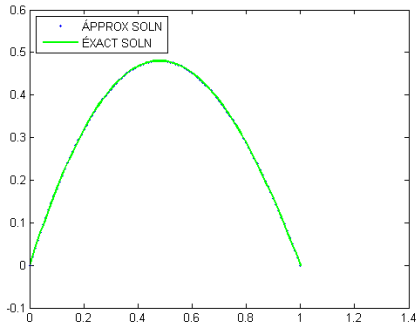

Figure 7: Exact solution vs Numerical solution in uniform mesh method

[6] Bhrawy, A.H., Alofi, A.S., Van Gorder, R.A.(2014), An Efficient Collocation Method for a Class of Boundary Value Problems Arising in Mathematical Physics and Geometry, Abstract and Applied Analysis, Article ID 425648, 9 pages.

[7] Dwivedi, K. and Singh, J.(2021), Numerical solution of two-dimensional fractional-order reaction advection sub-diffusion equation with finite-difference Fibonacci collocation method, Mathematics and Computers in Simulation, 181, 38-50.

[8] Geng,F. and Cui,M.(2007), Solving a nonlinear system of second order boundary value problems, Journal of Mathematical Analysis and Application , 327, 1167-1181.

[9] Glatzmaier, G.A.(2014), Numerical simulations of stellar convection dynamics at the base of the convection zone, Geophysical Fluid Dynamics, 31(1985), 137-150.

[10] Jain, M.K.(2014), Numerical Solution of Differential Equations(third edition), New Age International(P) Ltd., New Delhi.

[11] Jha, N., Bieniasz, L.K.(2015), A Fifth (Six) Order Accurate, Three-Point Compact Finite Difference Scheme for the Numerical Solution of Sixth Order Boundary Value Problems on Geometric Meshes, Journal of Scientific Compution, 64, 898–913.

[12] Kadalbajoo, M.K. and Bawa, R.K.(1993), Third Order Variable-Mesh Cubic Spline Methods for Singularly Perturbed Boundary Value Problems, Applied Mathematics and Computation, 59, 117-129.

[13] Keller, H.B.(1968), Numerical Methods for Two point Boundary value problems, Blaisdell Publications Co., New York.

[14] Khan, A. and Khandelwal, P.(2011), Solution of Non-linear Sixth-order Two Point Boundary-value Problems Using Parametric Septic Splines, International Journal of Nonlinear Science ,12(2), 184-195.

[15] Mohanty,R.K. and Evans, D.J.(2003), A Fourth Order Accurate Cubic Spline Alternating Group Explicit Method for Non-linear Singular Two Point Boundary Value Problems, International Journal of Computer Mathematics, 80, 479-492.

[16] Mohanty, R.K.,Sachdev, P.L. and Jha, N.(2004), An $O(h^4)$ Accurate Cubic Spline TAGE Method for Non-linear Singular Two Point Boundary Value Problems, Applied Mathematics and Computations, 158, 853-868.

[17] Mohanty,R.K., Jha, N. and Evans, D.J.(2004), Spline in Compression Method for the Numerical Solution of Singularly Perturbed Two Point Singular Boundary Value Problems , International Journal of Computer Mathematics, 81, 615-627 .

[18] Mohanty, R.K., Evans, D.J. and Khosla, N.(2005), An $O(h^3)$ Non-uniform Mesh Cubic Spline TAGE Method for Non-linear Singular Two-point Boundary Value Problems , International Journal of Computer Mathematics, 82, 1125-1139.

[19] Mohanty, R.K., Evans, D.J. and Arora,U.(2005) ,Convergent Spline in Tension Methods for Singularly Perturbed Two Point Singular Boundary Value Problems , International Journal of Computer Mathematics , 82, 55-66.

[20] Mohanty, R.K. and Jha, N. (2005), A Class of Variable Mesh Spline in Compression Methods for Singularly Perturbed Two Point Singular Boundary Value Problems, Applied Mathematics and Computations , 168, 704-716.

[21] Mohanty, R.K. and Khosla, N. (2005), A Third Order Accurate Variable Mesh TAGE Iterative Method for the Numerical Solution of Two Point Non-linear Singular Boundary Value Problems, International Journal of Computer Mathematics, 82, 1261-1273.

[22] Mohanty, R.K. and Arora, U.(2006), A Family of Non-uniform Mesh Tension Spline Methods for Singularly Perturbed Two Point Singular Boundary Value Problems with Significant First Derivatives, Applied Mathematics and Computations , 172, 531-544.

[23] Mohanty, R.K.(2006), A class of non-uniform mesh three point arithmetic average discretization for $y'' = f(x, y, y')$ and the estimates of y' , Applied Mathematics and Computation, 183, 477-485.

[24] O'Regan, D (1991), Solvability of some fourth (and higher) order singular boundary value problems, Journal of Mathematical Analysis and Applications, 161(1), 78-116.

[25] Sakai, M. and Usmani,R.(1983), Spline Solutions for Nonlinear Fourth-Order Two-Point Boundary Value Problems , Publication of Research Institute for Mathematical Sciences, Kyoto University , 19, 135-144.

[26] Siddiqi, S. S. and Twizell, E.H.(1996), Spline solutions of linear sixth- order boundary value problems, International Journal of Computer Mathematics, 60, 295-304.

[27] Terril, R. M.(1964), Laminar flow in a uniformly porous channel, Aeronaut Quarterly, 15(3), 299-310.

[28] Toomre, J., Zahn, J.R., Latour, J. and Spiegel, E.A.(1976), Stellar convection theory II:Single-mode study of the second convection zone in A-type stars, The Astophysical Journal, 207, 545-563.

[29] Twizell, E.H.(1986), A fourth-order extrapolation method for special nonlinear fourth-order boundary value problems, Communications in Applied Numerical Methods,John Wiley and Sons, 2, 593-602.

[30] Siddiqi, S. S. and Akram ,G.(2007), Solution of eighth-order boundary value problems using the non-polynomial spline technique, International Journal of Computer Mathematics, 84(3), 347-368.

[31] Siddiqi, S. S. and Akram ,G.(2008), Septic spline solutions of sixth-order boundary value problems, Journal of Computational and Applied Mathematics, 215, 288-301.

[32] Singh, J., Kilicman, A., Kumar D., Swaroop, R. and Md. Ali F.(2019), Numerical Study For Fractional Model Of Non-Linear Predator-Prey Biological Population Dynamical System, Thermal Science, 23 (6) , S2017-S2025.

[33] Varga, R.S. (1962), Matrix Iterative Analysis, Prentice-Hall, Englewood Cliffs, NJ.

Numerical study of the space fractional Burger's equation by using Lax-Friedrichs-implicit scheme

Swapnali Doley[1,*], A. Vanav kumar[1] and L. Jino[1,2]

December 25, 2021

Abstract

This paper deals with the numerical solution of space fractional Burger's equation using the implicit finite difference scheme and Lax-Friedrichs-implicit finite difference scheme respectively. The Riemann-Liouville based fractional derivative (non-integer order) is fitted for the diffusion term of fractional order $1.0 < \alpha \leq 2.0$. The Mathematical induction is used to estimate a stability of both the implicit and Lax-Friedrichs-implicit schemes. The study shows that the implicit based scheme is stable and the results are good in agreement with the exact solution. Finally, the significance of space fractional order with respect to the solution is discussed. It is noted that the solution of space fractional Burger's equation get affected by changing the space fractional order.

Key words: Lax-Friedrichs, implicit scheme, fractional calculus, finite difference method

1

1 Introduction

Fractional Calculus plays an important role in various fields of science and engineering. Examples include ground water flow modeling, electric circuit design, quantum mechanics, optics, plasma model, dengue fever transmission dynamics and atmospheric CO_2 dynamics model [1, 2, 3, 4, 5]. Due to its wide applications, solving techniques of those fractional equations are extensively improved by the researchers. For instance, Goswami et al. [6] used Homotopy perturbation Sumudu transform for solving time-fractional regularized long wave equations. Later, they used the techniques to find the solutions for the time fractional Schrdinger equations and fractional equal width equations (describes the

[1]Department of Basic and Applied Science, NIT Arunachal Pradesh, Arunachal Pradesh, India
[2] Department of Automobile Engineering, Sathyabama University, Chennai, India
* Email: swapnalidoley05@gmail.com

hydro-magnetic waves) [7, 8]. Also, Goswami et al. [9] made a mixed approach of Homotopy perturbation and Laplace transform to solve the fifth order KdV equations in order to illustrate the plasma's magneto-acoustic waves. Recently, Hashmi et al. [10] used B-spline method to solve the fractional telegraph equation and quoted that the scheme is efficient. In numerical methods there are numerous methods including finite difference method (FDM), finite element method, finite volume method etc. Out of this methods FDM is a pioneering tool used among the investigators. In the present investigation, we establish two schemes namely the implicit FDM and Lax-Friedrichs implicit FDM for the space fractional Burger's equation (SFBE).

Fractional calculus application gives a real system better than integer-order. The Burger's equations arises in various domain such as fluid and gas dynamics, theory of shock waves, traffic flow, etc [11, 12, 13, 14]. Many researchers have applied various analytical techniques, numerical algorithms/schemes for extracting the solution for the Burger's equation. The exact solution and explicit FDM solutions for the 1-D Burger's equation was surveyed by Kutluay et al. [15]. Aksan and Ozdes [16] constructed variational method for solving the Burger's equation. Inan and Bahadir [17] converted non-linear Burger's equation into linear using Hopf-Cole transformation and obtained Numerical solution (NS) using explicit exponential FDM. Pandey et al. [18] coupled Hopf-Cole transformation and Douglas FDM to get the NS with accuracy of second order in time and fourth order in space.

Zhang et al.[19] used the implicit FDM to solve the fractional convection-diffusion equation. It is found that the NS is unconditionally stable. Sousa [20] obtained the NS for the fractional advection diffusion equation using explicit-central difference FDM, explicit-upwind FDM and Lax-Wendroff FDM. The study consider Riemann-Liouville fractional derivative for space fractional and Caputo fractional derivative for the time derivative. The result shows that all the explicit FDM schemes are stable under restricted conditions. Later, Sousa [21] presented the explicit-Lax-Wendroff method for the Riemann-Liouville derivative based space fractional advection diffusion equation. The study illustrates that the scheme is second order accurate and conditionally stable. Bekir and Gnerb [22] and Das et al. [23] used (G'/G) expansion method to solve the modified Riemann-Liouville derivative based fractional Burger's equation. Esen and Tasbozan[24] solved the time fractional Burger's equation by applying the B-spline quadratic Galerkin method. Moreover, Esen and Tasbozan[25] used finite element method based cubic B-spline for the time fractional Burger's equation. They also compared the NS with the various exact solutions (ES) and found that the scheme is stable and accurate. Rawashdeh [26] proposed a new scheme named the fractional reduced differential transform to solve the TFBE. It is noted that the proposed scheme is accurate and good comparable with the ES. Yokus [27] studied the FDM based NS with respect to the fractional derivatives such as Caputo, shifted Grunwald and Riemann-Liouville and obtained the solutions using the software Mathematica 11. Saad and Eman[28] have applied the variational iteration method (VIM) for the Riemann-Liouville based fractional Burger's equation and compared the results with the ES.

In this work, we propose a numerical solution based on implicit FDM scheme and Lax-Friedrichs FDM scheme to solve a non-linear SFBE. Generally, the Lax-Friedrichs method is used for achieving the solutions for a hyperbolic based PDE's [29]. In general, an implicit scheme is the most well-known schemes for approximating the PDEs. This paper presents an approximation based on Lax-Friedrichs-implicit FDM to non-linear SFBE with appropriate initial/boundary conditions. The stability of a proposed scheme is analysed along with the numerical results.

2 Mathematical equation

Time fractional Burgers' equation was discussed in the articles [16, 24, 25, 26]. Following their study, we consider the non-linear SFBE as,

$$\frac{\partial u(x,t)}{\partial t} + u\frac{\partial u(x,t)}{\partial x} = \mu\frac{\partial^{\alpha} u(x,t)}{\partial x^{\alpha}}, (x,t) \in [a,b] \times (0, T_{max}] \tag{2.1}$$

included with initial values

$$u(x,0) = u_0(x) \tag{2.2}$$

and respective boundary values

$$u(0,t) = h_1(t); u(1,t) = h_2(t), t \in [0,T] \tag{2.3}$$

where $\mu > 0$ is kinematic viscosity, $u_0(x)$, $h_1(t)$ and $h_2(t)$ are specified boundaries. $u(x)$ is unknown functional.

To solve the SFBE in this work, let us consider the Riemann-Liouville fractional derivatives [20, 21, 30].

$$({}_0D_x^{\alpha})u(x,t) = \frac{1}{\Gamma(r-\alpha)}\frac{d^r}{dx^r}\int_L^x \frac{u(t)}{(x-t)^{\alpha-r+1}}dt, \alpha > 0 \tag{2.4}$$

where $\Gamma(.)$ is the Gamma function.

For space fractional derivative $({}_0D_x^{\alpha})u(x,t)$, we taken the Grunwald and shifted-Grunwald formula at level t_{n+1} [31].

$$\frac{\partial^{\alpha} u(x,t)}{\partial x^{\alpha}} = \frac{1}{h^{\alpha}}\sum_{j=0}^{i+1} g_j^{\alpha}\ u_{i-j+1}^{k+1} + O(h) \tag{2.5}$$

where $g_j^{\alpha} = \dfrac{\alpha(\alpha-1)\ldots.(\alpha-k+1)}{j!}$,

We can express, $\quad g_0^{\alpha} = 1, \ldots,\ g_j^{\alpha} = \left(1 - \dfrac{\alpha}{j}\right) g_{j-1}^{\alpha},\ j = 1, 2, 3, \ldots.$

2.1 Implicit scheme

The implicit scheme is one of the more accurate scheme for a non-linear Burger's equation [32]. Here, we consider a same for SFBE due to its stability than the explicit scheme [21, 31, 33, 34].

Let $u(x_i, t_k)$ is denoted as u_i^k. Define, $t_k = k\tau, \quad k = 0, 1, 2, ..., n;\ x_i = ih, \quad i = 0, 1, 2, ..., m$. Here, $h = L/m$ is the step size on space and $\tau = T/n$ is the step size on time respectively. Now,let us consider the nonlinear term, $u^{k+1}u_x^{k+1}$ by denoting it on Taylor expansion using the explicit time layer. We approximate the equation (2.1) by using an implicit FDM and approximated Riemann-Liouville derivatives equation (2.5) in space fractional viscous terms as follows.

$$\frac{(u_i^{k+1} - u_i^k)}{\tau} + \frac{u_i^k}{2}\left(\frac{u_{i+1}^{k+1} - u_{i-1}^{k+1}}{2h}\right) + \frac{u_i^{k+1}}{2}\left(\frac{u_{i+1}^k - u_{i-1}^k}{2h}\right) = \frac{\mu}{h^\alpha}\sum_{j=0}^{i+1} g_j^\alpha u_{i-j+1}^{k+1} \tag{2.6}$$

$$\left(u_i^{k+1} - u_i^k\right) + \tau\frac{u_i^k}{2}\left(\frac{u_{i+1}^{k+1} - u_{i-1}^{k+1}}{2h}\right) + \tau u_i^{k+1}\left(\frac{u_{i+1}^k - u_{i-1}^k}{4h}\right) = \tau\frac{\mu}{h^\alpha}\sum_{j=0}^{i+1} g_j^\alpha u_{i-j+1}^{k+1} \tag{2.7}$$

$$-\tau\left(\frac{u_i^k}{4h} + \frac{\mu}{h^\alpha}g_2^\alpha\right)u_{i-1}^{k+1} + \left(1 + \frac{\tau\left(u_{i+1}^k - u_{i-1}^k\right)}{4h} - \frac{\mu\tau}{h^\alpha}g_1^\alpha\right)u_i^{k+1} + \tau\left(\frac{u_i^k}{4h} - \frac{\mu}{h^\alpha}g_0^\alpha\right)u_{i+1}^{k+1} - \tau\frac{\mu}{h^\alpha}\sum_{j=3}^{i+1} g_j^\alpha u_{i-j+1}^{k+1} = u_i^k \tag{2.8}$$

When $k = 0$,

$$-\tau\left(\frac{u_i^0}{4h} + \frac{\mu}{h^\alpha}g_2^\alpha\right)u_{i-1}^1 + \left(1 + \frac{\tau\left(u_{i+1}^0 - u_{i-1}^0\right)}{4h} - \frac{\mu\tau}{h^\alpha}g_1^\alpha\right)u_i^1 + \tau\left(\frac{u_i^0}{4h} - \frac{\mu}{h^\alpha}g_0^\alpha\right)u_{i+1}^1 - \tau\frac{\mu}{h^\alpha}\sum_{j=3}^{i+1} g_j^\alpha u_{i-j+1}^1 = u_i^0 \tag{2.9}$$

When $k \geq 1$,

$$-\tau\left(\frac{u_i^k}{4h} + \frac{\mu}{h^\alpha}g_2^\alpha\right)u_{i-1}^{k+1} + \left(1 + \frac{\tau\left(u_{i+1}^k - u_{i-1}^k\right)}{4h} - \frac{\mu\tau}{h^\alpha}g_1^\alpha\right)u_i^{k+1} + \tau\left(\frac{u_i^k}{4h} - \frac{\mu}{h^\alpha}g_0^\alpha\right)u_{i+1}^{k+1} - \tau\frac{\mu}{h^\alpha}\sum_{j=3}^{i+1} g_j^\alpha u_{i-j+1}^{k+1} = u_i^k \tag{2.10}$$

Rewriting above equation, we get

$$a_i^k u_{i-1}^{k+1} + b_i^k u_i^{k+1} + c_i^k u_{i+1}^{k+1} = u_i^k + d_i^k \tag{2.11}$$

where, $a_i^k = -\tau\left(\frac{u_i^k}{4h} + \frac{\mu}{h^\alpha} g_2^\alpha\right)$, $b_i^k = \left(1 + \frac{\tau\left(u_{i+1}^k - u_{i-1}^k\right)}{4h} - \frac{\mu\tau}{h^\alpha} g_1^\alpha\right)$, $c_i^k = \tau\left(\frac{u_i^k}{4h} - \frac{\mu}{h^\alpha} g_0^\alpha\right)$, $d_i^k = \tau\frac{\mu}{h^\alpha}\sum_{j=3}^{i+1} g_j^\alpha u_{i-j+1}^{k+1}$

The boundary/initial conditions are,

$$u_i^0 = u(ih), \quad u_0^k = h_1(t), \quad u_m^k = h_2(t)$$

where $k = 0,\ 1,\ 2, ..., n, \quad i = 0,\ 1,\ 2,\ ...., m.$ The truncation error is $O\left(\tau^2, h^2\right)$.

2.1.1 Stability analysis - implicit FDM

Let us investigate the stability of the numerical implicit scheme (2.8) by using von-Neumann analysis. Let U_j^k is the ES of $u(x,t)$ at the point (x_j, t_k). Define

$$e_j^k = U_j^k - u_j^k \tag{2.12}$$

Then, by substituting Equation (2.12) into Equation (2.11),we have

$$a_i^k e_{i-1}^{k+1} + b_i^k e_i^{k+1} + c_i^k e_{i+1}^{k+1} = e_i^k + d_i^k \tag{2.13}$$

We put $e_i^k = \rho^k\ e^{ipjh}$ $(i = \sqrt{-1})$, in equation (2.6) and p is the wave number.

$$\rho^{k+1}\left[\tau\left(\frac{\rho^k\ e^{ipjh}}{2h}\right) isin(ph) + \left(1 + \frac{\tau\left(\ isin(ph)\,\rho^k\ \right)}{2h}\right) - \tau\frac{\mu}{h^\alpha}\sum_{r=0}^{i+1} g_j^\alpha\ e^{ip(1-r)h}\right] = \rho^k \tag{2.14}$$

$$\frac{\rho^{k+1}}{\rho^k} = \frac{1}{\left[\tau\left(\frac{\rho^k\ e^{ipjh}}{2h}\right) isin(ph) + \left(1 + \frac{\tau\left(\ isin(ph)\,\rho^k\ e^{ipjh}\ \right)}{2h}\right) - \tau\frac{\mu}{h^\alpha}\sum_{r=0}^{i+1} g_j^\alpha\ e^{ip(1-r)h}\right]} \leq 1 \tag{2.15}$$

It is obvious that the above scheme is unconditionally stable.

2.2 Lax-Friedrichs Scheme

As a result of its application to a nonlinear space fractional problem and the dissipative nature of the solution, the Lax-Friedrichs scheme is considered to be a classic first-order method. The Lax-Friedrichs scheme of the fractional equation (2.1) is approximated by as below:

$$\left(\frac{u_i^{k+1}-\frac{1}{2}\left(u_{i-1}^k+u_{i+1}^k\right)}{\tau}\right)+\frac{u_i^k}{2}\left(\frac{u_{i+1}^{k+1}-u_{i-1}^{k+1}}{2h}\right)+\frac{u_i^{k+1}}{2}\left(\frac{u_{i+1}^k-u_{i-1}^k}{2h}\right) = \frac{\mu}{h^\alpha}\sum_{j=0}^{i+1} g_j^\alpha u_{i-j+1}^{k+1} \tag{2.16}$$

$$-\tau(\frac{u^k}{4h})u_{i-1}^{k+1}+(1+\frac{\tau(u_{i+1}^k-u_{i-1}^k)}{4h})u_i^{k+1}+\tau\left(\frac{u^k}{4h}\right)u_{i+1}^{k+1}-\tau\frac{\mu}{h^\alpha}\sum_{j=0}^{i+1} g_j^\alpha u_{i-j+1}^{k+1} = \frac{1}{2}\left(u_{i-1}^k+u_{i+1}^k\right) \tag{2.17}$$

When $k=0$

$$-\tau(\frac{u^0}{4h})u_{i-1}^1+(1+\frac{\tau(u_{i+1}^0-u_{i-1}^0)}{4h})u_i^1+\tau(\frac{u^0}{4h})u_{i+1}^1-\tau\frac{\mu}{h^\alpha}\sum_{j=0}^{i+1} g_j^\alpha u_{i-j+1}^1 = \frac{1}{2}(u_{i-1}^0+u_{i+1}^0) \tag{2.18}$$

When $k\geq 1$

$$-\tau(\frac{u^k}{4h})u_{i-1}^{k+1}+(1+\frac{\tau(u_{i+1}^k-u_{i-1}^k)}{4h})u_i^{k+1}+\tau(\frac{u^k}{4h})u_{i+1}^{k+1}-\tau\frac{\mu}{h^\alpha}\sum_{j=0}^{i+1} g_j^\alpha u_{i-j+1}^{k+1} = \frac{1}{2}(u_{i-1}^k+u_{i+1}^k) \tag{2.19}$$

2.2.1 Stability Analysis - Lax-Friedrichs-implicit FDM

Let us consider the von-Neumann based method in preparation for estimating the stability of Lax-Friedrichs implicit scheme for SFBE. Let U_i^k be the approximate solution of fractional schemes (2.17).

$$e_i^k = U_i^k - u_i^k \tag{2.20}$$

Define, $e_i^k = \rho^k e^{ipjh} (i = \sqrt{(-1)}$ in Eq. (2.17), We get

$$\rho^{k+1} \left[\tau \left(\frac{\rho^k e^{ipjh}}{2h} \right) isin\,(ph) + \left(1 + \frac{\tau \left(\ isin\,(ph)\, e^{ipjh} \ \rho^k \right)}{2h} \right) - \tau \frac{\mu}{h^\alpha} \sum_{r=0}^{i+1} g_j^\alpha \ e^{ip(1-r)h} \right] = \left(\rho^k \ cos(ph) \right) \tag{2.21}$$

$$\frac{\rho^{k+1}}{\rho^k} = \frac{cos(ph)}{\left[\left(1 + \frac{\tau \left(\ isin\,(ph)\, e^{ipjh} \ \rho^k \right)}{2h} \right) + \tau \left(\frac{\rho^k e^{ipjh}}{2h} \right) isin\,(ph) \ - \tau \frac{\mu}{h^\alpha} \sum_{r=0}^{i+1} g_j^\alpha \ e^{ip(1-r)h} \right]} \tag{2.22}$$

We know, the value of the $sin\,(ph) \ and \ cos\,(ph) \ \leq 1$

3 Numerical Results

The verification of NS and accuracy of the schemes (implicit FDM and Lax-Friedrichs-implicit FDM) are illustrated in this section. In addition, the behavior of the solution with respect to change in the parameters are considered. This types of Burger's equation are used in predicting the important real world applications such as fluid flow, contaminant flow, boundary layer flow, aquifer flow, etc.

The accuracy of the FDM based schemes are measured using the L_∞ error norm, which is defined below:

$$L_\infty = \| \ U_k - u_N \ \|_\infty = Max_j |U_k - (u_N)_j| \tag{3.1}$$

where U_k and u_N denotes the ES and NS respectively at the node points x_k, for some fixed time.

3.1 Example 1

Consider the space fractional Burger's equation with source term to find error values as follows:

$$\frac{\partial u(x,t)}{\partial t} + u \frac{\partial u(x,t)}{\partial x} = \frac{\partial^\alpha u(x,t)}{\partial x^\alpha} + f(x,t), (x,t) \in [a,b] \times (0, T_{max}] \tag{3.2}$$

with initial and boundary conditions as

$$u\,(x,0) = x; \qquad and \quad u\,(0,t) = 0; \qquad u\,(1,t) = \frac{1}{1+t}$$

The exact solution [27]

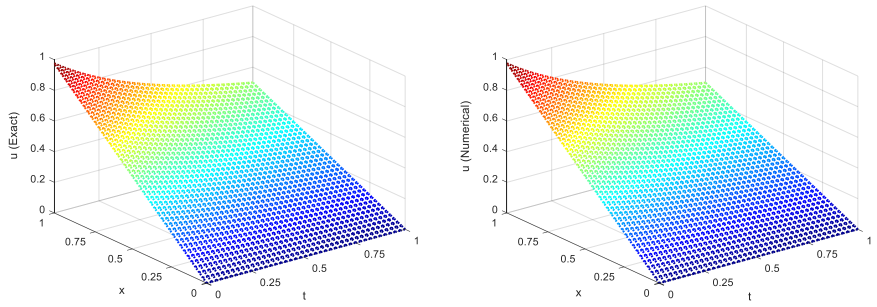

(a) (b)

Figure 1: Comparison of (a). ES and (b). NS

$$u(x,t) = \frac{x}{1+t} \tag{3.3}$$

and the respective source term is,

$$f(x,t) = -\frac{1}{1+t} \cdot \frac{1}{\Gamma(2-\alpha)} \mu x^{1-\alpha} \tag{3.4}$$

Table 1: Comparison the Maximum errors (L_∞) between ES and NS

τ	α	implicit FDM	Lax-Friedrichs FDM
1/100	1.9	$6.68689189E-03$	$4.27211449E-03$
1/100	1.7	$1.03293294E-02$	$9.42116044E-03$
1/100	1.5	$1.12734595E-02$	$1.07855788E-02$
1/100	1.3	$1.18441200E-02$	$1.14968475E-02$
1/100	1.1	$1.22581907E-02$	$1.18474280E-02$
1/1000	1.9	$3.30544871E-03$	$1.65415841E-03$
1/1000	1.7	$9.85641548E-03$	$7.98325112E-03$
1/1000	1.5	$9.89541454E-03$	$9.75634282E-03$
1/1000	1.3	$9.90254650E-03$	$9.76487132E-03$
1/1000	1.1	$9.91051481E-03$	$9.80037527E-03$

The verification of NS for the SFBE (2.18) with the ES is illustrated in the Fig. 1. The comparison is done against the time, $t = 0$ to 1 and space, $x = 0$ to 1. Both the NS and ES are good in comparable. Also, the Table. 3.1 shows the L_2 between the ES and NS. It is found that the Lax-Friedrichs-implicit FDM has lesser L_2 than the implicit FDM for every α.

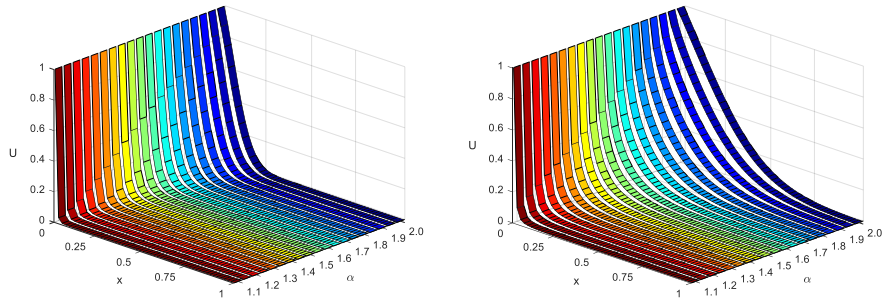

(a) (b)

Figure 2: variation of U at (a) $\mu = 0.1$ (b) $\mu = 1.0$

3.2 Example 2

Also, consider the SFBE without source term to find the characteristics of NS as

$$\frac{\partial U(x,t)}{\partial t} + u\frac{\partial U(x,t)}{\partial x} = \mu\frac{\partial^{\alpha} U(x,t)}{\partial x^{\alpha}} \tag{3.5}$$

with initial and boundary conditions as

$$U(x,0) = 0; \qquad U(0,t) = 1; \qquad U(1,t) = 0$$

Figure 2 shows the variation of U with respect to the space fractional parameter (α) and space coordinates (x) at kinematic viscosity $\mu = 0.1$ and 1.0 respectively. It is noted that, by increasing the parameter α, U decreases its intensity and travelling distance along the space.

4 Conclusion

The NS of SFBE has been evaluated by using implicit and Lax-Friedrichs-implicit FDM respectively. It is noted that both the implicit scheme is unconditionally stable and are good in agreement with the ES. It is found that L_2 of the Lax-Friedrichs-implicit is lesser than the implicit FDM. Also, it is found that the variation in space fractional order strongly affects the flow characteristics.

References

[1] M. Axtell and M. E. Bise, "Fractional calculus application in control systems," in *IEEE Conference on Aerospace and Electronics*, pp. 563–566, IEEE, 1990.

[2] V. V. Kulish and J. L. Lage, "Application of fractional calculus to fluid mechanics," *J. Fluids Eng.*, vol. 124, no. 3, pp. 803–806, 2002.

[3] D. Kumar and J. Singh, *Fractional Calculus in Medical and Health Science*. CRC Press, 2020.

[4] A. Goswami, J. Singh, D. Kumar, *et al.*, "Numerical computation of fractional kersten-krasilshchik coupled kdv-mkdv system occurring in multicomponent plasmas," *AIMS Mathematics*, vol. 5, no. 3, pp. 2346–2368, 2020.

[5] S. Kumar, R. Chauhan, J. Singh, and D. Kumar, "A computational study of transmission dynamics for dengue fever with a fractional approach," *Mathematical Modelling of Natural Phenomena*, vol. 16, p. 48, 2021.

[6] A. Goswami, J. Singh, D. Kumar, S. Gupta, and Sushila, "An efficient analytical technique for fractional partial differential equations occurring in ion acoustic waves in plasma," *Journal of Ocean Engineering and Science*, vol. 4, pp. 85–99, jun 2019.

[7] A. Goswami, J. Singh, D. Kumar, and Sushila, "An efficient analytical approach for fractional equal width equations describing hydro-magnetic waves in cold plasma," *Physica A: Statistical Mechanics and its Applications*, vol. 524, pp. 563–575, jun 2019.

[8] A. Goswami, S. Rathore, J. Singh, and D. Kumar, "Analytical study of fractional nonlinear schrödinger equation with harmonic oscillator," *Discrete & Continuous Dynamical Systems-S*, 2021.

[9] A. Goswami, J. Singh, and D. Kumar, "Numerical simulation of fifth order KdV equations occurring in magneto-acoustic waves," *Ain Shams Engineering Journal*, vol. 9, pp. 2265–2273, dec 2018.

[10] M. Hashmi, U. Aslam, J. Singh, and K. S. Nisar, "An efficient numerical scheme for fractional model of telegraph equation," *Alexandria Engineering Journal*, 2021.

[11] E. Medina, T. Hwa, M. Kardar, and Y.-C. Zhang, "Burgers equation with correlated noise: Renormalization-group analysis and applications to directed polymers and interface growth," *Physical Review A*, vol. 39, no. 6, p. 3053, 1989.

[12] X. Sun and M. J. Ward, "Metastability for a generalized burgers equation with applications to propagating flame fronts," *European Journal of Applied Mathematics*, vol. 10, no. 1, pp. 27–53, 1999.

[13] J. Baker, A. Armaou, and P. D. Christofides, "Nonlinear control of incompressible fluid flow: Application to burgers' equation and 2d channel flow," *Journal of Mathematical Analysis and Applications*, vol. 252, no. 1, pp. 230–255, 2000.

[14] A. R. Seadawy, W. Jun, *et al.*, "Mathematical methods and solitary wave solutions of three-dimensional zakharov-kuznetsov-burgers equation in dusty plasma and its applications," *Results in physics*, vol. 7, pp. 4269–4277, 2017.

[15] S. Kutluay, A. Bahadir, and A. Özdeş, "Numerical solution of one-dimensional burgers equation: explicit and exact-explicit finite difference methods," *Journal of Computational and Applied Mathematics*, vol. 103, no. 2, pp. 251–261, 1999.

[16] E. N. Aksan and A. Özdeş, "A numerical solution of burgers' equation," *Applied Mathematics and Computation*, vol. 156, no. 2, pp. 395–402, 2004.

[17] B. Inan and A. Bahadır, "An explicit exponential finite difference method for the burgers equation," *European International Journal of Science and Technology*, vol. 2, no. 10, pp. 61–72, 2013.

[18] K. Pandey, L. Verma, and A. K. Verma, "On a finite difference scheme for burgers equation," *Applied Mathematics and Computation*, vol. 215, no. 6, pp. 2206–2214, 2009.

[19] Y. Zhang, "A finite difference method for fractional partial differential equation," *Applied Mathematics and Computation*, vol. 215, no. 2, pp. 524–529, 2009.

[20] E. Sousa, "Finite difference approximations for a fractional advection diffusion problem," *Journal of Computational Physics*, vol. 228, no. 11, pp. 4038–4054, 2009.

[21] E. Sousa, "A second order explicit finite difference method for the fractional advection diffusion equation," *Computers & Mathematics with Applications*, vol. 64, pp. 3141–3152, nov 2012.

[22] A. Bekir and Ö. Güner, "The (G'/G) expansion method using modified RiemannLiouville derivative for some space-time fractional differential equations," *Ain Shams Engineering Journal*, vol. 5, pp. 959–965, sep 2014.

[23] A. Das, N. Ghosh, and K. Ansari, "Bifurcation and exact traveling wave solutions for dual power zakharov–kuznetsov–burgers equation with fractional temporal evolution," *Computers & Mathematics with Applications*, vol. 75, no. 1, pp. 59–69, 2018.

[24] A. Esen and O. Tasbozan, "Numerical solution of time fractional burgers equation," *Acta Univ. Sapientiae, Mathematica*, vol. 7, no. 2, pp. 167–185, 2015.

[25] A. Esen and O. Tasbozan, "Numerical solution of time fractional burgers equation by cubic b-spline finite elements," *Mediterranean Journal of Mathematics*, vol. 13, no. 3, pp. 1325–1337, 2016.

[26] M. S. Rawashdeh, "A reliable method for the space-time fractional burgers and time-fractional cahn-allen equations via the frdtm," *Advances in Difference Equations*, vol. 2017, no. 1, pp. 1–14, 2017.

[27] A. Yokus, "Numerical solution for space and time fractional order burger type equation," *Alexandria Engineering Journal*, vol. 57, no. 3, pp. 2085–2091, 2018.

[28] K. Saad and E. H. Al-Sharif, "Analytical study for time and time-space fractional burgers equation," *Advances in Difference Equations*, vol. 2017, no. 1, pp. 1–15, 2017.

[29] J. D. Towers, "The lax-friedrichs scheme for interaction between the inviscid burgers equation and multiple particles," *Networks and Heterogeneous Media*, vol. 15, no. 1, p. 143, 2020.

[30] I. Podlubny, *Fractional differential equations: an introduction to fractional derivatives, fractional differential equations, to methods of their solution and some of their applications*. Elsevier, 1998.

[31] F. Liu, P. Zhuang, V. Anh, I. Turner, and K. Burrage, "Stability and convergence of the difference methods for the space–time fractional advection–diffusion equation," *Applied Mathematics and Computation*, vol. 191, no. 1, pp. 12–20, 2007.

[32] V. K. Srivastava, M. K. Awasthi, and M. Tamsir, "A fully implicit finite-difference solution to one dimensional coupled nonlinear burgers equations," *Int. J. Math. Sci*, vol. 7, no. 4, p. 23, 2013.

[33] D. A. Murio, "Implicit finite difference approximation for time fractional diffusion equations," *Computers & Mathematics with Applications*, vol. 56, no. 4, pp. 1138–1145, 2008.

[34] S. T. Mohyud-Din, T. Akram, M. Abbas, A. I. Ismail, and N. H. Ali, "A fully implicit finite difference scheme based on extended cubic b-splines for time fractional advection–diffusion equation," *Advances in Difference Equations*, vol. 2018, no. 1, pp. 1–17, 2018.

Optimal Control of two-strain typhoid transmission using treatment and proper hygiene/sanitation practices

Tsegaye Kebede Irena[1], Sunita Gakkhar

December 26, 2021

Abstract

A mathematical model is developed to predict the optimum level of measures required to control a two-strain typhoid infection. The model considers symptomatic individuals and carriers together with environmental bacteria with different sensitivities to antimicrobials. Treatment for symptomatic individuals in each strain and use of sanitation and proper hygiene practices are considered as control measures. Our simulation results show that combining the three control interventions highly influenced the number of symptomatic individuals and environmental bacteria in both the strains. However, there are still a significant number of asymptomatic carriers in both the strains. This result shows that combating a two-strain typhoid infection requires some control interventions that reduce the number of asymptomatic carriers to near zero, along with optimal treatment combined with proper hygiene/sanitation practices. Further, efficiency analysis is used to investigate the impact of each control strategy on reducing the number of infected individuals and bacteria in both the strains. The study result suggests that implementing the combination of all the three control interventions is the most effective control strategy.

Key words: *Salmonella* Typhi; Two-strain typhoid infection; Asymptomatic carriers; Efficiency analysis

Mathematics Subject Classification(2010): 44A15; 46F12; 54B15; 46F99

1

1 Introduction

Typhoid, a disease caused by *Salmonella* Typhi bacteria, is a significant cause of illness and death in low-resource regions worldwide, especially Sub-Saharan

[1]Corresponding author: Department of Mathematics
Indian Institute of Technology Roorkee, Roorkee-247667, India

Africa and South/Southeast Asia [1]. It is a severe febrile illness often accompanied by headache, loss of appetite, malaise, abdominal pain, diarrhea, and (in severe cases) intestinal perforation and neurological complications [2]. It is estimated to cause nearly 12 million cases and over 128 000 deaths globally each year [6]. It is estimated that the case fatality rate for untreated patients ranges between 10 and 20%, but drops to 1–4% with appropriate and timely antimicrobial treatment [4, 3, 5]. The infection is usually spread through contaminated food and water from the environment and direct contact with an infected person [7, 8].

Typhoid fever can be prevented and controlled through public health interventions such as providing safe drinking water, promoting hygiene and sanitation, and ensuring adequate and timely patient care. Antimicrobial treatment is the cornerstone for reducing severe illness and even death. However, misuse of antimicrobials for treatment leads to the emergence of resistant strains of *Salmonella* Typhi, known as treatment-induced acquired resistance [9, 10]. In typhoid endemic areas, clinicians frequently prescribe antimicrobials to patients with suspected typhoid without blood culture confirmation. This practice results in delayed treatment leading to the development of antimicrobial resistance [3, 11, 12, 13]. Treatment-induced acquired resistance has complicated treatment, increasing morbidity and mortality, and is considered one of the most significant challenges in managing the disease [14, 15].

In existing litrature, several typhoid epidemiological models have been developed and analyzed to better understand the transmission dynamics of typhoid [16, 17, 18, 19, 20, 21, 22, 23]. Among them, only a few have explored the effect of control strategies for typhoid with optimal control theory [16, 17]. Optimal control theory is a mathematical optimization that deals with finding a control for a dynamical system over a period of time. Although the importance of optimal control theory in epidemiology is well recognized, its applications in typhoid dynamics are scarce. No attempts have been made to predict the optimal level of control measures required to combat a two-strain typhoid infection. Our aim is to investigate the optimal control strategies in a two-strain dynamic model involving antimicrobial-sensitive and resistant strains of typhoid. A mathematical model for a two-strain typhoid dynamics is explored considering treatment-induced acquired resistance and re-infection [24]. Three time-dependent controls are introduced in this model to explore the optimal control strategy for controlling the disease.

The paper is organized as follows: In Section 2, the model in [24] is modified by adding three time-dependent controls $u_1(t)$, $u_2(t)$ and $u_3(t)$, and three positive parameters ϵ, b_1 and b_2. Also, a description of these parameters is given. In Section 3, a mathematical analysis of the time-dependent model is performed. In Section 4, numerical simulations and discussions of the corresponding results are presented. A short conclusion of the study is made in Section 5.

2 Model with controls

The mathematical model developed by Irena and Gakkhar [24] is considered to investigate the infection dynamics in a two-strain typhoid disease. The state variables I_j, C_j, and $\mathcal{B}_j$ represent the number of symptomatic infectious individuals, asymptomatic carriers, and bacteria for the strain j, respectively, while S represents the susceptible individuals. The model presented in [24] is

$$\begin{cases} \frac{dS}{dt} = \pi - \mu S - (\lambda_1 + \lambda_2)S + (1-p)r_1 I_1 + r_2 I_2 \\ \frac{dI_1}{dt} = (1-\alpha)[\lambda_1 S - \psi\lambda_2 I_1] - (\mu + d_1 + r_1)I_1 + \phi_1 C_1 \\ \frac{dC_1}{dt} = \alpha\lambda_1 S - \psi\lambda_2 C_1 - (\mu + \phi_1)C_1 \\ \frac{d\mathcal{B}_1}{dt} = \delta_1 I_1 + \omega_1 C_1 - \xi_1 \mathcal{B}_1 \\ \frac{dI_2}{dt} = (1-\alpha)\lambda_2[S + \psi(I_1 + C_1)] + pr_1 I_1 - (\mu + d_2 + r_2)I_2 + \phi_2 C_2 \\ \frac{dC_2}{dt} = \alpha\lambda_2(S + \psi C_1) - (\mu + \phi_2)C_2 \\ \frac{d\mathcal{B}_2}{dt} = \delta_2 I_2 + \omega_2 C_2 - \xi_2 \mathcal{B}_2 \end{cases} \tag{2.1}$$

where

$$\lambda_j = \frac{\beta_j(I_j + \theta C_j)}{N} + \eta f(B) g_j(B)$$

and $j = 1, 2$ represent the sensitive and resistant strains, respectively.

On the basis of sensitivity analysis of the model, three time-dependent controls are introduced in the model: (i) treatment of the symptomatic individuals in each strain $(u_1(t), u_2(t))$, which were constant parameters in our previous work [24], and (ii) proper hygiene/sanitation practices in order to prevent contamination of food and water to reduce both direct and environmental transmission $(u_3(t))$. The first two controls, u_1 and u_2, also decrease the bacteria excretion of symptomatic individuals in both strains so that the bacteria shedding rates by symptomatic individuals δ_1 and δ_2 in model (2.1) are replaced by $(1-(1-p)u_1)\delta_1$ and $(1-\epsilon u_2)\delta_2$, respectively. The parameter ϵ represents the efficacy of treatment for symptomatic individuals with resistant strain. Also, the second control u_3 increases the decay rate of bacteria so that the bacteria decay rates ξ_1 and ξ_1 are replaced by $\xi_1 + b_1 u_3$ and $\xi_2 + b_2 u_3$, respectively. The parameters b_1 and b_2 denote the bacteria decay rates (sensitive and AMR strains, respectively) induced by sanitation and proper hygiene practices. The schematic diagram in Figure 1 shows the transmission dynamics of the time-dependent model. Thus, the resulting dynamic model is given by the following

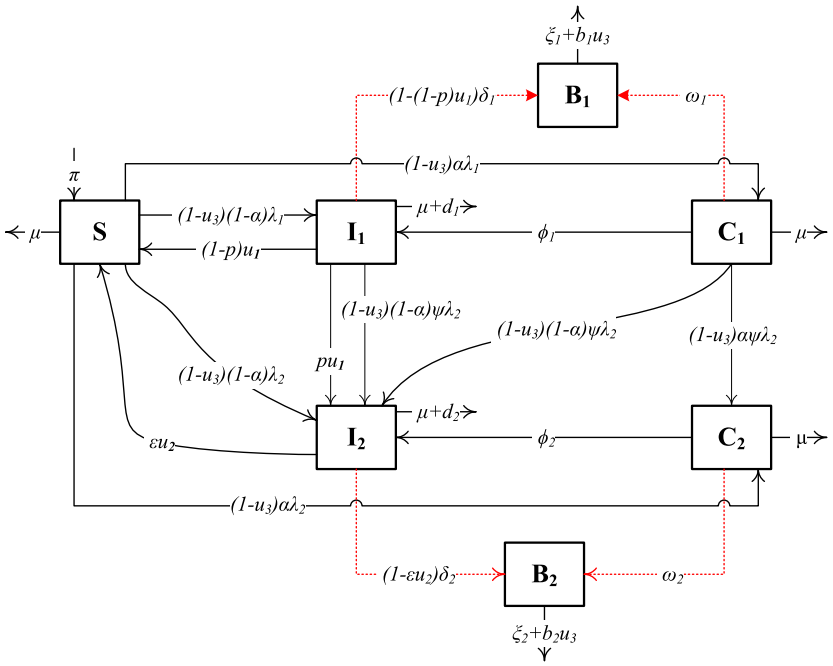

Figure 1: Flow diagram of the model.

system of nonlinear ODEs:

$$\begin{cases} \frac{dS}{dt} = \pi - \mu S - (1-u_3)(\lambda_1+\lambda_2)S + (1-p)u_1 I_1 + \epsilon u_2 I_2 \\ \frac{dI_1}{dt} = (1-u_3)(1-\alpha)[\lambda_1 S - \psi\lambda_2 I_1] - (\mu + d_1 + u_1)I_1 + \phi_1 C_1 \\ \frac{dC_1}{dt} = (1-u_3)[\alpha\lambda_1 S - \psi\lambda_2 C_1] - (\mu+\phi_1)C_1 \\ \frac{d\mathcal{B}_1}{dt} = \delta_1(1-(1-p)u_1)I_1 + \omega_1 C_1 - (\xi_1 + b_1 u_3)\mathcal{B}_1 \\ \frac{dI_2}{dt} = (1-\alpha)(1-u_3)\lambda_2[S+\psi(I_1+C_1)] + pu_1 I_1 \\ \qquad -(\mu + d_2 + \epsilon u_2)I_2 + \phi_2 C_2 \\ \frac{dC_2}{dt} = (1-u_3)\alpha\lambda_2(S+\psi C_1) - (\mu+\phi_2)C_2 \\ \frac{d\mathcal{B}_2}{dt} = \delta_2(1-\epsilon u_2)I_2 + \omega_2 C_2 - (\xi_2 + b_2 u_3)\mathcal{B}_2 \end{cases} \tag{2.2}$$

The model is associated with the nonnegative initial conditions:

$$S(0), \quad I_j(0), \quad C_j(0), \quad \mathcal{B}_j(0) \quad \text{for} \quad j = 1, 2.$$

The description of the associated model parameters are given in Table 1 and are assumed to be nonnegative.

Table 1: Description the model parameters.

Parameter	Description
α	Fraction of newly infected individuals who becomes asymptomatic carriers
β_1, β_2	Ingestion rate of sensitive and resistant strains of bacteria through human-to-human interaction
δ_1, δ_2	Shedding rate of bacteria by symptomatic cases with sensitive and resistant strains
ϵ	Efficacy of treatment of symptomatic individuals with resistant strain
η	Ingestion rate of bacteria from the contaminated environment
θ	Relative infectiousness of asymptomatic carriers
μ	Natural mortality rate of human population
ξ_1, ξ_2	Decay rate of sensitive and resistant strains of bacteria in the environment
π	Influx rate of individuals into susceptible class
ϕ_1, ϕ_2	Symptoms development rate by asymptomatic carriers with sensitive and resistant strains
ψ	Factor reducing the risk of re-infection with resistant strain due to activates of immune cells to the previous infection with a sensitive strain
ω_1, ω_2	Shedding rate of bacteria by asymptomatic carriers with sensitive and resistant strains
b_1, b_2	Sanitation-induced bacteria decay rates (sensitive and resistant strains)
d_1, d_2	Disease-induced death rate for symptomatic cases with sensitive and resistant strains
p	Fraction of those symptomatic individuals infected with a sensitive strain who acquire treatment-induced resistance

The objective functional to be minimized is

$$J(u_1,u_2,u_3)=\int_0^T\left(\sum_{i=1}^{2}A_i(I_i+C_i)+A_3\sum_{j=1}^{2}\mathcal{B}_j+\frac{1}{2}\sum_{k=1}^{3}D_ku_k^2\right)dt \qquad (2.3)$$

subject to the state system (2.2), where A_i and D_i $(i=1,2,3)$ are appropriate weight constants. The aim is to minimize the total number of infective individuals as well as bacteria while keeping the implementation cost of the strategies associated to the controls low.
We seek to find an optimal control triplet (u_1^*,u_2^*,u_3^*) such that

$$J(u_1^*,u_2^*,u_3^*)=\min_{\Omega}J(u_1,u_2,u_3)$$

where

$$\Omega=\left\{(u_1,u_2,u_3)\in L^1(0,T)\mid 0\le u_i\le 1,\ i=1,2,3\right\}$$

is the control set.

3 Optimal control analysis

The existence of optimal control triplet (u_1^*, u_2^*, u_3^*) is guaranteed due to a priori boundedness of the state solutions, convexity of the integrand of J on Ω, and the *Lipschitz* property of the state system [25].

The necessary conditions that an optimal solution must satisfy come from Pontryagin's Maximum Principle [26]. This principle converts (2.2) and (2.3) into a problem of minimizing pointwise a Hamiltonian $\mathbb{H}$ with respect to u_1, u_2 and u_3:

$$\begin{aligned}
\mathbb{H} = {} & A_1(I_1 + C_1) + A_2(I_2 + C_2) + A_3(\mathcal{B}_1 + \mathcal{B}_2) + \frac{D_1}{2}u_1^2 + \frac{D_2}{2}u_2^2 + \frac{D_3}{2}u_3^2 \\
& + \lambda_1[\pi - \mu S - (1-u_3)(\lambda_1 + \lambda_2)S + (1-p)u_1 I_1 + \epsilon u_2 I_2] \\
& + \lambda_2[(1-u_3)(1-\alpha)(\lambda_1 S - \psi\lambda_2 I_1) - (\mu + d_1 + u_1)I_1 + \phi_1 C_1] \\
& + \lambda_3[(1-u_3)(\alpha\lambda_1 S - \psi\lambda_2 C_1) - (\mu + \phi_1)C_1] \\
& + \lambda_4[\delta_1(1-(1-p)u_1)I_1 + \omega_1 C_1 - (\xi_1 + b_1 u_3)\mathcal{B}_1] \\
& + \lambda_5[(1-u_3)(1-\alpha)\lambda_2(S + \psi(I_1 + C_1)) + pu_1 I_1 \\
& \quad -(\mu + d_2 + \epsilon u_2)I_2 + \phi_2 C_2] \\
& + \lambda_6[(1-u_3)\alpha\lambda_2(S + \psi C_1) - (\mu + \phi_2)C_2] \\
& + \lambda_7[\delta_2(1-\epsilon u_2)I_2 + \omega_2 C_2 - (\xi_2 + b_2 u_3)\mathcal{B}_2]
\end{aligned} \tag{3.1}$$

where λ_i, $i = 1, 2, ..., 7$ are the adjoint functions.

By applying Pontryagin's Maximum Principle [26] and the existence result for the optimal control triplet from [25], the following adjoint system is obtained

together with transversality conditions $\lambda_k(T) = 0$:

$$\begin{aligned}
\frac{d\lambda_1}{dt} =& \frac{1}{\mathcal{B}_1+\mathcal{B}_2} \\
&\times [(1-u_3)\eta f(\mathcal{B})((\lambda_1-(1-\alpha)\lambda_2-\alpha\lambda_3)\mathcal{B}_1+(\lambda_1-(1-\alpha)\lambda_5-\alpha\lambda_6)\mathcal{B}_2) \\
&+\mu(\mathcal{B}_1+\mathcal{B}_2)\lambda_1] \\
&+\frac{(1-u_3)}{N^2}[\mathcal{B}_1(\lambda_1-(1-\alpha)\lambda_2-\alpha\lambda_3)(I_1+\theta C_1)(I_1+C_1+I_2+C_2)] \\
&+\frac{\beta_2(1-u_3)(I_2+\theta C_2)}{N^2}[(\lambda_1-(1-\alpha)\lambda_5-\alpha\lambda_6+(\lambda_5-\lambda_2)(1-\alpha)\psi)I_1 \\
&+(\lambda_1-(\lambda_5(1-\alpha)+\alpha\lambda-6)(1-\psi)-\psi\lambda_3)C_1 \\
&+(\lambda_1-(1-\alpha)\lambda_5-\alpha\lambda_6)I_2+(\lambda_1-(1-\alpha)\lambda_5-\alpha\lambda_6)C_2], \\
\frac{d\lambda_2}{dt} =& -A_1-[(1-p)u_1-S(1-u_3)\frac{\beta_1(S+(1-\theta)C_1+I_2+C_2)-\beta_2(I_2+\theta C_2)}{N^2}]\lambda_1 \\
&+(\mu+d_1+u_1)\lambda_2 \\
&-(1-u_3)(1-\alpha)[\frac{\beta_1 S(S+(1-\theta)C_1+I_2+C_2)}{N^2}-\frac{\beta_2\psi(S+C_1+I_2+C_2)(I_2+\theta C_2)}{N^2} \\
&-\frac{\psi\eta f(\mathcal{B})\mathcal{B}_2}{\mathcal{B}_1+\mathcal{B}_2}]\lambda_2-(1-u_3)[\frac{\alpha\beta_1 S(S+(1-\theta)C_1+I_2+C_2)}{N^2}+\frac{\beta_2\psi C_1(I_2+\theta C_2)}{N^2}]\lambda_3 \\
&-(1-u_1)\delta_1\lambda_4-pu_1\lambda_5 \\
&-(1-u_3)(1-\alpha)[\frac{\beta_2(I_2+\theta C_2)(S(\psi-1)+\psi(I_2+C_2))}{N^2}+\frac{\psi\eta f(\mathcal{B})\mathcal{B}_2}{\mathcal{B}_1+\mathcal{B}_2}]\lambda_5 \\
&+\frac{(1-u_3)\alpha\beta_2(S+\psi C_1)(I_2+\theta C_2)}{N^2}\lambda_6, \\
\frac{d\lambda_3}{dt} =& -A_1+S(1-u_3)\frac{\beta_1(-I_1+\theta(S+I_1+I_2+C_2))-\beta_2(I_2+\theta C_2)}{N^2}\lambda_1+(\mu+\phi_1)\lambda_3 \\
&+[(1-u_3)(1-\alpha)\frac{\beta_1 S(-I_1+\theta(S+I_1+I_2+C_2))+\beta_2\psi I_1(I_2+\theta C_2)}{N^2}+\phi_1]\lambda_2 \\
&-(1-u_3)\frac{\alpha\beta_1 S(-I_1+\theta(S+I_1+I_2+C_2))-\beta_2\psi(I_2+\theta C_2)(S+I_1+I_2+C_2)}{N^2}\lambda_3 \\
&+(1-u_3)\frac{\psi\eta f(\mathcal{B})\mathcal{B}_2}{\mathcal{B}_1+\mathcal{B}_2}\lambda_3-\omega_1\lambda_4 \\
&-(1-u_3)(1-\alpha)[\frac{\beta_2(I_2+\theta C_2)(S(\psi-1)+\psi(I_2+C_2))}{N^2}+\frac{\psi\eta f(\mathcal{B})\mathcal{B}_2}{\mathcal{B}_1+\mathcal{B}_2}]\lambda_5 \\
&-(1-u_3)\alpha[\frac{\beta_2(I_2+\theta C_2)(S(\psi-1)+\psi(I_1+I_2+C_2))}{N^2}+\frac{\psi\eta f(\mathcal{B})\mathcal{B}_2}{\mathcal{B}_1+\mathcal{B}_2}]\lambda_6,
\end{aligned}$$

$$
\begin{aligned}
\frac{d\lambda_4}{dt} =& - A_3 + \frac{(1-u_3)\eta S}{(1+\mathcal{B}_1)^2(1+\mathcal{B}_2)}\lambda_1 + (\xi_1 + b_1u_3)\lambda_4 \\
& - \frac{(1-u_3)\eta f(\mathcal{B})\mathcal{B}_2}{(\mathcal{B}_1+\mathcal{B}_2)^2}[(1-\alpha)((S+\psi I_1)\lambda_2 - (S+\psi(I_1+C_1))\lambda_5) \\
& + (\alpha S + \psi C_1)\lambda_3 - \alpha(S+\psi C_1)\lambda_6] - (1-u_3)\eta[\frac{\mathcal{B}_1 S((1-\alpha)\lambda_2 + \alpha\lambda_3)}{(1+\mathcal{B}_1)^2(1+\mathcal{B}_2)(\mathcal{B}_1+\mathcal{B}_2)} \\
& + \frac{\mathcal{B}_2\{-\psi C_1\lambda_3 + \alpha\lambda_6(S+\psi C_1) + \psi(-1+\alpha)\lambda_2 I_1 + (1-\alpha)\lambda_5\ (S+\psi(C_1+I_1))\}}{(1+\mathcal{B}_1)^2(1+\mathcal{B}_2)(\mathcal{B}_1+\mathcal{B}_2)}], \\
\frac{d\lambda_5}{dt} =& - A_2 - [u_2 + S(1-u_3)\frac{\beta_1(I_1+\theta C_1) - \beta_2(S+I_1+C_1+(1-\theta)C_2)}{N^2}]\lambda_1 \\
& + (1-u3)(1-\alpha)\frac{\beta_1 S(I_1+\theta C_1) + \beta_2\psi I_1(S+I_1+C_1+(1-\theta)C_2)}{N^2}\lambda_2 \\
& + (1-u3)\frac{\beta_1\alpha S(I_1+\theta C_1) + \beta_2\psi C_1(S+I_1+C_1+(1-\theta)C_2)}{N^2}\lambda_3 \\
& + [(\mu + d_2 + u_2) - \frac{(1-u_3)(1-\alpha)(S+I_1+C_1+(1-\theta)C_2)(S+\psi(I_1+C_1))\beta_2}{N^2}]\lambda_5 \\
& - \frac{(1-u_3)\alpha(S+\psi C_1)(S+I-1+C_1+(1-\theta)C_2)\beta_2}{N^2}\lambda_6 - (1-\epsilon u_2)\delta_2\lambda_7, \\
\frac{d\lambda_6}{dt} =& - A_2 + S(1-u_3)\frac{\beta_2(-I_2+\theta(S+I_1+C_1+I_2)) - \beta_1(I_1+\theta C_1)}{N^2}\lambda_1 \\
& + (1-u_3)(1-\alpha)\frac{\beta_1 S(I_1+\theta C_1) + \beta_2\psi I_1(-I_2+\theta(C_1+S+I_1+I_2))}{N^2}\lambda_2 \\
& + (1-u_3)\frac{\alpha\beta_1 S(I_1+\theta C_1) + \beta_2\psi C_1(-I_2+\theta(S+I_1+C_1+I_2))}{N^2}\lambda_3 \\
& - [\frac{(1-u_3)(1-\alpha)(S+\psi(I_1+C_1))(-I_2+\theta(S+I_1+C_1+I_2))\beta_2}{N^2} + \phi_2]\lambda_5 + (\mu+\phi_2)\lambda_6 \\
& - \frac{(1-u_3)\alpha(S+\psi C_1)(-I_2+\theta(S+I_1+C_1+I_2))\beta_2}{N^2}\lambda_6 - \omega_2\lambda_7, \\
\frac{d\lambda_7}{dt} =& - A_3 + \frac{(1-u_3)\eta S}{(1+\mathcal{B}_1)(1+\mathcal{B}_2)^2}\lambda_1 + (\xi_1 + b_1u_3)\lambda_4 \\
& - \frac{(1-u_3)\eta f(\mathcal{B})\mathcal{B}_1}{(\mathcal{B}_1+\mathcal{B}_2)^2}[(1-\alpha)((S+\psi I_1)\lambda_2 - (S+\psi(I_1+C_1))\lambda_5) \\
& + (\alpha S + \psi C_1)\lambda_3 - \alpha(S+\psi C_1)\lambda_6] - (1-u_3)\eta[\frac{\mathcal{B}_1 S((1-\alpha)\lambda_2 + \alpha\lambda_3)}{(1+\mathcal{B}_1)(1+\mathcal{B}_2)^2(\mathcal{B}_1+\mathcal{B}_2)} \\
& + \frac{\mathcal{B}_2\{-\psi C_1\lambda_3 + \alpha\lambda_6(S+\psi C_1) + \psi(-1+\alpha)\lambda_2 I_1 + (1-\alpha)\lambda_5(S+\psi(C_1+I_1))\}}{(1+\mathcal{B}_1)(1+\mathcal{B}_2)^2(\mathcal{B}_1+\mathcal{B}_2)}]
\end{aligned}
\tag{3.2}
$$

Furthermore, the optimal control characterization is

$$\begin{aligned} u_1^* &= max\left\{0, min\left(\frac{(\lambda_2+(1-p)(\delta_1\lambda_4-\lambda_1)-p\lambda_5)I_1^*}{D_1}, 1\right)\right\} \\ u_2^* &= max\left\{0, min\left(\frac{\epsilon(\lambda_5+\delta_2\lambda_7-\lambda_1)I_2^*}{D_2}, 1\right)\right\} \\ u_3^* &= max\left\{0, min\left(\tilde{u}_3, 1\right)\right\} \end{aligned} \tag{3.3}$$

where

$$\begin{aligned} \tilde{u}_3 = \frac{\eta f(\mathcal{B})}{D_3}[&-\lambda_1 S^* + \frac{S^*\mathcal{B}_1^*(1-\alpha)\lambda_2+\alpha\lambda_3}{\mathcal{B}_1^*+\mathcal{B}_2^*} \\ &+\frac{\mathcal{B}_2^*\left(\psi(1-\alpha)(\lambda_5-\lambda_2)I_1^*+((1-\alpha)\lambda_5+\alpha\lambda_6)(S^*+\psi C_1^*)-\psi\lambda_3 C_1^*\right)}{\mathcal{B}_1^*+\mathcal{B}_2^*}] \\ &+\frac{b_1\lambda_4\mathcal{B}_1^*+b_2\lambda_7\mathcal{B}_2^*}{D_3} - \frac{\beta_1}{D_3N^*}(I_1^*+\theta C_1^*)(\lambda_1-\lambda_2+\alpha(\lambda_2-\lambda_3))S^* \\ &-\frac{\beta_2}{D_3N^*}(I_2^*+\theta C_2^*)[\lambda_1 S^*+\psi\lambda_3 C_1^*+(S^*+\psi C_1^*)(-\lambda_5+\alpha(\lambda_5-\lambda_6)) \\ &+\psi(1-\alpha)(\lambda_2-\lambda_5)I_1^*]. \end{aligned}$$

4 Numerical results

This section presents the numerical simulation results by solving the optimality system, which comprises the state system (2.2), adjoint system (3.2), control characterization (3.3), and corresponding initial and final conditions, using the forward-backward sweep method [27, 28].

For numerical simulations, we consider the model parameter values presented in Table 2.

Table 2: Model parameter values used in numerical simulations [24], the unit is per week if appropriate.

$\alpha = 0.3$	$\beta_1 = 0.006$	$\beta_2 = 0.0052$	$\delta_1 = 1.0$
$\delta_2 = 1.05$	$\eta = 1.379 \times 10^{-10}$	$\theta = 0.35$	$\mu = 0.0005$
$\xi_1 = 0.2415$	$\xi_2 = 0.2415$	$\pi = 10^5/52$	$\phi_1 = 0.00096$
$\phi_2 = 0.0017$	$\psi = 0.95$	$\omega_1 = 0.05$	$\omega_2 = 0.06$
$d_1 = 0.00125$	$d_2 = 0.002$	$p = 0.1$	

Additionally, the following parameter values are chosen:

$A_1 = A_2 = 10,\ A_3 = 25,\ D_1 = 5,\ D_2 = 8,\ D_3 = 10,\ b_1 = 0.2,\ b_2 = 0.1,$
$\epsilon = 0.75,\ T = 100$ weeks.

The following control strategies are explored in order to determine the optimum strategy that significantly reduces typhoid transmission:

A: Treatment of the symptomatic individuals in each strain (u_1, u_2) only;

B: Employing sanitation and proper hygiene (u_3) only;

C: Employing all the three control interventions $(u_1,\ u_2,\ u_3)$.

The control profile for each control strategy is shown in Fig. 2, and the effect of each control strategy on the reduction of infection is depicted in Fig. 3.

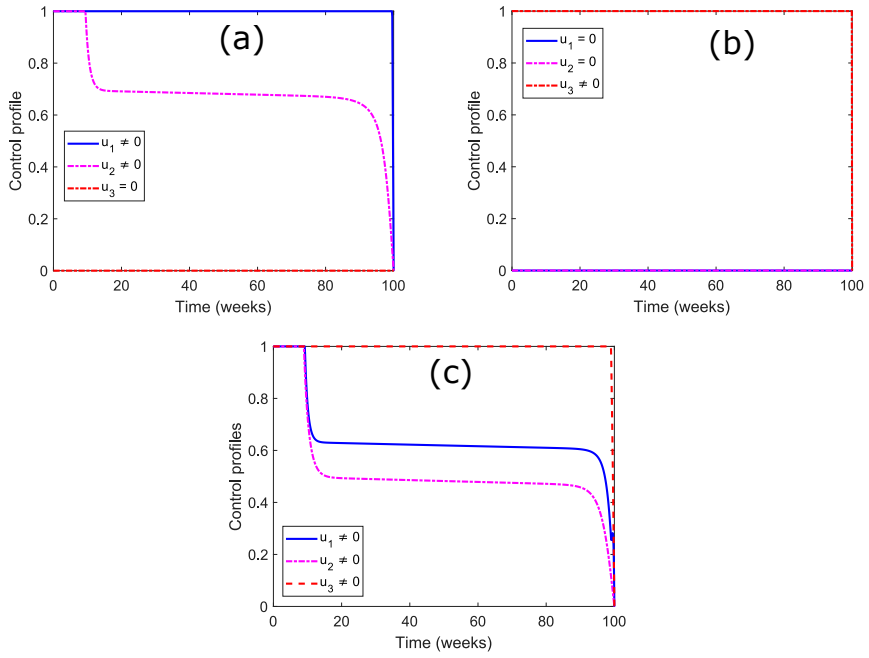

Figure 2: Control profile for (a) optimal treatment only, (b) optimal sanitation and proper hygiene only, and (c) optimal treatment combined with sanitation and proper hygiene

Our simulation results reveal that the combination of all control interventions highly influenced the symptomatic individuals and environmental bacteria in both the strains. However, there are still a significant number of asymptomatic carriers in both the strains, which play an important role in the evolution and transmission of typhoid infections. This reflects that asymptomatic carriers may have long-term impacts on the spread of typhoid infection even in the presence of the two control interventions.

4.1 Efficiency analysis

Here an efficiency analysis is performed to determine the best control strategy without considering costs associated with each control strategy [29, 30]. So, we

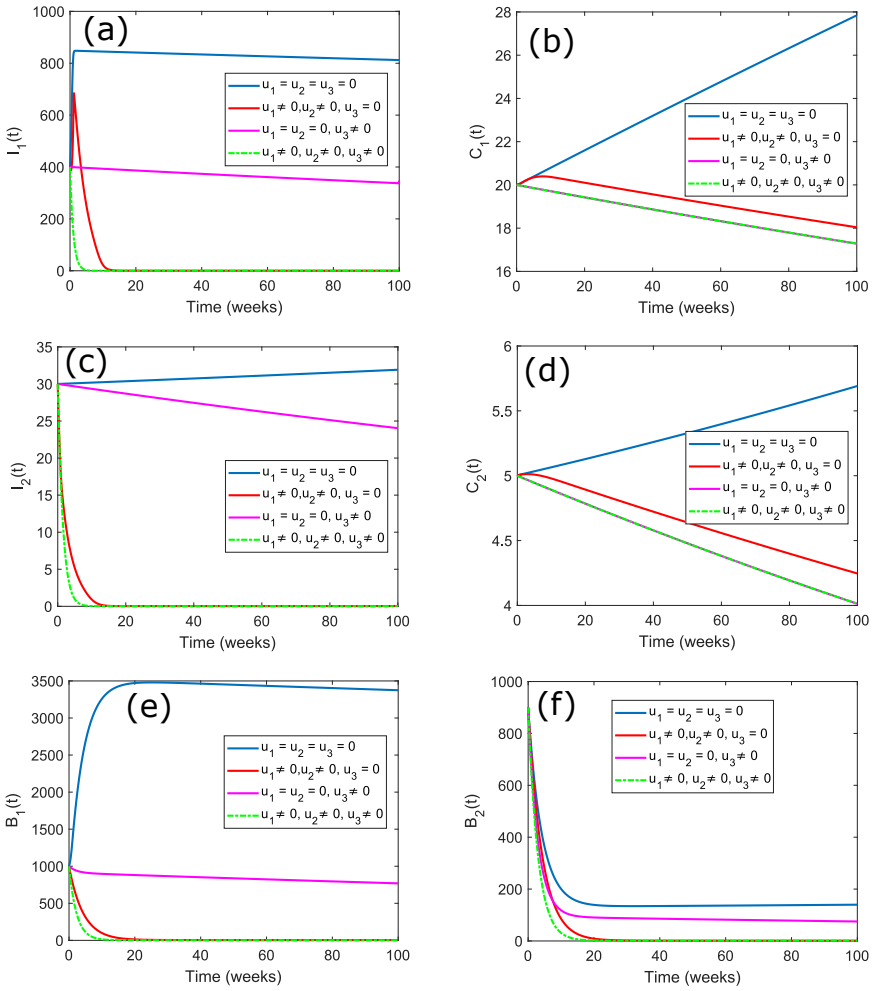

Figure 3: Effect of each control strategy on reducing the number of infectious humans and bacteria: (a) Symptomatic individuals with sensitive strain, (b) Asymptomatic carriers with sensitive strain, (c) Symptomatic individuals with resistant strain, (d) Asymptomatic carriers with resistant strain, (e) Sensitive strain of bacteria in the environment, (f) Resistant strain of bacteria in the environment

investigate the impact of each control strategies on the reduction of infectious humans and bacteria by introducing the efficiency index, $\mathbb{F}$. The efficiency index for human and bacteria population in the strain j are, respectively, computed

as:

$$\mathbb{F}^{I_j+C_j} = \left(1 - \frac{A_c^{I_j+C_j}}{A_o^{I_j+C_j}}\right) \times 100 \quad \text{and} \quad \mathbb{F}^{\mathcal{B}_j} = \left(1 - \frac{A_c^{\mathcal{B}_j}}{A_o^{\mathcal{B}_j}}\right) \times 100$$

where

$$A^{I_j+C_j} = \int_0^T \Big(I_j(t) + C_j(t)\Big)dt \quad \text{and} \quad A^{\mathcal{B}_j} = \int_0^T \mathcal{B}_j(t)dt$$

represent the cumulative number of infectious humans and bacteria with strain j, respectively, during the time interval $[0, T]$. The efficiency index is calculated for human and bacteria population in both the strains and presented in Table 3. Note that the control strategy with the highest efficiency index will be the best. From Table 3, it follows that strategy C is the most effective for reducing

Table 3: Efficiency index

Strategy	$A_c^{I_1+C_1}$	$A_c^{\mathcal{B}_1}$	$\mathbb{F}^{I_1+C_1}$	$\mathbb{F}^{\mathcal{B}_1}$	$A_c^{I_2+C_2}$	$A_c^{\mathcal{B}_2}$	$\mathbb{F}^{I_2+C_2}$	$\mathbb{F}^{\mathcal{B}_2}$
No control	87084	340679	0.0	0.0	3617	16767	0.0	0.0
A	1958	4567	97.75	98.66	508	3933	85.96	76.54
B	6541	12887	92.45	96.22	3143	10817	13.11	35.49
C	1918	2525	97.80	99.23	493	2792	86.37	83.35

the disease burden, followed by strategy A and strategy B.

5 Conclusions

The novelty of this study is its ability to predict the optimal level of control interventions that include treatment and proper hygiene/ sanitation practices. On the basis of sensitivity analysis of a two-strain typhoid model incorporating symptomatic infection, asymptomatic carriers, and environmental bacteria, some control measures were suggested in [24]. Accordingly, the time-dependent functions representing the treatment of sensitive and resistant strains are considered as control measures. Proper hygiene and sanitation are also considered as another control measure to prevent contamination of food and water. The necessary and sufficient conditions for the existence of optimal controls are established and the optimality system is developed. The characterization of the optimal control is determined by the Pontryagin's maximum principle. The numerical simulations are performed for every single control and combination of the two controls. The simulation results reveal that with the combination of the two control interventions, the number of symptomatic individuals and doses of *S.* Typhi bacteria in both the strains reduced to near zero. However, there is still a significant number of asymptomatic carriers in both strains, which play an essential role in the evolution and transmission of typhoid infections. So, additional preventive measures need to be implemented in order to further reduce the population of asymptomatic carriers. The effects of each control strategy on

the reduction of infection in both the strains is investigated through efficiency analysis. From the study results, we conclude that the fight against a two-strain typhoid infection requires some control interventions that reduce the number of asymptomatic carriers to near zero, along with optimal treatment combined with sanitation and proper hygiene.

Acknowledgement

The first author is financially supported by Indian Council for Cultural Relations (ICCR) during his Ph.D. study. The authors are thankful to the anonymous reviewers for their valuable comments and suggestions, which helped us to improve the quality of our original manuscript.

References

[1] Vos T, Abajobir AA, Abate KH, Abbafati C, Abbas KM, Abd-Allah F, Abdulkader RS, Abdulle AM, Abebo TA, Abera SF, Aboyans V (2017) Global, regional, and national incidence, prevalence, and years lived with disability for 328 diseases and injuries for 195 countries, 1990–2016: a systematic analysis for the Global Burden of Disease Study 2016. The Lancet, 390(10100), 1211-1259.

[2] Dougan G, Baker S (2014) Salmonella enterica serovar Typhi and the pathogenesis of typhoid fever. Annual review of microbiology, 68, 317-336.

[3] Bhutta ZA (1996) Impact of age and drug resistance on mortality in typhoid fever. Archives of disease in childhood, 75(3), 214-217.

[4] Pieters Z, Saad NJ, Antillón M, Pitzer VE, Bilcke J (2018) Case fatality rate of enteric fever in endemic countries: a systematic review and meta-analysis. Clinical Infectious Diseases, 67(4), 628-638.

[5] Khan MI, Soofi SB, Ochiai RL, Khan MJ, Sahito SM, Habib MA, Puri MK, Von Seidlein L, Park JK, You YA, Ali M (2012) Epidemiology, clinical presentation, and patterns of drug resistance of Salmonella Typhi in Karachi, Pakistan. The Journal of Infection in Developing Countries, 6(10), 704-714.

[6] Antillón M, Warren JL, Crawford FW, Weinberger DM, Kürüm E, Pak GD, Marks F, Pitzer VE (2017) The burden of typhoid fever in low-and middle-income countries: a meta-regression approach. PLoS neglected tropical diseases, 11(2), e0005376.

[7] Baker S, Holt KE, Clements AC, Karkey A, Arjyal A, Boni MF, Dongol S, Hammond N, Koirala S, Duy PT, Nga TV (2011) Combined high-resolution genotyping and geospatial analysis reveals modes of endemic urban typhoid fever transmission. Open biology, 1(2), 110008.

[8] Browne AJ, Hamadani BH, Kumaran EA, Rao P, Longbottom J, Harriss E, Moore CE, Dunachie S, Basnyat B, Baker S, Lopez AD (2020) Drug-resistant enteric fever worldwide, 1990 to 2018: a systematic review and meta-analysis. BMC medicine, 18(1), 1-22.

[9] Crump JA, Mintz ED (2010) Global trends in typhoid and paratyphoid fever. Clinical infectious diseases, 50(2), 241-246.

[10] Parry CM, Threlfall EJ (2008) Antimicrobial resistance in typhoidal and nontyphoidal salmonellae. Current opinion in infectious diseases, 21(5), 531-538.

[11] Azmatullah A, Qamar FN, Thaver D, Zaidi AK, Bhutta ZA (2015) Systematic review of the global epidemiology, clinical and laboratory profile of enteric fever. Journal of global health, 5(2).

[12] Andrews JR, Vaidya K, Bern C, Tamrakar D, Wen S, Madhup S, Shrestha R, Karmacharya B, Amatya B, Koju R, Adhikari SR (2018) High rates of enteric fever diagnosis and lower burden of culture-confirmed disease in peri-urban and rural Nepal. The Journal of infectious diseases, 218(suppl˙4), S214-S221.

[13] John J, Van Aart CJ, Grassly NC (2016) The burden of typhoid and paratyphoid in India: systematic review and meta-analysis. PLoS neglected tropical diseases, 10(4), e0004616.

[14] Sehra D, Sehra S, Relia P, Sehra ST (2013) An altered drug resistance pattern in Salmonella typhi. American Journal of Infectious Diseases and Microbiology, 1(5), 84-85.

[15] Singh Y, Saxena A, Bohra J, Kumar R, Kumar A, Saxena MK (2019) Anti microbial resistance in salmonella, Journal of Basic & Applied Sciences, 15, 27–31.

[16] Mushayabasa S (2016) Modeling the impact of optimal screening on typhoid dynamics. International Journal of Dynamics and Control, 4(3), 330-338.

[17] Tilahun GT, Makinde OD, Malonza D (2017) Modelling and optimal control of typhoid fever disease with cost-effective strategies. Computational and mathematical methods in medicine, 2017.

[18] Kaufhold S, Yaesoubi R, Pitzer VE (2019) Predicting the impact of typhoid conjugate vaccines on antimicrobial resistance. Clinical Infectious Diseases, 68(Supplement˙2), S96-S104.

[19] Edward S, Nyerere N (2016) Modelling typhoid fever with education, vaccination and treatment. Eng. Math, 1(1), 44-52.

[20] Mushanyu J, Nyabadza F, Muchatibaya G, Mafuta P, Nhawu G (2018) Assessing the potential impact of limited public health resources on the spread and control of typhoid. Journal of mathematical biology, 77(3), 647-670.

[21] Nyaberi HO, Musaili JS (2021) Mathematical modeling of the impact of treatment on the dynamics of typhoid. Journal of the Egyptian Mathematical Society, 29(1), 1-11.

[22] Pitzer VE, Feasey NA, Msefula C, Mallewa J, Kennedy N, Dube Q, Denis B, Gordon MA, Heyderman RS (2015). Mathematical modeling to assess the drivers of the recent emergence of typhoid fever in Blantyre, Malawi. Clinical Infectious Diseases, 61(suppl˙4), S251-S258.

[23] Nthiiri JK, Lawi GO, Akinyi CO, Oganga DO, Muriuki WC, Musyoka MJ, Otieno PO, Koech L (2016) Mathematical modelling of typhoid fever disease incorporating protection against infection. Journal of Advances in Mathematics and Computer Science, 1-10.

[24] Irena TK, Gakkhar S (2021) Modelling the dynamics of antimicrobial-resistant typhoid infection with environmental transmission. Applied Mathematics and Computation, 401, 126081.

[25] Fleming WH, Rishel RW (2012) Deterministic and stochastic optimal control (Vol. 1). Springer Science & Business Media.

[26] Pontryagin LS (1987) Mathematical theory of optimal processes. CRC press.

[27] Lenhart S, Workman JT (2007) Optimal control applied to biological models. Chapman and Hall/CRC.

[28] Rodrigues HS, Monteiro MT, Torres DF (2014) Optimal control and numerical software: an overview. arXiv preprint arXiv:1401.7279.

[29] Carvalho SA, da Silva SO, da Cunha Charret I (2019) Mathematical modeling of dengue epidemic: control methods and vaccination strategies. Theory in Biosciences, 138(2), 223-239.

[30] Yang HM, Ferreira CP (2008) Assessing the effects of vector control on dengue transmission. Applied Mathematics and Computation, 198(1), 401-413.

Bicomplex Laplace Transform of Fractional Order, Properties and applications

Urvashi Purohit Sharma and Ritu Agarwal*

December 25, 2021

Abstract

The aim of this research article is to define bicomplex Laplace transform of fractional order or fractional Laplace transform by the application of the Mittag-Leffler function. Various properties of bicomplex fractional Laplace transform along with the convolution theorem have also been given. Inverse bicomplex fractional Laplace transform has also been defined. Application of bicomplex fractional Laplace transform in the solution of diffusion equation has been given.

Key words: Bicomplex numbers, Fractional derivative, fractional Laplace transform, Mittag-Leffler function.

Mathematics Subject Classification(2010): 30G35, 44A10, 33E12.

1 Introduction

In recent years, mathematicians and physicists have focused their efforts on bicomplex algebra. In 1882, Segre [25] introduced bicomplex numbers. Detailed study of bicomplex numbers are presented by Riley [20], Price [18], Rönn [24]. A bicomplex number is defined as an ordered pair of complex numbers, similar like how a complex number is defined as an ordered pair of real numbers.

In recent years, the fractional order differential equations with boundary conditions have gained more attention in a variety of scientific and engineering domains. The Mittag-Leffler function (see, e.g. [7, 10]) has an important contribution in the study of fractional calculus, it has been used to solve fractional order differential equations. The Mittag-Leffler function has caught the interest of a number of authors working in the field of fractional calculus (FC) and its applications such as, usage of a fractional operator involving Mittag–Leffler function for the generalized Casson fluid flow [29], to established the fractional calculus operators with Appell function kernels and Caputo-type fractional differential operators [16], Epidemiological analysis of fractional order COVID-19 model with Mittag-Leffler kernel [6]. In recent developments authors have worked on

*Corresponding author: Department of Mathematics, Malaviya National Institute of Technology, Jaipur-302017, INDIA, Email: ragarwal.maths@mnit.ac.in

the area of fractional calculus such as, to study a guava fruit model associated with a non-local additionally non-singular fractional derivative [27], the approximate solution of nonlinear Caudrey-Dodd-Gibbon equation of fractional order [28], analysis of fractional blood alcohol model [26].

Many authors have studied the applications of the fractional integral transform [9, 13, 14, 17, 23]. Efforts have been made by authors to introduce the Mittag-Leffler function (ML function) in bicomplex space along with applications to fractional calculus and integral transform [4, 5]. In 2011 bicomplex Laplace transform is introduced by Kumar et al. [15] and its convolution theorem and applications in bicomplex space are discussed by Agarwal et al. [1], bicomplex double Laplace transform is derived by Goswami et al. [8].

Following the path, efforts are made to extend the fractional Laplace transform in bicomplex space. Fractional Laplace transformation method is a effective and strong tool for finding a solution of the fractional differential equation. In this article bicomplex fractional Laplace transform and its properties in bicomplex space are introduced.

2 Preliminaries

2.1 Bicomplex Numbers

Definition 2.1 (Bicomplex Number)**.** A bicomplex number $\xi \in \mathbb{T}$ can be written as [25]

$$\xi = x_0 + i_1 x_1 + i_2 x_2 + j x_3, \text{ where } x_0,\ x_1,\ x_2,\ x_3 \in \mathbb{R}. \tag{2.1}$$

Here $\mathbb{T}$, $\mathbb{R}$ represents the set of bicomplex numbers and real numbers respectively.

We shall use the notations, $x_0 = \mathrm{Re}(\xi),\ x_1 = \mathrm{Im}_{i_1}(\xi),\ x_2 = \mathrm{Im}_{i_2}(\xi),\ x_3 = \mathrm{Im}_j(\xi)$.

Idempotent representation is particularly important since it allows for term-by-term addition, multiplication, and division.

Definition 2.2 (Idempotent Representation)**.** Every bicomplex number has following idempotent representation [18]

$$\xi = z_1 + i_2 z_2 = (z_1 - i_1 z_2)e_1 + (z_1 + i_1 z_2)e_2. \tag{2.2}$$

Hence if $\xi_1 = (z_1 - i_1 z_2)$ and $\xi_2 = (z_1 + i_1 z_2)$ then

$$\xi = \xi_1 e_1 + \xi_2 e_2, \tag{2.3}$$

where $e_1,\ e_2$ are idempotent elements in $\mathbb{T}$ such that $e_1 = \dfrac{1 + i_1 i_2}{2} = \dfrac{1 + j}{2}$, $e_2 = \dfrac{1 - i_1 i_2}{2} = \dfrac{1 - j}{2}$ and $e_1 + e_2 = 1,\ e_1.e_2 = 0$.

Projection Mappings

$P_1 : \mathbb{T} \to T_1 \subseteq \mathbb{C}$, $P_2 : \mathbb{T} \to T_2 \subseteq \mathbb{C}$ for a bicomplex number $\xi = z_1 + i_2 z_2$ are

given by (see, e.g. [2, 22]):

$$P_1(\xi) = P_1(z_1 + i_2 z_2) = (z_1 - i_1 z_2) \in T_1, \tag{2.4}$$

and

$$P_2(\xi) = P_2(z_1 + i_2 z_2)(z_1 + i_1 z_2) \in T_2, \tag{2.5}$$

where

$$T_1 = \{\xi_1 = z_1 - i_1 z_2 \,|z_1, z_2 \in \mathbb{C}\} \text{ and } T_2 = \{\xi_2 = z_1 + i_1 z_2 \,|z_1, z_2 \in \mathbb{C}\}. \tag{2.6}$$

2.2 Bicomplex One-Parameter Mittag-Leffler Function

The bicomplex one parameter ML function defined Agarwal et al. [5] is given by

$$\mathbb{E}_\alpha(\xi) = \sum_{n=0}^{\infty} \frac{\xi^n}{\Gamma(\alpha n + 1)}, \tag{2.7}$$

where $\xi, \alpha \in \mathbb{T},\ \xi = z_1 + i_2 z_2$ and $|\mathrm{Im_j}(\alpha)| < \mathrm{Re}(\alpha)$.

2.3 Modified Riemann- Liouville Derivative

Definition 2.3 (Modified Riemann-Liouville Derivative, [12])**.** Let $g : \mathbb{R} \to \mathbb{R},\ y \to g(y)$ represents a continuous function (not necessarily differentiable) function

1. If $g(y)$ is a constant M then its fractional derivative of order μ is given by

$${}^J D_y^\mu M = \begin{cases} \frac{M}{\Gamma(1-\mu) y^\mu} & if\ \mu \le 0, \\ 0 & if\ \mu > 0. \end{cases}$$

2. If $g(y)$ is not a constant then its fractional derivative of order μ is given by

$$\begin{aligned} {}^J D_y^\mu (g(y) - g(0)) &= \frac{1}{\Gamma(-\mu)} \int_0^y \frac{g(\zeta) d\zeta}{(y-\zeta)^{\mu+1}},\ \mu < 0, & (2.8) \\ {}^J D_y^\mu (g(y) - g(0)) &= {}^J D_y^\mu g(y) = {}^J D_y (g^{\mu-1}(y)),\ \mu > 0, & (2.9) \\ (g^\mu(y)) &= \left(g^{\mu-n}(y)\right)^{(n)},\ n \le \mu \le n+1,\ n \ge 1. & (2.10) \end{aligned}$$

2.4 Laplace Transform of Fractional Order

Let $g(x)$ denotes the function which vanishes for negative values of the variable x. Its Laplace transform (LT) of order α is defined by the expression (see, e.g. [13, 14, 19]), when it is finite,

$$L_\alpha(g(x)) = \int_0^\infty E_\alpha(-s^\alpha x^\alpha) g(x) (dx)^\alpha,\ 0 < \alpha < 1, \tag{2.11}$$

where $s \in \mathbb{C}$.
Sufficient condition for this integral to be finite is that (see, e.g.[13])

$$\int_0^\infty |g(x)|(dx)^\alpha < M < \infty. \tag{2.12}$$

If $g(u)$ is a continuous function, the integral with respect to $(du)^\alpha$ is defined as (see, e.g. [14]) the fractional differential equation's solution $y(u)$

$$dy = g(t)(du)^\alpha,\ x \geq 0,\ y(0) = 0, \tag{2.13}$$

where

$$y = \int_0^u g(v)(dv)^\alpha = \alpha \int_0^u \frac{g(v)}{(u-v)^{1-\alpha}} dv,\ 0 < \alpha < 1. \tag{2.14}$$

Jumarie [11] gave the the proof of the above result as follows:

$$x^{(\alpha)}(u) = g(u),\ 0 < \alpha \leq 1. \tag{2.15}$$

Its solution is obtained by fractional derivative as

$$x(u) = D^{-\alpha} g(u) = \frac{1}{\Gamma\alpha} \int_0^u (u-t)^{\alpha-1} g(t) dt. \tag{2.16}$$

Again

$$d^\alpha x = g(u)(du)^\alpha, \tag{2.17}$$

or

$$\Gamma(\alpha+1) dx = g(u)(du)^\alpha. \tag{2.18}$$

On integrating

$$x(u) = \frac{1}{\Gamma(\alpha+1)} \int_0^u g(t)(dt)^\alpha. \tag{2.19}$$

From equations (2.16) and (2.19), equation (2.14) can be obtained.

3 Bicomplex Laplace transform of Fractional order

In this section we introduce the bicomplex fractional Laplace transform with convergence conditions using the bicomplex ML function.

Definition 3.1 (Class $\mathcal{C}$)**.** Let $\mathcal{C}$ be the class of bicomplex-valued functions defined with the following properties, for any $f \in \mathcal{C}$

1. $f(x)$ vanishes for negative values of the variable x.
2. f is piecewise continuous in the interval $(0, a]$ for any $a \in (0, +\infty)$.

3. $\int_0^\infty |f(x)|_j (dx)^\alpha < M < \infty$.

Now we introduce the bicomplex Laplace transform of fractional order α as follows:
Let Laplace transform of order α of $f(t) \in \mathcal{C}$ for $t \geq 0$ can be written as

$$L_\alpha(f(t))_{s_1} = F_\alpha(s_1) = \int_0^\infty E_\alpha(-s_1^\alpha t^\alpha) f(t)(dt)^\alpha,\ 0 < \alpha < 1, \tag{3.1}$$

where $s_1 \in \mathbb{C}$ and take another LT of order α of $f(t) \in \mathcal{C}$ for $s_2 \in \mathbb{C}$

$$L_\alpha(f(t))_{s_2} = F_\alpha(s_2) = \int_0^\infty E_\alpha(-s_2^\alpha t^\alpha) f(t)(dt)^\alpha,\ 0 < \alpha < 1. \tag{3.2}$$

Now we take linear combination of $F_\alpha(s_1)$ and $F_\alpha(s_2)$ with e_1 and e_2 such as

$$\begin{aligned}
&L_\alpha(f(t))_{s_1} e_1 + L_\alpha(f(t))_{s_2} e_2 \\
&\quad = F_\alpha(s_1)e_1 + F_\alpha(s_2)e_2 \\
&\quad = \int_0^\infty E_\alpha(-s_1^\alpha t^\alpha) f(t)(dt)^\alpha e_1 + \int_0^\infty E_\alpha(-s_2^\alpha t^\alpha) f(t)(dt)^\alpha e_2 \\
&\quad = \int_0^\infty \left(E_\alpha(-s_1^\alpha t^\alpha)e_1 + E_\alpha(-s_2^\alpha t^\alpha)e_2\right) f(t)(dt)^\alpha \\
&\quad = \int_0^\infty E_\alpha(-\xi^\alpha t^\alpha) f(t)(dt)^\alpha \\
&\quad = F_\alpha(\xi) \\
&\quad = L_\alpha(f(t))_\xi,
\end{aligned} \tag{3.3}$$

where $\xi = s_1 e_1 + s_2 e_2 \in \mathbb{T}$.
Since $F_\alpha(s_1)$ and $F_\alpha(s_2)$ are complex valued functions which are convergent and analytic for respectively, so by application of decomposition theorem of Ringleb [21], (see, e.g. [20]) bicomplex valued function $F_\alpha(\xi) = F_\alpha(s_1)e_1 + F_\alpha(s_2)e_2$ will be convergent and analytic.

Definition 3.2 (Bicomplex Laplace Transform of Fractional Order)**.** Let $g(t) \in \mathcal{C}$ be a bicomplex valued function. Then bicomplex Laplace transform of fractional order α of $g(t)$ for $t \geq 0$ can be defined as

$$L_\alpha(g(t))_\xi = G_\alpha(\xi) = \int_0^\infty E_\alpha(-\xi^\alpha t^\alpha) g(t)(dt)^\alpha = \lim_{\mathcal{M}\to\infty} \int_0^{\mathcal{M}} E_\alpha(-\xi^\alpha t^\alpha) g(t)(dt)^\alpha, \tag{3.4}$$

where $0 < \alpha < 1,\ \xi = s_1 e_1 + s_2 e_2 \in \mathbb{T},\ s_1,\ s_2 \in \mathbb{C}$.

3.1 Some Basic Properties of Bicomplex Fractional Laplace Transform

Theorem 3.3 (Linearity Property)**.** *Let $F_\alpha(\xi)$ and $G_\alpha(\xi)$ be the bicomplex fractional Laplace transform of order α of class $\mathcal{C}$ functions $f(t)$ and $g(t)$ respectively, then*

$$L_\alpha\left(f(t)+g(t)\right)=F_\alpha(\xi)+G_\alpha(\xi). \tag{3.5}$$

Proof. Let $\xi=s_1e_1+s_2e_2\in\mathbb{T},\ s_1,\ s_2\in\mathbb{C}$ and $0<\alpha<1$ then

$$\begin{aligned}
L_\alpha\left(f(t)+g(t)\right)&=\int_0^\infty E_\alpha(-\xi^\alpha t^\alpha)\left(f(t)+g(t)\right)(dt)^\alpha\\
&=\int_0^\infty E_\alpha(-s_1^\alpha t^\alpha)\left(f_1(t)+g_1(t)\right)(dt)^\alpha e_1\\
&\quad+\int_0^\infty E_\alpha(-s_2^\alpha t^\alpha)\left(f_2(t)+g_2(t)\right)(dt)^\alpha e_2\\
&=\int_0^\infty E_\alpha(-s_1^\alpha t^\alpha)f_1(t)(dt)^\alpha e_1+\int_0^\infty E_\alpha(-s_1^\alpha t^\alpha)g_1(t)(dt)^\alpha e_1\\
&\quad+\int_0^\infty E_\alpha(-s_2^\alpha t^\alpha)f_2(t)(dt)^\alpha e_2+\int_0^\infty E_\alpha(-s_2^\alpha t^\alpha)g_2(t)(dt)^\alpha e_2\\
&=\int_0^\infty E_\alpha(-\xi^\alpha t^\alpha)f(t)(dt)^\alpha+\int_0^\infty E_\alpha(-\xi^\alpha t^\alpha)g(t)(dt)^\alpha\\
&=L_\alpha\left(f(t)\right)+L_\alpha\left(g(t)\right)\\
&=F_\alpha(\xi)+G_\alpha(\xi).
\end{aligned} \tag{3.6}$$

□

Theorem 3.4. *Let $F_\alpha(\xi)$ be the bicomplex fractional Laplace transform of order α of function $f(t)\in\mathcal{C}$ and $\xi=s_1e_1+s_2e_2\in\mathbb{T},\ s_1,\ s_2\in\mathbb{C},\ 0<\alpha<1$ and k is a constant then*

$$L_\alpha\left(kf(t)\right)=kF_\alpha(\xi). \tag{3.7}$$

Proof. Let $\xi=s_1e_1+s_2e_2\in\mathbb{T},\ s_1,\ s_2\in\mathbb{C}$ and $0<\alpha<1$, then

$$\begin{aligned}
L_\alpha\left(kf(t)\right)&=\int_0^\infty E_\alpha(-\xi^\alpha t^\alpha)\left(kf(t)\right)(dt)^\alpha\\
&=\int_0^\infty E_\alpha(-s_1^\alpha t^\alpha)\left(kf_1(t)\right)(dt)^\alpha e_1+\int_0^\infty E_\alpha(-s_2^\alpha t^\alpha)\left(kf_2(t)\right)(dt)^\alpha e_2\\
&=k\int_0^\infty E_\alpha(-s_1^\alpha t^\alpha)f_1(t)(dt)^\alpha e_1+k\int_0^\infty E_\alpha(-s_2^\alpha t^\alpha)f_2(t)(dt)^\alpha e_2\\
&=k\int_0^\infty E_\alpha(-\xi^\alpha t^\alpha)f(t)(dt)^\alpha\\
&=kL_\alpha\left(f(t)\right)\\
&=kF_\alpha(\xi).
\end{aligned} \tag{3.8}$$

□

Theorem 3.5 (Bicomplex Fractional Laplace Transform of Derivatives)**.** *Let $F_\alpha(\xi)$ be the bicomplex fractional LT of order α of function $f(t) \in \mathcal{C}$ and $\xi = s_1e_1 + s_2e_2 \in \mathbb{T},\ 0 < \alpha < 1$ then*

$$L_\alpha\left({}^JD^\alpha f(t)\right) = \xi^\alpha F_\alpha(\xi) - f(0), \tag{3.9}$$

where ${}^JD^\alpha$ is defined in the definition (2.3).

Proof. Let $\xi = s_1e_1 + s_2e_2 \in \mathbb{T}$ and $0 < \alpha < 1$ then

$$\begin{aligned} L_\alpha\left({}^JD^\alpha f(t)\right) &= \int_0^\infty E_\alpha(-\xi^\alpha t^\alpha)\left(D^\alpha f(t)\right)(dt)^\alpha \\ &= \left[f(t)E_\alpha(-\xi^\alpha t^\alpha)\right]_0^\infty - \int_0^\infty f(t)\left(-\xi^\alpha E_\alpha(-\xi^\alpha t^\alpha)\right)(dt)^\alpha \\ &= -f(0) + \xi^\alpha \int_0^\infty f(t)E_\alpha(-\xi^\alpha t^\alpha)(dt)^\alpha \\ &= \xi^\alpha L_\alpha\left(f(t)\right) - f(0) \\ &= \xi^\alpha F_\alpha(\xi) - f(0). \end{aligned} \tag{3.10}$$

□

Corollary 3.6. *Let $F_\alpha(\xi)$ be the bicomplex fractional LT of order α of function $f(t) \in \mathcal{C}$ and $\xi = s_1e_1 + s_2e_2 \in \mathbb{T},\ 0 < \alpha < 1$ then*

$$L_\alpha\left({}^JD^{2\alpha} f(t)\right) = \xi^{2\alpha}F_\alpha(\xi) - \xi^\alpha f(0) - f^\alpha(0), \tag{3.11}$$

where ${}^JD^{2\alpha}$ is defined in the definition (2.3).

Proof. Let $\xi = s_1e_1 + s_2e_2 \in \mathbb{T},\ 0 < \alpha < 1$ and $D^\alpha f(t) = F(t)$ then

$$\begin{aligned} L_\alpha\left({}^JD^{2\alpha} f(t)\right) &= L_\alpha\left({}^JD^\alpha F(t)\right) \\ &= \xi^\alpha L_\alpha\left(F(t)\right) - F(0) \\ &= \xi^\alpha L_\alpha\left({}^JD^\alpha f(t))\right) - f^\alpha(0) \\ &= \xi^\alpha\left(\xi^\alpha L_\alpha\left(f(t)\right) - f(0))\right) - f^\alpha(0) \\ &= \xi^{2\alpha}L_\alpha\left(f(t)\right) - \xi^\alpha f(0) - f^\alpha(0) \\ &= \xi^{2\alpha}F_\alpha(\xi) - \xi^\alpha f(0) - f^\alpha(0). \end{aligned} \tag{3.12}$$

□

Proceeding in similar manner, we obtain the result contained in the following corollary:

Corollary 3.7. *Let $F_\alpha(\xi)$ be the bicomplex fractional LT of order α of function $f(t) \in \mathcal{C}$ and $\xi = s_1e_1 + s_2e_2 \in \mathbb{T},\ 0 < \alpha < 1$ then*

$$\begin{aligned} &L_\alpha\left({}^JD^{n\alpha} f(t)\right) \\ &= \xi^{n\alpha}F_\alpha(\xi) - \left(\xi^{n\alpha-\alpha}f(0) + \xi^{n\alpha-2\alpha}f^\alpha(0) + \xi^{n\alpha-3\alpha}f^{2\alpha}(0) + \cdots + f^{n\alpha-\alpha}(0)\right), \end{aligned} \tag{3.13}$$

where ${}^JD^{n\alpha}$ is defined in the definition (2.3).

Theorem 3.8 (Change of Scale Property)**.** *Let $F_\alpha(\xi)$ be the bicomplex fractional Laplace transform of order α of function $f(t) \in \mathcal{C}$ and $\xi = s_1e_1 + s_2e_2 \in \mathbb{T},\ s_1,\ s_2 \in \mathbb{C},\ a > 0$ and $0 < \alpha < 1$ then*

$$L_\alpha(f(at)) = (1/a)^\alpha F_\alpha\left(\frac{\xi}{a}\right). \tag{3.14}$$

Proof. Let $\xi = s_1e_1 + s_2e_2 \in \mathbb{T},\ s_1,\ s_2 \in \mathbb{C}$ and $0 < \alpha < 1$ then from equations (3.4) and (2.14) we have

$$\begin{aligned}
L_\alpha(f(at)) &= \int_0^\infty E_\alpha(-\xi^\alpha t^\alpha) f(at)(dt)^\alpha \\
&= \lim_{\mathcal{M}\to\infty} \int_0^{\mathcal{M}} E_\alpha(-\xi^\alpha t^\alpha) f(at)(dt)^\alpha \\
&= \lim_{\mathcal{M}\to\infty} \alpha \int_0^{\mathcal{M}} (\mathcal{M}-t)^{\alpha-1} E_\alpha(-\xi^\alpha t^\alpha) f(at)(dt) \\
&= \lim_{\mathcal{M}\to\infty} \alpha \int_0^{\mathcal{M}} (\mathcal{M}-t)^{\alpha-1} E_\alpha(-s_1^\alpha t^\alpha) f_1(at)(dt)e_1 \\
&\quad + \lim_{\mathcal{M}\to\infty} \alpha \int_0^{\mathcal{M}} (\mathcal{M}-t)^{\alpha-1} E_\alpha(-s_2^\alpha t^\alpha) f_2(at)(dt)e_2,
\end{aligned} \tag{3.15}$$

putting $at = x \Longrightarrow dt = \frac{dx}{a},\ a > 0,$

$$\begin{aligned}
L_\alpha(f(at)) &= \lim_{\mathcal{M}\to\infty} \alpha \int_0^{a\mathcal{M}} \left(\mathcal{M} - \frac{x}{a}\right)^{\alpha-1} E_\alpha\left(-s_1^\alpha \frac{x^\alpha}{a^\alpha}\right) f_1(x)\frac{dx}{a}e_1 \\
&\quad + \lim_{\mathcal{M}\to\infty} \alpha \int_0^{a\mathcal{M}} \left(\mathcal{M} - \frac{x}{a}\right)^{\alpha-1} E_\alpha\left(-s_2^\alpha \frac{x^\alpha}{a^\alpha}\right) f_2(x)\frac{dx}{a}e_2 \\
&= \lim_{\mathcal{M}\to\infty} \alpha \int_0^{a\mathcal{M}} \frac{(a\mathcal{M}-x)^{\alpha-1}}{a^{\alpha-1}} E_\alpha\left(-s_1^\alpha \frac{x^\alpha}{a^\alpha}\right) f_1(x)\frac{dx}{a}e_1 \\
&\quad + \lim_{\mathcal{M}\to\infty} \alpha \int_0^{a\mathcal{M}} \frac{(a\mathcal{M}-x)^{\alpha-1}}{a^{\alpha-1}} E_\alpha\left(-s_2^\alpha \frac{x^\alpha}{a^\alpha}\right) f_2(x)\frac{dx}{a}e_1 \\
&= (1/a)^\alpha F_\alpha\left(\frac{\xi_1}{a}\right)e_1 + (1/a)^\alpha F_\alpha\left(\frac{\xi_2}{a}\right)e_2 \\
&= (1/a)^\alpha F_\alpha\left(\frac{\xi}{a}\right).
\end{aligned} \tag{3.16}$$

□

Theorem 3.9 (Shifting Property)**.** *Let $F_\alpha(\xi)$ be the bicomplex fractional Laplace transform of order α of $f(t) \in \mathcal{C}$ and $\xi = s_1e_1 + s_2e_2 \in \mathbb{T},\ s_1,\ s_2 \in \mathbb{C},\ c > 0$ and $0 < \alpha < 1$ then*

$$L_\alpha(f(t-c)) = E_\alpha(\xi^\alpha c^\alpha) F_\alpha(\xi). \tag{3.17}$$

Proof. Let $\xi = s_1e_1 + s_2e_2 \in \mathbb{T},\ s_1,\ s_2 \in \mathbb{C}$ and $0 < \alpha < 1$ then from equations (3.4) and (2.14) we have

$$\begin{aligned} L_\alpha(f(t-c)) &= \int_0^\infty E_\alpha(-\xi^\alpha t^\alpha) f(t-c)(dt)^\alpha \\ &= \lim_{\mathcal{M}\to\infty} \int_0^{\mathcal{M}} E_\alpha(-\xi^\alpha t^\alpha) f(t-c)(dt)^\alpha \\ &= \lim_{\mathcal{M}\to\infty} \alpha \int_0^{\mathcal{M}} (\mathcal{M}-t)^{\alpha-1} E_\alpha(-\xi^\alpha t^\alpha) f(t-c)(dt) \qquad (3.18) \\ &= \lim_{\mathcal{M}\to\infty} \alpha \int_0^{\mathcal{M}} (\mathcal{M}-t)^{\alpha-1} E_\alpha(-s_1^\alpha t^\alpha) f_1(t-c)(dt)e_1 \\ &\quad + \lim_{\mathcal{M}\to\infty} \alpha \int_0^{\mathcal{M}} (\mathcal{M}-t)^{\alpha-1} E_\alpha(-s_2^\alpha t^\alpha) f_2(t-c)(dt)e_2. \end{aligned}$$

Putting $t - c = x \Longrightarrow dt = dx$

$$\begin{aligned} &= \lim_{\mathcal{M}\to\infty} \alpha \int_0^{\mathcal{M}-c} (\mathcal{M}-x-c)^{\alpha-1} E_\alpha(-s_1^\alpha (x+c)^\alpha) f_1(x)(dx)e_1 \\ &\quad + \lim_{\mathcal{M}\to\infty} \alpha \int_0^{\mathcal{M}-c} (\mathcal{M}-x-c)^{\alpha-1} E_\alpha(-s_2^\alpha (x+c)^\alpha) f_2(x)(dx)e_2 \\ &= E_\alpha(-s_1^\alpha c^\alpha) \lim_{\mathcal{M}\to\infty} \alpha \int_0^{\mathcal{M}-c} (\mathcal{M}-x-c)^{\alpha-1} E_\alpha(-s_1^\alpha x^\alpha) f_1(x)(dx)e_1 \qquad (3.19) \\ &\quad + E_\alpha(-s_2^\alpha c^\alpha) \lim_{\mathcal{M}\to\infty} \alpha \int_0^{\mathcal{M}-c} (\mathcal{M}-x-c)^{\alpha-1} E_\alpha(-s_2^\alpha x^\alpha) f_2(x)(dx)e_2 \\ &= E_\alpha(\xi^\alpha c^\alpha) L_\alpha(f(t)) \\ &= E_\alpha(\xi^\alpha c^\alpha) F_\alpha(\xi). \end{aligned}$$

□

Theorem 3.10 (Bicomplex Fractional Laplace Transform of Integrals)**.** *Let $F_\alpha(\xi)$ be the bicomplex fractional Laplace transform of order α of $f(t) \in \mathcal{C}$ and $\xi = s_1e_1 + s_2e_2 \in \mathbb{T},\ 0 < \alpha < 1$ then*

$$L_\alpha\left(\int_0^t f(v)(dv)^\alpha\right) = \frac{1}{\xi^\alpha \Gamma(1+\alpha)} L_\alpha(f(t)). \qquad (3.20)$$

Proof. Since

$${}^J D_t^\alpha \int_0^t f(v)(dv)^\alpha = \alpha!\, f(t), \qquad (3.21)$$

by using equation (3.9)

$$\begin{aligned} L_\alpha\left({}^J D_t^\alpha \int_0^t f(v)(dv)^\alpha\right) &= \xi^\alpha L_\alpha\left(\int_0^t f(v)(dv)^\alpha\right), \\ L_\alpha\left(\alpha!\, f(t)\right) &= \xi^\alpha L_\alpha\left(\int_0^t f(v)(dv)^\alpha\right). \end{aligned} \qquad (3.22)$$

Hence,

$$L_\alpha\left(\int_0^t f(v)(dv)^\alpha\right) = \Gamma(\alpha+1)\xi^{-\alpha}L_\alpha\left(f(t)\right). \tag{3.23}$$

□

Theorem 3.11. *Let* $\xi = s_1e_1 + s_2e_2 \in \mathbb{T},\ s_1,\ s_2 \in \mathbb{C}$ *and* $0 < \alpha < 1$ *then*

(i) $L_\alpha(t^\alpha f(t)) = -{}^J D_\xi^\alpha L_\alpha(f(t))$,

(ii) $L_\alpha(E_\alpha(-c^\alpha t^\alpha)f(t))_\xi = F_\alpha(\xi + c)$,

(iii) $L_\alpha(-t^\alpha f(t)) = {}^J D_\xi^\alpha L_\alpha(f(t))$.

Proof. (i) Let $\xi = s_1e_1 + s_2e_2 \in \mathbb{T},\ s_1,\ s_2 \in \mathbb{C}$ and $0 < \alpha < 1$ then from equation (3.4) we have

$$\begin{aligned}
&L_\alpha(t^\alpha f(t)) \\
&= \int_0^\infty E_\alpha(-\xi^\alpha t^\alpha)t^\alpha f(t)(dt)^\alpha \\
&= \int_0^\infty E_\alpha(-s_1^\alpha t^\alpha)t^\alpha f_1(t)(dt)^\alpha e_1 + \int_0^\infty E_\alpha(-s_2^\alpha t^\alpha)t^\alpha f_2(t)(dt)^\alpha e_2 \\
&= -\ {}^J D_{s_1}^\alpha \int_0^\infty E_\alpha(-s_1^\alpha t^\alpha)f_1(t)(dt)^\alpha e_1 - \ {}^J D_{s_2}^\alpha \int_0^\infty E_\alpha(-s_2^\alpha t^\alpha)f_2(t)(dt)^\alpha e_2 \\
&= -\ {}^J D_\xi^\alpha L_\alpha(f(t)).
\end{aligned} \tag{3.24}$$

(ii) Let $\xi = s_1e_1 + s_2e_2 \in \mathbb{T},\ s_1,\ s_2 \in \mathbb{C}$ and $0 < \alpha < 1$ then from equation (3.4) we have

$$\begin{aligned}
L_\alpha(E_\alpha(-c^\alpha t^\alpha)f(t))_\xi &= \int_0^\infty E_\alpha(-\xi^\alpha t^\alpha)E_\alpha(-c^\alpha t^\alpha)f(t)(dt)^\alpha \\
&= \int_0^\infty E_\alpha(-(\xi+c)^\alpha t^\alpha)f(t)(dt)^\alpha \\
&= F_\alpha(\xi + c).
\end{aligned} \tag{3.25}$$

(iii) Let $\xi = s_1e_1 + s_2e_2 \in \mathbb{T},\ s_1,\ s_2 \in \mathbb{C}$ and $0 < \alpha < 1$ then from equation (3.4) we have

$$\begin{aligned}
&L_\alpha(-t^\alpha f(t)) \\
&= \int_0^\infty E_\alpha(-\xi^\alpha(-t)^\alpha)t^\alpha f(t)(dt)^\alpha \\
&= \int_0^\infty E_\alpha(-s_1^\alpha t^\alpha)t^\alpha f_1(t)(dt)^\alpha e_1 + \int_0^\infty E_\alpha(-s_2^\alpha t^\alpha)t^\alpha f_2(t)(dt)^\alpha e_2 \\
&= -\ {}^J D_{s_1}^\alpha \int_0^\infty E_\alpha(-s_1^\alpha t^\alpha)f_1(t)(dt)^\alpha e_1 - \ {}^J D_{s_2}^\alpha \int_0^\infty E_\alpha(-s_2^\alpha t^\alpha)f_2(t)(dt)^\alpha e_2 \\
&= -\ {}^J D_\alpha^\xi L_\alpha(f(t)).
\end{aligned} \tag{3.26}$$

□

3.2 Convolution Theorem

Convolution is a mathematical operation on two functions $f,\ g.$ which is useful in signal theory, image processing. Convolution of order μ of the functions $f(t),\ g(t)$ defined by Jumarie [14] given by

$$(f * g)(t) = \int_0^t f(t-v)g(v)(dv)^{\mu}. \tag{3.27}$$

Theorem 3.12. *Let $f,\ g \in \mathcal{C}$ and Let $F_\alpha(\xi)$ and $G_\alpha(\xi)$ be the bicomplex fractional Laplace transform of order α of functions $f(t)$ and $g(t)$ respectively, then*

$$L_\alpha\left(f * g\right)(t) = F_\alpha(\xi)G_\alpha(\xi) = L_\alpha\left(f(t)\right)L_\alpha\left(g(t)\right). \tag{3.28}$$

Proof.

$$\begin{aligned}
L_\alpha\left(f(t) * g(t)\right) &= \int_0^\infty (dt)^\alpha E_\alpha(-\xi^\alpha t^\alpha)\int_0^t f(t-v)g(v)(dv)^\alpha \\
&= \int_0^\infty (dt)^\alpha E_\alpha(-(s_1e_1+s_2e_2)^\alpha t^\alpha)\int_0^t f(t-v)g(v)(dv)^\alpha \\
&= \left(\int_0^\infty (dt)^\alpha E_\alpha(-s_1^\alpha t^\alpha)\int_0^t f(t-v)g(v)(dv)^\alpha\right)e_1 \\
&\quad + \left(\int_0^\infty (dt)^\alpha E_\alpha(-s_2^\alpha t^\alpha)\int_0^t f(t-v)g(v)(dv)^\alpha\right)e_2 \\
&= \left(\int_0^\infty (dt)^\alpha E_\alpha(-s_1^\alpha (t-v)^\alpha)E_\alpha(-s_1^\alpha v^\alpha)\int_0^t f(t-v)g(v)(dv)^\alpha\right)e_1 \\
&\quad + \left(\int_0^\infty (dt)^\alpha E_\alpha(-s_2^\alpha (t-v)^\alpha)E_\alpha(-s_2^\alpha v^\alpha)\int_0^t f(t-v)g(v)(dv)^\alpha\right)e_2.
\end{aligned} \tag{3.29}$$

Put $p = t-v,\ q = v$, to obtain

$$\begin{aligned}
L_\alpha\left(f(t) * g(t)\right) &= \left(\int_0^\infty\int_0^\infty (dp)^\alpha E_\alpha(-s_1^\alpha p^\alpha)E_\alpha(-s_1^\alpha q^\alpha)f(p)g(q)(dq)^\alpha\right)e_1 \\
&\quad + \left(\int_0^\infty\int_0^\infty (dp)^\alpha E_\alpha(-s_2^\alpha p^\alpha)E_\alpha(-s_2^\alpha q^\alpha)f(p)g(q)(dq)^\alpha\right)e_2 \\
&= \left(\int_0^\infty\int_0^\infty E_\alpha(-s_1^\alpha p^\alpha)E_\alpha(-s_1^\alpha q^\alpha)f(p)g(q)(dp)^\alpha(dq)^\alpha\right)e_1 \\
&\quad + \left(\int_0^\infty\int_0^\infty E_\alpha(-s_2^\alpha p^\alpha)E_\alpha(-s_2^\alpha q^\alpha)f(p)g(q)(dp)^\alpha(dq)^\alpha\right)e_2
\end{aligned} \tag{3.30}$$

Hence,

$$\begin{aligned} L_\alpha\left(f(t) * g(t)\right) &= \left(F_\alpha(s_1)G_\alpha(s_1)\right)e_1 + \left(F_\alpha(s_2)G_\alpha(s_2)\right)e_2 \\ &= F_\alpha(\xi)G_\alpha(\xi) \\ &= L_\alpha(f(t))L_\alpha(g(t)). \end{aligned} \tag{3.31}$$

□

4 Bicomplex Fractional Inverse Laplace Transform

Definition 4.1. Generalized Dirac's function $\delta_\alpha(x)$ of fractional order $\alpha,\ 0 < \alpha < 1$ is given by (see, e.g. [14])

$$\int_{\mathbb{R}} f(x)\delta_\alpha(x)(dx)^\alpha = \alpha f(0). \tag{4.1}$$

The relation between Dirac's function and ML function is given by (see, e.g. [14]) the following result

$$\frac{\alpha}{(M_\alpha)^\alpha}\int_{-i_1\infty}^{+i_1\infty} E_\alpha(i_1(-\omega x)^\alpha)(d\omega)^\alpha = \delta_\alpha(x), \tag{4.2}$$

where M_α is the period of the complex-valued ML function defined by the relation $E_\alpha(i_1(M_\alpha)^\alpha) = 1$.

Theorem 4.2. *Let $F_\alpha(\xi)$ be the bicomplex fractional Laplace transform of order α of function $f(t) \in \mathcal{C}$ and $\xi = s_1e_1 + s_2e_2 \in \mathbb{T}$ and $0 < \alpha < 1$ then*

$$f(t) = \frac{1}{(M_\alpha)^\alpha}\int_H E_\alpha(\xi^\alpha x^\alpha)F_\alpha(\xi)(d\xi)^\alpha, \tag{4.3}$$

where H is closed contour in $\mathbb{T}$.

Proof. Let $F_\alpha(\xi)$ be the bicomplex fractional Laplace transform of bicomplex-valued function $f(t)$. Then $F_\alpha(\xi) = F_\alpha(s_1)e_1 + F_\alpha(s_2)e_2$. The inverse formula for complex fractional Laplace transform (see, e.g. [14]) are

$$\begin{aligned} f_1(t) &= \frac{1}{(M_\alpha)^\alpha}\int_{-i_1\infty}^{+i_1\infty} E_\alpha(s_1^\alpha x^\alpha)F_\alpha(s_1)(ds_1)^\alpha \\ &= \frac{1}{(M_\alpha)^\alpha}\int_{\gamma_1} E_\alpha(s_1^\alpha x^\alpha)F_\alpha(s_1)(ds_1)^\alpha, \end{aligned} \tag{4.4}$$

and

$$\begin{aligned} f_2(t) &= \frac{1}{(M_\alpha)^\alpha}\int_{-i_1\infty}^{+i_1\infty} E_\alpha(s_2^\alpha x^\alpha)F_\alpha(s_2)(ds_2)^\alpha \\ &= \frac{1}{(M_\alpha)^\alpha}\int_{\gamma_2} E_\alpha(s_2^\alpha x^\alpha)F_\alpha(s_2)(ds_2)^\alpha, \end{aligned} \tag{4.5}$$

where M_α is the period of the complex-valued ML function defined by the relation $E_\alpha(i_1(M_\alpha)^\alpha) = 1$ and γ_1 and γ_2 be closed contours taken along the the vertical lines as follows $\gamma_1 = -i_1\infty$ to $i_1\infty$,$\gamma_2 = -i_1\infty$ to $i_1\infty$.

Now, using complex inversions (4.4) and (4.5), we get

$$\begin{aligned} f(t) &= f_1(t)e_1 + f_2(t)e_2 \\ &= \frac{1}{(M_\alpha)^\alpha}\left(\int_{\gamma_1} E_\alpha(s_1^\alpha x^\alpha)F_\alpha(s_1)(ds_1)^\alpha\ e_1 + \int_{\gamma_2} E_\alpha(s_2^\alpha x^\alpha)F_\alpha(s_2)(ds_2)^\alpha\ e_2\right) \\ &= \frac{1}{(M_\alpha)^\alpha}\int_{(\gamma_1,\gamma_2)} E_\alpha((s_1e_1+s_2e_2)^\alpha x^\alpha)F_\alpha(s_1e_1+s_2e_2)\left((ds_1)^\alpha e_1 + (ds_2)^\alpha e_2\right) \\ &= \frac{1}{(M_\alpha)^\alpha}\int_H E_\alpha(\xi^\alpha x^\alpha)F_\alpha(\xi)(d\xi)^\alpha, \end{aligned} \tag{4.6}$$

where $H = (\gamma_1, \gamma_2)$ and

$$\xi = s_1e_1 + s_2e_2 \Rightarrow d\xi = ds_1e_1 + ds_2e_2 \Rightarrow (d\xi)^\alpha = (ds_1)^\alpha e_1 + (ds_2)^\alpha e_2. \tag{4.7}$$

□

5 Application of Bicomplex Fractional Laplace Transform

Agarwal et al.[3] discussed fractional differential equations in bicomplex space. Bicomplex fractional Laplace transform has great advantage in finding the solution of fractional order differential equations. We have solved the following homogeneous fractional order differential equations using bicomplex fractional Laplace transform.

$$(D^{2\alpha} + 2D^\alpha + 2)y(t) = 0, \tag{5.1}$$

where $y(0) = 1$ and $y^\alpha(0) = -1$.
By taking bicomplex fractional LT on both sides of order α, we get

$$L_\alpha\left(y^{2\alpha} + 2y^\alpha + 2y\right) = 0, \tag{5.2}$$

$$s^{2\alpha}L_\alpha(y(t)) - s^\alpha y(0) - y^\alpha(0) + 2\left(s^\alpha L_\alpha y(t) - y(0)\right) + 2L_\alpha y(t) = 0, \tag{5.3}$$

$$\left(s^{2\alpha} + 2s^\alpha + 2\right)L_\alpha y(t) = s^\alpha + 1, \tag{5.4}$$

$$\Rightarrow \quad L_\alpha y(t) = \frac{s^\alpha + 1}{\left(s^\alpha + 1\right)^2 + 1}. \tag{5.5}$$

Hence,

$$L_\alpha y(t) = L_\alpha\left(\mathbb{E}_\alpha(-t^\alpha)\cos_\alpha(t^\alpha)\right). \tag{5.6}$$

Therefore

$$y(t) = \mathbb{E}_\alpha(-t^\alpha)\cos_\alpha(t^\alpha), \tag{5.7}$$

where $\cos_\alpha(t^\alpha)$ is fractional order cosine function (see, e.g. [13, 19]).

5.1 Application to Diffusion equation

Consider the following partial fractional differential equation

$$D_t^{\alpha} u(x,t) = cD_x^{\beta} u(x,t),\ 0 < \alpha, \beta < 1, \tag{5.8}$$

with initial condition $u(x,t) = f(x)$. It is very simple case of diffusion equation (see, e. g. [13]).
By taking bicomplex fractional LT of the equation (5.8) with respect to t,

$$s^{\alpha}\bar{u}(x,s) - f(x) = cD_x^{\beta}\bar{u}(x,s). \tag{5.9}$$

Taking fractional Fourier transform of equation (5.9) defined by Jumarie [13] with respect to x,

$$s^{\alpha}\hat{\bar{u}}(\zeta,s) - \hat{f}(\zeta) = c(-i_1\zeta^{\beta})\hat{\bar{u}}(\zeta,s), \tag{5.10}$$

or

$$(s^{\alpha} + i_1 c\zeta^{\beta})\hat{\bar{u}}(\zeta,s) = \hat{f}(\zeta), \tag{5.11}$$

$$\hat{\bar{u}}(\zeta,s) = \frac{\hat{f}(\zeta)}{(s^{\alpha} + i_1 c\zeta^{\beta})}. \tag{5.12}$$

By taking inverse Bicomplex fractional Laplace transform

$$\hat{u}(\zeta,t) = \hat{f}(\zeta)E_{\alpha}(-i_1 c\zeta^{\beta}t^{\alpha}), \qquad \text{(From [19, Property 3.4])}. \tag{5.13}$$

Finally by taking Inverse Fractional Fourier transform defined by Jumarie [13] of the equation (5.13)

$$u(x,t) = \frac{1}{(M_{\beta})^{\beta}} \int_{-\infty}^{+\infty} E_{\beta}(i_1\zeta^{\beta}x^{\beta})\ E_{\alpha}(-i_1 c\zeta^{\beta}t^{\alpha})\ \hat{f}(\zeta)\ (d\zeta)^{\alpha}. \tag{5.14}$$

6 Conclusion

In this paper, the Laplace transform of fractional order or fractional Laplace transform in bicomplex space, the extension of complex Laplace transform of fractional order has been derived. Various properties along with the convolution theorem have also been derived. Bicomplex fractional Laplace transform may be used in finding the solution of bicomplex fractional Schrödinger equation.

References

[1] Agarwal, R., Goswami, M. P., and Agarwal, R. P. (2014). Convolution theorem and applications of bicomplex Laplace transform. *Advances in Mathematical Sciences and Applications*, 24(1):113–127.

[2] Agarwal, R., Goswami, M. P., and Agarwal, R. P. (2017a). Mellin transform in bicomplex space and its applications. *Studia Universitatis Babes-Bolyai Mathematica*, 62(2):217–232.

[3] Agarwal, R., Goswami, M. P., and Agarwal, R. P. (2017b). A study of Mellin transform of fractional operators in bicomplex space and applications. *Journal of Fractional Calculus and Applications*, 8(2):211–226.

[4] Agarwal, R. and Sharma, U. P. (2020). Bicomplex Mittag-Leffler function and applications in integral transform and fractional calculus. *Accepted, Proceedings of the conference, 22nd FAI-ICMCE-2020.*

[5] Agarwal, R., Sharma, U. P., and Agarwal, R. P. (2022). Bicomplex Mittag-Leffler Function and associated properties. *Journal of Nonlinear Sciences and Applications*, 15:48–60.

[6] Farman, M., Akgül, A., Nisar, K. S., Ahmad, D., Ahmad, A., Kamangar, S., and Saleel, C. A. (2022). Epidemiological analysis of fractional order COVID-19 model with Mittag-Leffler kernel. *AIMS Mathematics*, 7(1):756–783.

[7] Gorenflo, R., Kilbas, A. A., Mainardi, F., and Rogosin, S. V. (2014). *Mittag-Leffler functions, Related Topics and Application.* Springer Berlin Heidelberg.

[8] Goswami, M. P., Agarwal, R., and Agarwal, R. P. (2019). Double Laplace transform in bicomplex space with applications. *Advances in Mathematical Sciences and Applications*, 28(2):255–271.

[9] Gupta, V. G., Shrama, B., and Kiliçman, A. (2010). A note on fractional Sumudu transform. *Journal of Applied Mathematics*, 2010:1–9.

[10] Haubold, H. J., Mathai, A. M., and Saxena, R. K. (2011). Mittag-Leffler functions and their applications. *Journal of Applied Mathematics*, 2011:1–51.

[11] Jumarie, G. (2005). On the representation of fractional Brownian motion as an integral with respect to $(dt)^a$. *Applied Mathematics Letters*, 18:739–748.

[12] Jumarie, G. (2006). Modified Riemann -Liouville derivative and fractional Taylor series of non-differentiable functions Further results. *Computer and Mathematics with Applications*, 51:1367–1376.

[13] Jumarie, G. (2008). Fourier's transform of fractional order via Mittag-Leffler function and modified Riemann-Liouville derivative. *J Appl. Math. and Informatics*, 26(5-6):1101–1121.

[14] Jumarie, G. (2009). Laplace's transform of fractional order via the Mittag-Leffler function and modified Riemann-Liouville derivative. *Appl. Math. Lett*, 22:1659–1664.

[15] Kumar, A. and Kumar, P. (2011). Bicomplex version of Laplace transform. *International Journal of Engineering and Technology*, 3(3):225–232.

[16] Nisar, K. S., Suthar, D., Agarwal, R., and Purohit, S. (2020). Fractional calculus operators with Appell function kernels applied to Srivastava polynomials and extended Mittag-Leffler function. *Advances in Difference Equations*, 2020(1):1–14.

[17] Omran, M. and Kiliçman, A. (2016). Natural transform of fractional order and some properties. *Cogent Mathematics*, 3(1):1251874.

[18] Price, G. B. (1991). *An Introduction to Multicomplex Spaces and Functions*. Marcel Dekker Inc. New York.

[19] Raj, S. R. and Jernith, S. S. (2017). Analytic solution of linear fractional differential equation using fractional Laplace transform. *Annals of Pure and Applied Mathematics*, 15(2):209–214.

[20] Riley, J. D. (1953). Contributions to the theory of functions of a bicomplex variable. *Tohoku Mathematical Journal*, 5(2):132–165.

[21] Ringleb, F. (1933). Beiträge zur funktionentheorie in hyperkomplexen systemen. *I. Rendiconti del Circolo Matematico di Palermo*, 57:311–340.

[22] Rochon, D. and Shapiro, M. (2004). On algebraic properties of bicomplex and hyperbolic numbers. *Analele Universitatii din Oradea. Fascicola Matematica*, 11:71–110.

[23] Rogowski, K. (2020). General response formula for CFD pseudo-fractional 2D continuous linear systems described by the Roesser model. *Symmetry*, 12(12):1934.

[24] Rönn, S. (2001). Bicomplex algebra and function theory. *arXiv:0101200v1 [Math.CV]*, pages 1–71.

[25] Segre, C. (1892). Le rappresentazioni reale delle forme complessee Gli Enti Iperalgebrici. *Math. Ann.*, 40:413–467.

[26] Singh, J. (2020). Analysis of fractional blood alcohol model with composite fractional derivative. *Chaos, Solitons & Fractals*, 140:110127.

[27] Singh, J., Ganbari, B., Kumar, D., and Baleanu, D. (2021a). Analysis of fractional model of guava for biological pest control with memory effect. *Journal of Advanced Research*, 32:99–108.

[28] Singh, J., Gupta, A., and Baleanu, D. (2021b). On the analysis of an analytical approach for fractional Caudrey-Dodd-Gibbon equations. *Alexandria Engineering Journal*.

[29] Tassaddiq, A., Khan, I., Nisar, K. S., and Singh, J. (2020). MHD flow of a generalized Casson fluid with Newtonian heating: A fractional model with Mittag-Leffler memory. *Alexandria Engineering Journal*, 59(5):3049–3059.

TABLE OF CONTENTS, JOURNAL OF COMPUTATIONAL ANALYSIS AND APPLICATIONS, VOL. 30, NO. 2, 2022